Doctoral theses at NTNU, 2010:64

Nicola Chiesa

Power Transformer Modeling for Inrush Current Calculation

Doctoral thesis

NTNU
Norwegian University of
Science and Technology
Thesis for the degree of
Philosophiae Doctor
Faculty of Information Technology,
Mathematics and Electrical Engineering
Department of Electric Power Engineering

NTNU
Norwegian University of
Science and Technology

Nicola Chiesa

Doctoral theses at NTNU, 2010:64

NTNU

Nicola Chiesa

Power Transformer Modeling for Inrush Current Calculation

Thesis for the degree of Philosophiae Doctor

Trondheim, June 2010

Norwegian University of Science and Technology
Faculty of Information Technology,
Mathematics and Electrical Engineering
Department of Electric Power Engineering

NTNU
Norwegian University of
Science and Technology

NTNU
Norwegian University of Science and Technology

Thesis for the degree of Philosophiae Doctor

Faculty of Information Technology,
Mathematics and Electrical Engineering
Department of Electric Power Engineering

ISBN 978-82-471-2086-6 (printed ver.)
ISBN 978-82-471-2087-3 (electronic ver.)
ISSN 1503-8181

Doctoral theses at NTNU, 2010:64

Printed by NTNU-trykk

to Laura,
endless spring of love and joy.

Preface

This thesis is the result of my work at the Department of Electric Power Engineering at the Norwegian University of Science and Technology (NTNU) from 2005 to 2009. The main topic of the project is the investigation of power transformer behavior under switching operation, with special attention to the inrush current phenomena. This Ph.D. project has been part of the KMB project "Thermal and electromagnetic performance of transformers" supervised by SINTEF Energy Research and supported by the Norwegian Research Council, Hafslund Nett, Statnett SF, Statkraft Energi AS, NVE, EDF, Nynäs Petroleum AB, as well as ABB.

First and foremost I would like to thank my supervisor Prof. Hans Kristian Høidalen, who has been my mentor since I first arrived in Norway in 2004. At that time I was a young and inexperienced student pursuing my first accademic achievement, the M.Sc. Thank you for giving me the opportunity to develop as a researcher and reach this new, bigger accomplishment, the Ph.D. Hopefully we will continue our collaboration in the future, as well.

I own Prof. Bruce Mork many thanks for his many advices and insightful discussions during these four years. Thank you for inviting me to stay at your Department of Electrical & Computer Engineering at Michigan Technological University. I also would like to thank the whole research team at MTU, in particular Alejandro Avendaño and Dmitry Ishchenko.

I am very thankful to the people working in the NTNU Service Lab and Workshop, as well as to many SINTEF Energy Research employees for their help with my experimental setup. In particular, I would like to thank Bård Almås, Vladimir Kublicka, Oddvar Landrø, and last but certainly not least, Horst Førster.

I have been employed at SINTEF Energy Research, Department of Energy System since September 2009. I would like to thank my employer and my colleges for their understanding and support during the finishing phase of my thesis. It has been an honor to start working with you and be part of a prestigious research center.

Beyond all doubt, I am very happy I have had the fortune to meet many good friends in Trondheim and Michigan, within and outside the university, and from all the corners of the world. You are too many to be named, thank you for making these years unforgettable.

I want to express all my gratitude to my father Mario, mother Mirella and brother Lorenzo. Thank you for always believing in me, I could have never make it so far without your support as a family. You will always be in my heart even if I will not be so close to you – geographically. To all my relatives from the Chiesa and Mangili families, thank you to make me feel always close to you and beying a large united family. A special thank goes to my cousins Matteo and Luisa for sharing with me their interest in scientific research and being always a source of inspiration. We should write our first article together now.

Finally, the most important person in my life is my girlfriend Laura. Thank you for being supportive in these last busy months. It is your turn now, I will do my best to help you finish your Ph.D. In front of us is only a wonderful future, together we will discover unforgettable moments and extraordinary emotions.

Trondheim, April 2010
Nicola Chiesa

Abstract

In this thesis a general purpose transformer model for low and medium frequency transient studies is developed and verified. The inrush current phenomena during no-load energization of power transformer is analyzed with special attention. The main challenge is to develop a general model that is valid for a wide range of studies, while it relies on a limited number of commonly available input data. The development of such engineering model is the ultimate research goal.

The power transformer is an essential component in power systems and with exception of transmission lines, it has the greatest exposure to electrical transients of all devices. The models used to predict its transient behaviors are however not always adequate due to both lack of data/measurements and knowledge. Situations of special concern are inrush currents, switching and lightning impulse stresses, induced overvoltages and harmonics.

To predict the electromagnetic stresses on transformers, a calculation model must be established. The single-phase based equivalent representation used in most of the present simulation packages does not sufficiently account for the coupling between phases and the differences caused by various iron core structures. The representation of hysteresis, anomalous losses and remanence also needs improvements.

A valuable way to achieve a deeper understanding of the inrush current phenomena is through extensive laboratory measurements on distribution transformers and field measurements on power transformers. Experimental data are highly beneficial in the verification of the developed model.

Research questions:

- Parameter estimation is complex and not fully standardized. It may be a source of error both in the way parameters are measured and post processed.
- When saturation is a concern, the importance of a correct representation of the core is often underestimated. Several factors have to be taken into account as core topology, behavior in extreme saturation, residual flux initialization.
- Manual initialization of the residual fluxes in a transformer model is not simple. The understanding of the deenergization transient is important for the appropriate estimation of the residual flux values.

Main contributions:

- The development of a general transformer model for transient studies.
- A proposed method for parameter estimation supported by sensitivity studies.
- Systematic measurements and simulations of ringdown and inrush transients have revealed novel patterns in the inrush current first peak.
- Potential contribution to new mitigation methods.
- Measurements on three large power transformers of several MVA.

Units of Measurement

MAGNETIC CIRCUITS

NAME	SYMBOL [UNIT]	EQUATION
Magnetomotive force (mmf)	$\mathfrak{F}$ [A-t]	$\mathfrak{F} = NI$
Magnetic field intensity	H [A-t/m]	$H = NI/l$ (l = length)
Flux density	B [T] [Wb/m^2]	$B = \mu H$
Permeability	μ [H/m]	$\mu = \mu_0 \mu_r$ $\mu_0 = 4\pi 10^{-7}$
Flux	Φ [Wb]	$\Phi = BA$ (A = cross-sectional area)
Flux linkage	λ [Wb-t]	$\lambda = N\Phi$
Inductance	L [H]	$L = \lambda/I = N^2/\mathfrak{R} = N^2\Lambda$
Reluctance	$\mathfrak{R}$ [H^{-1}]	$\mathfrak{R} = 1/\Lambda$
Permeance	Λ [H]	$\Lambda = \mu_0 \mu_r A/l$

OHM'S LOW ANALOGY

ELECTRIC		MAGNETIC	
$V = RI$		$\mathfrak{F} = \mathfrak{R}\Phi$	
Current	I [A]	Φ [Wb]	Flux
emf	V [V]	$\mathfrak{F}$ [A-t]	mmf
Resistance	R [Ω]	$\mathfrak{R}$ [H^{-1}]	Reluctance
Conductivity	σ [S/m]	μ [H/m]	Permeability

CONTENTS

Preface i

Abstract iii

Units of Measurement v

Contents vii

List of Figures ix

List of Tables xi

1 Introduction 1
- 1.1 Scope of Work . . . 2
- 1.2 Research Context . . . 4
- 1.3 Thesis Outline . . . 4
- 1.4 Publications . . . 6

2 Background / State of the Art 9
- 2.1 Low-frequency Transformer Modeling . . . 10
  - 2.1.1 Models based on a magnetic circuit . . . 11
  - 2.1.2 Models based on an equivalent electric circuit . . . 13
  - 2.1.3 Model based on an hybrid approach . . . 18
  - 2.1.4 Parameter estimation . . . 20
  - 2.1.5 Extension to higher frequency . . . 22
- 2.2 Inrush Current . . . 23
  - 2.2.1 Simulation of inrush current transients . . . 24
  - 2.2.2 Analytical calculation of inrush current . . . 27
  - 2.2.3 Inrush current mitigation techniques . . . 30

2.2.4 Ringdown transient and residual fluxes 31
2.3 Iron Core Modeling 32
2.3.1 Dynamic hysteresis models 34
2.4 Challenges in Power Transformer Modeling for Inrush Current Calculation 36

3 Inrush Current Measurements **37**
3.1 Laboratory setup 37
3.1.1 Test objects, configuration and measuring equipment 37
3.1.2 Data acquisition procedure 41
3.2 Systematic measurements on a 300 kVA and 800 kVA distribution transformers 44
3.3 Field measurements on large transformers 57
3.3.1 Field measurement 1, 300 MVA 58
3.3.2 Field measurement 2, 50 MVA 61
3.3.3 Field measurement 3, 300 MVA 61

4 Discussion **67**
4.1 Model Development 67
4.2 Leakage Model 72
4.3 Jiles-Atherton Model 79

5 Conclusions **91**
5.1 Contribution of the Publications 91
5.2 Concluding Remarks 96
5.3 Recommendations for Further Work 96

References **99**

A Implementation of the Jiles-Atherton Model in ATP **111**

B Journal Publications and Conference Proceedings **115**
Analytical algorithm for the calculation of magnetization and loss curves of delta connected transformers 117
On the ringdown transient of transformers 137
Hysteretic iron-core inductor for transformer inrush current modeling in EMTP 155
Systematic switching study of transformer inrush current: simulation and measurements 173
Transformer model for inrush current calculations: simulations, measurements and sensitivity analysis 193
Novel approach for reducing transformer inrush currents. Laboratory measurements, analytical interpretation and simulation studies 219

LIST OF FIGURES

2.1 Low frequency model of a single phase transformer. 10
2.2 Model based on a magnetic circuit. 12
2.3 Model based on an equivalent electric circuit. 14
2.4 Duality transformation: identification of the equivalent components. 16
2.5 Duality transformation: series and parallel equivalent connections. . 16
2.6 Duality transformation: derivation of a dual circuit. 17
2.7 Model based on a hybrid approach. 19
2.8 Qualitative representation of the inrush current phenomenon and the effect of the residual flux. 24
2.9 Analytical estimation of inrush current. 28
2.10 Modeling of a nonlinear iron-core inductor. 33
2.11 Loss components contributing to total iron loss in grain oriented material electrical steel. 35

3.1 Laboratory layout. 38
3.2 Test objects: 800 kVA transformer on the left, 300 kVA transformer on the right. 39
3.3 Connection of the high voltage deviders and vacuum breakers. The voltage deviders are connected directly to the transformer terminals in the final set-up. 39
3.4 GUI for the transient recorder. 42
3.5 Structured text file specifing the timings for automated multiple measurements. 42
3.6 Trigger signals and systematic variation of the switching times. . . . 43
3.7 Double triggering procedure. 43
3.8 Ringdown transient, 300 kVA transformer. 46
3.9 Inrush current transient, 300 kVA transformer. 47
3.10 Ringdown transient, 800 kVA transformer. 48

3.11 Inrush current transient, 800 kVA transformer. 49
3.12 Residual flux, 300 kVA transformer. 50
3.13 Residual flux, 800 kVA transformer. 50
3.14 Measurements of the first peak inrush current pattern, Yyn coupling. 300 kVA transformer, 3D pattern. 51
3.15 Measurements of the first peak inrush current pattern, Yyn coupling. 300 kVA transformer, absolute value. 52
3.16 Measurements of the first peak inrush current pattern, Yyn coupling. 300 kVA transformer, extended pattern. 53
3.17 Measurements of the first peak inrush current pattern, Yyn coupling. 800 kVA transformer, 3D pattern. 54
3.18 Measurements of the first peak inrush current pattern, Yyn coupling. 800 kVA transformer, absolute value. 55
3.19 Measurements of the first peak inrush current pattern, Yyn coupling. 800 kVA transformer, extended pattern. 56
3.20 Ringdown transient, 300 MVA transformer (F.M. 1). 59
3.21 Inrush current transient, 300 MVA transformer (F.M. 1). 60
3.22 Ringdown transient, 50 MVA transformer (F.M. 2). 62
3.23 Inrush current transient, 50 MVA transformer (F.M. 2). 63
3.24 Ringdown transient, 300 MVA transformer (F.M. 3). 64
3.25 Inrush current transient, 300 MVA transformer (F.M. 3). 65
3.26 Effect of CTs and current probes on inrush current measurements. . 66

4.1 Three-legged three-winding transformer. Magnetic core and winding structure. 68
4.2 Discretization of the flux paths. 69
4.3 Magnetic circuit. 70
4.4 Equivalent electric circuit obtained by duality transformation. 71
4.5 Concentric windings. 73
4.6 Sandwich windings. 74
4.7 Mixed windings, configuration 1. 75
4.8 Mixed windings, configuration 2. 76
4.9 Equivalent mesh network for leakage representation. 78
4.10 Geometrical model for leakage representation of concentric windngs. 78
4.11 Anhisteretic curve fitting. 84
4.12 Test report and calculated rms no-load current. 85
4.13 Test report and calculated losses. Constant parameters. 85
4.14 Test report and calculated losses. Variable parameters. 86
4.15 Current wave at rated excitation. 87
4.16 Hysteresis loop at rated excitation. 88
4.17 Expansion of hysteresis loops 89

LIST OF TABLES

3.1 Core and Windings design data, 300 kVA transformer. 40
3.2 Core and Windings design data, 800 kVA transformer. 40
3.3 Comparison of maximum inrush current first peak and maximum residual flux for different transformers. 57

4.1 Open-Circuit Data. 83

CHAPTER 1

INTRODUCTION

The market liberalization of the electrical energy sector started in Europe in the 1990s, with the objective of opening up the electricity market by gradually introducing competition. Businesses and private customers are theoretically able to choose their suppliers freely in a competitive marketplace. To allow different players to enter the market, production and distribution activities have to be run independently from network operation. Under this situation, efficiency improvement, cost management and investment reduction are the necessary tools to be more competitive. At the same time, the demand for a reliable supply of energy has increased considerably requiring nearly a no-fault operation of power systems.

This scenario is very challenging from the network operation and planing point of view. The failure of equipment due to overloading, overvoltages, ageing, and misoperations of protective devices is likely to increase. The advent of smart and micro grids systems with energy storage capabilities and/or private generation allows to trade electrical energy in a dynamic way. More switching operations regulated by the energy spot price are predicted. The number of electrical transient situations is therefore believed to increase in a distributed power generation regime.

The age distribution of the transformer population is entering in a critical era. Many transformers subjected to overload conditions and/or accelerating ageing might be near at their end-of-life. A power transformer is a rather large and expensive unit therefore, in a competitive and fairly low margin market, utilities tend to postpone as much as possible the replacement of aged units. This inconveniently reduces the

network reliability. A transformer breakdown could have consequences on the rest of the power system and in addition the repair time of transformers is long. Time to delivery for new power transformers is in the range of one year. To overcome this problem the scientific community is asked to answer the question: "When should a power transformer be replaced?".

The main approach to address this question is the study of materials ageing. This involves ageing models of paper and press board, acid formation and voltage withstand reduction schemes. However, ageing studies and aging control techniques (e.g. oil refurbishment) are believed to be insufficient to overcome the problem alone. Unfavorable network situations have to be restrained as much as possible to limit electromagnetic stresses, especially in case of aged units.

The withstand of electrical apparatus to overvoltages is assumed reduced both due to aging and optimized design practice. Most of the electrical equipment installed in the networks approaches a critical age. While condition assessment is arduous, improved protection of electrical apparatus may extend their functional life and increase the overall system reliability. In addition, the trend to cut the manufacturing costs by optimization of insulating materials leads to a smaller margin in the design practice. Increased accuracy in insulation coordination studies is required to identify the vulnerable spots in a system in order to minimize the damages as a consequence of steady-state, dynamic and transient overvoltages.

The number of transient situations is believed to increase in a distributed power generation regime. A wind farm will be extensively exposed both to switching and lightning over-stresses. The large number of generators and connecting cables in such plants will also increase the risk of resonant phenomena. The understanding and prediction of these situations can result in better protection schemes and integration of power transformers in the network. Hazardous operations manifest as electromagnetic transients and are usually difficult to accurately predict. They are inrush currents, overvoltages, internal resonances, and lightning impulse stresses. Even though they cannot be eliminated, it can be possible to limit and reduce them to a harmless state.

High inrush currents can result in voltage dips and tripping of differential current relays both leading to a power quality reduction. Some providers have installed synchronized breakers to migrate high inrush currents, but this practice generally results in higher overvoltages and increases the risk of resonances. The trend of increased short circuit capacity and reduced losses in power systems intensifies the inrush current problem and makes the proper setting of relays more difficult.

1.1 Scope of Work

Calculation models must be established to predict electromagnetic stresses on transformers. The single-phase based equivalent model used in most of the present simulation packages does not accurately represent the coupling between phases caused

by the configuration of the iron core and its construction. The representation of hysteresis, core losses and remanence should also be improved. Lack of input data is the main problem as the typical test report procedure is often insufficient to establish an accurate model.

The objective of this work is to perform a detailed study of power transformers and to develop a transformer model to be used in transient simulation studies. A transformer is a sophisticated electrical machine and its modeling is a challenge. The focus is on transformer modeling from power frequencies and upwards below the first resonant frequency at some kilohertz.

The inrush current occurring at the energization of a transformer may be considered as one of the most demanding low-frequency transient to be modeled in a transformer. Inrush currents are caused by saturation effects in the iron core when a transformer is energized. The work puts a strong emphasis on inrush current modeling as it is believed that if a transformer model can accurately predict inrush current transients, it can predict most of the switching transients.

The main challenge in transformer modeling is the proper representation of the nonlinear core. A topologically correct model is required to predict the saturation effect in each part of the core. Special attention will be paid to saturation, core losses, and hysteresis loops. Another important characteristic for the model is the ability of flux initialization. For this reason an advanced nonlinear inductor model is required.

Test report data is the "identification card" of a transformer and is usually the only information available. The use of standardly available input data imposes a limit on the detail level of a model. However, a model established mainly from this data will be a fairly general model in contrast to design-based model (suitable for a specific transformer only).

Generally, a better low frequency/electromagnetic transformer model will improve the capability of estimating inrush currents and switching transients. A better knowledge of network transients may produce a power quality improvement and reduce the risk of failures. The overall benefits from this project will have relevance both for the end users and for the manufacturers of materials and transformers. From the utilities, transformer manufacturers and service providers' point of view this work has the following points of interest:

- The availability of accurate and reliable simulation tools.
- The setting of protective relays to avoid tripping at transformer energization for minimum inrush and maximum power quality.
- A way to better define rules for synchronized switching of transformers.
- The identification of situations that can result in transient overvoltages.
- The investigation of the causes of failures and the ways to avoid their repetition.
- The reduction of transformer stress situations.

1.2 Research Context

The PhD work is part of a larger KMB[1] project administrated by SINTEF Energy Research with title "Thermal and electromagnetic performance of transformers". The project is composed by three main activities: winding aging and maintenance, electromagnetic modeling, and copper sulfur. It has been financed by the Norwegian Research Council and several industrial partners: Hafslund Nett, Statnett SF, Statkraft Energi AS, NVE, EDF, Nynäs Petroleum AB and ABB. The PhD work was financed for 75% by the electromagnetic modeling part of this project.

Concerning my work, the research questions delineated by the project were related to the improvement of transformer models available for electromagnetic transient programs. In particular, an enhanced representation of energization transients was desired. As a restraint, the model parameters should have been estimated primarily from standardly available test report data.

Synergetic collaboration with Prof. B. A. Mork at Michigan Technological University (MTU) was maintained during the whole duration of the PhD. In particular, I have been visiting MTU in 2006 for the duration of six months. The interchange was extended for another six months welcoming at our institution the PhD student A. Avendaño from MTU. The collaboration with this PhD student was relevant for the project. In spite of the common interest in transformer modeling, the research topics remained clearly distinguished. The research of A. Avendaño has a main focus on the leakage model, with splitting of the winding representation in subsections for extension to higher frequency and modeling of internal faults. I was more involved in transformer core and inrush current issues as extensively documented in this thesis.

1.3 Thesis Outline

The principal focus of this document is to provide background information and state of the art knowledge on the main aspects of transformer modeling. The main contributions and results are reported in publications in journals and conference proceedings as outlined in Section 1.4.

This first **Chapter 1** outlines the motivations and the context of this work.

Chapter 2 is the principal part of the document and is divided in three main sections: state of the art of low-frequency transformer modeling, background information on inrush current, and overview on modeling of a nonlinear hysteretic inductor.

Chapter 3 details the laboratory and test setup. The systematic energization and deenergization measurements performed on two distribution transformer are shown. In

[1] Knowledge-building project with user involvement (KMB), http://www.forskningsradet.no/

addition, few field measurements carried out on large power transformers are presented.

Chapter 4 discusses several topics that were triggered by this work and may be inspiration for future research activities. In particular, it treats 1) the development of the model, 2) the generalization of the leakage reactance representation for different configuration and number of windings, and 3) the possible improvements to the Jiles-Atherton model when used for transformer modeling.

Chapter 5 contains the main conclusion of this work and suggests topics for further research.

The code of the Jiles-Atherton model implemented in ATP based on the MODELS language for the trapezoidal rule of integration is given in **Appendix A**.

The reprints of the most significant journal publications and conference proceedings produced during this work are included in **Appendix B**.

1.4 Publications

The main results of this work are published or accepted for publication in the following journal and conference proceedings:

[Pb1] N. Chiesa and H. K. Høidalen, "Analytical algorithm for the calculation of magnetization and loss curves of delta connected transformers," *IEEE Trans. Power Del.*, 2010, accepted for publication, TPWRD-00589-2009.

[Pb2] H. K. Høidalen, B. A. Mork, F. Gonzalez, D. Ishchenko, and N. Chiesa, "Implementation and verification of the hybrid transformer model in ATPDraw," *Electr. Power Syst. Res.*, vol. 79, no. 3, pp. 454 – 459, Mar. 2009, special Issue: Papers from the 7th International Conference on Power Systems Transients (IPST).

[Pb3] A. Avendaño, N. Chiesa, B. A. Mork, H. K. Høidalen, D. Ishchenko, F. Gonzalez, and A. P. Kunze, "Transformer short-circuit representation: Investigation of phase-to-phase coupling," in *IPST'07 - International Conference on Power System Transients*, no. IPST-232, Lyon, France, Jun. 2007.

[Pb4] N. Chiesa, A. Avendaño, H. K. Høidalen, B. A. Mork, D. Ishchenko, and A. P. Kunze, "On the ringdown transient of transformers," in *IPST'07 - International Conference on Power System Transients*, no. IPST-229, Lyon, France, Jun. 2007.

[Pb5] N. Chiesa and H. K. Høidalen, "Hysteretic iron-core inductor for transformer inrush current modeling in EMTP," in *PSCC 2008 - 16th Power Systems Computation Conference*, Glasgow, Scotland, Jul. 2008.

[Pb6] N. Chiesa and H. K. Høidalen, "Systematic switching study of transformer inrush current: simulation and measurements," in *IPST'09 - International Conference on Power System Transients*, no. IPST-139, Kyoto, Japan, Jun. 2009.

[Pb7] N. Chiesa, B. A. Mork, and H. K. Høidalen, "Transformer model for inrush current calculations: Simulations, measurements and sensitivity analysis," *IEEE Trans. Power Del.*, 2010, accepted for publication, TPWRD-00942-2009.

[Pb8] N. Chiesa and H. K. Høidalen, "Novel approach for reducing transformer inrush currents. Laboratory measurements, analytical interpretation and simulation studies," *IEEE Trans. Power Del.*, 2010, accepted for publication, TPWRD-00953-2009.

Publications relevant to the topic but not discussed in this document:

[Pb9] N. Chiesa and H. K. Høidalen, "On the calculation of flux linkage/current-characteristic for Δ-coupled transformer windings," in EEUG Meeting 2005, European EMTP-ATP Conference*, Warsaw, Poland, Sep. 2005.*

[Pb10] N. Chiesa and H. K. Høidalen, "Modeling of nonlinear and hysteretic iron-core inductors in ATP," in EEUG Meeting 2007, European EMTP-ATP Conference*, Leon, Spania, Sep. 2007.*

My role in [Pb2] is related to the implementation of the core section of the model. My contribution to [Pb3] is marginal and related to laboratory measurements and implementation of the model in the simulation program. I am the main contributor of all the remaining publications. The reprints of [Pb1, Pb4, Pb5, Pb6, Pb7, Pb8] are included in **Appendix B**.

CHAPTER 2

BACKGROUND / STATE OF THE ART

Transformer modeling is a broad topic and models are widely used for the simulation of transient behaviors [1–5]. An accurate representation of every transient situation requires a model valid for a frequency range from dc to several MHz. This is very difficult and in most of the cases is not feasible. Transformer models can be developed to be accurate for a specific range of frequencies. A classification of frequency ranges of transients is proposed in [4] in accordance with what recommended by the CIGRE WG 33.02:

- slow transients: from 5 Hz to 1 kHz.
- switching transients: from the fundamental power frequency up to 10 kHz.
- fast front transients: from 10 kHz up to 1 MHz.
- very fast front transients: from 100 kHz to 50 MHz

Each range of frequencies corresponds to some particular transient phenomena. Transformer models with a different level of details can be developed to represent the transients in the frequency range of interest as briefly outlined below [4].

Examples of slow transients are torsional oscillations, transient torsional torques, turbine blade vibrations, fast bus transfers, controller interactions, harmonic interactions, and resonances. Classical low frequency transformer models similar to the

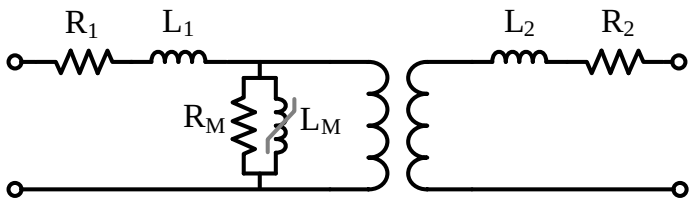

Figure 2.1: Low frequency model of a single phase transformer.

one shown in Fig. 2.1 can be used for the simulation of low frequency dynamics. Three-phase transformer models are developed from this representation with a proper connection of primary and secondary windings.

Switching transients are caused by energization and de-energization of system components. The study of switching phenomena is useful for insulation co-ordination, determination of arrester characteristics, calculation of transient recovery voltages, and establishment of transient mitigation solutions. Transformer are usually represented by lumped parameter coupled-winding models. A sufficient number of R-L-C elements ensures the appropriate frequency response of a model. The nonlinear characteristic of the core is usually included, and for transients below 3-5 kHz the frequency characteristic of the core may be neglected.

One of the primary cause of fast front transients are lightning strokes on overhead transmission lines and substations. Studies are aimed to the design of transmission lines and substations, and to the protection of equipments. Here transformer are represented by their stray capacitances to ground. A model can be enhanced by adding the inductive transformer model and relevant capacitances between windings. The influence of the magnetic core is usually neglected in the study of high frequency transients.

Very fast front transients typically occur in gas insulated substations. For such high frequency transients, it is common to model a transformer as a capacitor. Inter winding capacitances are represented when the voltage transfer has to be calculated. At very high frequency the leakage and magnetizing impedances can be neglected.

The scope of this work is to examine transformer models for the study of low-frequency switching transients where saturation effects, nonlinearities, and losses representation are the main concerns. This chapter present the state of the art of the central topics of this work: low-frequency transformer modeling, estimation of inrush current, and representation of nonlinear hysteretic inductors.

2.1 Low-frequency Transformer Modeling

The two main components to be considered when creating a low-frequency transformer model are the windings and the iron core. The windings representation deter-

mines the transfer characteristic of the transformer (short-circuit response), while the iron core representation controls the flux balance (no-load response) and the phase-to-phase coupling (transformer topology).

A review of transformer modeling for low-frequency transients is given in [6–10]. These references suggest that a transformer model for transient studies should be based on a topologically correct representation of the magnetic and winding structures. In most of the cases, a single-phase equivalent black-box model is not adequate for representing unbalanced operations and nonlinear behaviors of three-phase networks [11].

There are two main approaches for the modeling of transformers in the low frequency range that retain the topological representation of the magnetic structure. On one side, an equivalent magnetic circuit can be used to represent a transformer. An interface between the magnetic model and the electrical network is then required. On the other side, an equivalent electric circuit derived by duality transformation of the magnetic circuit can be used to model a transformer directly in the electrical domain. Both methods are appropriate for the representation of the transformer magnetic core where the flux path are well defined, but rely on approximations for the representation of the leakage flux paths.

2.1.1 Models based on a magnetic circuit

The electromagnetic structure of a transformer can be directly represented using reactances. Relatively complex structures can be examined as a magnetic model is obtained by inspection as shown in Fig. 2.2. The accuracy of the magnetic circuit is highly related to the assumptions made to discretize the magnetic structure in a lumped parameter magnetic circuit. Nonlinear reactances are used to represent iron limbs and linear reactances to represent air paths, [8,12,13]. In [12] a high order polynomial function is used to model nonlinearity and hysteresis effects. The connection between the magnetic structure and an electric network is not easily accomplished and an interface need to be established. The windings have the function to connect the two interdependent sub-systems through electric and magnetic equations:

$$v(t) = \mathrm{d}\lambda(t)/\mathrm{d}t \tag{2.1}$$

$$i(t) = \mathfrak{F}(t)/N \tag{2.2}$$

Core and winding losses cannot be directly included in the magnetic model and are connected at the winding terminals [14, 15] in a similar way as shown in Fig. 2.2. In [12] the eddy current losses in the core are accounted for by a voltage-dependent resistance on the transformer terminals. Several assumptions of the flux distribution among the three phases are required [16] to concentrate eddy current losses at the winding terminals instead of at the corresponding core limbs. It is therefore difficult to obtain a topological distribution of the core losses.

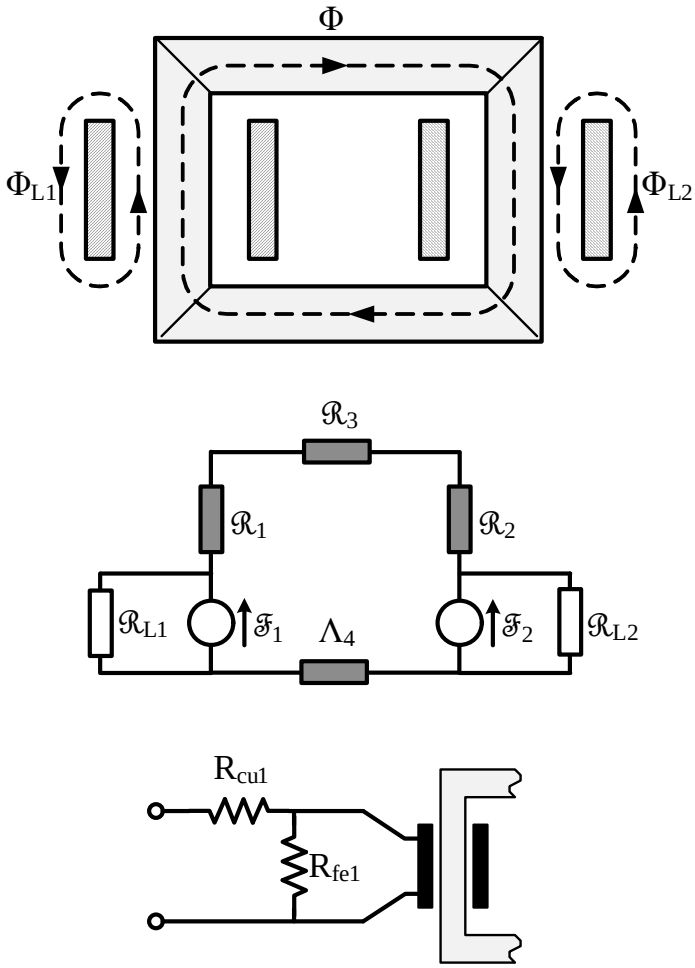

Figure 2.2: Model based on a magnetic circuit.

Elleuch and Poloujadoff [8] used a reluctance based model to study the influence of zero sequence and leakage inductances on inrush current transients. In a following work [17, 18], they used the same modeling approach to investigate the anisotropy of magnetic materials and examine the flux distribution in the central T-joint. The model has been used to simulate inrush current transients and is able to reproduce spatial inequality of the flux distribution, the distortion of localized flux waveform, and the circulating fluxes in a T-joint.

2.1.2 Models based on an equivalent electric circuit

The implementation of a reluctance model in an electromagnetic transient program is complicated as an electric and a magnetic subnetworks have to be established and mutually interconnected. An equivalent electric circuit of the reluctance model can be derived by mean of a duality transformation as shown in Fig. 2.3 and as explained below. The final circuit is a pure electric circuit that can be easily implemented with standard electrical components. In addition, resistances can be connected in parallel to the inductors to represent core losses, establishing an inclusive topological structure.

Maxwell equations can be deciphered to help defining general rules for the discretization of magnetic circuits.

$$\nabla \cdot \vec{D} = \rho_\nu \tag{2.3}$$

$$\nabla \cdot \vec{B} = 0 \tag{2.4}$$

$$\nabla \times \vec{E} = -\frac{\partial \vec{B}}{\partial t} \tag{2.5}$$

$$\nabla \times \vec{H} = \vec{J} + \frac{\partial \vec{D}}{\partial t} \tag{2.6}$$

Equation (2.4) defines that there are no sources of magnetic flux, thus all the flux lines have to be closed. This means that the net flux flowing inside and outside the surface defined by a winding have to be equal. Electric potential and variation of magnetic flux density are related as defined by (2.5). In the presence of an ideal short circuit in a winding (E=0), the net flux flowing inside the surface surrounded by a winding has to be zero. An electric short-circuit is therefore equivalent to a magnetic open-circuit. It is reasonable to assume the space charges ρ_ν and the displacement current $\partial\vec{D}/\partial t$ identical to zero for this problem. Equation (2.6) simplifies to $\nabla \times \vec{H} = \vec{J}$. This last equation implies that the magnetic field is deformed by a current flowing in a winding. A winding with no current is neutral to the magnetic field and does not modify the flux paths. This is represented by an electric open-circuit and the flux is free to cross the area surrounded by the winding. The voltage induced in an open-circuited winding is then defined by the net flux in the inner (or outer) area of the winding due to (2.5). To satisfy the Maxwell equations, at least one magnetic branch on the inside and one on the outside of a winding need to be available and be part of

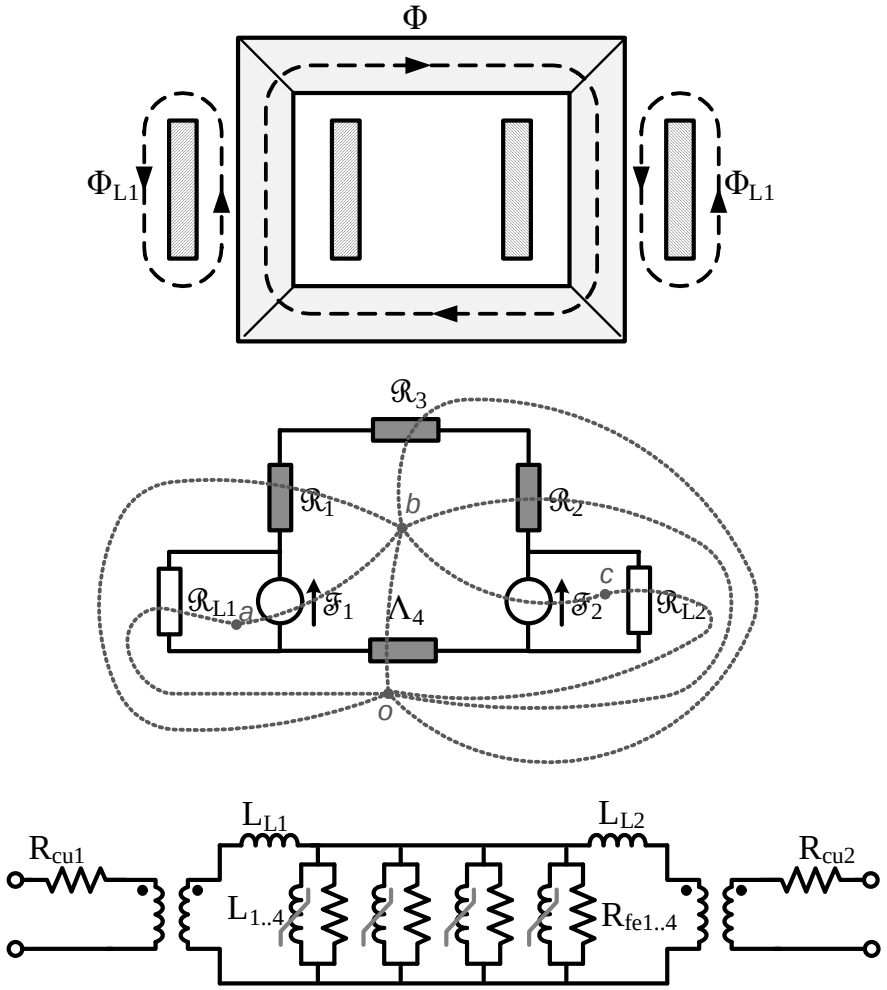

Figure 2.3: Model based on an equivalent electric circuit.

the same circuit. In addition, each magnetic node has to be connected to at least two magnetic branches to form a mesh.

The duality between electric and magnetic circuits and an efficient topological approach for constructing dual circuits were proposed by Colin Cherry [19] and have been further formalized in [20]. The topological approach proposed by Colin Cherry is valid for planar network and is limited to a maximum of three windings. For a number of winding higher than three, the electrical network can be equivalent in term of external effects, but is not representative of the internal fields. For example, a n-winding planar magnetic network can be construct neglecting the multiple-linked air fluxes. The practical application of the derivation of an equivalent circuit for three-phase transformer is presented by Slemon in [21].

The conversion of the magnetic circuit to an electric equivalent representation does not introduce approximations and is obtained by duality transformation. In this sense, the phenomena of establishing a flux in a magnetic circuit due to the effect of a magnetomotive force ($\Phi = \Lambda \cdot \mathfrak{F}$) is dual of the creation of an electromotive force due to the effect of a variable current ($v = L \cdot \frac{\mathrm{d}i}{\mathrm{d}t}$) [22]. The magnetic across variable magnetic potential drop (M) is dual of the electric through variable current (i), and the magnetic through variable flux (Φ) is dual of the electric across variable voltage (v). The identification of the equivalent components is illustrated in Fig. 2.4: the electric equivalent of a permeance (Λ) is an inductance (L), and the electric equivalent of a mmf source ($\mathfrak{F}$) is a current source (i). The duality transformation of series and parallel connections is shown in Fig. 2.5. An example of the application of the topological method for constructing a dual circuit proposed by C. Cherry [19] is shown in Fig. 2.6 for a simple structure. In Fig. 2.6 the magnetic structure is first discretized and represented by a magnetic circuit. Then, a knot is defined and numbered at the center of each mesh of the magnetic circuit. In addition a knot "0" is placed externally. Finally, the topology of the electric circuit can be obtained drawing a line between different knots according to few simple rules:

1. A line cannot cross the connections of the magnetic circuit (solid lines) but only its elements (mmf sources and permeances).
2. If two knots need to be connected together, the connection must cross a single element.
3. Each single element is crossed only once by a single line.
4. All elements have to be crossed by a line.
5. Each knot must have at least two connections.

The dashed line in Fig. 2.6 are sketched according to these rules. These lines represent the electric connections and the electric circuit can be obtain by substituting the magnetic components with their electric equivalent. The directions of one current source is chosen arbitrary to defines the correlation between the direction of mmf and current sources. The remaining current sources needs to follow the same convention.

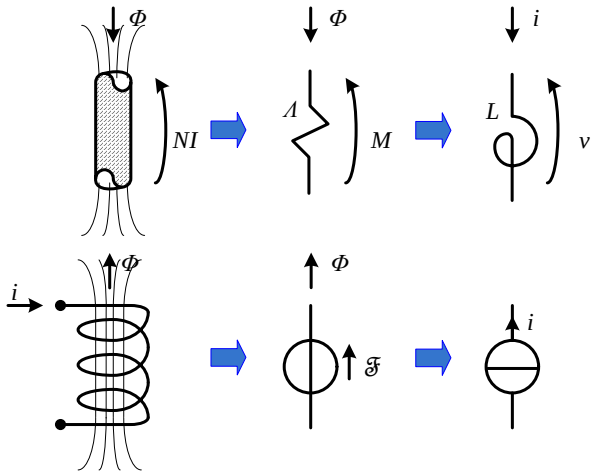

Figure 2.4: Duality transformation: identification of the equivalent components.

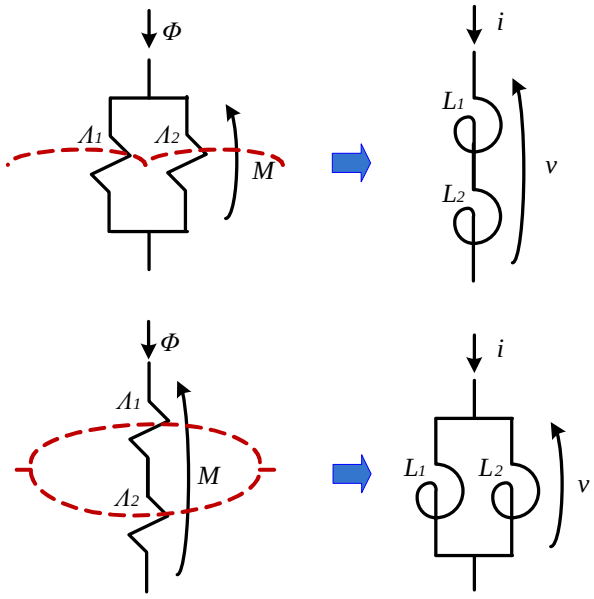

Figure 2.5: Duality transformation: series and parallel equivalent connections.

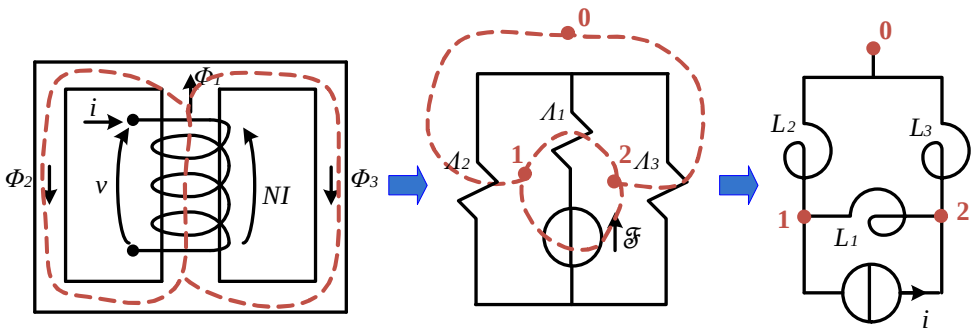

Figure 2.6: Duality transformation: derivation of a dual circuit.

Saldaña and Calzolari [23] present some theoretical aspect on how to obtain electric circuit of a transformer based on the principle of duality. They observe that the accuracy of the dual electric circuit is largely dependent on the manner in which the magnetic system is discretized into a magnetic circuit.

A detailed equivalent circuit model is presented by Dick and Watson in [24]. This model is based on a topologically correct electrical equivalent representation of the core and the windings. The linear inductances can be related to the physical geometry of the transformer windings, while nonlinear inductances are a direct representation of the reluctances of the iron core. The authors observe how in their model the magnetizing inductance of a core leg results connected to the respective inner winding, while the zero sequence inductance and the delta connection used to model the effect of a three-limb core should be attached at the outer winding terminals.

The limitation of a per-phase equivalent circuit and the need to represent the core topology for the investigation of overvoltages is discussed in [11, 21]. A model of a five-legged wound-core transformer composed by four single cores bounded together is proposed in [11]. One of the first complete implementation of a topological equivalent model of a five-limb transformer is given by Arturi [25]. He highlights the importance of an air-branch in parallel to each iron-branch to model the heavy saturated behavior. Ideal transformers are used to interface the core model to the external electric circuit, to take into account the actual number of turns, and to allow star or delta connection of the windings. This model has been successfully used for the analysis of out-of-phase synchronization involving heavy saturation.

Mork [26] proposes a five-legged wound-core transformer model for the investigation of ferroresonance effects. The model's equivalent circuit is derived using the duality transformation. The author stresses the importance to use a duality based model for ferroresonance studies in order to correctly represent phase-to-phase magnetic coupling. The paper points out the importance to improve core equivalent model representation, nonlinear core losses modeling and handling of nonzero initial fluxes in further works.

2.1.3 Model based on an hybrid approach

Transformers are modeled in electromagnetic transient programs using different approaches [27]. Branch resistance and inductance matrices $[R]$ and $[L]$ are used in the XFORMER support routine to represent the self and mutual inductances. Transformers can be represented as coupled $[R]$-$[L]$-branches only if the exciting current is not ignored and are based on the following equation:

$$[v] = [R][i] + [L][di/dt] \tag{2.7}$$

The elements of the $[X] = j\omega[L]$ matrix contain the information of the exciting current with the short circuit reactances being represented indirectly by the small difference between each matrix element pair X_{ii} and X_{ij}. The short circuit reactance may be lost unless very high accuracy is used to input the numerical values (ill-conditioned matrix).

An equivalent star circuit representation is used in the STC (saturable transformer component) support routine. It is based on the matrices $[R]$ and $[L]^{-1}$ with the constituting equation:

$$[L]^{-1}[v] = [L]^{-1}[R][i] + [di/dt] \tag{2.8}$$

While the $[L]$ matrix does not exist if the exciting current is ignored, the $[L]^{-1}$ can always be determined, and is not ill-conditioned. When the exciting current is ignored, the core representation can be externally connected to the star point. This approach may give unstable responses if one of the leakage inductance in a three-winding transformer becomes negative [28]. Since the unsaturated magnetizing reactance is much larger than the short-circuit reactance, it can be connected to a winding terminal as well. This is reported also as a mean to avoid instabilities of the model [29]. This representation is in general not valid for more than three windings.

The branch admittance matrix formulation

$$[I] = [Y][V] \tag{2.9}$$

is used in BCTRAN and TRELEG support routines. A transformer is represented by an equivalent mesh network extracted from short-circuit measurements. For transient studies, the resistance and inductance parts need to be separated. The winding resistances form a diagonal matrix $[R]$ and $[Y]$ is purely inductive ($j\omega[Y] = [L]^{-1}$). Blume [1] and later Shipley [30] propose a method for calculating the equivalent circuit of multi-winding transformers. It is based on an admittance matrix formulation that can be determined by inspection and without inversion process. It is relatively simple to obtain a model that match terminal short-circuit measurements. The method produces a very accurate short circuit representation and can be extended to any number of windings, however it does not directly take into account the magnetizing current. This approach is implemented in the standard EMTP BCTRAN transformer model [27, 31]. The BCTRAN model is regarded as a generally reliable

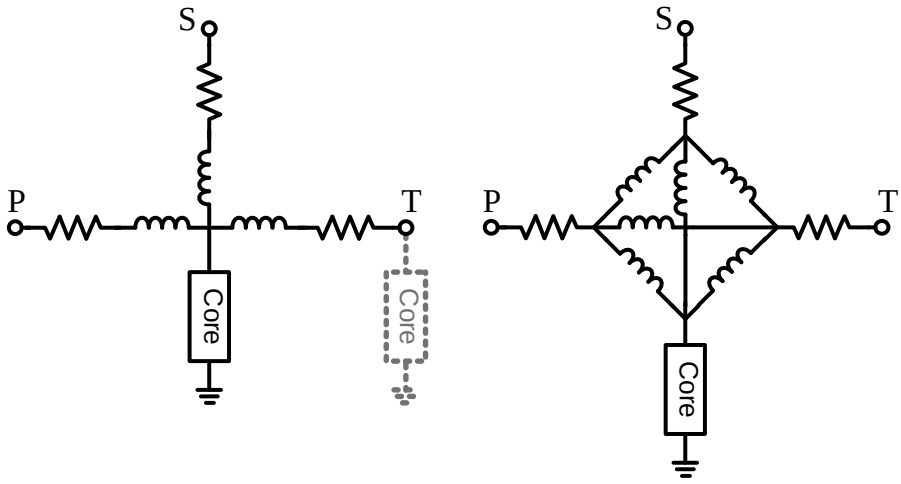

(a) *Equivalent star circuit.* (b) *Equivalent mesh circuit.*

Figure 2.7: Model based on a hybrid approach.

model, been successfully tested under a wide range of phenomena [32]. This approach does not have stability issues as the cross-admittances always have positive values. In the $[L]^{-1}$ matrix representation, the internal node of the star circuit is not available, and the magnetizing inductance must therefore be connected across one of the external terminals.

The representation of three-phase transformers is obtained by extension of the previous approaches with the inclusion of zero-sequence reluctances. However, it is difficult to include the non symmetric transformer construction to accurately represent the phase-to-phase magnetic coupling and the unbalanced magnetization currents. In an hybrid approach, it is assumed that the no-load and the short-circuit behaviors of a transformer are decoupled. The magnetic structure of a transformer is represented either by a magnetic or an equivalent electric circuit, and the windings are described by their leakage inductance and turns ratio. Both the star-equivalent and the mesh-equivalent circuit can be used to model the transformer leakage reactance as depicted in Fig. 2.7. This is a hybrid approach in the sense that two different modeling methods are combined together. The element identified as "core" in Fig. 2.7 can be a very detailed representation of the magnetic structure of a transformer (single- or three-phase). It may be connected to the star point or to a winding terminal for an equivalent star circuit as shown in Fig. 2.7(a). In case of an equivalent mesh circuit, the core representation can be added to a winding terminal. Since the number of winding is not limited to three for the mesh equivalent circuit, an additional fictitious winding can be defined as the connection point for the core model as shown in Fig. 2.7(b).

The hybrid approach strategy is proposed by de Leon in [7, 33] as a way to com-

bine a duality based model with a model based on leakage inductances. The concept of a fictitious-turn used to interface the core and leakage model is introduced here. Elleuch [8] uses a hybrid approach combining self and mutual inductances with a magnetic circuit. Fuchs [13] combines a leakage inductance model together with a magnetic circuit representation. Nagarg and Brierley [34] describe the hybrid approach philosophy in the development of their TOPMAG model. Practical application and ease of derivation of the parameters from test data are the main leading motivations for the development of a hybrid model. The model is based on a topologically correct electrical equivalent representation of the core, while it relays on an inverse inductance matrix for the representation of the short circuit behavior.

The model proposed by Mork in [26] is further developed in a low-frequency transformer model based on a hybrid topology where leakage inductances can be derived from short-circuit measurements at the terminals, and a fictitious winding is used as connection point between a leakage admittance matrix and a dual equivalent core representation [35–38]. Under the assumption of the separation of short-circuit and no-load effects, the correct short circuit representation is provided by a leakage admittance matrix, and the topologically correct representation of the core is achieved by a simplified equivalent electric model.

2.1.4 Parameter estimation

The detail level of a model is mainly determined by the data available for the estimation of the parameters. A sophisticated model that requires confidential design data or atypical measurements can rarely find application in a practical study. A less complex model based on commonly available data and measurements, and empirical parameters is adequate for most of the low-frequency and switching transients studies.

Test reports used for the certification of transformers according to standards [39–41] are the majour source of information for the parameter estimation of transformer models. Inductances, winding losses, capacitances, and core are the main elements in a transformer model. An estimation method based either on test report data, simplified design data, or typical values is given in [36, 38].

The estimation of winding resistances and capacitances is relatively effortless for low frequency models. Winding resistance measurements at dc is usually available from the test report and the ac resistance is extracted from short-circuit test data. The winding shunt capacitances are also standardly measured. The modeling of shunt capacitances is important for the higher frequencies and for the calculation of residual fluxes, but may be omitted in other contexts. Leakage inductances are calculated from short-circuit measurements, and no-load measurements are used for the estimation of core parameters. An approach for the estimation of leakage inductances based on the admittance matrix formulation is discussed in [35]. Here the parameters for a three-phase multi-winding autotransformer are derived from short circuit measurements.

The main concern in literature is the estimation of the transfer characteristic and core losses. Dick and Watson [24] discuss in their paper the importance of the proper representation of the saturation behavior in a transformer model. The paper propose a measurement procedure to determine saturation and air-core inductance using low-power dc supply. Hysteresis loop are recorded and minor loops are discussed. The paper analyzes three different modeling approaches in relation to the proper representation of iron-core inductances. First, a common star-equivalent circuit model is considered inadequate due to large discrepancies between measured and calculated air-core inductances. A detailed equivalent circuit is then proposed. This model is based on a dual electric circuit that account for winding thickness, core topology and flux-leakage paths. This model gives a very accurate representation of the air-core leakages, however due to the elevated number of elements the circuit is considered too cumbersome for most studies. A simplified equivalent model is then proposed. This has the same number of elements as the star-equivalent circuit, but their relocation improves the overall accuracy. Based on the detailed equivalent circuit, it has been observed that the delta connection required to model the effect of a three limb core should be made at the outer winding terminals. It is observed that hysteresis is important only for certain type of simulations (transformer deenergization, current chopping, low-current ferroresonance with series capacitance) and can be neglected in other studies (effect of saturation on overvoltages, high current ferroresonance from excess shunt capacitance).

Ewart [42] proposes that a core model has to represent the separate effects of hysteresis, saturation, and free-space (air-core). These three effects are somewhat independent and can be analyzed separately. Hysteresis and saturation are further discussed in Section 2.3.

The free-space or air-core inductance is defined both by the leakage inductances and by the saturated inductance of the core. The importance of a correct winding leakage representation in transient simulations where the core reaches saturation is discussed in [29]. A leakage model based on geometrical data is proposed. This model uses negative inductances to account for the thickness of the winding. The same approach is mention by Arturi in [25] as a way to improve the winding leakage representation in a model based on duality transformation. A technique for measuring air-core and leakage inductances using a low power dc supply is proposed in [24]. The air-core inductance can be estimated from inrush current waveforms as proposed in [43]: the magnetization curves extracted from inrush current measurements are first compensated for the unknown residual flux and then used to extend the manufacturer no-load test data.

The importance of the air-core reactance is also emphasize in [44]. The authors of this paper propose a method for the calculation of the air-core reactance from highly detailed winding design data. It is observed that the total transformer reactance is different for different winding configurations. Nakachi in [45] strengthen the importance of the air-core inductance for the correct representation of the behavior in saturation and the accurate determination of inrush current transients. De Leon and

Martinez propose in [46] a way to match leakage inductance measurements using a set of mutually coupled inductances that avoid the use of a negative inductance in a star-equivalent representation.

2.1.5 Extension to higher frequency

At low frequency, from dc to few kHz, transformer modeling is difficult as frequency- and voltage-dependent nonlinear effects have to be taken into account at the same time.

De Leon and Semlyen proposed a transformer model with a topologically correct core valid for the study of high frequency transients. In a first paper [6] the procedure for the calculation of turn-to-turn leakage inductance and capacitance is proposed. In a follow-up paper [33] the same authors propose a reduction of the high-order turn-to-turn model of the windings and interface this with an iron core model using the principle of duality. The approach described in this paper shows how a transformer model valid for low frequency transient can be extended to higher frequency substituting lumped elements with components that represent frequency dependency. A complete transformer model is then proposed in a third paper [7] where also the nonlinear and frequency dependent effects of the core are modeled with a Cauer equivalent circuit. However, hysteresis is not modeled due to its complex nature. The complete model is composed of three main parts representing the linear electric subsystem, the nonlinear and frequency dependent core magnetization, and the frequency dependent winding losses. These subsystems are interdependent. An iterative approach is used to solve the state equations and achieve the convergence of the complete model. The state equations can be solved with trapezoidal rule of integration and the solution is considered valid for frequency up to 1-10MHz. Semlyen and de Leon [47] described the use of an add-on circuit based on a Foster equivalent circuit for the representation of frequency dependent Ri^2 eddy current effects. This model can be added to any existing transformer model.

A similar approach is used in [48] to model high frequency effects for lightning studies. Each frequency dependent effect is represented by a circuit block and added to the fundamental circuit of a transformer. The effects taken into account by the model are:

- winding-to-winding and winding-to-enclosure capacitances using series RLC network,
- skin effect of winding conductors and iron core using first order foster circuit (valid below the first resonance),
- multiple resonance due to combination of winding inductance and turn-to-turn capacitance.

The model does not consider the saturation and hysteresis effects in the core.

A different approach for the inclusion of frequency dependent effect for harmonic studies based on rated parameters is proposed in [49]. Here the transformer admittance matrix has been modified to include frequency dependent effects. The model is verified to be valid for frequencies up to 5kHz.

For even higher frequency (10kHZ-10MHz), transformers are modeled using different approaches. In general, transformer models valid at high frequencies are linear, neglect the core, and are less accurate for the representation of low frequency transients. In [50] a black-box model is created from impedance measurements and from the knowledge of core and winding geometrical arrangement. In [51] a linear wideband transformer model is obtained via frequency-domain measurements and rational approximation of the terminal admittance matrix Y. The transmission-line theory has been used in [52, 53] to model internal winding voltage distribution.

2.2 Inrush Current

The saturation of the magnetic core of a transformer is the main cause of an inrush current transient. The saturation of the core is due to an abrupt change in the system voltage which may be caused by switching transients, out-of-phase synchronization of a generator, external faults and faults restoration. The energization of a transformer yield to the most severe case of inrush current and the flux in the core can reach a maximum theoretical value of two to three times the rated flux peak [1]. Fig. 2.8 illustrates how flux-linkage and current relates.

There is no direct evidence that the energization of a transformer can cause an immediate failure due to high inrush currents. However, insulation failures in power transformers which are frequently energized under no load condition support the suspicion that inrush currents have a hazardous effect [54]. A more typical problem caused by the energization of transformers is due to harmonics interaction with other system components that develops into overvoltages and resonant phenomena. The study of the energization of a transformer installed in an industrial facility carried out in [55] highlights problems due to harmonics, overvoltages and resonances. In [56] the authors show how the harmonic distortions caused by the switching of lightly loaded or unloaded transformers may be amplified during a power system restoration process, creating high harmonic overvoltages. In [57] the energization of large size transformers in EHV substations with long transmission lines is discovered to cause significant temporary disturbances when harmonic resonances are reached. In particular, when there are transformers already connected to the bus, the disturbances caused by the energization of one more transformer have greater duration and intensity. In [58] it is discussed how transformer inrush current can excite resonance frequencies in inter-connected offshore power systems.

To overcome these and other possible unpredictable situations, the possibility to model transformer energization transients in detail and with good accuracy is of great

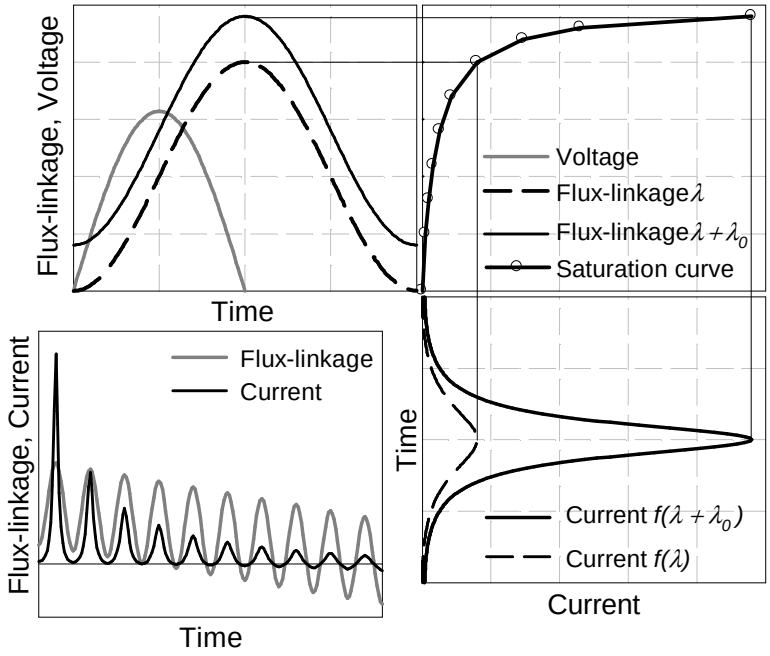

Figure 2.8: Qualitative representation of the inrush current phenomenon and the effect of the residual flux.

value. A selected list of references are presented in the next sections to highlight the main issues related to the modeling of inrush current transients. The investigation is limited to the inrush current generated upon the energization of a no-load transformer. The main topics discussed in this section concern simulation, analytical calculation, and mitigation of energization transients. The residual flux influence on inrush current and its estimation is also briefly discussed.

2.2.1 Simulation of inrush current transients

The inrush current transient occurring at the energization of a transformer is a highly nonlinear phenomena. The simulation of this behavior is rather complex and a transformer has to be modeled in great detail to represent the nonlinear behavior of the magnetization, losses, and saturation effects in the core [59].

The main difficulties in the simulation of transformer nonlinearities in EMTP-like programs related to the solution method are discussed in [60]. The classical compensation method is found inadequate when multiple dependent nonlinearities have to be modeled. The Thevenin equivalent cannot always be determined due to possible floating network formation. A transformer model for inrush current simulation based on separate magnetic and electric equivalent circuits is proposed in the paper. Nonlinearities are linearized and included in the system matrices. The Newton-Raphson

iterative methods is used for solving the circuit and it is shown to give improved efficiency and accuracy compared to the predictor-corrector method. The predictor-corrector method is found to be not suitable for transformer inrush current modeling and simulation. In [61, 62] a piecewise linear inductance and resistance is implemented as switched elements. The model is solved with the backward differential formulas (BDF) numerical method that eliminates numerical oscillation problems common of the traditional trapezoidal rule.

An alternative approach to the time-domain solution is presented in [63]. A model based on analytical equations is solved in the frequency domain using operational matrices and assuming periodic train of impulses. The problem is not discretized in time-steps but needs to be solved iteratively. The nonlinearities are linearized around the operating point. This approach gives results comparable to EMTP, however it is difficult to integrate such solution method into standard transient program based on time-domain solution methods.

The three standard ATP/EMTP models BCTRAN, TRELEG and STC (saturable transformer component) are compared in [64] for the calculation of inrush current transients. It is concluded that the type of model is not important as they all give a similar result. The correct estimation of parameters is critical, especially the estimation of the inductance of the saturated transformer core (air-core inductance), the parameter for the modeling of nonlinear behavior (magnetization curve), and the estimation of residual fluxes (model initialization). Substantial differences in the current waveforms are observed between simulations and measurements. This may be explained by the lack of a topologically correct core representation. The use of an admittance matrix based model (BCTRAN) with hysteretic inductor (type-96) externally connected to the low-voltage terminals is used in [65] for the study of an inrush current mitigation strategy.

Reference [66] presents a model based on a mixed electrical and magnetic system equations solved together. The authors of this paper recognize the importance of modeling the leakage channel between inner winding and core for highly saturated condition. Neglecting this may cause errors from 50% for small transformers, to 150-250% for large transformers in the estimation of the inrush current first peak.

A model based on a magnetic network is effectively employed in [67–69] for inrush current mitigation studies. A Jiles-Atherton based model is used to represent the ferromagnetic hysteresis behavior and to calculate residual fluxes in the model.

The effect of mechanical forces acting on the windings upon the energization of a transformer is a recurring question in the literature. The comparison of the maximum values of short circuit and inrush currents for single phase transformers is performed in [70]. Analytical equations are derived based on the physical dimensions of a transformer. It is concluded that for a typical transformer construction, a short circuit current is in the range of 2 to 6 times the magnitude of the worst case inrush current.

The estimation of inrush current first peak based on reluctance model, 2D and 3D

field calculation is compared in [71]. The motivation of the study is the calculation of the axial forces in hydraulic plants due to frequent switch on-off. The 3D model is chosen as a reference as it is assumed to be the most accurate. The results obtained with the permeance network model are far more accurate than the one obtained with 2D field calculations. This proves that lumped parameter models are accurate enough for the study of inrush current transients.

Mechanical forces within transformer coils under inrush transients are compared to those occurring at short circuit in [54] using models based on 2D and 3D field calculations. The result shows that inrush peak of 70% the rated short circuit current cause local forces of magnitude as those at short circuit. Short-circuit currents and worst-case inrush currents are in the same order of magnitude (with inrush occurring more frequently as it is considered a normal service operation). Inrush currents are normally smaller but with longer exposure time (tens of seconds) than short circuit currents (a fault is cleared within tens of milliseconds). For the transformer considered in the paper, the ratio i_{pk-IR}/i_{pk-SC} is 0.4, and normal ratio is given in the range 0.15-0.6.

3D and 2D FEM simulations are used in [72] to calculate radial and axial forces during inrush. It results that 2D models are not adequate. Using a 3D model, it is proved that when assuming the same current amplitude for short-circuit and inrush currents, the axial forces due to inrush currents are larger than those due to short circuit currents. Radial forces due to an inrush current on the LV winding are 40% lower than those due to a short circuit current. On the HV winding the forces during inrush are three times those during short circuit. It is also pointed out that the differences between inrush currents and short circuit currents are due to the unbalanced excitation and unbalanced ampere-turn resulting in the development of axial forces. In addition, inrush currents have a longer duration than short-circuit currents.

A transformer is design to withstand short-circuit currents. The forces generated during an inrush current transient with a typical transformer design are normally lower and differently allocated than those during a short-circuit. It can be concluded that the damage of a transformer due to a single inrush-current transient is therefore remote. However, a degradation of the insulation capability can be expected from severe and repeated inrush-current transients.

The study of inrush current as a statistical phenomena is proposed in [73] using a Monte-Carlo technique. The inrush current magnitude is calculated as a function of the random variables switching angle and remanent flux. The study is based on a single phase transformer and a simple model. The study concludes that the probability of inrush current higher than 2.6 p.u. is negligible when combining the statistical effect of residual flux and switching angle.

Sympathetic interaction between transformers, both for series and parallel connection is presented in [74]. The analysis is based upon the model of [66]. The phenomenon is triggered by the voltage drop across the system impedance produced by the inrush current. It is suggested that this interaction will become more significant with the use

of transformers with amorphous core or superconducting winding. The interaction is greatly reduced if the series impedance is small or if the electrical distance between transformers is large.

Ultra-saturation and excessive ultra-saturation phenomena in transformers appear when the flux has no zero crossing as explained in [75]. They are likely to occur during the energization of a loaded transformer. The second harmonic is very low in these circumstances and the inrush current may cause relay misoperation (normal relay setting is $I_{2nd} > 15\% I_{1st}$).

2.2.2 Analytical calculation of inrush current

Standard analytical formulas for the calculation of inrush peak and rate of decay are derived from single-phase transformer theory. The inrush current on a three-phase transformer can be calculated analytically based on the analytical formulas for a single-phase transformer and an empirical scaling factor. This factor accounts for the number of phases, core construction and coupling of the transformer [1, 5, 76].

Bertagnolli [77] proposes a relatively simple equation based on a sustained exponential decay of the inrush current:

$$\hat{i}(n) = \frac{\sqrt{2}U}{\sqrt{R_W^2 + \omega^2 \cdot L_{air-core}^2}} \left(\frac{2 \cdot B_N + B_R - B_S}{B_N} \right) \cdot e^{-\frac{t_n}{\tau}} \tag{2.10}$$

$$\tau = \frac{2 \cdot L_{air-core}}{R_W} \tag{2.11}$$

This equation is useful for rapid hand calculations due to its simplicity.

The analytical formula proposed by Specht [78] is somewhat more accurate as the decay of the dc component of the flux (B_R) is considered only during saturation ($B > B_S$):

$$i(n) = \frac{\sqrt{2}U}{\omega L_{air-core}} (1 - \frac{B_S - B_N - \tilde{B_R}(n)}{B_N}) \tag{2.12}$$

$$\tilde{B_R}(n) = \tilde{B_R}(n-1) - B_N \cdot \frac{R_W}{\omega L_{air-core}} \cdot 2(\sin\theta - \theta\cos\theta) \tag{2.13}$$

Holcomb [79] proposes an improved analytical equation:

$$i(t) = \frac{\sqrt{2}U}{\sqrt{R_W^2 + \omega^2 L_{air-core}^2}} \cdot \left(\sin(\omega t - \phi) - e^{-\frac{R_W}{L_{air-core}}(t - t_s)} \sin(\omega t_s - \phi) \right) \tag{2.14}$$

$$\phi = \tan^{-1} \frac{\omega \cdot L_{air-core}}{R_W} \tag{2.15}$$

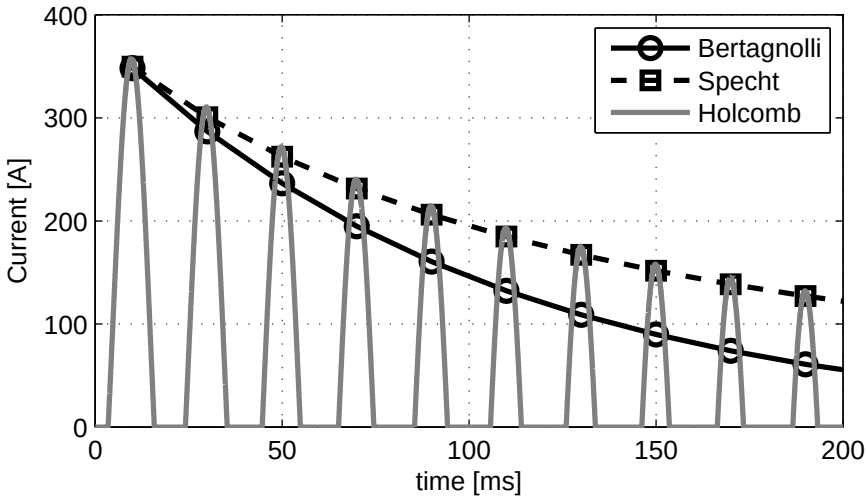

Figure 2.9: Analytical estimation of inrush current.

where t_s is the time when the core begins to saturate ($B(t) > B_s$). It is assumed that the inrush current is different from zero only between t_s and t_0, where t_0 is the time when the inrush current reaches zero at each cycle.

Equation (2.10) and (2.12) calculate only the envelope of the inrush current peaks, not the actual waveform. Equation (2.14) can be used to calculate analytically an approximate waveform of the inrush current. These three approaches are compared in Fig. 2.9 using a common set of parameters.

The air-core inductance $L_{air-core}$ of the a winding can be calculated as:

$$L_{air-core} = \mu_0 \cdot N_{HV}^2 \cdot \frac{A_{HV}}{h_{eq\_HV}} \tag{2.16}$$

with h_{eq_HV} being the equivalent height of the winding including fringing effects. The equivalent height is obtained by dividing the winding height by the Rogowski factor K_R (< 1.0) [5]. This factor is usually determined empirically and is a function of the height, mean diameter, and radial width of a winding.

These type of formulas are commonly used by manufacturers for the estimation of the inrush-current first peak and rate of decay. In-house developed experience factors are used to fine tune these analytical formulas for the design and materials of each specific transformer. In particular, those factors are used to tune the calculation of the angle of saturation, the maximum current, and the rate of decay. In addition, the choice of the empirical formula for the calculation of the transformer reactance $\omega L_{air-core}$ affects the final result. It is reported in [78] that an accuracy of $\pm 40\%$ should be expected from analytical formulas for the calculation of inrush current.

Other more advanced analytical methods are proposed in literature. Analytical formulas are used in [70] to investigate the forces inside a winding during an inrush

current transient. The analytical calculation of inrush current in three-phase transformers is presented in [80]. The influence of the connection for transformer banks with independent magnetic circuit for each phase is investigated. The study of voltage sag and inrush current caused by the clearing of a fault with simultaneous closing of all three phases is presented in [81]. Analytical expressions are used to model electric and magnetic circuits.

An analytical formula for inrush current calculation is proposed in [82]. The approach is based on the solution of a nonlinear inductor modeled by a two segments piecewise linear saturation curve in series with a resistor. This is used to determine the impact of a damping resistor on the transformer inrush current. The result is in agreement with the "standard" analytical formulas for inrush current estimation. This approach is used to prove that the inrush current peak is not a function of the unsaturated magnetizing inductance.

Analytical calculation of peak and second harmonic of inrush current for present design transformer is presented in [83]. The paper analyses the influence of modern design methods on the inrush current, specifically the influence of core design flux density, core material, core joint geometry, power rating, winding connection, and number of phases. The main findings are:

- The 2nd harmonic in today's power transformers differ substantially from that in older design, therefore a careful selection of the proper relay protection is important.
- Core design flux density: peak inrush current increases and I_{2nd}/I_{1st} decreases as the induction level increases ($I_{2nd}/I_{1st} < 5\%$).
- Power rating: lower MVA gives higher ratio peak inrush versus rated load current. Reduced insulation and smaller cooling duct give lower leakage inductance, thus result in higher current in p.u. For distribution size transformer the peak inrush current can reach levels greater than the short-circuit current. The MVA size has negligible effect on the 2nd harmonic.
- Core material: highly grain oriented and domain-refined (HD) material is compared with regular grain oriented (R) electrical steel type. HD materials have higher value of saturation flux density, a larger linear portion of the magnetization curve, and a lower remanence flux density. For the same flux density HD has lower inrush and higher 2nd harmonic. However, since better material allows better utilization, a higher core design induction is used in order to compensate for the extra cost. It results that HD and R have the same inrush current for $B_{HD} \approx 110\% B_R$.
- Core joint geometry: core joint gives high reluctance that reduces the residual flux in the transformer compared to the remanence flux of the material. Modern step-lap type joints have lower reluctance than mitered joints, thus exhibit higher inrush and lower second harmonic.

- Winding connection & number of phases: scaling factors have to be used depending on the winding connection. Winding connection has no effect on the 2nd harmonic.

2.2.3 Inrush current mitigation techniques

Several technologies exist to mitigate energization transients in transformers. The most common are pre-insertion resistors and point-on-wave (POW) controlled closing. Pre-insertion resistors require relatively large resistors to be installed in parallel to the main circuit breaker and an effective reduction of inrush current is achieved only by an optimal choice of the resistance value and the pre-insertion time. Transformer controlled switching is considered an economical and reliable alternative to pre-insertion resistors.

The first commercial controlled breakers were adopted in the 1990's, with few installation existent in 1995. A larger adoption occurred at the end of 1990's thanks to the introduction of effective compensation algorithms for the variation of the operation timing. Controlled switching technology is mainly used for insertion of capacitor ($\approx$66%). Fewer installations are reported for the energization of transformer and reactors, and an insignificant quantity for line switching [84]. Controlled switching is used to energize transformers to mitigate the inrush currents and avoid power quality degradation, false relay tripping, and reduction of internal mechanical stresses. The most common controlled switching strategy implies to energize a first phase at its voltage peak and delay the energization of the remaining two phases by a quarter of a period of the fundamental frequency (5 ms in a 50 Hz system). No commercial system taking into account residual fluxes is reported available before 2002. Controlled de-energization is proposed as a mean to control residual fluxes.

The main factors affecting the magnetizing inrush current are identified in [85] and are:

- POW voltage at the instant of energization,
- magnitude and polarity of remanent flux,
- total resistance of the primary winding,
- power source inductance,
- air-core inductance between the energizing winding and the core,
- geometry of the transformer core,
- the maximum flux-carrying capability of the core material.

Based on these considerations, a method for controlling the POW closing instant and defining a value of residual flux using a dc coil is proposed.

The influence of the tap changer on an inrush current is investigated in [86]. Higher number of excited turns gives lower flux density in the core. Changing from the 0.9 p.u. to the 1.1 p.u. tap position results in almost a 50% reduction in the inrush current first peak. The authors of this paper suggest therefore to energize the transformer positioning the tap changer to give the highest number of turns to be excited.

The state of the art of controlled switching with and without the consideration of residual fluxes is given in [87]. This publication also discusses the practical calculation of the residual fluxes from integration of voltage waveforms and the possible influence of network disturbances.

Three different synchronized switching strategies (rapid closing, delayed closing and simultaneous closing) are extensively examined and discussed in [88, 89]. The work has been followed up in [90] and experimental results are presented. Synchronized switching with delayed closing and rapid closing outperform the proposed simultaneous closing strategy.

The application of controlled switching with measurement of residual fluxes is reported in several publications in the last 10 years [68, 69, 91, 92]. Closing time scatter and residual flux measurement uncertainties reduce the field performance of controlled switching as reported in [93].

Alternative methods for inrush current mitigation are continuously been proposed. Prikler *et. al.* [65] present a synchronized switching method for three-pole spring-driven circuit breaker with fixed delay between poles (mechanically staggered). Optimum energization is obtained by controlling the residual flux with controlled de-energization. An inrush mitigation strategy based on a pre-insertion neutral resistor is presented in [94]. This technique is however restricted to star grounded transformers.

2.2.4 Ringdown transient and residual fluxes

One of the main difficulties encountered in transformer modeling is the accurate estimation of the residual flux left in the core after the de-energization.

In a large Cigré survey (carried out in 1984 on more than 500 transformers) [95] the maximum residual flux is given only for two transformers (0.75 and 0.9 p.u). Reference [80] dated 1986 suggests different residual flux ranges varying between 0.4 and 0.8 p.u. It also discusses the importance of residual flux and the practical difficulties concerning its estimation or measurement. The residual flux for a 545-MVA transformer is measured to be slightly higher than 0.4 p.u. (worst case out of 10 random de-energization) in [92]. One single measurement of the de-energization of a 170-MVA transformer is reported in [96] and has a residual flux of 0.31 p.u. Recent measurements on a 400-kVA transformer report a 0.6 p.u. maximum residual flux [93].

In general, there is a lack of information published in literature on actual residual flux measurements performed for different transformer sizes and designs. This makes it difficult to estimate a correct range of values for residual flux initialization.

The ringdown transient occurring after the de-energization of a transformer is explained in [97]. The discharge of a capacitor trough a VT creates a nonlinear ringdown. It is observed that the size of the capacitance strongly influences the development of the flux-linked in the VT. This behavior is similar to the case when stray and shunt capacitances in a transformers are being discharged. As observed in [84], the residual flux is influenced by the stray capacitances of the transformer and any other shunt capacitance. A decrease of the residual flux is expected in presence of larger capacitances. It is therefore important to include capacitances in a simulation if the transformer model has the capability to calculate residual fluxes.

2.3 Iron Core Modeling

The low-frequency modeling of a transformer is complicated by the nonlinear magnetic core characteristics. Saturation, hysteresis and eddy current losses are the main nonlinear effects to be considered in the modeling of an iron-core inductor as illustrated in Fig. 2.10.

The inductance in Fig. 2.10 represents the anhysteretic magnetization curve used to characterized the nonlinearity of the magnetic material. The rigorous definition of anhysteretic curve is given in [98] as the thermodynamic equilibrium state of a ferromagnetic material. The nonlinear characteristic is extracted from $V_{rms} - I_{rms}$ curves and no-load losses at rated frequency [99–102]. This curve can be described as a piecewise linear function [27] or approximated by a fitting function [101, 103, 104] and is considered a reasonable approximation of the anhysteretic curve. Specific test procedures have been proposed in literature [105–107] for a direct limb-by-limb calculation of the saturation and loss curves of a multi-phase transformer. These are based on single-phase or dc excitation of the transformer, however they are impractical outside a controlled laboratory environment.

The use of resistances to model iron losses is based on a semi-empirical description of the loss components. Hysteresis and eddy current losses are often considered separately [108]. In the most simple case, hysteresis losses can be neglected as they represent a small contribution to the total losses and eddy current losses are assumed proportional to $(B_m \cdot f)^2$. This allows a convenient representation using an ordinary linear resistance [103]. In [109] instantaneous core losses are investigated and it is observed that the hysteresis curve tends to widen out more at the knee than at zero flux level, thus a linear or voltage-dependent resistance can represent the average loss per period, but fails to accurately reproduce the exact waveforms and hysteresis loops.

The conventional model of a nonlinear inductance in parallel with a constant re-

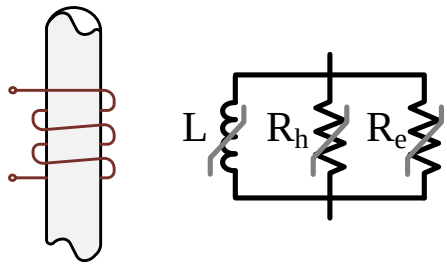

Figure 2.10: Modeling of a nonlinear iron-core inductor.

sistance is reported to be accurate accurate within 5% up to about 3kHz [110]. In order to retain the accuracy at higher frequency, Foster circuits or discretized models have to be used. The inclusion of nonlinearities in higher order models is discussed in [110, 111]. Neves and Dommel [111] observe that for inrush current and ferroresonance no major improvement is observed in representing the frequency dependent effect of the core.

To achieve a more accurate representation, the total transformer core losses can be divided in three components: hysteresis, classic eddy current, and excess eddy current.

$$P_0 = P_{hyst} + P_{cls} + P_{exc} \tag{2.17}$$

Bertotti [112] characterizes the three loss components based on the properties of a magnetic material:

$$P_0(t) = P_{hyst}(t) + \frac{\sigma d^2}{12}\left(\frac{dM}{dt}\right)^2 + \sqrt{\sigma G S V_0}\left|\frac{dM}{dt}\right|^{3/2} \tag{2.18}$$

$$P_0 = W(M_{max})f + \frac{\pi^2}{6}\sigma d^2 (M_{max} f)^2 + 8\sqrt{\sigma G S V_0}(M_{max} f)^{3/2} \tag{2.19}$$

$$H_{cls}(t) = \frac{\sigma d^2}{12}\frac{dB}{dt} \tag{2.20}$$

$$H_{exc}(t) = \frac{n_0 V_0}{2}\left(\sqrt{1 + \frac{4\sigma G S}{n_0^2 V_0}\frac{dM}{dt}} - 1\right) \tag{2.21}$$

with M the average magnetization in the laminations, d the lamination thickness, S the lamination cross-sectional area, σ the conductivity of the magnetic material, G a geometrical factor, n_0 and V_0 phenomenological parameters.

With the assumption that the flux is uniformly distributed over the cross-sectional area of a limb, the following statements between magnetic flux and electrical voltage are adopted:

$$\frac{dM}{dt} = \frac{1}{2Ld}\left\langle\frac{d\phi}{dt}\right\rangle \propto \frac{d\phi}{dt} \tag{2.22}$$

$$B(t) \propto \phi(t) \propto \int v(t)dt \tag{2.23}$$

with $2L$ the domain wall spacing. Equations (2.18)-(2.21) can then be translated in the following proportionality relations:

$$P_{cls} \propto B_{max}^2 f^2 \tag{2.24}$$

$$P_{exc} \propto B_{max}^{1.5} f^{1.5} \tag{2.25}$$

$$H_{cls}(t) \propto \frac{dB}{dt} \propto v(t) \tag{2.26}$$

$$H_{exc}(t) \propto \sqrt{\frac{dB}{dt}} \propto \sqrt{v(t)} \tag{2.27}$$

For a sinusoidal flux, (2.24) and (2.25) are proportional to the rms voltage:

$$\lambda = \frac{\sqrt{2}V}{2\pi f} \tag{2.28}$$

$$B_{max}^n f^n \propto V^n \tag{2.29}$$

According to (2.26) and (2.27), equation (2.18) is simplified in term of average electrical quantities to:

$$i_{0\,tot}(t) = i_{hyst}(t) + k_1 \cdot v(t) + k_2 \cdot \sqrt{v(t)} \tag{2.30}$$

$$P_0(t) = P_{hyst}(t) + k_1 \cdot v(t)^2 + k_2 \cdot v(t)^{3/2} \tag{2.31}$$

where $i_{hyst}(t)$ and $P_{hyst}(t)$ can then be evaluated from simple hysteresis models [48, 107] or by a magnetization model as Stone-Wolhfart, Jiles-Atherton, Globus, or Preisach models [113].

The loss components of the total losses for different grain oriented electrical steel is shown in Fig. 2.11. The data for the 60 Hz losses are obtained from [114] and the values at 50 Hz are scaled assuming: $P_{hyst} \propto f$, $P_{cls} \propto f^2$, and $P_{exc} \propto f^{1.5}$. This figure highlights the importance of a correct splitting of the losses and the need to model all the three loss components. At 1.7 T, approximately a standard rated excitation, each loss component is between 30% and 40% of the total core losses.

2.3.1 Dynamic hysteresis models

The representation of hysteresis is important because [115]:

- together with the deenergization condition determines the residual flux values that can affect a subsequent inrush current transient,
- can exert a significant damping effect on long term dynamic transients and is crucial if resonance phenomena are present.

De Leon and Semlyen [116] give a very complete review of hysteresis models and divide the approaches for modeling hysteresis in ferromagnetic material in three main

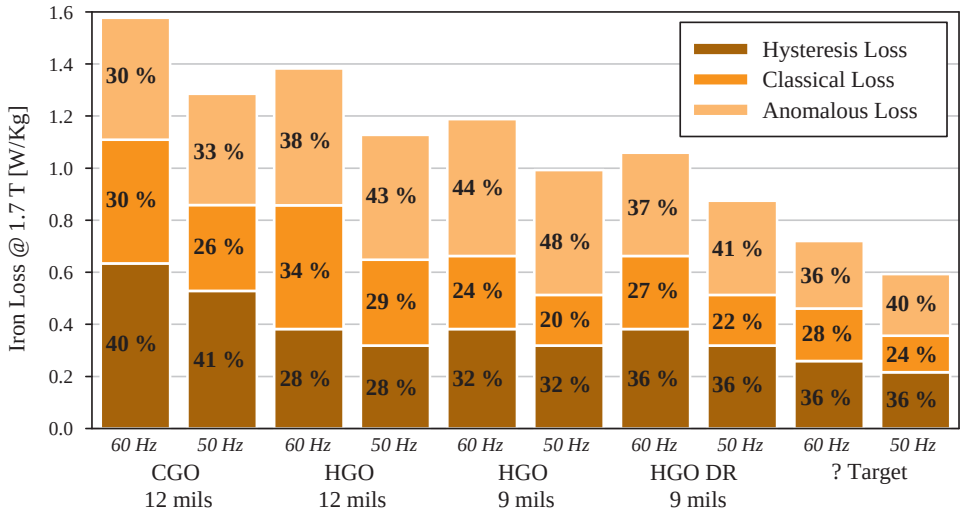

Figure 2.11: Loss components contributing to total iron loss in grain oriented material electrical steel. Adapted from [114].

categories according to the target audience. The models used by physicists are based on a detailed physical description of a material properties and consider all known energy on a very small scale. Mathematical models that relay on a macroscopic description of the underlying physics of the material are useful when designing an electromagnetic machine. These models have the main focus on the prediction of electromagnetic fields as they relate micro-structural parameters to the macroscopic responses of the material to outside fields [113]. Simple models that ignore the underlying physics and represent the hysteresis loops using a path tracing approach [117,118] are preferred in power system engineering. These simplified models are based on the scaling and expansion of a defined primary hysteresis loop.

Physical models are not investigated here as they result too cumbersome for being implemented in a transformer model and their high detail level is not required. The models based on a mathematical representation or on a path tracing approach are both suitable for time-domain modeling depending on the scope of a study.

Relevant models based on a path tracing approach are proposed in [24, 115, 117]. These models allow an approximated representation of residual flux and require a fairly limited input data. However, these have been criticized mainly due to their simplistic representation of sub-loop operations.

In order to achieve a better representation of sub-loop operations and remanent flux, a mathematical model should be preferred to path tracing approaches, [104]. Several macroscopic models are proposed in literature with four of the most common compared in [113]: Stoner-Wolhfarth, Jiles-Atherton, Globus, and Preisach models. Among these, the Jiles-Atherton and Preisach models are the only able to reproduce minor loops and demagnetization. A comparison of these two models is performed

in [119] with the following conclusions:

- The Preisach model fits better the minor loops than the Jiles-Atherton model.
- The Preisach model requires extensive measurements but hardly no fitting to identify the model parameters, the contrary is true for the Jiles-Atherton model.
- The correspondence with the measurements is generally better for Preisach model than for the Jiles-Atherton model, especially if several levels of excitation of higher order loops are considered.
- In their generalized form, the Jiles-Atherton model is ten times computationally more efficient than the Preisach model.

The Jiles-Atherton model is described in [120–122] and with inclusion of eddy current losses in [123–125]. The parameters can be estimated from specific measurements on a magnetic material as detailed in [126, 127]. The use of variable parameters as proposed in [128, 129] seems to enhance the accuracy of simulations when the maximum magnetic field is not constant. The capability of this model to represent residual magnetization is confirmed in [130]. The implementation of the Jiles-Athorton model in transformer for transient simulation is reported in [131] for a current transformer, and in [124, 125, 132] for a single-phase power transformer.

The classical Preisach model is described in [133] and the generalized version with inclusion of eddy current losses in [134, 135]. The model has been applied to the modeling of a single-phase transformer in [136], and of a three-phase transformer in [137].

2.4 Challenges in Power Transformer Modeling for Inrush Current Calculation

The main challenges in the calculation of inrush current with a transformer model are related to:

- Correct representation of the behavior in complete saturation.
- Modeling of nonlinear and hysteretic iron-core.
- Representation of frequency dependent core and winding losses.
- Determination of the initialization condition, in particular residual fluxes.
- Description of the concurrent magnetic and electric coupling in a multi-phase transformer.
- Estimation of the model parameters.
- Collection of data measurements for the verification of a model.

CHAPTER 3

INRUSH CURRENT MEASUREMENTS

3.1 Laboratory setup

3.1.1 Test objects, configuration and measuring equipment

The controlled environment of the laboratory gives the possibility to perform extensive measurements, otherwise not possible on a power transformer installed in a high-voltage network. The purpose of the testing is to perform systematic measurement where the breakers operation is accurately controlled.

Two distribution transformers have been used for laboratory investigations. They are unloaded, connected to a low-impedance 11-kV medium voltage grid, and energized by two sets of controlled circuit breakers. A schema of the laboratory setup with the voltage and current measurement points is shown in Fig. 3.1. The components in the dashed box of Fig. 3.1 are a fixed laboratory installation and cannot be modified.

The test objects are three-phase oil-filled distribution transformers with a three-legged core. The transformers are rated 300 kVA and 800 kVA and share the same voltage levels at 11.430/0.235 kV Yyn. They were manufactured by Møre Trafo AS between 1975 and 1976 and are pictured in Fig. 3.2. The main core and windings dimensions of the two transformers are given in Tabs. 3.1, 3.2. In addition, a detail

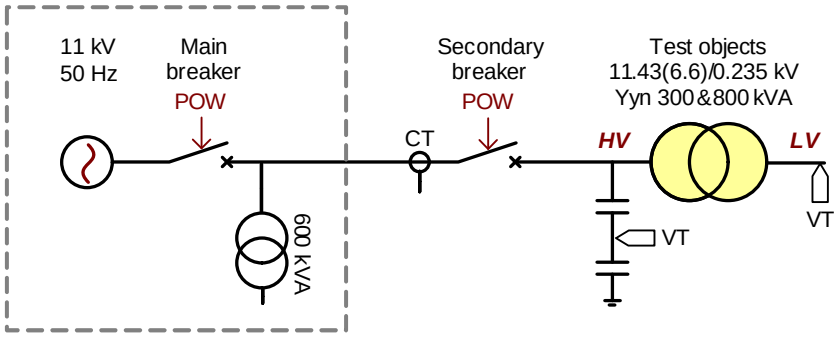

Figure 3.1: Laboratory layout.

of the connection of the high voltage dividers and the secondary vacuum breaker is shown in Fig. 3.3.

Two vacuum breakers are used in the setup. The main breaker installed in the laboratory is an old 6.6 kV ABB-Sace vacuum breaker. It has been tested to give a stable closing operation time with repeatability of approximately 1 ms. The secondary vacuum breaker is composed by three separate poles that are operated independently by electromagnetic relays. Its operation time has been verified to be stable such that each pole of the breaker can operate with accuracy and repeatability of approximately 1 ms. This vacuum breaker is delivered by *Ross Engineering Corp.*[1] (Type HB51). The main breaker is used for the energization and the secondary breaker set is used for the de-energization. The reason for this dual breaker setup is a fixed transformer installed on the source side that otherwise would interact with the test-object during ringdown. The secondary breaker decouples the ringdown of the two transformers, however it cannot be used for energization due to contact bouncing. The fixed source-side transformer does not influence the inrush current as the source voltage has a low impedance (200 MVA short circuit power).

A National Instrument PXI transient recorder[2] (acquisition modules: *PXI-6133* ad *PXI-6122*) has been used to record voltages and currents at the high voltage terminals as well as the induced voltages on the low voltage terminals. A total of twelve analogue input channels with simulataneous sampling are available, eight 14-bit and four 16-bit channels. The input voltage can be selected among ± 1.25 V, ± 2.50 V, ± 5.0 V, and ± 10.0 V. Signals are recorded at a sampling frequency of 100 kS/s. The digital output channels have been used to operate and synchronize the breakers with a common triggering reference.

The PXI transient recorder is specifically programmed in LabWindows/CVI to synchronize the operation of the circuit breakers and the recording of the voltage and current waveforms. The graphical user interface is shown in Fig. 3.4. A structured text file containing the configuration and the timings for multiple recordings can be

[1] http://www.rossengineeringcorp.com/
[2] http://www.ni.com/pxi/

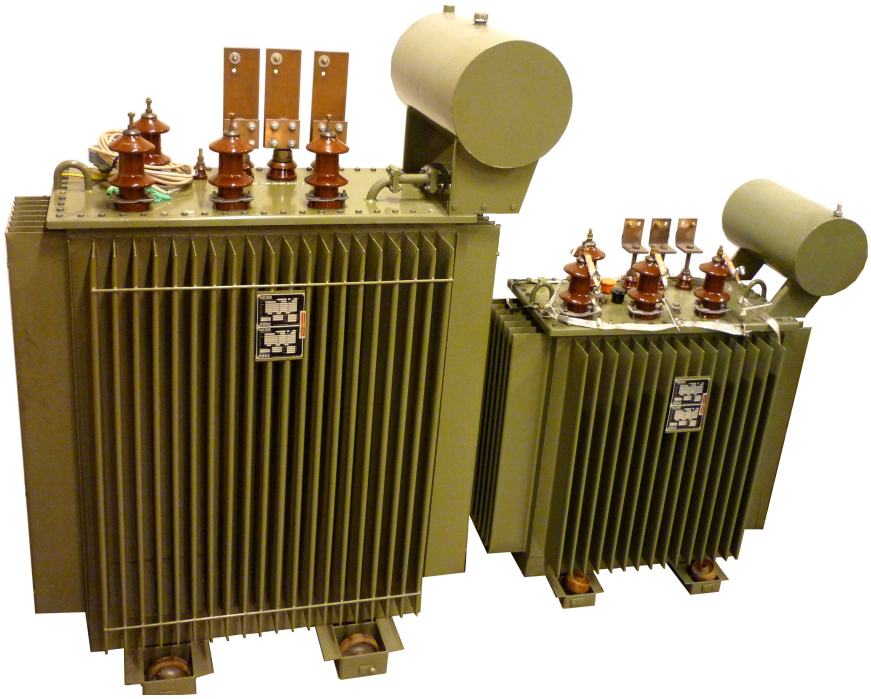

Figure 3.2: Test objects: 800 kVA transformer on the left, 300 kVA transformer on the right.

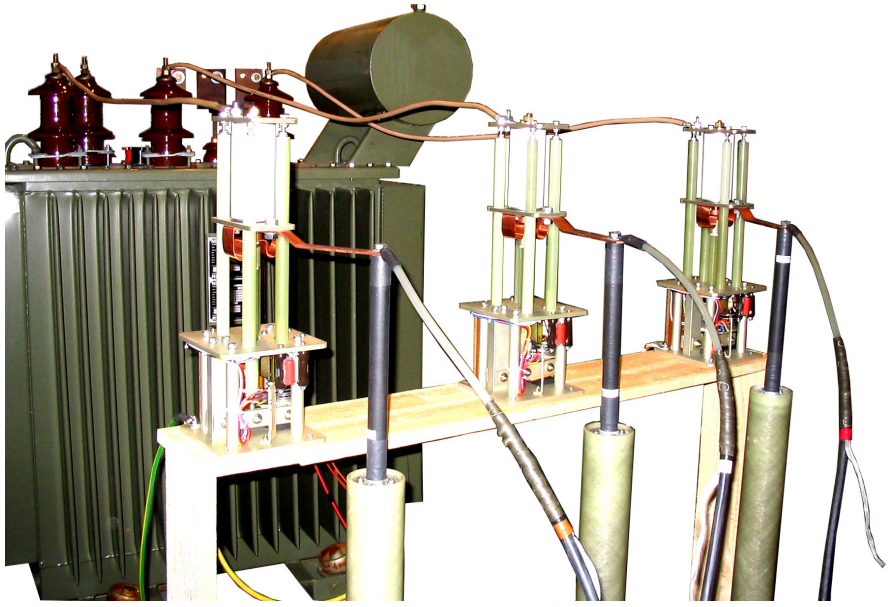

Figure 3.3: Connection of the high voltage deviders and vacuum breakers. The voltage deviders are connected directly to the transformer terminals in the final set-up.

TABLE 3.1
CORE AND WINDINGS DESIGN DATA, 300 KVA TRANSFORMER.

CORE	**Legs**	**Yokes**
Net cross-sectional area	0.0175 m^2	0.0198 m^2
Max lamination width	0.150 m	0.170 m
Window height	0.500 m	
Legs dist. center-to-center	0.290 m	

WINDINGS	**Low Voltage**	**High Voltage**
Number of turns	21	1074
Height	0.452 m	0.452 m
Inner diameter	0.162 m	0.222 m
Thickness	0.017 m	0.0225 m

TABLE 3.2
CORE AND WINDINGS DESIGN DATA, 800 KVA TRANSFORMER.

CORE	**Legs**	**Yokes**
Net cross-sectional area	0.0260 m^2	0.0295 m^2
Max lamination width	0.180 m	0.200 m
Window height	0.850 m	
Legs dist. center-to-center	0.370 m	

WINDINGS	**Low Voltage**	**High Voltage**
Number of turns	14	716
Height	0.790 m	0.706 m
Inner diameter	0.206 m	0.278 m
Thickness	0.021 m	0.0265 m

read by the software. An example of such file is given in Fig. 3.5. The acquired waveforms are then automatically saved in a compact binary format for a later conversion and processing in MATLAB. This setup allows to operate the recording system in a completely automatic mode and to perform systematic measurement with a minimum supervision of the operator required.

The currents on the high voltage side are measured with high precision current transducers (LEM IT-400) based on the *closed loop (compensated) fluxgate technology* with claimed accuracy of 0.0033%. Such high accuracy together with a large vertical resolution of the transient recorder (16-bit) allows to accurately measure steady state no-load currents (less then one ampere) as well as severe inrush currents with peak of several hundred amperes. A custom build wiring and a battery power supply were required to avoid the injection of noise when measuring very low currents.

The voltage at the high-voltage terminals is measured with capacitive voltage dividers with a high voltage capacitor of 200 pF with 200 Ω resistance in series. The low voltage capacitor is rated 400 nF resulting in a voltage scaling of 1/2000. The bandwidth of such dividers is measured to be around 1 MHz. The voltage on the low-voltage terminal is measured through a voltage probe with ratio of 1/200.

3.1.2 Data acquisition procedure

The breakers have a stable operation time and can be controlled with accuracy and repeatability of approximately ± 1 ms. Two trigger signals synchronous to the zero crossing of the line voltage V_{RS} on the high voltage side are used to control the time where de-energization and energization occur. The de-energization and energization transients are linked together as the ringdown transient determines the value of the residual fluxes in the transformer that is a fundamental initial condition for the following energization. The residual flux is calculated by the time integral of the induced voltage during the ringdown transient. Once it reaches a stable value, it is assumed constant until the next energization. In order to limit the uncertainties on the residual flux estimation, the de-energization and energization transients are performed in rapid sequence with a delay of approximately 1 s.

The measurement procedure consists of two separate recordings as the frequency of power systems is not fixed at 50 Hz but shows a slow dynamic. A double triggering and double acquisition procedure is therefore necessary to accurately synchronize the operation of the circuit breakers with the point-on-wave (POW) timings. As shown in Fig. 3.6, the opening time (Δt_{open}) is relative to the trigger signal t_{trg1} and is varied systematically between 0 ms and 20 ms. In the same way, the closing time (Δt_{close}) is relative to the trigger signal t_{trg2} and is also varied systematically between 0 ms and 20 ms. The systematic variation of the opening and closing times of the breakers with a time resolution of 1 ms allows to perform a total of 400 (20x20) measurements to map the whole range of inrush current and residual flux combinations in a period.

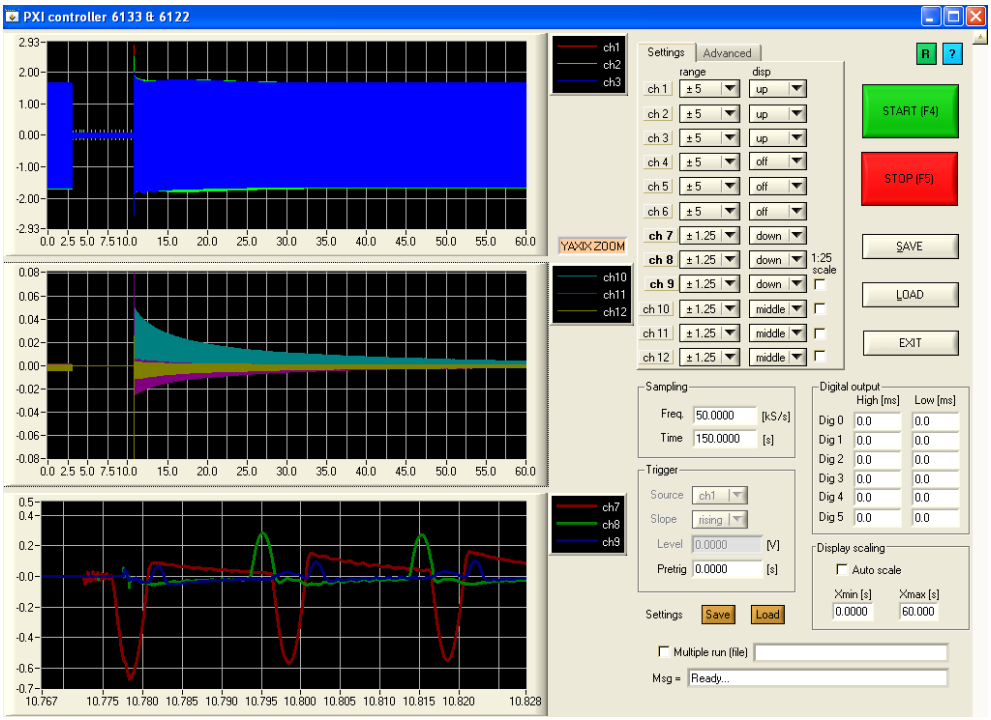

Figure 3.4: GUI for the transient recorder.

```
300_kVA_No-synch                # Test ID
300kVA_OUTscanIN14ms_
40                              # Number of runs
20 18 19 54 54 0                # Response time IN [ms] NB! 6 values required
13 14 12 0 0 0                  # Response time OUT
1.0 0                   # Acquisition and waiting time [s], run 1a
0 0 0 0 500 0           # IN times [ms] after trigger for each 6 channels, run 1a
400 400 400 0 900 0     # OUT times [ms] after trigger for each 6 channels, run 1a
20.0 5                  # Acquisition time [s], run 1b
100 100 100 414 0 0     # IN times [ms] after trigger for each 6 channels, run 1b
0 0 0 1000 0 0          # OUT times [ms] after trigger for each 6 channels, run 1b
1.0 0                   # TIME 2a
0 0 0 0 500 0           # IN   2a
401 401 401 0 900 0     # OUT  2a
20.0 5                  # TIME 2b
100 100 100 414 0 0     # IN   2b
0 0 0 1000 0 0          # OUT  2b
1.0 0                   # TIME 3a
0 0 0 0 500 0           # IN   3a
402 402 402 0 900 0     # OUT  3a
20.0 5                  # TIME 3b
100 100 100 414 0 0     # IN   3b
0 0 0 1000 0 0          # OUT  3b
```

Figure 3.5: Structured text file specifing the timings for automated multiple measurements.

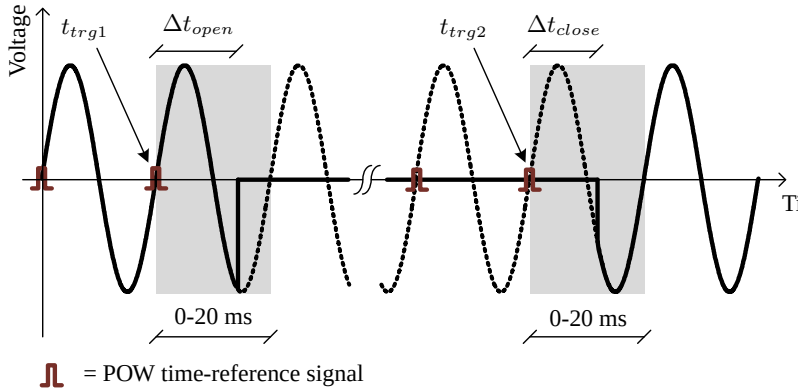

Figure 3.6: Trigger signals and systematic variation of the switching times.

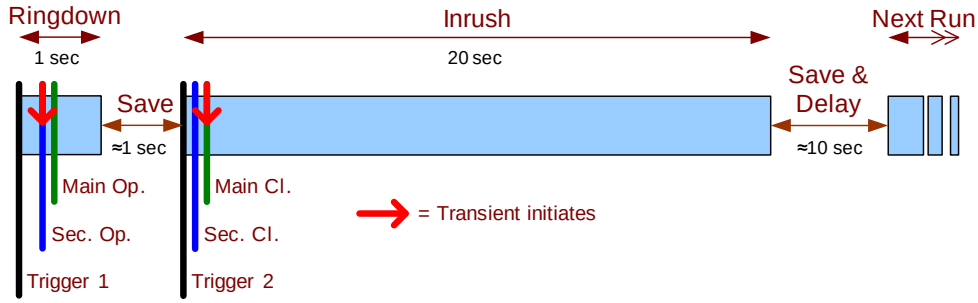

Figure 3.7: Double triggering procedure.

The automated sequence of operations for the acquisition of a de-energization/energization sequence is shown in Fig. 3.7 and can be outlined in six repeating stages:

- *Steady State:* The transformer is energized and in steady state (no-load).
- *Ringdown:* The vacuum breaker opens at $t_{trg1}+\Delta t_{open}$ and the de-energization transient initiates. The main breaker opens slightly after without any effect on the test object. The transient is recorded for the duration of 1 s.
- *Storing Data:* Recorded data are stored and a delay of 1 s is introduced between ringdown and inrush stages.
- *Inrush:* The vacuum breaker closes without delay. The main circuit breaker closes at $t_{trg2} + \Delta t_{close}$ and the energization transient initiates. The transient is recorded for the duration of 20 s.
- *Storing Data & Delay:* Recorded data are stored followed by a 10 s delay where the transformer reaches steady state.
- *Ready for Next Run:* The system is ready and in steady state. A new measurement sequence can start.

3.2 Systematic measurements on a 300 kVA and 800 kVA distribution transformers

The ringdown and inrush measurements performed on the 300 kVA and 800 kVA transformers are presented here. More than 400 de-energization/energization measurement sequences have been performed for each transformer. One single time domain measurement of the ringdown and inrush current transients for each transformer is shown here in Figs 3.8-3.11[3]. The measurements for both transformers refer to the same opening-closing sequence with $\Delta t_{open} = 0\ ms$ and $\Delta t_{close} = 10\ ms$. This timing sequence corresponds to one of the most severe inrush current transient registered during the measurements. The current first-peak is above 200 A and 560 A for the 300 kVA and 800 kVA transformers, respectively. The flux-linkage is calculated as the time integral of the phase voltage at the low voltage terminals. The stable value reached after a de-energization is used as the initial value for the following energization.

The residual flux reached after each de-energization is shown in Figs. 3.12 and 3.13 for the two transformers. For each disconnection time Δt_{open} a total of 20 residual flux points are shown and the continuous lines in the figures represent the average residual flux value. The maximum residual flux is estimated to be approximately 0.55 p.u. and 0.6 p.u. for the 300 kVA and 800 kVA transformers, respectively. The two transformers have approximately the same rated flux density[4]. They were built by the same company in the same years so they presumably share the same core material. The different maximum residual flux is therefore due to a different core construction and dimensions. It is also valuable to note that the residual flux as a function of the disconnection time can be approximated with a sine function and the residual flux curves as a function of Δt_{open} have a phase shift of $2\pi/3$ for the three phases. This is further discussed in [Pb8].

The inrush current first peaks of all the measurements are represented in Figs. 3.14-3.16 for the 300 kVA transformer and in Figs. 3.17-3.19 for the 800 kVA transformer. These representations are proposed in this work as they provide a remarkable overview of the inrush current first-peak variation as a function of the opening and closing times. A three-dimensional representation of the measurements is shown in Figs. 3.14 and 3.17. However, a 3D representation may be difficult to visualize on a flat surface. A filled 2D contour plot is proposed in Figs. 3.15 and 3.18 as a better visualization alternative. In these last figures the absolute value of the first-peak inrush current is represented. The dark blue areas represent low magnitude inrush currents and a characteristic pattern can be observed. In order to better

[3] For the rest of this chapter, when no legend is specified in the figures the following color code is valid: BLUE: phase R, GREEN: phase S, RED: phase T. For line voltages: BLUE: phase R-S, GREEN: phase S-T, RED: phase T-R.

[4] $B_{300} = \frac{\sqrt{2}V}{\sqrt{3}\omega N_{300} A_{300}} = 1.662\text{T}$, $B_{800} = \frac{\sqrt{2}V}{\sqrt{3}\omega N_{800} A_{800}} = 1.678\text{T}$, $\frac{B_{800}}{B_{300}} = 1.01$, $\frac{\lambda_{res800}}{\lambda_{res300}} = 1.09$

visualize this pattern, a grid of 40x40 ms is shown in Figs. 3.16 and 3.19. These figures are obtained assuming a 2π periodicity of the inrush current first peaks such that the measured first-peak inrush current pattern (inside the black frame) is extended by duplication. The implications of this characteristic pattern are further discussed in [Pb8].

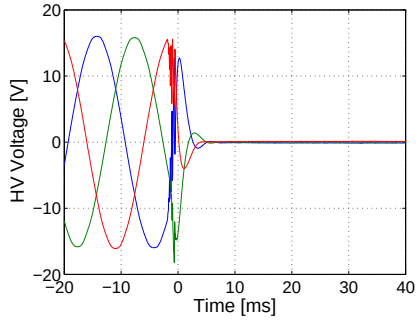

(a) *Line voltage at the HV terminals*

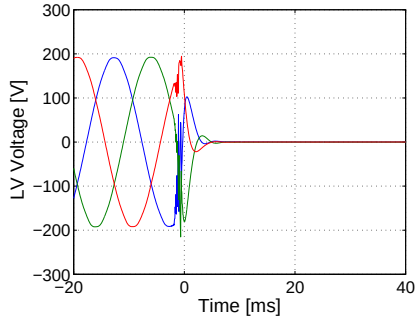

(b) *Phase voltage at the LV terminals*

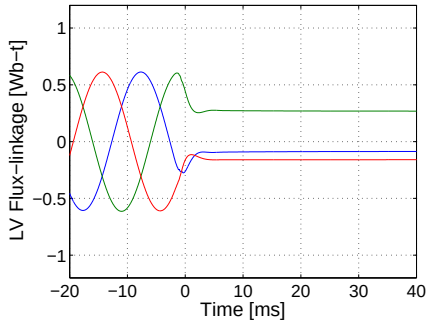

(c) *Flux-linkage at the LV terimanls*

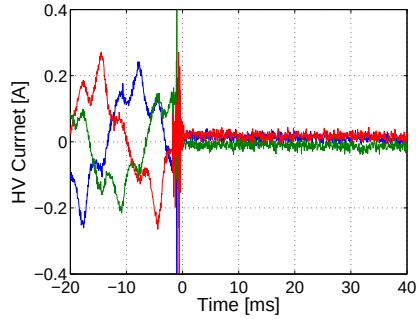

(d) *Line current at the HV terminals*

Figure 3.8: Ringdown transient, 300 kVA transformer.

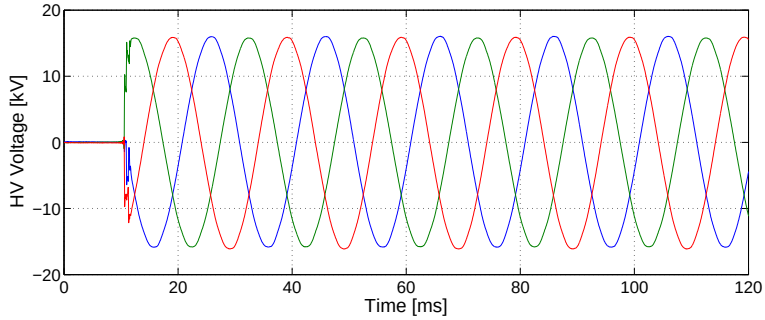

(a) *Line voltage at the HV terminals*

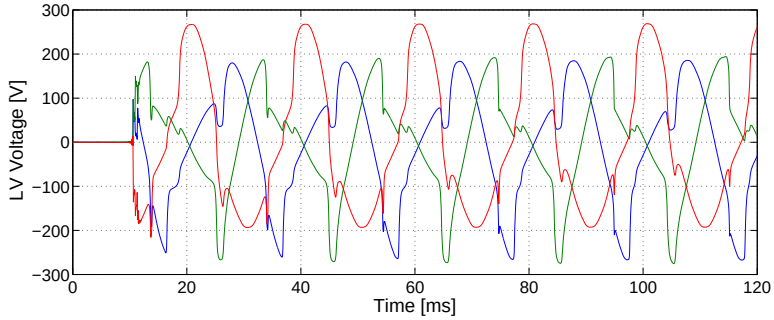

(b) *Phase voltage at the LV terminals*

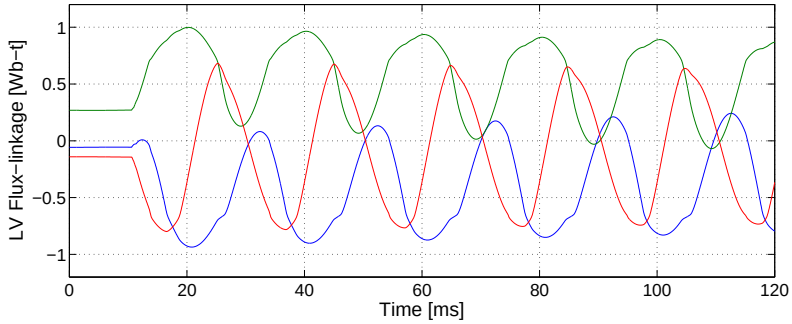

(c) *Flux-linkage at the LV terminals*

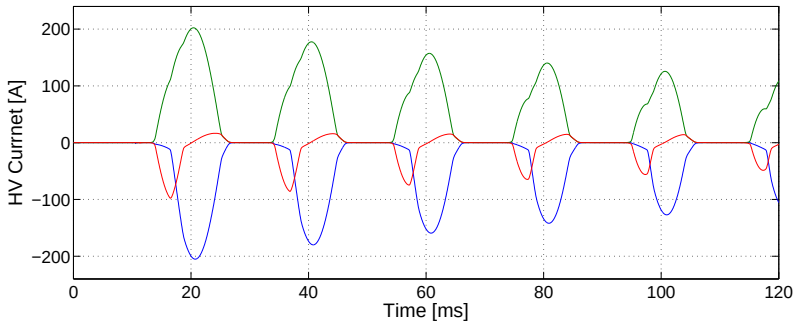

(d) *Line current at the HV terminals*

Figure 3.9: Inrush current transient, 300 kVA transformer.

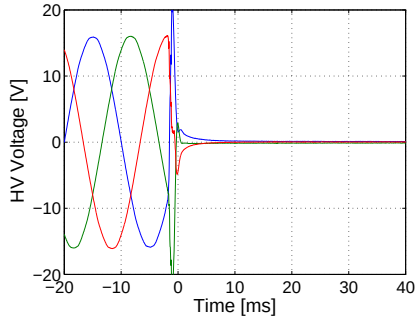

(a) *Line voltage at the HV terminals*

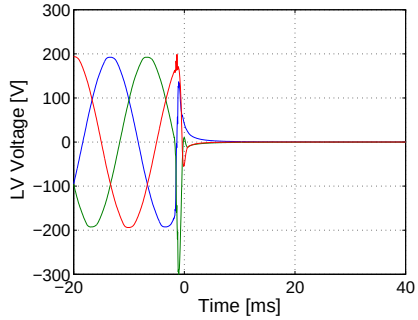

(b) *Phase voltage at the LV terminals*

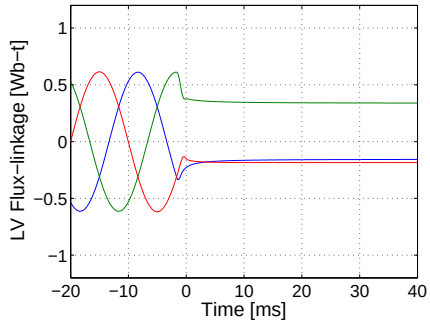

(c) *Flux-linkage at the LV terminals*

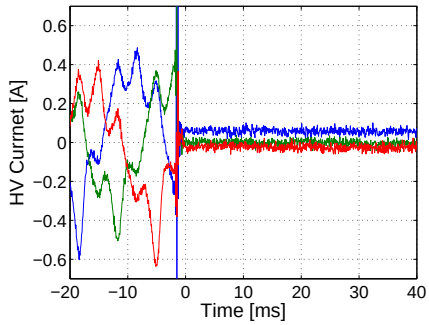

(d) *Line current at the HV terminals*

Figure 3.10: Ringdown transient, 800 kVA transformer.

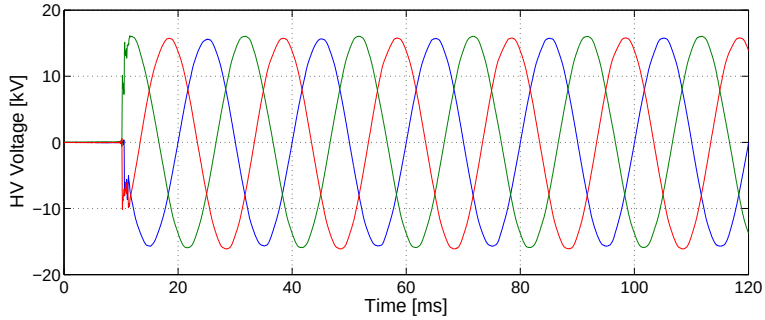

(a) *Line voltage at the HV terminals*

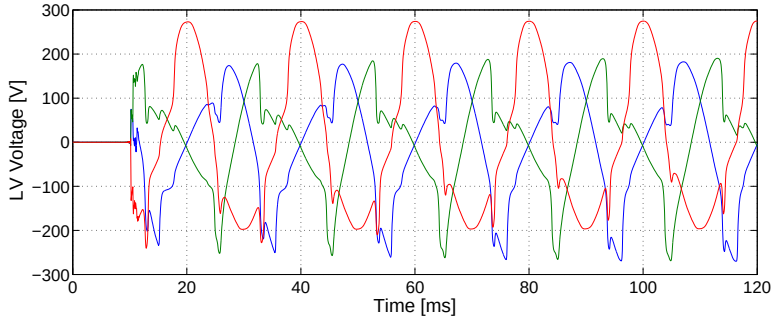

(b) *Phase voltage at the LV terminals*

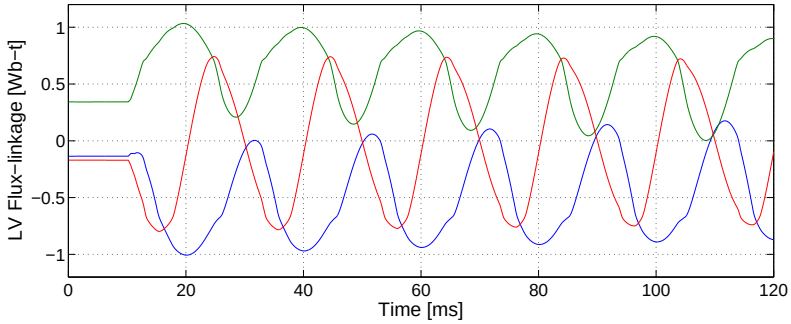

(c) *Flux-linkage at the LV terminals*

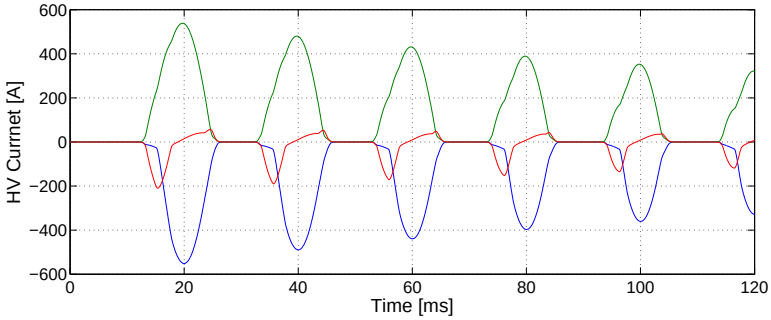

(d) *Line current at the HV terminals*

Figure 3.11: Inrush current transient, 800 kVA transformer.

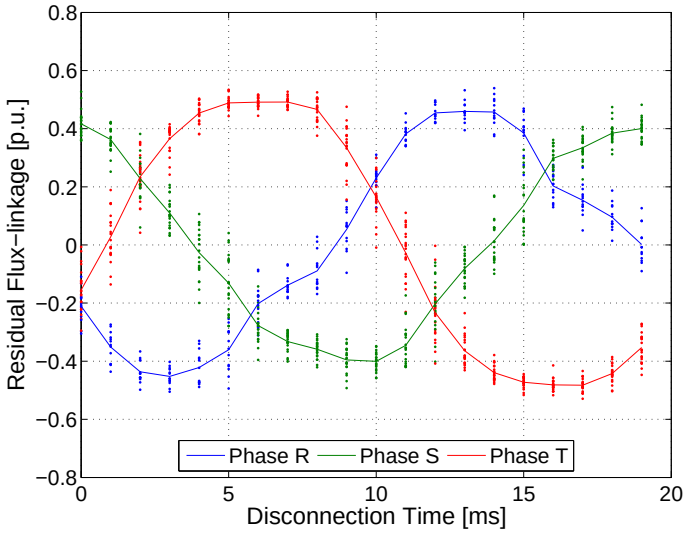

Figure 3.12: Residual flux, 300 kVA transformer.

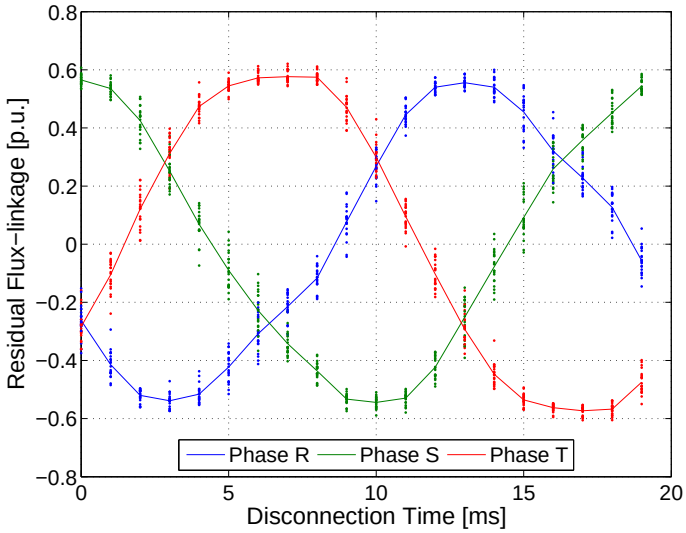

Figure 3.13: Residual flux, 800 kVA transformer.

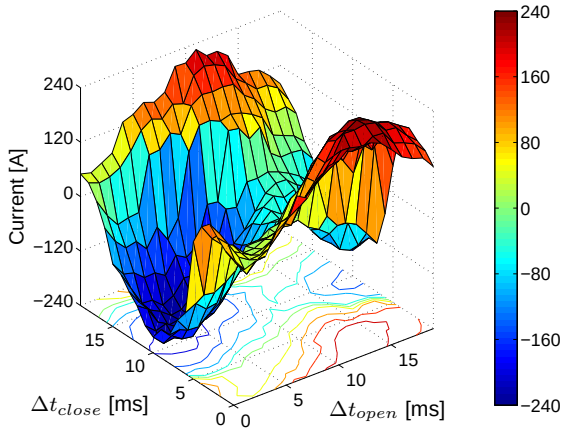

(a) *Phase R*

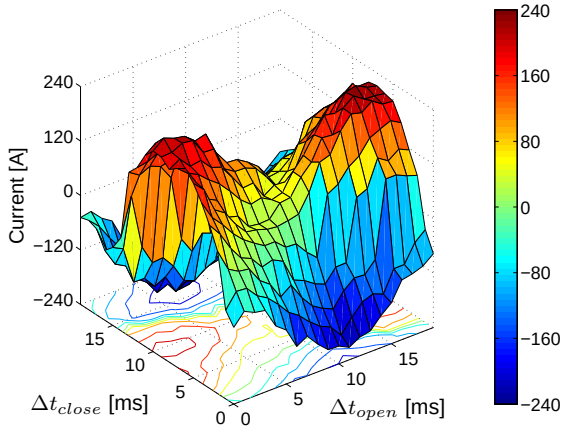

(b) *Phase S*

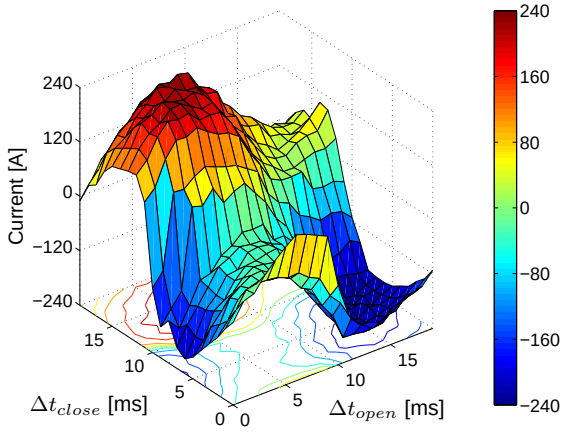

(c) *Phase T*

Figure 3.14: Measurements of the first peak inrush current pattern, Yyn coupling. 300 kVA transformer, 3D pattern.

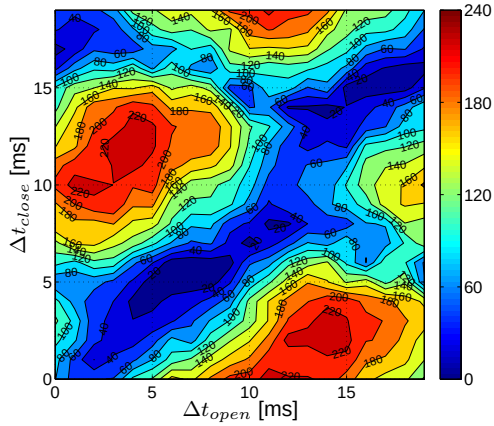

(a) *Phase R*

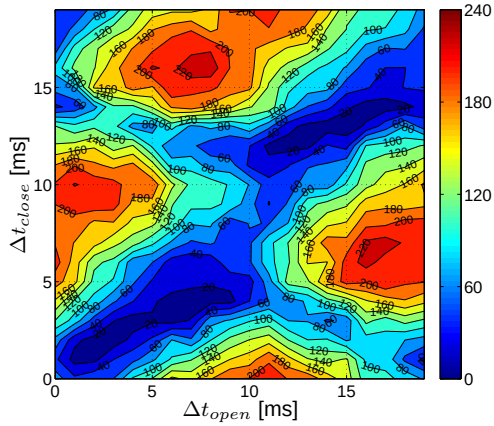

(b) *Phase S*

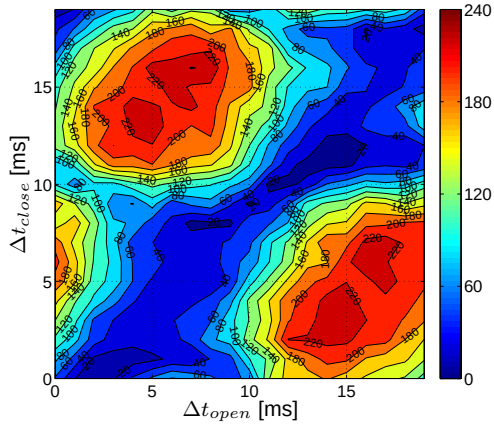

(c) *Phase T*

Figure 3.15: Measurements of the first peak inrush current pattern, Yyn coupling. 300 kVA transformer, absolute value.

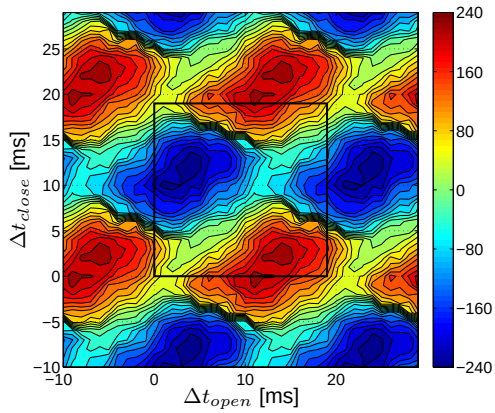

(a) *Phase R*

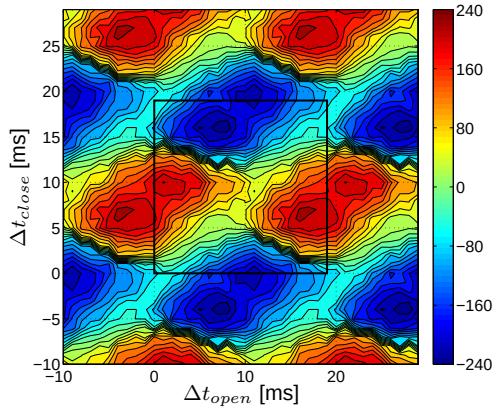

(b) *Phase S*

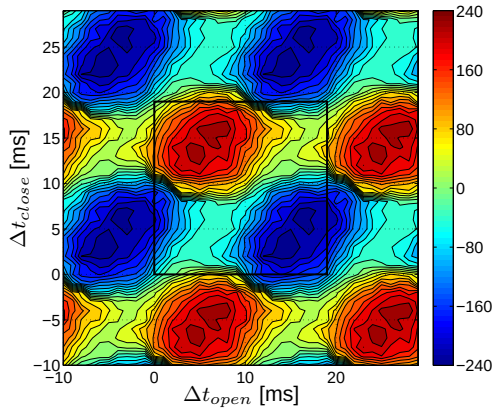

(c) *Phase T*

Figure 3.16: Measurements of the first peak inrush current pattern, Yyn coupling. 300 kVA transformer, extended pattern.

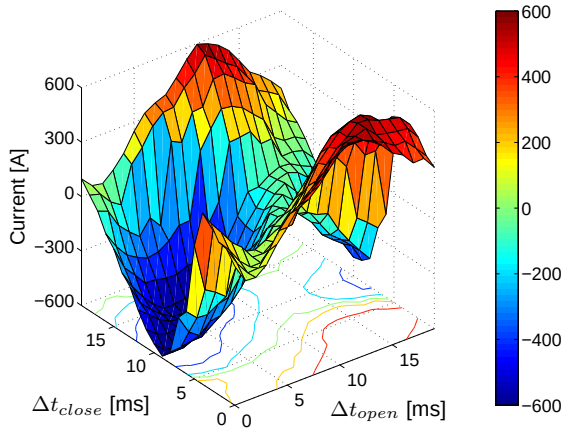

(a) *Phase R*

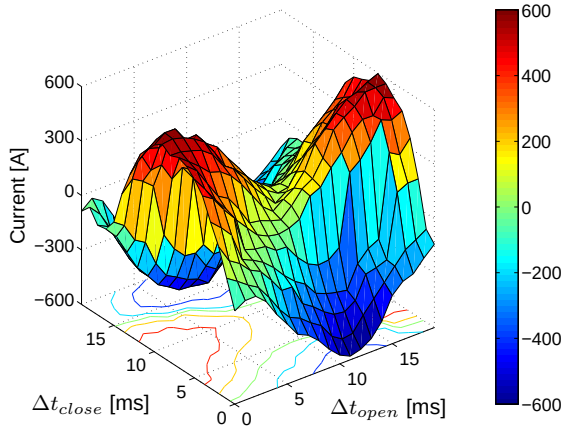

(b) *Phase S*

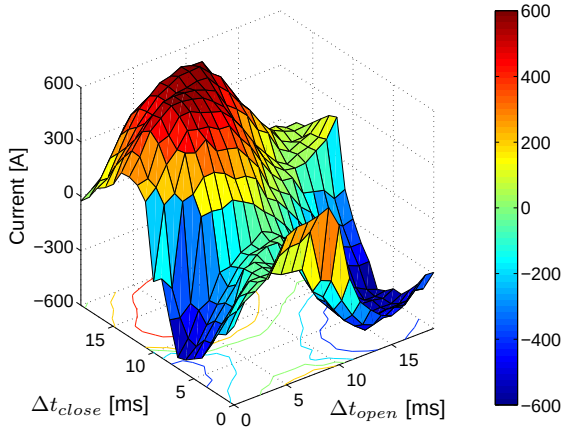

(c) *Phase T*

Figure 3.17: Measurements of the first peak inrush current pattern, Yyn coupling. 800 kVA transformer, 3D pattern.

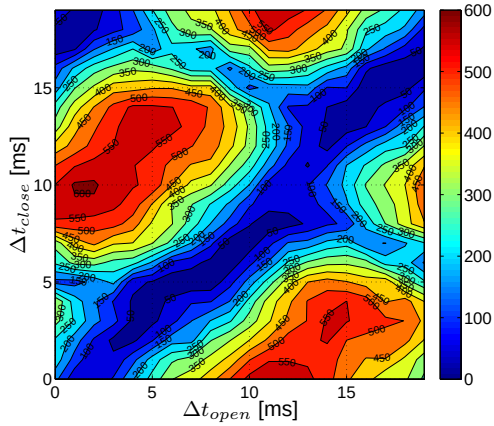

(a) *Phase R*

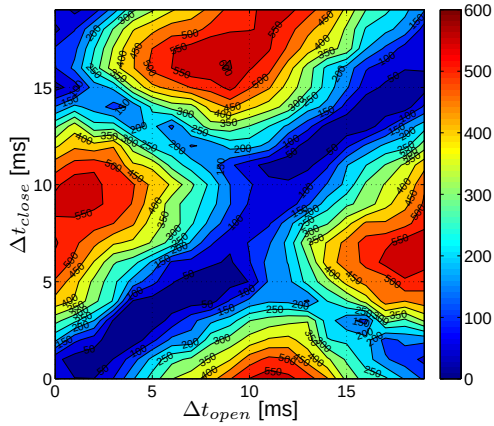

(b) *Phase S*

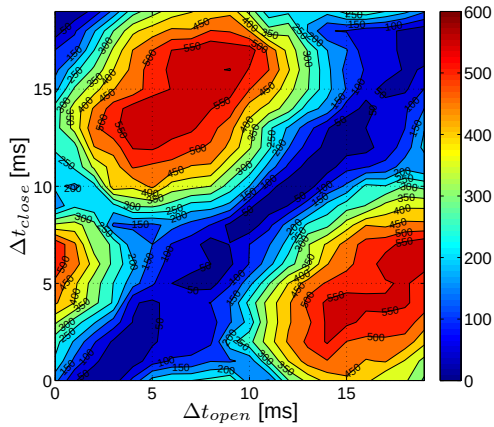

(c) *Phase T*

Figure 3.18: Measurements of the first peak inrush current pattern, Yyn coupling. 800 kVA transformer, absolute value.

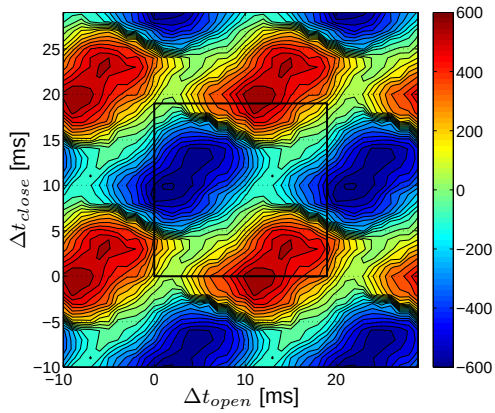

(a) *Phase R*

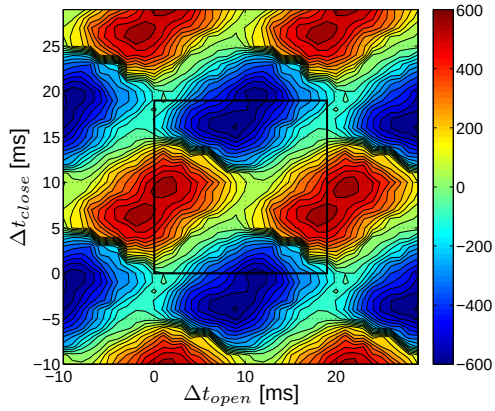

(b) *Phase S*

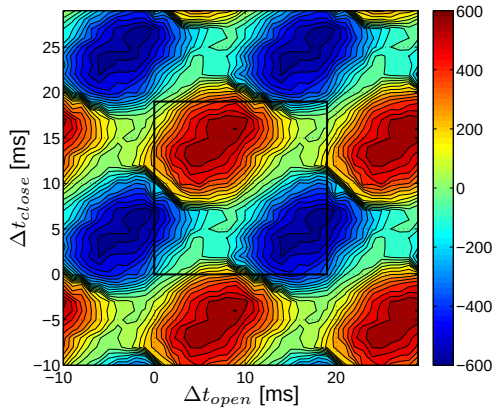

(c) *Phase T*

Figure 3.19: Measurements of the first peak inrush current pattern, Yyn coupling. 800 kVA transformer, extended pattern.

3.3 Field measurements on large transformers

Live measurements have been performed on three power transformers rated 50 MVA and 300 MVA (two units). Table 3.3 summarizes the results of the tests and compares the worst case inrush current and maximum residual flux recorded for the different transformers. The systematic measurements performed in the controlled laboratory environment (L.M.) ensure a statistical validity of the values for the two distribution transformers. The results from the field measurements (F.M.) are based on a relatively limited number of de-energization and energization transients. Therefore, there is a high level of uncertainty and a high probability that the worst case values have not been captured. The comparison of the per-unit values in Table 3.3 shows that worst case inrush current first peak is much higher in distribution transformers (15-20 p.u.) compared to power transformers (2-4 p.u.).

Large power transformers are very seldom disconnected from the grid. It is very expensive and inconvenient to take a large power transformer out of service for the only purpose of performing measurements. The field measurements of the transformers were coordinated with the utility and transformer manufacturer. All three cases took place when the new transformers were placed in service for the first time. The first energization of a transformer is quite a chaotic moment as several engineers are present to calibrate the protection relays and assist in the different required operations. In this situation inrush current measurements are given relatively low priority and a rather short time-frame is available for measurements.

Collaboration with utilities and transformer manufacturers was required to identify the proper study cases. The main restriction are related to the availability and location of measurement points. It is important to have a VT and a CT on the energization side, either before or after the primary circuit breaker to monitor the source voltage and line current. A VT on the unloaded side of the transformer is required to have access to the induced voltage measurements needed for the estimation of flux-linkages and residual fluxes. This VT has to be connected to the transformer terminals and therefore located before the secondary side circuit breaker. This is a relatively rare

TABLE 3.3
COMPARISON OF MAXIMUM INRUSH CURRENT FIRST PEAK AND MAXIMUM RESIDUAL FLUX FOR DIFFERENT TRANSFORMERS.

	300 kVA	**800 kVA**	**50 MVA**	**300 MVA**	**300 MVA**	
Inrush first	241	605	1436	1545	2060	[A]
peak	20.5	14.4	2.34	3.75	3.57	[p.u.]
Residual	0.33	0.38	13	83	231	[Wb-t]
flux	0.54	0.62	0.45	0.24	0.67	[p.u.]
	L.M.	L.M.	F.M. 2	F.M. 1	F.M. 3	

configuration that limited the number of suitable test cases. In addition, in most of the situations safety regulations did not allow to install additional voltage and current measurement devices.

The close collaboration with utilities and transformer manufacturers made it possible to specify additional non-standard factory measurements and obtain design data of the two transformer of F.M 2 and F.M. 3. These data and measurements are confidential and are not published in this work.

The main challenges encountered in field measurements compared to the controlled laboratory environment are:

- Limited time frame, usually few hours. This limit the possibility to perform extensive and systematic measurements.
- Restrictions on the number of measurements prevent conclusive and statistically relevant conclusion of the residual flux and inrush current ranges.
- Uncertainties related to the measurements. The accuracy of the installed VTs and CTs, the noise collected by the long cable of the measurement circuit, and the poor dc performance of the CTs and VTs highly affect the overall accuracy of the measurements (current measurements and flux-linkage estimation mainly).
- Uncertainties related to the network configuration. Network source impedance, cables and reactors may complicate the modeling and the verification of a model with field measurements.

3.3.1 Field measurement 1, 300 MVA

The measurements were performed in October 2007 at a transformer station in Norway. The testes transformer is rated 420/132/32 kV 300/300/100 MVA YNyn0d11 and has a five-legged core. The neutral points on 420 kV and 132 kV are ungrounded but connected through an arrester to ground. The breaker is equipped with a synchronized switching control unit. In total 7 de-energization/energization measurements were performed (5 random energization and 2 controlled energization).

The available measurement point were:

- VT on 420kV side, only phase voltage of phase S available for measurements. Before the circuit breaker.
- VT on 132kV side.
- CT on 420kV side. Before the circuit breaker.

The measured de-energization and energization transients for the most severe inrush current case are shown in Figs. 3.20 and 3.21. The current during the ringdown tran-

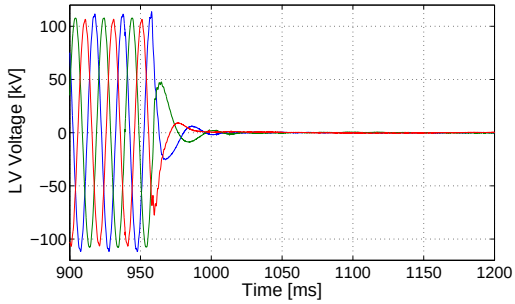

(a) *Phase voltage at the LV terminals*

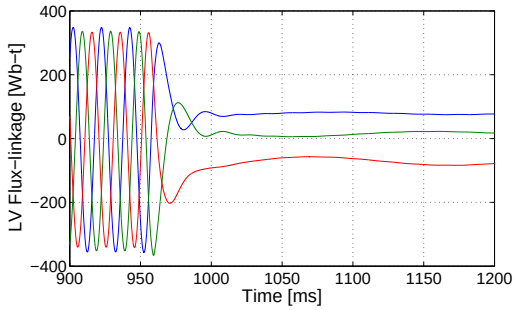

(b) *Flux-linkage at the LV terminals*

Figure 3.20: Ringdown transient, 300 MVA transformer (F.M. 1).

sient is not shown as it was not possible to record such a low current with the installed CT. In Fig. 3.21 we observe:

- The voltage on the 420 kV bus is distorted. This may cause power quality degradation issues.
- The voltage on the 132 kV bus is highly distorted, see the zoom window in Fig. 3.21(b).
- The dc-offset component of the flux-linkage has unusual fluctuations. It is not sure if this is the correct behavior or is an effect caused by the accumulated error in the time integral.
- The current has a sudden decrease in magnitude after the seventh period. At the same time, an unusual dc-component in the current is recorded. This may be due to saturation of the CT that is not able to correctly measure low-frequency and dc components of the current. This also explains why passed the seventh period the sum of the measured currents is not zero although the transformer is ungrounded.

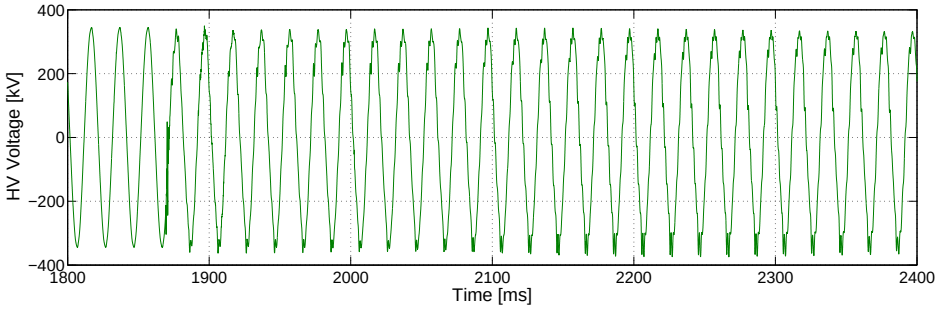

(a) *Phase voltage at the HV terminals (Ph. S)*

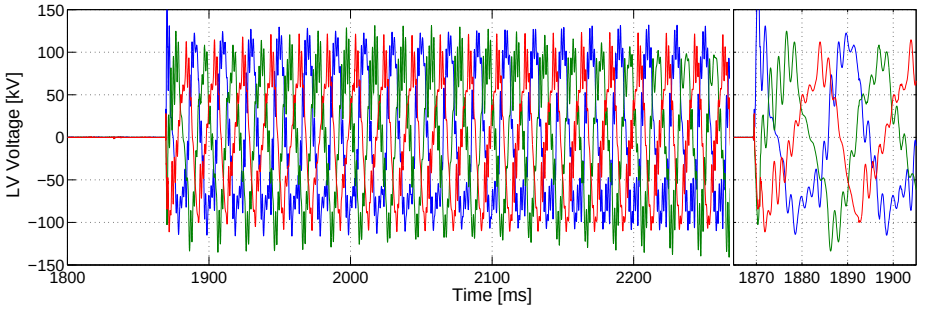

(b) *Phase voltage at the LV terminals (with zoom)*

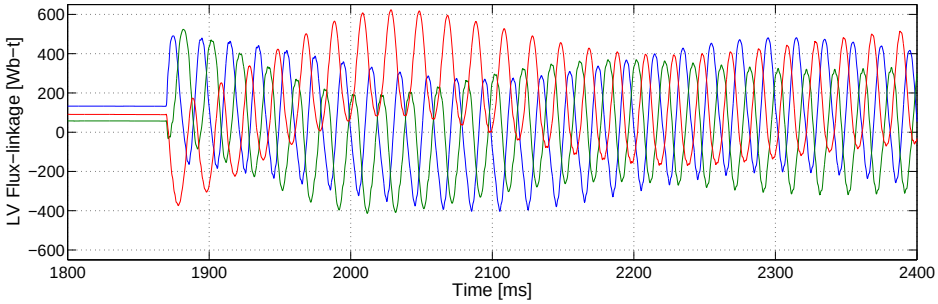

(c) *Flux-linkage at the LV terminals*

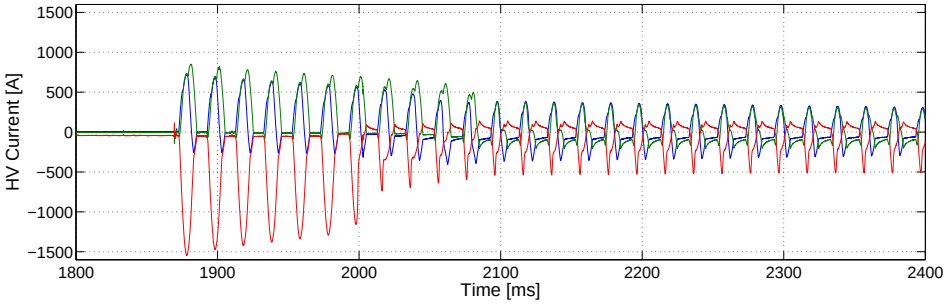

(d) *Line current at the HV terminals*

Figure 3.21: Inrush current transient, 300 MVA transformer (F.M. 1).

3.3.2 Field measurement 2, 50 MVA

The measurements were performed in September 2008 at a district heating station in Norway. The tested transformer is rated 47/11 kV 50 MVA YNyn0 and has a three-legged core. The transformer is energized through a breaker located in a station at approximately 2 km distance. A damping reactor and 1.7 km cable connect the secondary side of the circuit breaker to the high voltage side of the transformer.

Only the measurements of the 11 kV side voltage were available in the heating station (VT). Temporary capacitive voltage dividers and Rogowski current probes were installed on the 47 kV side for the measurements of voltages and currents. Since the neutral on the 11 kV side is ungrounded, an additional capacitive voltage derider was installed to measure the neutral-point voltage.

A total of 13 random de-energization/energization measurements were performed. The waveform measurements of the de-energization transient with the highest residual flux are shown in Fig. 3.22. The ringdown transient of this transformer is particularly interesting as the damping reactor and the cable remain connected to the transformer after the circuit breaker opens. The ringdown transient is influenced by additional shunt capacitances installed in the system. The effect is evident in Fig. 3.22 after the disconnection at approximately 700 ms. Contrarily to the previous case, here the ringdown transient develops over several periods. This induces a temporary core saturation effect: the no-load current with a peak of approximately 3 A increases up to 22 A after the opening of the circuit breaker. This effect is further discussed in [Pb4].

The waveform measurements of the most severe inrush transient recorded are shown in Fig. 3.23. The induce voltage and inrush current waveforms are qualitatively similar to the waveforms measured in the laboratory on the smaller distribution transformers (Figs. 3.9, 3.11). The 50 MVA transformer and the distribution transformers tested in the laboratory share the same ungrounded wye coupling, have no tertiary delta winding, and have a three-legged core.

3.3.3 Field measurement 3, 300 MVA

The measurements were performed in October 2009 at a transformer station in Norway. The tested transformer is rated 300(420)/132/47 kV 300/300/100 MVA YNyn0d11 and has a five-legged core. The neutral points on the 300 kV and 132 kV are ungrounded. The breaker is equipped with a synchronized switching control unit. A total of 17 energizations have been performed. For most of the energizations, the controlled switching unit was activated as a differential protection relay was constantly tripping (after 4 seconds) when the transformer was energized with no synchronized switching control. Only two attempts of a random de-energization/energization were successful. The waveforms for the one with the highest inrush current magnitude are shown in Figs. 3.24 and 3.25. The max inrush

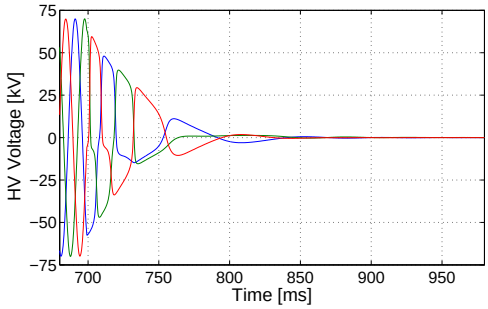

(a) *Line voltage at the HV terminals*

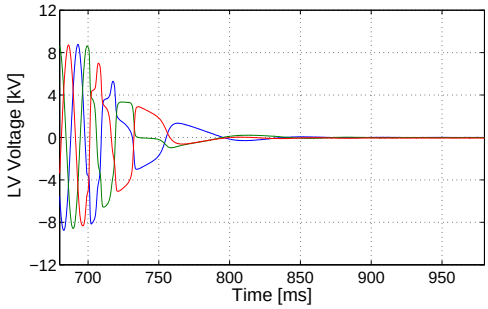

(b) *Phase voltage at the LV terminals*

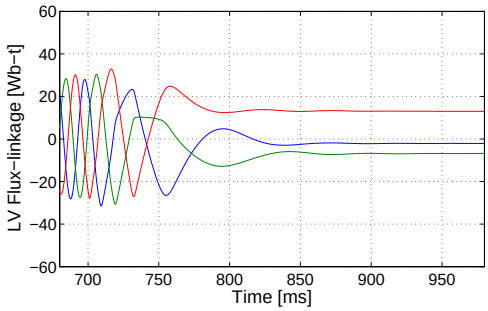

(c) *Flux-linkage at the LV terminals*

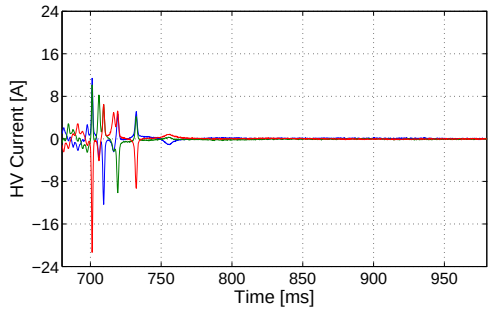

(d) *Line current at the HV terminals*

Figure 3.22: Ringdown transient, 50 MVA transformer (F.M. 2).

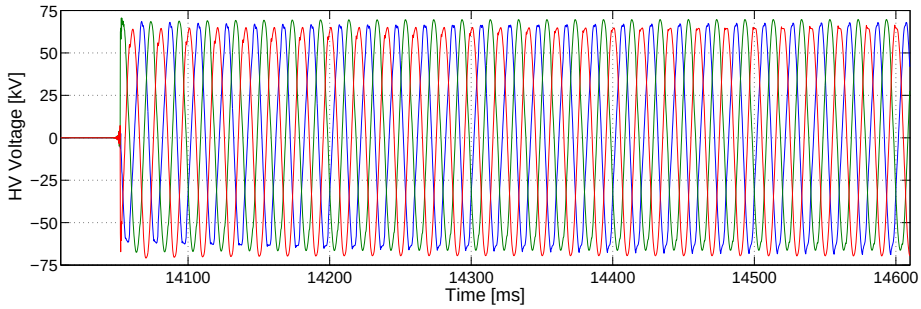

(a) *Line voltage at the HV terminals*

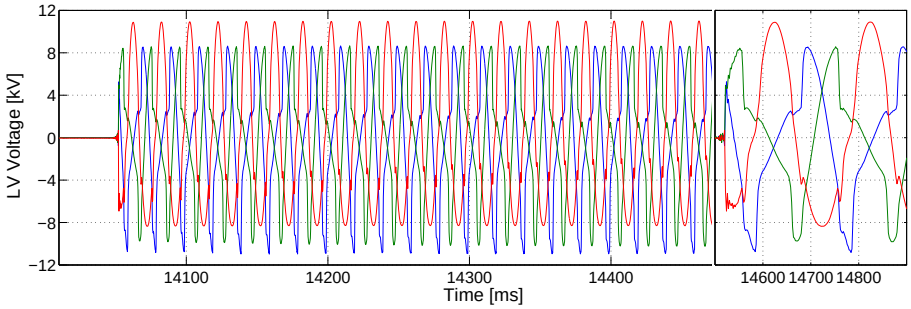

(b) *Phase voltage at the LV terminals (with zoom)*

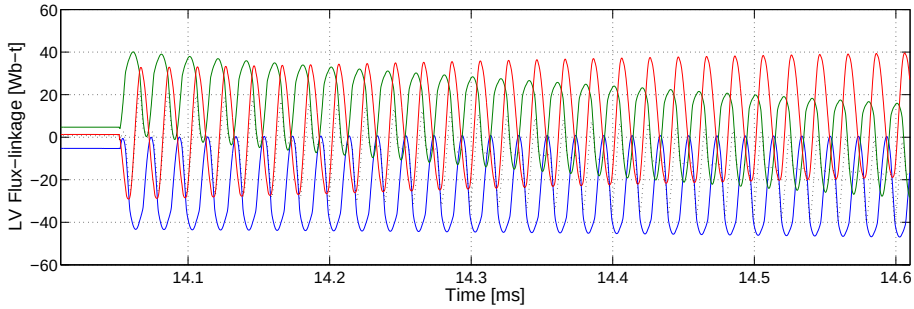

(c) *Flux-linkage at the LV terminals*

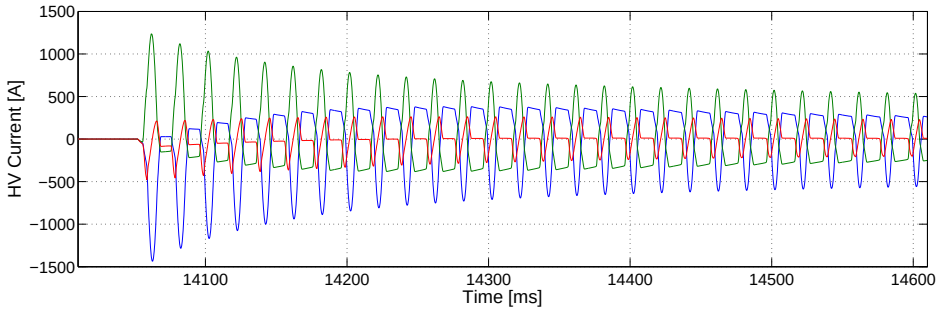

(d) *Line current at the HV terminals*

Figure 3.23: Inrush current transient, 50 MVA transformer (F.M. 2).

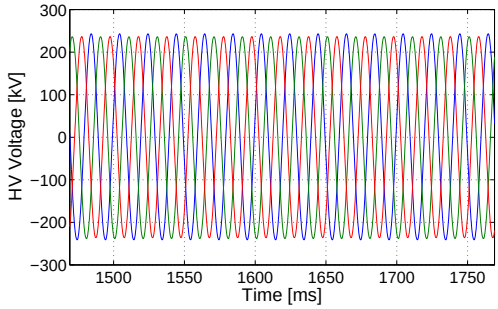

(a) *Phase voltage at the HV terminals*

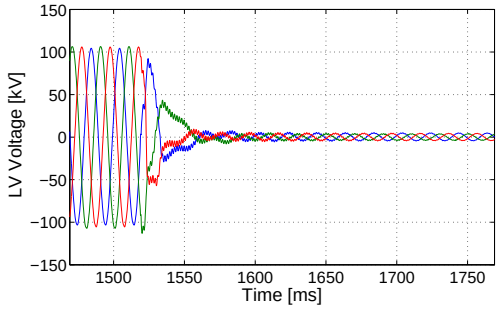

(b) *Phase voltage at the LV terminals*

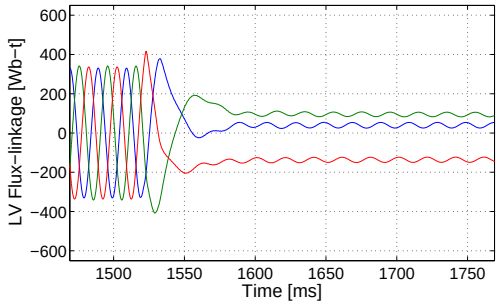

(c) *Flux-linkage at the LV terminals*

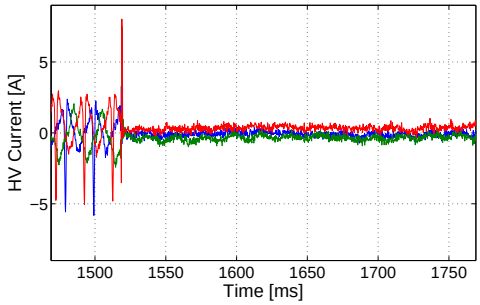

(d) *Line current at the HV terminals*

Figure 3.24: Ringdown transient, 300 MVA transformer (F.M. 3).

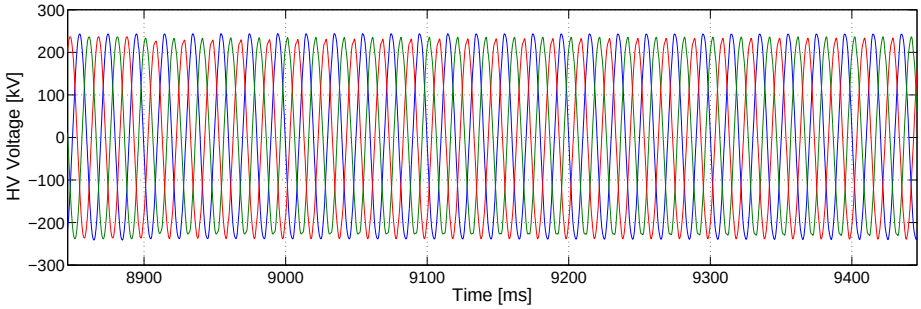

(a) *Phase voltage at the HV terminals*

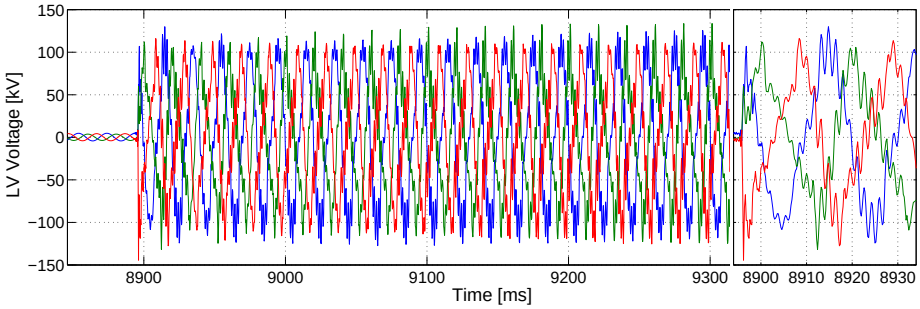

(b) *Phase voltage at the LV terminals (with zoom)*

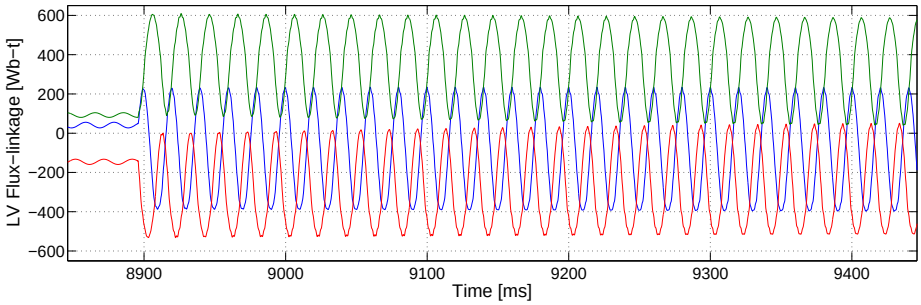

(c) *Flux-linkage at the LV terminals*

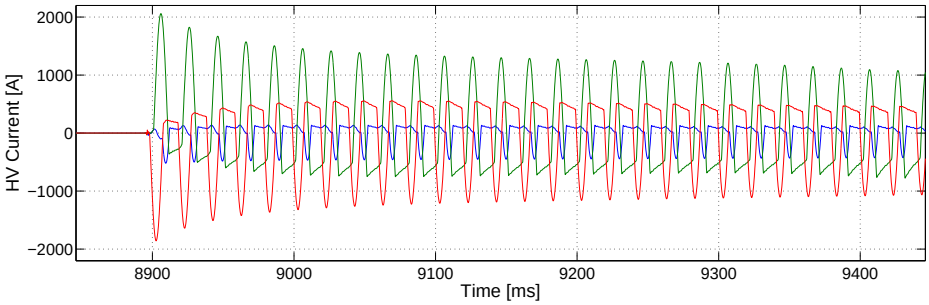

(d) *Line current at the HV terminals*

Figure 3.25: Inrush current transient, 300 MVA transformer (F.M. 3).

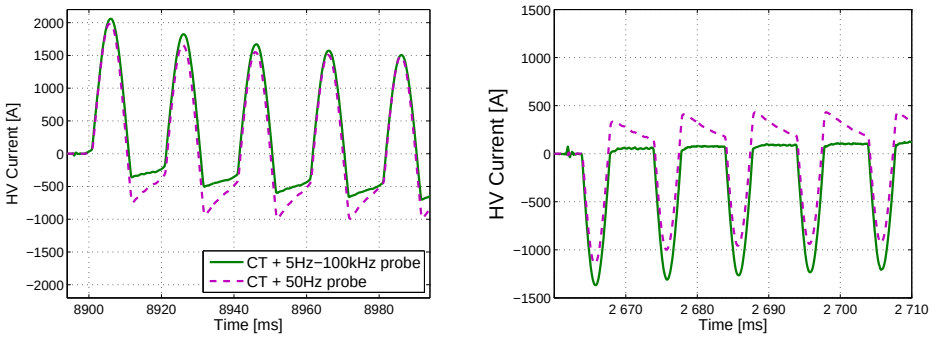

Figure 3.26: Effect of CTs and current probes on inrush current measurements.

current measured during the test is 2415 A (4.18 p.u.). However, it followed an unsuccessful energization and the residual fluxes may have been outside the range reached by a normal de-energization. In Figs. 3.24(c) and 3.25(c) is possible to note that the flux-linkage does not reach a steady value after de-energization but exhibit low amplitude oscillations. This may either by caused by a low voltage transferred to the 300 kV terminals of the transformer by the grading capacitors of the circuit breaker, or by electromagnetic noise collected by the cables of the measurement circuit.

In order to record the measurements of the line currents, a transient recorder has to be connected to the CT measurement circuit through a current probe. Two different current probes were used in parallel here. One current probe is more accurate and has a frequency response of 5 Hz-100 kHz. The other probe is cheaper and less accurate, with a narrow frequency response at 50 Hz. The same current measurements recorded with the two different probes are compared in Fig. 3.26. We observe how the probe with a limited frequency response induce more distortions in the measurements. A similar effect is assumed to be introduced by the main CT. The atypical dc-offset in the currents recorded in the field measurement is therefore due to a limited low frequency response of the measurement circuit (low-pass filter effect) and the dc current component cannot be correctly measured. This effect has not been observed in the laboratory measurements as the current probes used there have a frequency response of from DC to 500 kHz.

CHAPTER 4

DISCUSSION

4.1 Model Development

The modeling approach preferred in this work is based on an equivalent electric circuit derived by duality transformation introduced in Section 2.1.2. The main reasons why this is preferred over magnetic and hybrid modeling approaches are:

- A magnetic model requires the implementation of core and electric networks as separate but interconnected models. This might be difficult to implement in EMTP-like program using standard components.
- Core losses representation is more difficult in a magnetic model as lossy element cannot be directly modeled. They have to be relocated far from their topological location in the electric section of the model as equivalent resistances.
- The discretization of the flux paths is performed for any approach. The duality transformation from a discretized magnetic circuit to an electric circuit does not introduce loss of accuracy.
- The assumption of decoupled magnetic and leakage fluxes used in an hybrid approach is doubtful at high saturation.

The magnetic core of a three-legged three-winding transformer is represented in Fig. 4.1. The procedure to establish a topological electrical equivalent model of this

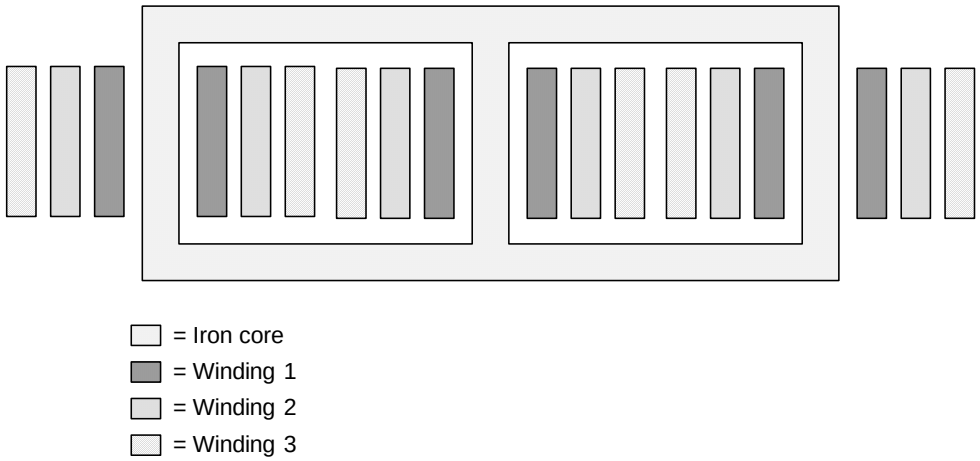

Figure 4.1: Three-legged three-winding transformer. Magnetic core and winding structure.

transformer is described here step-by-step. First, the magnetic structure needs to be discretized.

The discretization of a magnetic structure into a magnetic circuit is the most sensitive operation. The magnetic paths needs to be identified and represented by reluctances. The paths in the iron are easily determined as the high permeability of the core provides a preferred route for the flux. The magnetic field is not confined only in the iron core but can leaks in the open space between the windings. Different winding configurations result therefore in different magnetic circuits.

The magnetic knots and the assumed flux paths for the structure of Fig. 4.1 are depicted in Fig. 4.2. Six magnetic knots are identified in this structure. They determine the points of departure of the flux paths and set the discretization level of the structure. A larger number of knots allows a higher level of discretization but increases the complexity of the final model. The flux paths are distinguished in three categories:

1. *Linkage fluxes*: are the magnetic paths in the iron core. The linkage between different phases are trough the ferromagnetic material. They are characterized by being nonlinear, with high permeability in normal condition. When saturated, the permeability decreases and approaches μ_0. They describe the open-circuit behavior of the transformer and the coupling between phases.

2. *Leakage fluxes*: are the fluxes in the air. The space between two windings is particularity important because of the high energy density. These paths are linear and have permeability μ_0. They describe the short-circuit behavior of the transformer. In addition, a leakage path is identified between each innermost winding and its relative leg. This path is particularly important in saturated condition to account for the non ideal concatenation of the innermost winding with the core. The coupling between different phases due to leakage fluxes is

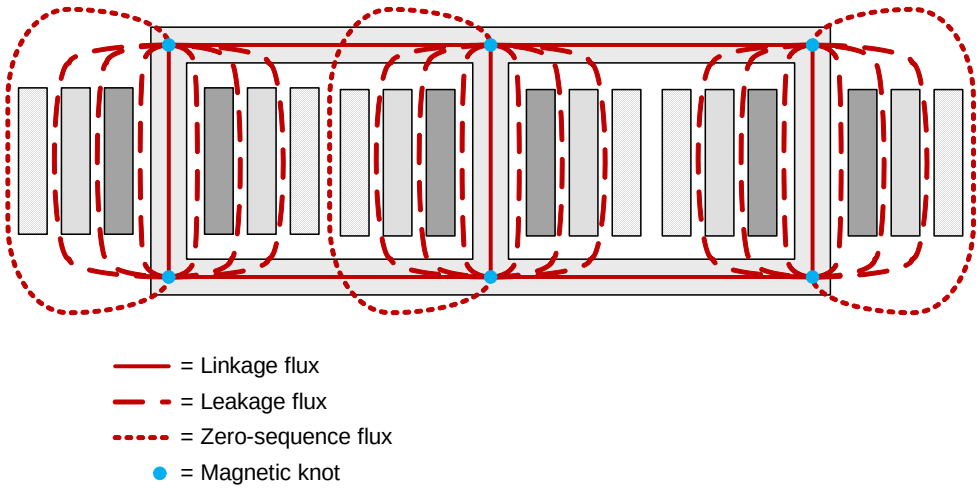

Figure 4.2: Discretization of the flux paths.

negligible [Pb3].

3. *Zero-sequence fluxes*: are the homopolar flux paths that flows in the transformer tank and oil. They describe the zero-sequence behavior of the transformer. Due to the relatively large air-gap filled by oil between the core and the tank, they can be considered linear and with permeability μ_0. In case of a five-legged transformer, the zero-sequence flux mainly flows in the outer transformer legs, that in this case are nonlinear.

The meshes of the magnetic model are directly identified by the flux paths in Fig. 4.2. In a magnetic model the across variable is the magnetic-potential drop and the through variable is the flux. Each path is a magnetic branch that is represented either by a linear or nonlinear reactance. In addition, the windings are modeled as magnetomotive force (mmf) sources. The windings that act to magnetize the same iron-core limb are placed in series.

The interconnection of reactances and mmf sources is not straightforward. The three bottom knots expand as additional knots needs to be introduced to have a topological location of the mmf sources. A simple rule valid for concentric windings can be used to correctly position the mmf sources in the magnetic circuit.

The outermost winding surrounds all the leakage flux paths, while the innermost winding encloses only one leakage flux path. Proceeding from the outermost to the innermost winding, the mmf source corresponding to outermost winding ($\mathfrak{F}_3$) is connected to the bottom knot, and all the leakage path are located on top of it. The mmf source of the next inner winding ($\mathfrak{F}_2$) is also above of $\mathfrak{F}_3$. The leakage flux between winding 2 and 3 is not enclosed by the winding 2, therefore needs to be connected to the knot between $\mathfrak{F}_2$ and $\mathfrak{F}_3$. The difference between the flux of the winding 2 and 3 flows in the reactance $\mathfrak{R}_{23}$. In the same way, $\mathfrak{R}_{12}$ is connected to the knot

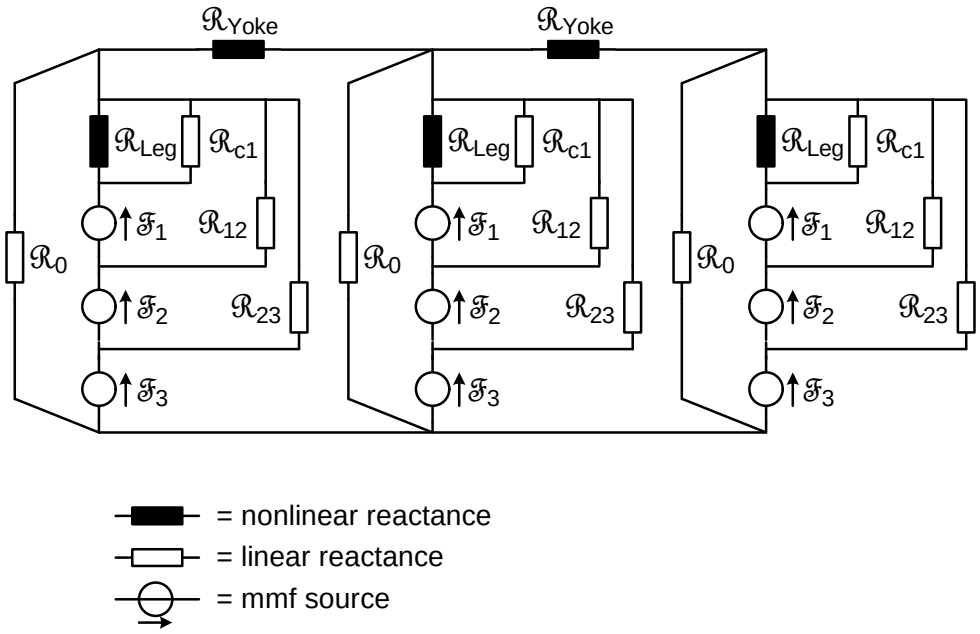

Figure 4.3: Magnetic circuit.

between $\mathfrak{F}_1$ and $\mathfrak{F}_2$. The flux generated by the innermost winding and therefore by $\mathfrak{F}_1$ flows solely in the leg ($\mathfrak{R}_{Leg}$) and in the space between the leg and the winding 1 ($\mathfrak{R}_{c1}$). The second terminal of the leakage reactances is then connected to a common top knot. The direction of the mmf sources is arbitrary. The final result is shown in Fig. 4.3.

The rules for the conversion of a magnetic circuit into its electric equivalent depicted in Section 2.1.2 can be applied to the more complex magnetic circuit of Fig. 4.3. After the substitution of the current sources with ideal transformers, and the addition of the winding resistances at one terminal of the ideal transformers, the equivalent electric circuit of Fig. 4.4 is obtained.

The ideal transformers take into account the windings' turns ratio and allow the connection of the model to other network components. The winding coupling and phase shift is obtained by appropriately connecting the $r - r'$, $s - s'$ and $t - t'$ terminals of the ideal transformer together. The connections r, s and t identify the terminals on the top of a winding, and r', s' and t' the terminals on the bottom of a winding.

All the key components of a transformer model can be identified in Fig. 4.4, namely:

- The core model: it is spread across the model with the representation of the leg (L_{Leg}) and yoke (L_{Yoke}) limbs respectively on the left and right side of the circuit. The nonlinear and lossy behavior of the core is represented here.
- The leakage model: it is decoupled between the three phases and represented by the linear inductances L_{c1}, L_{12} and L_{23}. The short-circuit behavior of the

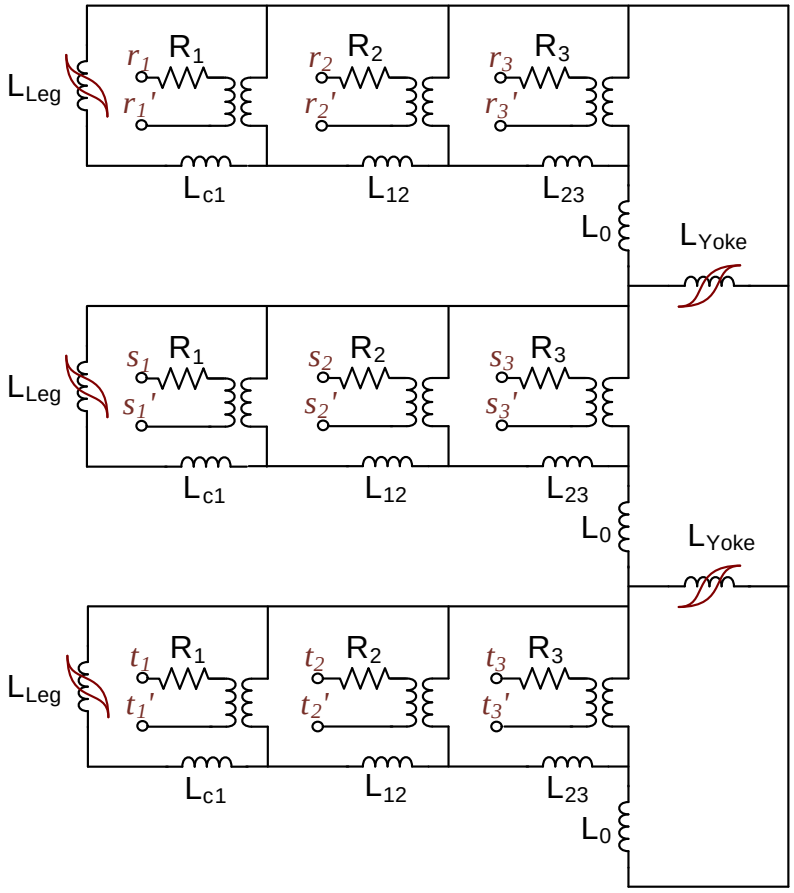

Figure 4.4: Equivalent electric circuit obtained by duality transformation.

transformer is represented here. This part is further discussed below.

- The zero-sequence model: depicted by the linear inductances L_0.
- The winding resistances: concentrated at the windings' terminals.
- The voltage ratio: modeled by ideal transformers.

The hysteresis model used to represent the iron-core nonlinear and lossy behavior is described in Section 4.3. The core losses are properly distributed at their topological position on legs and yokes. It is interesting to highlight that the voltage across the inductor L_{Leg} is the voltage of the innermost winding (minus the voltage drop on the inductance L_{c1}). The voltage across the yoke inductors L_{Yoke} is the voltage of the outermost winding of phase R and T (minus the voltage drop on the inductance L_0). Therefore, the fluxes in the transformer legs are mainly determined by the innermost winding voltages, while the outermost windings control the fluxes in the transformer yokes. The difference between leg and yoke fluxes flows in the leakage inductances (L_{c1}, L_{12} and L_{23}) and in the zero-sequence inductances L_0.

This transformer model is intrinsically asymmetric and accurately model the behavior of a three-phase core transformer. The different equivalent impedance seen from the center s and outer r and t phases is mainly due to the asymmetrical location of the yoke sections. A two-winding version of the model of Fig. 4.4 has been successfully employed for the representation of inrush current transients in [Pb6, Pb7, Pb8].

4.2 Leakage Model

The modeling of the leakage fluxes in a topological model depends on the winding configuration. Concentric windings (foil, layer and disk windings) is the most common topology found in power and distribution transformers. Simplified representations of different winding topologies are shown in Fig. 4.5 for concentric windings, in Fig. 4.6 for sandwich winding, and in Figs. 4.7-4.8 for two mixed configurations. A possible derivation of the magnetic and electric equivalent circuits is shown in the figures. The transformer core has not been fully represented in these figures as the focus here is on the leakage model.

The derivation of the magnetic and electric equivalent circuits for the concentric winding topology is relatively simple and previously explained for the three-legged transformer case. The leakage inductance L_{c1} can be interpreted as a short-circuit inductance between the innermost winding and a fictitious infinitively-thin winding placed on the core surface. This inductance represents the physical gap between the core and the innermost winding that is filled with oil and has permeability μ_0. The example of Fig. 4.5 can therefore be considered as a four winding transformer.

For a general n-winding transformer the number of independent elements (degree of freedom) required to represent the relations between its n-terminals are $n(n-1)/2$

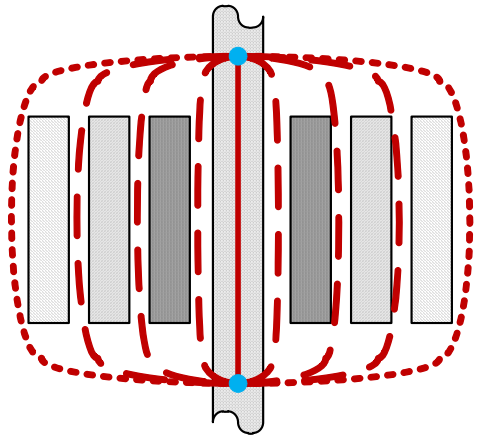

(a) *Core and winding structure. Identification of the flux paths.*

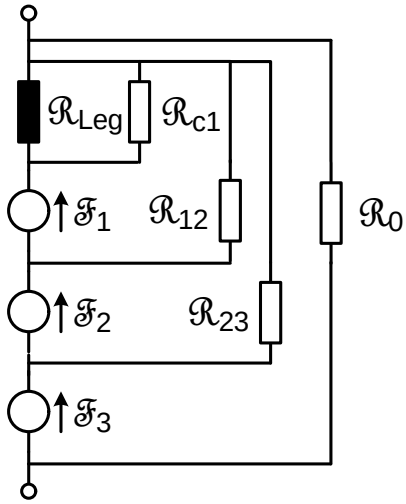

(b) *Magnetic circuit.*

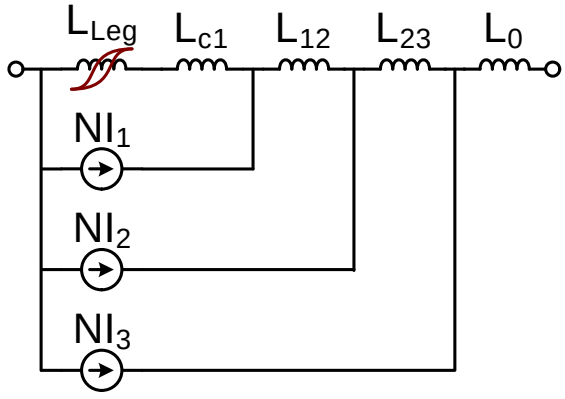

(c) *Electric equivalent circuit.*

Figure 4.5: Concentric windings.

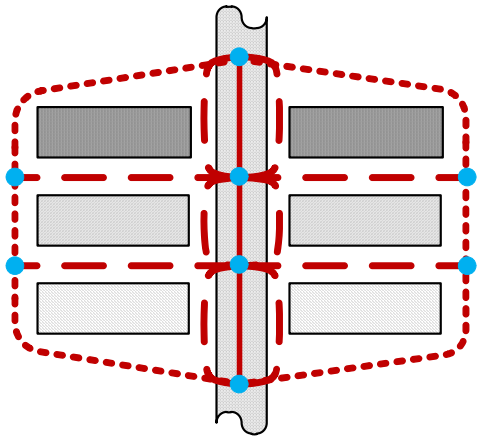

(a) *Core and winding structure. Identification of the flux paths.*

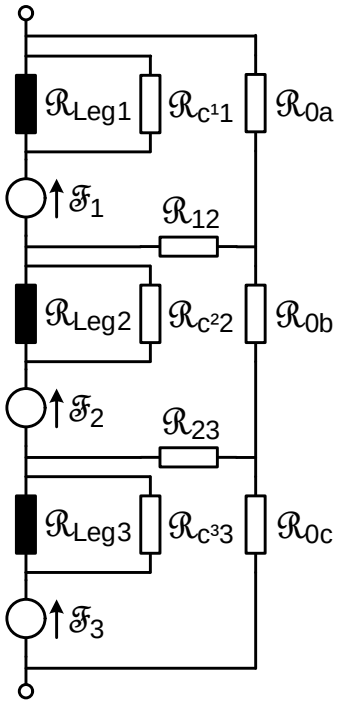

(b) *Magnetic circuit.*

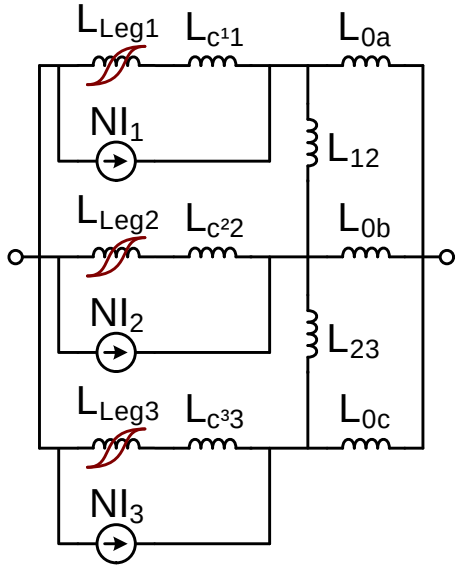

(c) *Electric equivalent circuit.*

Figure 4.6: Sandwich windings.

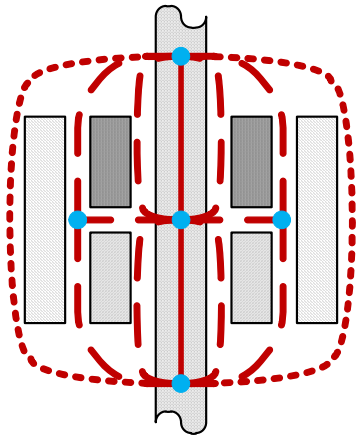

(a) *Core and winding structure. Identification of the flux paths.*

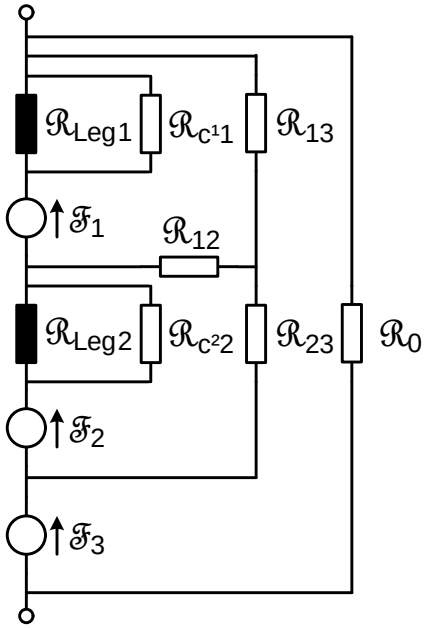

(b) *Magnetic circuit.*

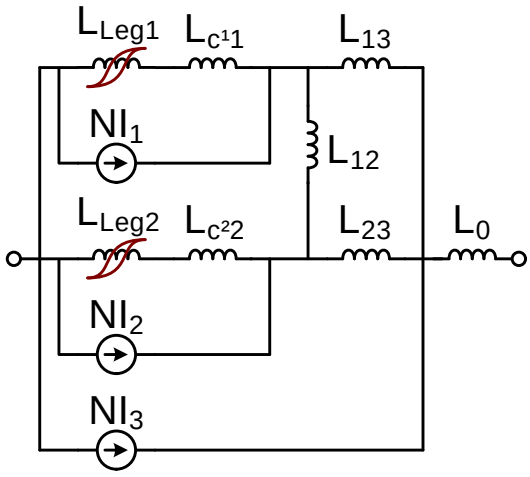

(c) *Electric equivalent circuit.*

Figure 4.7: Mixed windings, configuration 1.

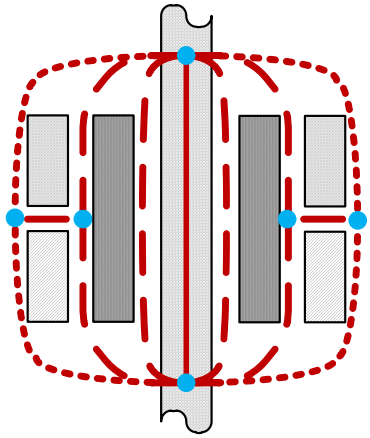

(a) *Core and winding structure. Identification of the flux paths.*

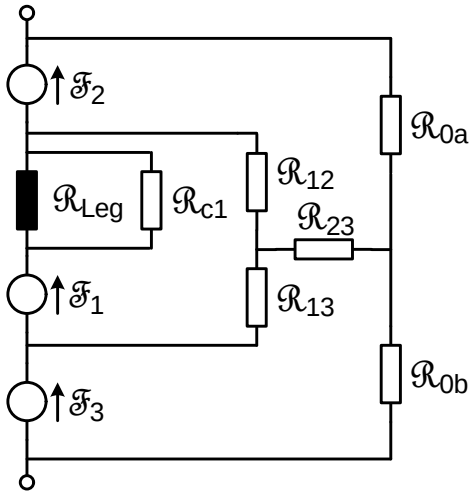

(b) *Magnetic circuit.*

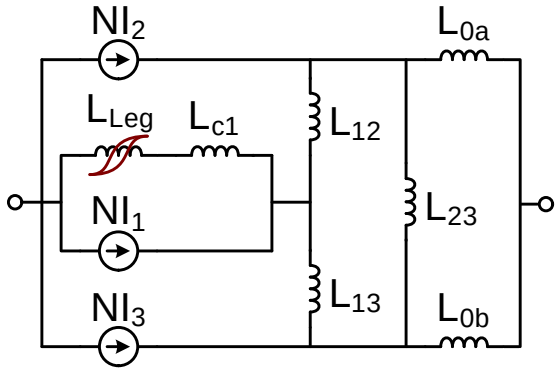

(c) *Electric equivalent circuit.*

Figure 4.8: Mixed windings, configuration 2.

[1]. This would require 6 independent inductances for a four-winding transformer. In the case of concentric windings the following three constraint can be assumed valid:

$$L_{c2} = L_{c1} + L_{12} \tag{4.1}$$

$$L_{13} = L_{12} + L_{23} \tag{4.2}$$

$$L_{c3} = L_{c1} + L_{12} + L_{23} \tag{4.3}$$

The degrees of freedom are therefore reduced to three and the system can be represented by the three inductances L_{c1}, L_{12} and L_{23}.

In case of a sandwich winding, the core limb and the fictitious winding on the core surface are divided into three parts. This topology can be regarded as three two-winding transformer sections magnetically in series. In this case the number of terminal is $n = 6$ with 15 degrees of freedom. The number of independent inductances is reduced to five: $L_{c^1 1}$, $L_{c^2 2}$, $L_{c^3 3}$, L_{12} and L_{23} assuming:

$$L_{13} = L_{12} + L_{23} \tag{4.4}$$

$$L_{c^m n} = 0 \, , m \neq n \text{ (6 eq.)} \tag{4.5}$$

$$L_{c^m c^n} = 0 \text{ (3 eq.)} \tag{4.6}$$

The zero-sequence path is also split in three part to provide a closed path for the leakage fluxes.

The two mixed configuration with one concentric and two sandwich windings are given as examples how topological models can be derived for more complicated winding topologies. It is clear that the degree of complexity increases as the topology varies from simple concentric and sandwich configurations.

An equivalent mesh network [1] provides a general approach to represent an equivalent leakage model. Its application to a three-winding transformer with inclusion of a core terminal is shown in Fig. 4.9. This representation is independent from the winding topology, therefore the network elements have no physical meaning. The number of independent elements of a mesh network is $n(n-1)/2$. This ensures that any winding configuration can be modeled using this approach, and any measured short-circuit impedance can be represented without the knowledge of the actual winding configuration. With the assumptions (4.1)-(4.3), the model based on a mesh network is equivalent to the case of Fig. 4.5(c).

A geometrical model is proposed in [29] and is applied to the structure of Fig. 4.5(a). This model is based on the calculation of leakage inductances from the winding geometry [5]. The leakage inductance between two concentric coils i and j is:

$$L_{ij} = \frac{\mu_0 \pi N^2}{H_{eq}} \cdot \sum_{k=1}^{n} ATD_{ij} \tag{4.7}$$

$$ATD_{ij} = 1/3 \cdot T_i \cdot D_i + T_g \cdot D_g + 1/3 \cdot T_j \cdot D_j \tag{4.8}$$

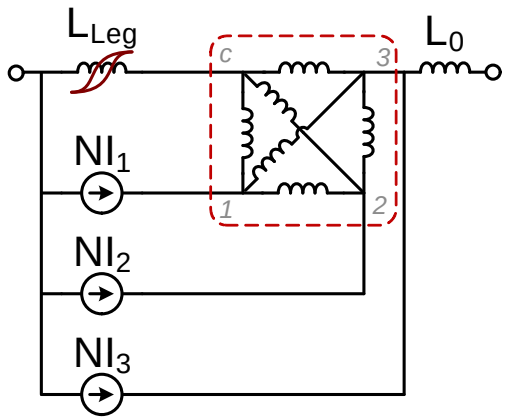

Figure 4.9: Equivalent mesh network for leakage representation.

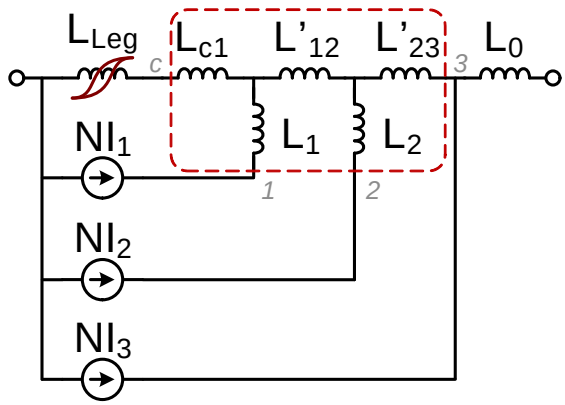

Figure 4.10: Geometrical model for leakage representation of concentric windngs.

with N the number of turns, H_{eq} the equivalent height of the coil included of the fringing effects, T the radial width of a winding, T_g the thickness of the air-gap between two windings, and D the mean diameter. The model can be represented by the geometrical equivalent electric network of Fig. 4.10. The sum of $L_{c1} + L'_{12} + L'_{23}$ represents the total leakage inductance between the core and the outermost winding. For concentric windings it is normally $L_{13} > L_{12} + L_{23}$ due to the linear magnetization in the winding thickness[1]. The negative inductances L_1 and L_2 compensate for the thickness of the windings. This network is intrinsically passive as the negative inductances L_1 and L_2 are smaller than L_{c1}, L'_{12} and L'_{23}:

$$L_{c1} \propto \frac{D_1 - D_c}{2} \tag{4.9}$$

$$L'_{12} \propto \frac{D_2 - D_1}{2} \tag{4.10}$$

$$L'_{23} \propto \frac{D_3 - D_2}{2} - \frac{T_3}{6} \tag{4.11}$$

$$L_1 \propto -\frac{T_1}{6} \tag{4.12}$$

$$L_2 \propto -\frac{T_2}{6} \tag{4.13}$$

The degrees of freedom of this representation is 5 as the constraints (4.1) and (4.2) are removed. In general this geometrical model provide $2n - 3$ independent impedance links for a n-winding transformer. The geometrical model is equivalent to the case of Fig. 4.5(c) if it is assumed $L_1 = 0$ and $L_2 = 0$.

The electric equivalent circuit of Figs. 4.6(c), 4.7(c), 4.8(c),4.9 and 4.10 can be replaced in Fig. 4.4 according to the appropriate winding configuration. The model can be extended to a number of winding higher than three using the same approach described here.

4.3 Implementation of the Jiles-Atherton Model and Parameter Estimation

The transient occurring after the disconnection of a transformer is called de-energization or ringdown transient and has been investigated in [Pb4]. Different models have been proposed to describe the hysteresis phenomenon, but only a few of them can represent demagnetization [113]. Two of the most relevant models are the Jiles-Atherton and the Preisach models introduced in Section 2.3.1. The Jiles-Atherton model is selected over the Preisach model for its simpler implementation and reduced computational effort [119]. In addition, the Preisach distribution function has to be identified using dedicated measurements techniques and only one of the model

[1] $L_{12} = L'_{12} + L_1 + L_2$, $L_{23} = L'_{23} + L_2$, and $L_{13} = L'_{12} + L'_{23} + L_1$ with L_1 and $L_2 < 0$

parameter is measurable, while all the Jiles-Atherton parameters are measurable and have a physical meaning [113].

The Jiles-Atherton hysteresis model is based on the magnetic quantities B, H, M, and μ. It is used to describe the nonlinear magnetization of electrical steel with focus on the behavior of a single lamination sheet. The model parameters can be extracted from hysteresis loops [126] measured with an Epstein frame or an analogous technique. The level of details can be greatly reduced when the interest is on the average response of the entire transformer core formed by a stack of laminations. This requires the reinterpretation of the Jiles-Atherton model in term of average quantities that are better described by the electric quantities flux-linkage and current:

$$\lambda = N\phi = BAN \tag{4.14}$$

$$i = \frac{Hl}{N} \tag{4.15}$$

$$B = \mu_0 \mu_r H \tag{4.16}$$

$$\lambda = Li \tag{4.17}$$

$$L = \mu_0 \mu_r N^2 \frac{A}{l} \tag{4.18}$$

$$\lambda(t) = \int v(t)\mathrm{d}t \tag{4.19}$$

Hysteresis loops of the magnetic material used in a transformer are rarely accessible for the calculation of the model parameters. Open-circuit test report data are normally the only information available for identifying the Jiles-Atherton parameters and extensive fitting is required.

The Jiles-Atherton model is converted from $B - H$ to $\lambda - i$ quantities by redefining the fundamental constructive equation:

$$B = \mu_0 \left(M + H\right) \tag{4.20}$$

$$\lambda = L_{inf} \left(i_M + i_E\right) \tag{4.21}$$

with i_M and i_E respectively defined as a magnetization and an electric currents, and L_{inf} as the differential slope of the hysteresis loop in complete saturation. The basic

Jiles-Atherton equations in term of $\lambda - i$ and in differential form are [Pb5]:

$$i_{Eeff} = i_E + \alpha\, i_M \tag{4.22}$$

$$i_{Man} = i_{Msat}\, \frac{a_1\, i_{Eeff} + i_{Eeff}^2}{a_3 + a_2\, i_{Eeff} + i_{Eeff}^2} \tag{4.23}$$

$$\delta = sign\left(\frac{\mathrm{d}i_E}{\mathrm{d}t}\right) \tag{4.24}$$

$$\frac{\mathrm{d}i_M}{\mathrm{d}i_E} = \left(c\, \frac{\mathrm{d}i_{Man}}{\mathrm{d}i_{Eeff}} + T\right) \frac{1}{1 - \alpha\, c\, \dfrac{\mathrm{d}i_{Man}}{\mathrm{d}i_{Eeff}}} \tag{4.25}$$

$$T = \begin{cases} 0 & \text{for } (i_{Man} - i_M)\delta > 0 \\ \dfrac{i_{Man} - i_M}{\frac{\delta\, K}{L_{inf}} - \frac{\alpha(i_{Man} - i_M)}{1-c}} & \text{for } (i_{Man} - i_M)\delta \leq 0 \end{cases} \tag{4.26}$$

These can be implemented in an EMTP program based on the trapezoidal rule of integration as following:

$$\Delta\lambda = \left((v(t - \mathrm{d}t) + v(t))\frac{\mathrm{d}t}{2}\right) \cdot \frac{1}{A_{REL}} \tag{4.27}$$

$$\lambda(t) = \lambda(t - \mathrm{d}t) + \Delta\lambda \tag{4.28}$$

$$\begin{cases} \Delta i_{Emax} = \dfrac{\Delta\lambda}{L_{inf}} \\ \Delta i_E = Q \cdot \Delta i_{Emax} \\ \Delta i_M = \Delta i_{Emax} - \Delta i_E \\ i_E(t) = i_E(t - \mathrm{d}t) + \Delta i_E \\ i_M(t) = i_M(t - \mathrm{d}t) + \Delta i_M \\ \delta = sign(\Delta\lambda) \\ \Delta i_{Eeff} = i_{Eeff}(t) - i_{Eeff}(t - \mathrm{d}t) \\ \Delta i_{Man} = i_{Man}(t) - i_{Man}(t - \mathrm{d}t) \\ \dfrac{\mathrm{d}i_M}{\mathrm{d}i_E} = \left(c\, \dfrac{\Delta i_{Man}}{\Delta i_{Eeff}} + T\right) \dfrac{1}{1 - \alpha\, c\, \dfrac{\Delta i_{Man}}{\Delta i_{Eeff}}} \end{cases} \tag{4.29}$$

$$Q = \frac{1}{\dfrac{\mathrm{d}i_M}{\mathrm{d}i_E} + 1} \tag{4.30}$$

$$i(t) = (i_E(t) + i_{clc}(t) + i_{exc}(t)) \cdot l_{REL} = \tag{4.31}$$

$$= \left(i_E(t) + k_1\, v(t) + k_2\, \sqrt{v(t)}\right) \cdot l_{REL} \tag{4.32}$$

where the set of equations (4.29) uses a guessed initial value of Q $(0 < Q < 1)$ and has to be iterated in order to satisfy (4.30). The variables are defined as:

- λ: flux-linkage;
- i_E: electric current;
- i_{Eeff}: effective electric current;
- i_{Emax}: electrical current of a coreless transformer;
- i_M: magnetization current;
- i_{Man}: anhysteretic magnetization current;
- A_{REL}, l_{REL}: relative core dimensions.

It is possible to initialize the residual flux in (4.28) defining $\lambda(t = 0) = \lambda_{res}$.

A total of eight (plus two optional) parameters have to be estimated:

- L_{inf}: inductance in complete saturation;
- i_{Msat}: saturation level of the anhysteretic curve;
- a_1, a_2, a_3: parameters of the anhysteretic curve
- α: interdomain coupling, controls the slope of the hysteresis loop
- c: ratio of the initial normal to the initial anhysteretic susceptibility, controls the transition smoothness of the knee area;
- K: width of the base of the hysteresis loop, main contribution to the losses;
- k_1, k_2: rate dependent terms for classical and excessive eddy current (optional).

A comprehensive explanation of the function and the numerical determination of each parameter can be found in [127]. The implementation of this model in an ATP routine is reported in Appendix A.

To illustrate the capabilities of the implemented Jiles-Atherton module and the parameter estimation procedure, a simple example is presented here. A single-phase transformer is chosen to avoids many of the complication related to the fitting of the parameters for topology-correct three-phase models. The parameter estimation approach detailed here is applicable also to three-phase transformer modeled as single-phase equivalent (disregarding the core topology). The data used for this example are for a 63 kVA 135.7 V single-phase transformer and are given in Table 4.1. The parameter fitting process is divided in two parts: anhysteretic curve and loss parameters.

The Jiles-Atherton parameters i_{Msat}, a_1, a_2, and a_3 describe the anhysteretic magnetization curve of (4.23). The values of Table 4.1 are converted to flux-linkage and current peak values using the approach described in [Pb1]. Equation (4.23) is then fitted to the peak flux-linkage/current values with a numerical optimization

TABLE 4.1
OPEN-CIRCUIT DATA.

Voltage [pu,rms]	**Losses** [%]	**Current** [%,rms]
0.80	0.56	0.27
0.95	0.85	0.54
1.00	0.96	0.70
1.03	1.06	0.88
1.07	1.19	1.24
1.11	1.33	1.84
1.15	1.49	2.90
1.20	1.76	5.55
1.28	2.47	15.28

routine[2]. The result is shown in Fig. 4.11 where the flux linkage is calculated[3] by $\lambda_{an} = L_{inf}\,(i_{Man} + i_{Eeff})$. L_{inf} is estimated from geometrical design data as detailed in [Pb7].

It is reasonable to assume that the shape of the anhysteretic curve does not change as a function of frequency and magnetization level. The anhysteretic curve parameters are therefore assumed constant and are not changed during the estimation of the remaining parameters.

The traditional Jiles-Atherton model only account for rate independent losses, that are hysteresis losses. Rate dependent losses due to eddy current can be added to the model as introduced in Section 2.3. The focus of the model proposed in this work is to represent the mean response of the bulk magnetic material, therefore the flux is assumed uniformly distributed in the cross-sectional area of of a limb.

The values for "HGO DG 9 mils" at 50 Hz of Fig. 2.11 (36%, 22%, and 41%) are used here for the splitting of the total no-load losses at rated excitation. The coefficient k_1 and k_2 can then be determined from (2.31) and the eddy current loss contributions estimated as a function of the excitation.

The remaining Jiles-Atherton model parameters α, c, and K are then calculated with an optimization procedure. A least-squares curve-fitting method is used to fit the losses calculated with the model to the test-report losses.

The rms values of test-report and calculated no-load currents are compared in Fig. 4.12 as a function of the excitation level. The rms value of the total no-load current is accurately predicted by the model. The test report and the calculated losses are compared in Fig. 4.13. In this case the agreement between test report and calcu-

[2]In MATLAB, the "lsqcurvefit" function solves nonlinear curve-fitting problems in least-squares sense.

[3]This is a valid approximation as $\alpha << 1$ such that $\alpha i_M << i_E$ resulting in $i_E \approx i_{Eeff}$.

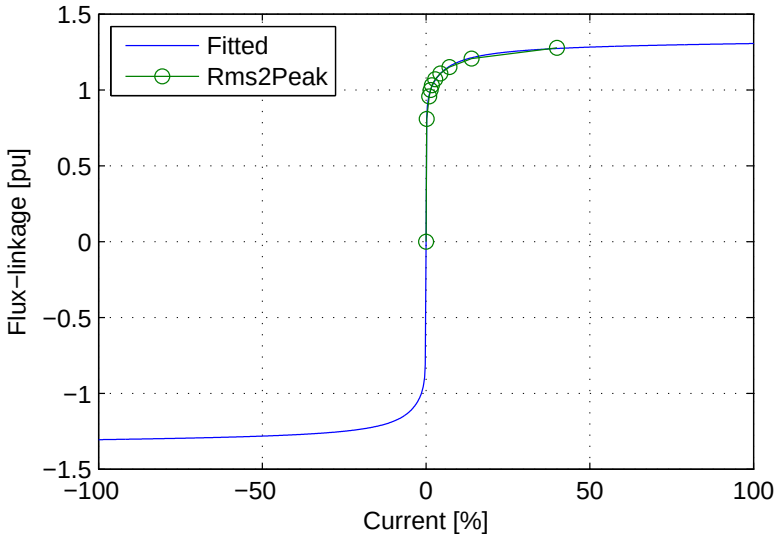

Figure 4.11: Anhisteretic curve fitting.

lated losses is quite poor. The model parameter are selected to fit the losses at rated excitation, but the model fails to represent the nonlinear loss curve. This has been observed also for the three-phase transformer modeled in [Pb5].

References [128,129] suggest that the Jiles-Atherton parameters are not constant, but should be expressed as a function of the excitation level. Wang *et al.* [128] propose empirical functions that modifies both the anhysteretic curve parameters and the loss parameters. Toman *et al.* [129] propose a Gaussian function to vary the single parameter K (parameter that strongly relates to the losses). In this work, very simple empirical functions are proposed to vary three model parameters:

$$K = K_0 \cdot \frac{|v(t)|}{\sqrt{2}V_{n\,ph}} \quad \text{with} \quad K \geq K_0 \tag{4.33}$$

$$c = c_0 \cdot \frac{\sqrt{2}V_{n\,ph}}{|v(t)|} \quad \text{with} \quad c \geq c_0 \tag{4.34}$$

$$\alpha = \alpha_0 \cdot \frac{|\lambda(t)|}{\lambda_n} \tag{4.35}$$

Fig. 4.14 shows that a much improved fitting of the test report values can be acheived using a Jiles-Atherton model with variable parameters. The current waveforms and the shape of the hysteresis loops are compared in Figs. 4.15-4.17 for the models with constant and variable parameters. The physical validity of the hysteresis loops of Fig. 4.17(b) has to be verified and the functions describing the variation of the model parameters (4.33)-(4.35) may be improved. It is difficult to collect published material that discusses the variation of the hysteresis loops and losses as a function of both excitation and frequency for the same material. An experimental setup needs to be established to gather data in order to continue the development of a robust method for estimating the Jiles-Atherton parameters from open-circuit test-report data.

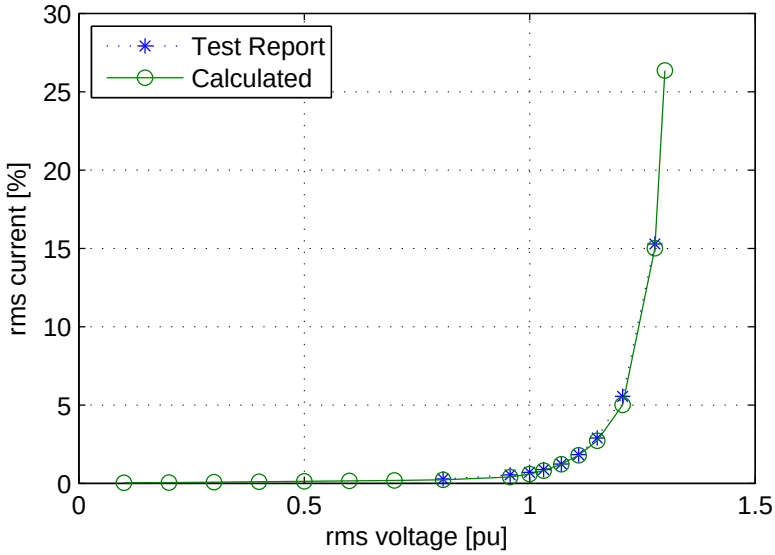

Figure 4.12: Test report and calculated rms no-load current.

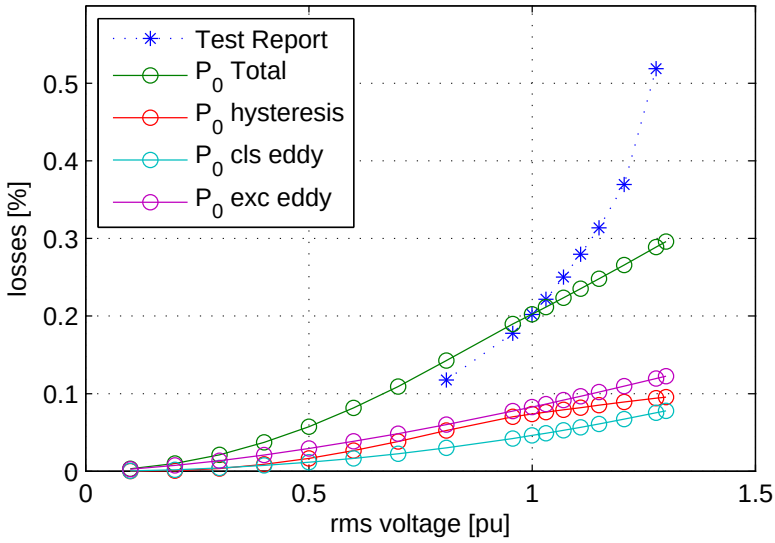

Figure 4.13: Test report and calculated losses. Constant parameters.

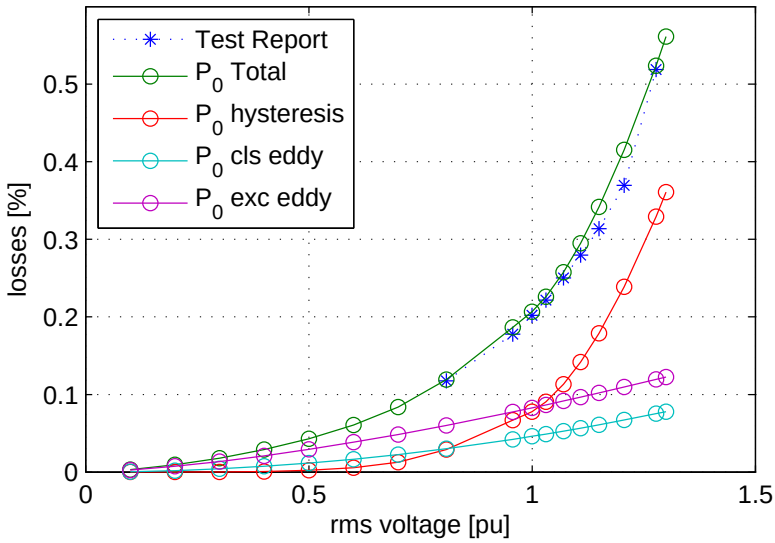

Figure 4.14: Test report and calculated losses. Variable parameters.

The fitting procedure is non-trivial for three-phase transformer models with a topologically correct core model. The core is divided in several sections as shown in Fig. 4.4. Several instances of the Jiles-Atherton module, one for each transformer limb, have to be solved together. An extensive fitting and optimization procedure is required to determine the parameters for each transformer limb. The circuit of Fig. 4.4 is simplified by disregarding the leakage inductances and the winding resistances. The reduced circuit is valid for the representation of an open-circuit test as long as the no-load current remains relatively low and the voltage drops on the disregarded inductances and resistances can be neglected. The average rms value of the three-phase currents and the total active losses calculated with the simplified model for different voltage levels are fitted to the test-report data. This is a nonlinear and multidimensional optimization problem. It can be solved numerically with least-squares or genetic algorithm optimization routines. It is reasonable to assume that the core material has the same characteristics in all transformer limbs. The nonlinear characteristic of two blocks of the same material is therefore scaled based on their relative cross-sectional area and length dimensions:

$$L_1(i) = \mu(i)\frac{A_1}{l_1}N^2 \tag{4.36}$$

$$L_2(i) = \mu(i)\frac{A_2}{l_2}N^2 \tag{4.37}$$

$$L_2(i) = L_1(i)\frac{A_2}{A_1}\frac{l_1}{l_2} = L_1(i)\frac{A_{REL}}{l_{REL}} \tag{4.38}$$

The total number of parameters to be estimated for the Jiles-Atherton model remains the same as for a single-phase transformer and does not multiply by the number of limbs.

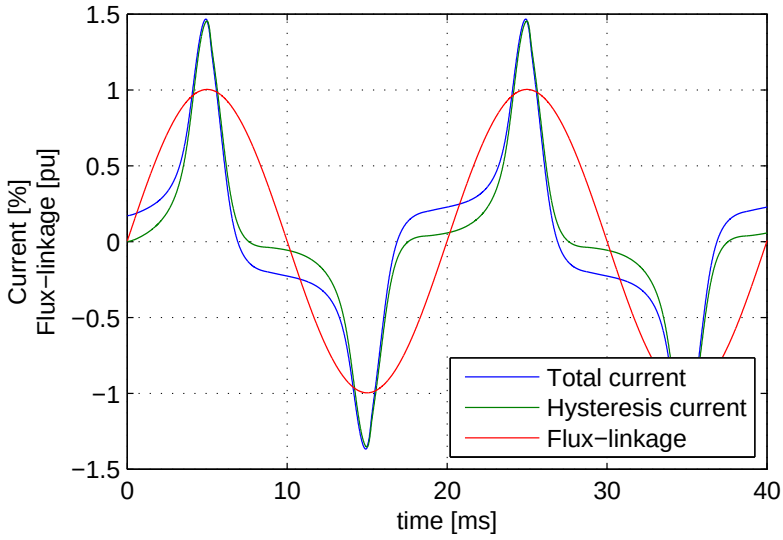

(a) *Model with constant parameters.*

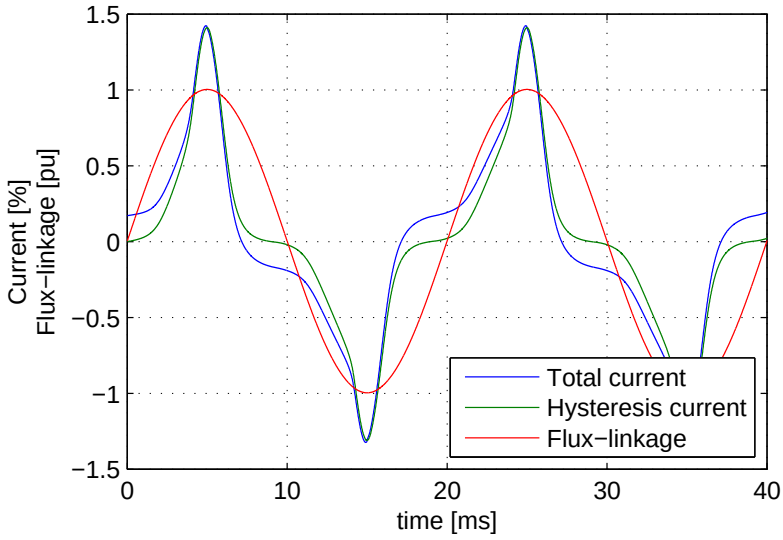

(b) *Model with variable parameters.*

Figure 4.15: Current wave at rated excitation.

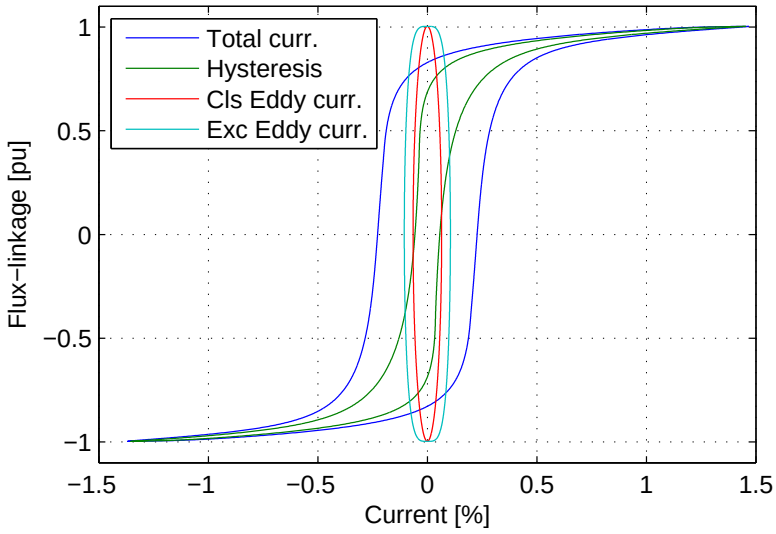

(a) *Model with constant parameters.*

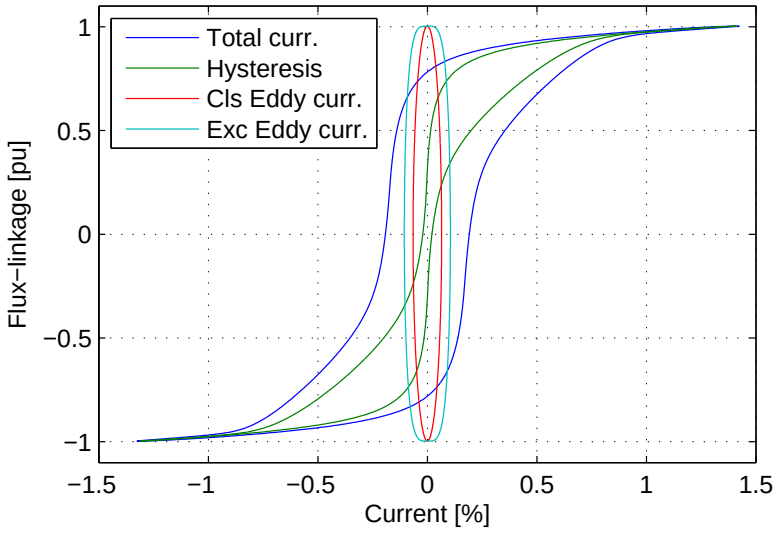

(b) *Model with variable parameters.*

Figure 4.16: Hysteresis loop at rated excitation.

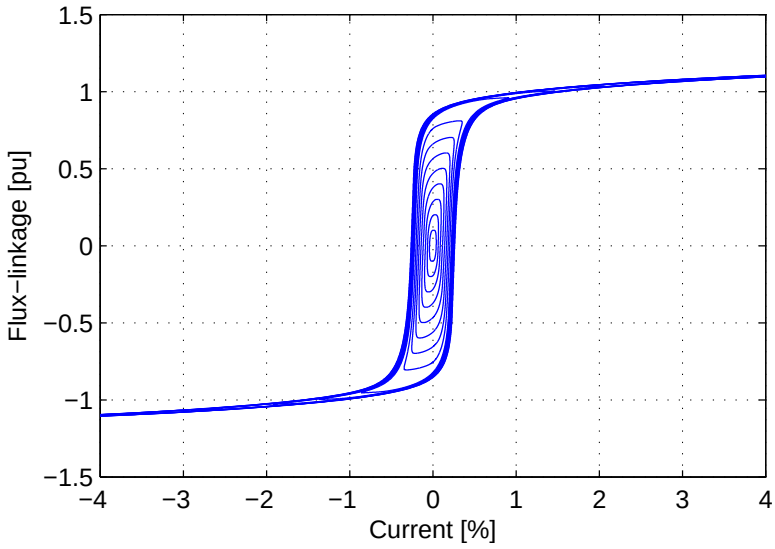

(a) *Model with constant parameters.*

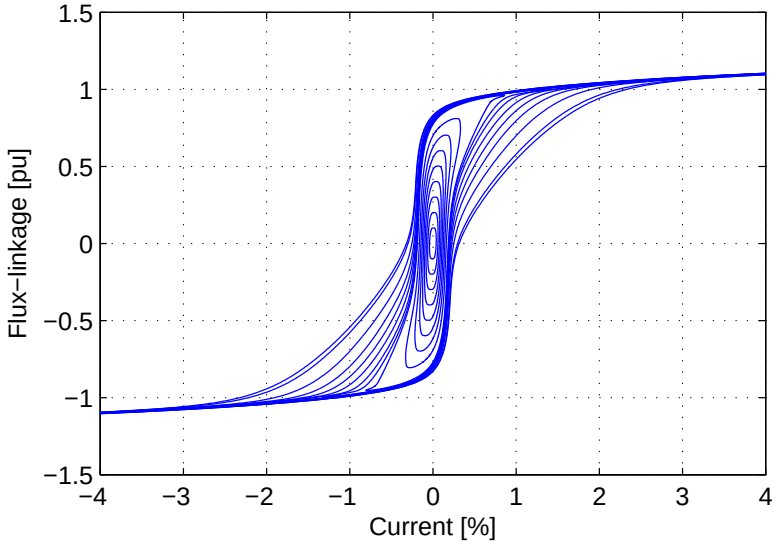

(b) *Model with variable parameters.*

Figure 4.17: Expansion of hysteresis loops

CHAPTER 5

CONCLUSIONS

5.1 Contribution of the Publications

[Pb1] Analytical Algorithm for the Calculation of Magnetization and Loss Curves of Delta Connected Transformers

Abstract - This paper proposes an analytical algorithm for the computation of the magnetization and loss curves for a transformer from standard no-load test report data. This is the input to standard transformer models for power system simulation. In the case of delta coupled windings the conversion from test report rms line quantities to peak phase values requires processing of the triplen harmonics in the current. This is handled analytically in the paper with utilization of the concept of incremental inertance and conductance. The analysis shows that only the third harmonic needs to be treated to reach sufficient accuracy within the measurement errors. The test case with a 290 MVA GSU transformer shows an increase in the calculated current of above 10% at rated voltage with proper triplen harmonic handling. This difference will increase considerably with excitation voltage.

Contribution - Frequently, the saturation curve is not defined as $\lambda = f(i)$, but as root-mean-square characteristics $V_{RMS} = f(I_{RMS})$. The contribution of this paper is the investigation of the influence of the delta connection in a three-phase transformer. In particular, the major contribution of this paper is the development of an analytical algorithm able to handle a delta connection.

[Pb2] Implementation and Verification of the Hybrid Transformer Model in ATPDraw

Abstract - The paper documents a new transformer model in ATPDraw called XFMR. This model handles 3-phase transformers with two or three windings. Autotransformers and all Wye and Delta couplings are supported. The model includes an inverse inductance matrix for the leakage description, optional frequency dependent winding resistance, capacitive coupling, and a topologically correct core model (3- and 5-legged) with individual saturation and losses in legs and yokes. Three different sources of parameters are supported; typical values, standard test reports, and design information. The hybrid model XFMR is compared to the UMEC model in PSCAD showing good agreement at rated, stationary operation, but considerable differences in transient situations. Both models need further benchmarking and development to reproduce all switching transient behaviors properly.

Contribution - The transformer model described in here can, to some extent, be considered as the state-of-the-art in low-frequency transformer model and constitute the starting point for this work. The main contribution of this paper in connection with this work is to emphasize the main weaknesses of two transformer models: the accuracy of the response in complete saturation and the representation of remanence.

[Pb3] Transformer Short-Circuit Representation: Investigation of Phase-To-Phase Coupling

Abstract - Transformer short-circuit behavior is typically represented in electromagnetic transient simulation programs by the inverse of the leakage inductance matrix, also known as the A-matrix or [A]. The terms of [A] represent the magnetic coupling (flux linkages) between windings, i.e. between coils on the same core leg. In addition to the representation of coupling between windings of the same phase, intra-phase coupling effects can also be included. This paper investigates the sensitivities of results of EMTP-type simulation to intra-phase entries of [A]. A method for obtaining [A] that includes intra-phase coupling is developed and verified by comparing simulation results with laboratory measurements. The percent error between measured and simulated short-circuit currents that result from implementing a full and simplified [A] was quantified. A correlation of the size of the elements representing intra-phase coupling in [A] with transformer MVA size is investigated and valuable conclusions and recommendations are made.

Contribution - The main contribution of this work is the verification that intra-phase entries of [A] are small as the contribution from phase-to-phase leakage fluxes is insignificant. The phase-to-phase coupling can therefore be assumed concentrated in the transformer core and the leakage representation decoupled for the three phases.

[Pb4] On the Ringdown Transient of Transformers

Abstract - This paper details the analysis of transformer ringdown transients that determine the residual fluxes. A novel energy approach is used to analyze the causes of transformer saturation during de-energization. Coupling configuration, circuit breaker and shunt capacitor influence on residual flux have been studied. Flux-linked initialization suggestions are given at the end of the paper.

Contribution - The study of the remanence or residual flux in a transformer is addressed in this paper. A ringdown transient occurs after the disconnection of a transformer and determines the residual fluxes. The main contributions of this paper are: a novel energy approach for the analysis of a ringdown transient, the observation that shunt capacitances has a main influence on the residual magnetization and ringdown transient duration, and that there may exist a phase correlation between rated flux-linkage and residual magnetization.

[Pb5] Hysteretic Iron-Core Inductor for Transformer Inrush Current Modelling in EMTP

Abstract - A crucial element of transformer models for transient simulation is the representation of the core. The modelling of non-linear hysteretic inductors required to properly represent a transformer core is a challenge in an electromagnetic transient program. The simulation of transients such as inrush and ferroresonance require a correct handling of nonlinear and frequency dependent losses, accurate hysteresis loop representation, possibility of flux initialization, and a proper automatic initialization by disconnection transients. This paper analyses standard available models and tests an advanced hysteretic model based on the Jiles-Atherton theory. This model is implemented in a topologically correct core representation and the parameters are obtained from test report data. Due to the interaction of several nonlinear elements, the solution of such model is still a challenge in classical EMTP programs based on compensation method. Good agreement with ringdown and inrush measurements is achieved.

Contribution - The study carried out in [Pb2, Pb4] highlights the importance of the representation of residual fluxes in a transformer model. A Jiles-Atherton module including eddy current effects is proposed here to enable the estimation of residual fluxes and the self-initialization of the residual fluxes in a transformer model by de-energization. The Jiles-Atherton magnetic model has been typically used to represent the magnetic properties of ferromagnetic material. Parameters are normally extracted from $B - H$ hysteresis loops. Here the Jiles Atherton model is implemented based on electrical quantities and the parameters are obtained from standard open-circuit test report data. This paper also reveal that the classical Jiles-Atherton model has some limitations in the representation of the average core losses as a function of the excitation level.

[Pb6] Systematic Switching Study of Transformer Inrush Current: Simulations and Measurements

Abstract - The verification of a transformer model for the representation of transient behaviors such as inrush and ringdown is not trivial as several parameters may influence measurements and simulations. The purpose of this paper is to suggest a laboratory testing strategy and to present an enhanced transformer model. A special emphasis is given to parameters estimation. The objective is to be able to obtain most of the model data directly from standard test report data. Design data are used to verify the parameters and to have a better estimation of scaling factors. The model is verified against few measurements and good agreement is observed for residual flux, inrush current first peak and decay.

Contribution - A three-phase three-legged transformer model for the simulation of inrush currents is proposed here. The model has been extensively verified for its capability to accurately predict both residual flux values and energization transients. The residual fluxes calculated with the proposed model are in agreement with measurements. While it is typical to tune transformer parameters to match a single inrush current measurement this has not been done here. The main contribution of the paper is the verification that a lumped parameter transformer model derived from test-report data can accurately represent inrush currents of different magnitudes.

[Pb7] Transformer Model for Inrush Current Calculations: Simulations, Measurements and Sensitivity Analysis

Abstract - The modeling of inrush currents that occur upon energization of a transformer is a challenge for EMTP-type programs due to limitations in available transformer models and ability to determine and specify initial flux. The estimation of transformer model parameters is also an issue. This paper presents a transformer model for low- and mid- frequency transient studies with focus on the behavior in saturation and the estimation of residual fluxes. The comparison of the simulation results with analytical calculations and measurements proves the capability of the model to accurately represent energization and de-energization transients of a three-legged-core distribution transformer. A novel property is the ability of auto initialization after disconnection, made possible by the implementation of a hysteretic core model which properly simulates and remembers residual flux from the previous de-energization. Special attention is paid to parameter estimation. Detailed core and winding design data are not used as they are seldom available from the manufacturer. A sensitivity analysis is performed to verify the influence of each parameter on the inrush current envelope curve. It is observed that the parameter that most influences the current amplitude is the slope of the magnetization curve at extreme saturation.

Contribution - The three-phase three-legged transformer model with focus on the behavior in saturation is further detailed here. The model is verified with analytical

formula and measurements. A sensitivity analysis is performed to verify the influence of the model parameters on the inrush current first peak and rate of decay. The main contribution of the papers is the development of a transformer model whose parameters are derived mainly from test-report data, with a limited number of low-detail design data required to achieve high accuracy. The model has been verified against inrush current measurements. It is shown that is able to reproduce inrush current transient over a wide range of current magnitude without a tuning of the parameters. The paper also suggests to include additional data valuable for transformer modeling in the test report.

[Pb8] Novel Approach for Reducing Transformer Inrush Currents. Laboratory Measurements, Analytical Interpretation and Simulation Studies

Abstract - Transformer inrush currents can lead to a reduction of transformer life time and inadvertent tripping of relays. This paper investigates a novel approach for minimizing the inrush current with a potential application in circuit breaker control strategies without independent-pole operation and residual flux estimation. For the analyzed transformer, the worst case inrush current is halved compared to the rapid-closing switching strategy. Measurements of inrush current transients are performed on an unloaded 11 kV distribution transformer varying disconnection and connection instants systematically. This reveals a characteristic pattern in the extremal value of the inrush current as a function of switching times. The pattern is reproduced with simulations and extended to alternative winding configurations. A condition for minimum inrush currents, consistent for all phases and winding configurations, is identified and explained physically. The impact of the current chopping capability of the circuit breaker is important and is discussed in this paper.

Contribution - The capability of auto-initialization of the model after disconnection is due to a core model based on Jiles-Atherton hysteretic modules. This capability has been exploited here where a possible application of the model is depicted. The systematic measurements reveal a characteristic map of the inrush current peaks that the proposed model is capable to reproduce. A further investigation of this pattern leads to the definition of a novel inrush current mitigation strategy. The laboratory setup used to perform systematic open-close switching operations is also presented.

5.2 Concluding Remarks

The transformer model developed in this work has been verified from inrush current measurements on a 300 kVA 11.430/0.235 kV Yyn-coupled unit. In addition, measurements performed on a larger distribution transformer and on three power transformers qualitatively confirm the validity of the study for larger units.

The Jiles-Atherton model has been implemented for complex core topology. The benefit is the possibility to perform de-energization simulations and automatically initialize the residual fluxes in the transformer limbs. This allowed to reproduce the systematic switching pattern measured in the laboratory.

The proposed model enables to perform studies and obtain results that would have been difficult to achieve without such advanced model. For example, the application of this model to the study of energization transients allowed to propose a novel inrush current mitigation strategy.

An analytical handling of no-load data for the derivation of the magnetization characteristic for transformer with delta-coupling has also been proposed. The benefit is a more accurate estimation of some of the transformer parameters.

5.3 Recommendations for Further Work

The proposed transformer model is considered to be a general model. However, it has been tested to produce accurate results only for inrush current with simultaneous switching and ungrounded wye connection. Further verification of the model is required to prove its accuracy under unbalanced energization, synchronized switching and other type of transients.

Systematic measurements should be performed for grounded wye and delta coupled transformers. This has not been carried out due to technical limitations of the laboratory.

It is suggested that the model is tested for large power transformers. The main difficulty here is related to the availability of a good test case: accessibility to transformer data and accurate measurements are required.

The residual flux is assumed to be constant after the disconnection of the transformer. This assumption should be further verified as slow decay of the residual flux may be possible in minutes or hours from its de-energization. An accurate and repeatable measurement technique should be developed for the estimation of residual fluxes. The calculation of the residual flux by time integral of the voltage is not suitable over such long time intervals.

The Jiles-Atherton model needs to be improved and verified for the accurate representation of core losses. Recommendations for further improvements in this field are

discussed in Section 4.3.

The availability of some of the model parameters is still a concern. These parameter are often difficult to measure or estimate, and have an high impact on the accuracy of the simulation results. The scientific community interested in transformer modeling should work for the awareness of the transformer manufacturers and utilities regarding the transformer modeling issues. This may have an impact on the refinement of standards for the inclusion in factory test reports of additional data relevant for the transient modeling of a transformer.

REFERENCES

[1] L. F. Blume, *Transformer engineering : a treatise on the theory, operation, and application of transformers*, 2nd ed. New York, N.Y.: John Wiley and Sons, Inc., 1951.

[2] A. Greenwood, *Electrical Transients in Power Systems*, 2nd ed. Troy, N.Y.: John Wiley and Sons, Inc., 1991.

[3] M. J. Heathcote, *J&P Transformer Book*, 12th ed. Newnes, 1998.

[4] A. Gole, J. A. Martinez-Velasco, and K. A. J. F., *Modeling and Analysis of System Transients Using Digital Programs*. IEEE PES Special Publication, Jan. 1999, no. TP-133-0.

[5] S. V. Kulkarni and S. A. Khaparde, *Transformer engineering: design and practice*, ser. Power engineering. New York, N.Y.: Marcel Dekker, Inc., 2004, vol. 25.

[6] F. de Leon and A. Semlyen, "Efficient calculation of elementary parameters of transformers," *IEEE Trans. Power Del.*, vol. 7, no. 1, pp. 376–383, Jan. 1992.

[7] F. de Leon and A. Semlyen, "Complete transformer model for electromagnetic transients," *IEEE Trans. Power Del.*, vol. 9, no. 1, pp. 231–239, 1994.

[8] M. Elleuch and M. Poloujadoff, "A contribution to the modeling of three phase transformers using reluctances," *IEEE Trans. Magn.*, vol. 32, no. 2, pp. 335–343, Mar. 1996.

[9] J. A. Martinez and B. A. Mork, "Transformer modeling for low- and mid-frequency transients - a review," *IEEE Trans. Power Del.*, vol. 20, no. 2 II, pp. 1625–1632, 2005.

[10] J. A. Martinez, R. Walling, B. A. Mork, J. Martin-Arnedo, and D. Durbak, "Parameter determination for modeling system transients - part III: Transformers," *IEEE Trans. Power Del.*, vol. 20, no. 3, pp. 2051–2062, Jul. 2005.

[11] D. L. Stuehm, B. A. Mork, and D. D. Mairs, "Five-legged core transformer equivalent circuit," *IEEE Trans. Power Del.*, vol. 4, no. 3, pp. 1786–1793, Jul. 1989.

[12] X. S. Chen and P. Neudorfer, "Digital model for transient studies of a three-phase five-legged transformer," *IEE Proceedings Generation, Transmission and Distribution*, vol. 139, no. 4, pp. 351–358, Jul. 1992.

[13] E. F. Fuchs, Y. You, and D. J. Roesler, "Modeling and simulation, and their validation of three-phase transformers with three legs under DC bias," *IEEE Trans. Power Del.*, vol. 14, no. 2, pp. 443–449, Apr. 1999.

[14] W. Enright, O. B. Nayak, G. D. Irwin, and J. Arrillaga, "An electromagnetic transients model of multi-limb transformers using normalized core concept," in *IPST'97 - International Conference on Power System Transients*, Seattle, Washington, Jun. 1997, pp. 93–98.

[15] W. Enright, O. Nayak, and N. Watson, "Three-phase five-limb unified magnetic equivalent circuit transformer models for PSCAD V3," in *IPST'99 - International Conference on Power System Transients*, Budapest, Hungary, Jul. 1999, pp. 462–467.

[16] A. D. Theocharis, J. Milias-Argitis, and T. Zacharias, "Three-phase transformer model including magnetic hysteresis and eddy currents effects," *IEEE Trans. Power Del.*, vol. 24, no. 3, pp. 1284–1294, Jul. 2009.

[17] M. Elleuch and M. Poloujadoff, "Anisotropy in three-phase transformer circuit model," *IEEE Trans. Magn.*, vol. 33, no. 5, pp. 4319–4326, Sep. 1997.

[18] M. Elleuch and M. Poloujadoff, "New transformer model including joint air gaps and lamination anisotropy," *IEEE Trans. Magn.*, vol. 34, no. 5, pp. 3701–3711, Sep. 1998.

[19] E. C. Cherry, "The duality between interlinked electric and magnetic circuits and the formation of transformer equivalent circuits," *Proceedings of the Physical Society. Section B*, vol. 62, pp. 101–111, Feb. 1949.

[20] S. Leva and A. P. Morando, "Topological transition from magnetic networks to the electric equivalent ones when iron losses are present," in *Proc. 43rd IEEE Midwest Symposium on Circuits and Systems*, vol. 2, Aug. 8–11, 2000, pp. 642–645.

[21] G. R. Slemon, "Equivalent circuits for transformers and machines including non-linear effects," *Proceedings of the Institution of Electrical Engineers*, vol. 100, no. 1, pp. 129 – 143, Jul. 1953.

[22] A. P. Morando and S. Leva, *Mutuo induttore tempo invariante*, 1st ed. Bologna, IT: Esculapio, Jun. 2001.

[23] C. Saldana and G. Calzolari, "Analysis of core type transformer models based on the principle of duality in electromagnetic transients studies," in *IPST'97 - International Conference on Power System Transients*, Seattle, Washington, Jun. 1997, pp. 87–92.

[24] E. P. Dick and W. Watson, "Transformer models for transient studies based on field measurements," *IEEE Trans. Power App. Syst.*, no. 1, pp. 409–419, Jan. 1981.

[25] C. M. Arturi, "Transient simulation and analysis of a three-phase five-limb step-up transformer following an out-of-phase synchronization," *IEEE Trans. Power Del.*, vol. 6, no. 1, pp. 196–207, Jan. 1991.

[26] B. A. Mork, "Five-legged wound-core transformer model: derivation, parameters, implementation and evaluation," *IEEE Trans. Power Del.*, vol. 14, no. 4, pp. 1519–1526, Oct. 1999.

[27] H. W. Dommel and et.al., *Electromagnetic Transients Program Reference Manual (EMTP Theory Book)*. Portland, OR: Prepared for BPA, Aug. 1986.

[28] T. Henriksen, "How to avoid unstable time domain responses caused by transformer models," *IEEE Trans. Power Del.*, vol. 17, no. 2, pp. 516–522, Apr. 2002.

[29] T. Henriksen, "Transformer leakage flux modeling," in *IPST'01 - International Conference on Power System Transients*, no. 059, Rio de Janeiro, Brazil, Jun. 2001.

[30] R. B. Shipley, D. Coleman, and C. F. Watts, "Transformer circuits for digital studies," *Transactions of the American Institute of Electrical Engineers, Part III (Power Apparatus and Systems)*, vol. 81, no. 64, pp. 1028 – 1031, Feb. 1963.

[31] V. Brandwajn, H. W. Dommel, and I. I. Dommel, "Matrix representation of three-phase n-winding transformers for steady-state and transient studies," *Power Apparatus and Systems, IEEE Transactions on*, vol. PAS-101, no. 6, pp. 1369 –1378, June 1982.

[32] B. C. Papadias, N. D. Hatziargyriou, J. A. Bakopoulos, and J. M. Prousalidis, "Three phase transformer modelling for fast electromagnetic transient studies," *Power Delivery, IEEE Transactions on*, vol. 9, no. 2, pp. 1151 –1159, Apr 1994.

[33] F. de Leon and A. Semlyen, "Reduced order model for transformer transients," *IEEE Trans. Power Del.*, vol. 7, no. 1, pp. 361–369, Jan. 1992.

[34] A. Narang and R. H. Brierley, "Topology based magnetic model for steady-state and transient studies for three-phase core type transformers," *IEEE Trans. Power Syst.*, vol. 9, no. 3, pp. 1337–1349, Aug. 1994.

[35] B. A. Mork, F. F. Gonzalez, and D. Ishchenko, "Leakage inductance model for autotransformer transient simulation," in *IPST'05 - International Conference on Power System Transients*, no. IPST05-248, Montreal, Canada, Jun. 2005.

[36] B. A. Mork, F. Gonzalez, D. Ishchenko, D. L. Stuehm, and J. Mitra, "Hybrid transformer model for transient simulation: Part I: development and parameters," *IEEE Trans. Power Del.*, vol. 22, no. 1, pp. 248–255, Jan. 2007.

[37] B. A. Mork, F. Gonzalez, D. Ishchenko, D. L. Stuehm, and J. Mitra, "Hybrid transformer model for transient simulation: Part II: laboratory measurements and benchmarking," *IEEE Trans. Power Del.*, vol. 22, no. 1, pp. 256–262, Jan. 2007.

[38] B. A. Mork, D. Ishchenko, F. Gonzalez, and S. D. Cho, "Parameter estimation methods for five-limb magnetic core model," *IEEE Trans. Power Del.*, vol. 23, no. 4, pp. 2025–2032, Oct. 2008.

[39] *IEEE standard test code for liquid-immersed distribution, power, and regulating transformers*, IEEE Std. C57.12.90-1999, 1999.

[40] *Guide for Transformer Loss Measurement*, IEEE Std. C57.123, 2002.

[41] *Power transformer - Part 1: General*, IEC Std. 60 076-1 Ed. 2.1, Apr. 2000.

[42] D. N. Ewart, "Digital computer simulation model of a steel-core transformer," *IEEE Trans. Power Del.*, vol. 1, no. 3, pp. 174–183, Jul. 1986.

[43] S. G. Abdulsalam, W. Xu, W. L. A. Neves, and X. Liu, "Estimation of transformer saturation characteristics from inrush current waveforms," *IEEE Trans. Power Del.*, vol. 21, no. 1, pp. 170–177, Jan. 2006.

[44] M. Rioual, T. Guillot, and C. C., "Determination of the air-core reactance of transformers by analytical formulae for different topological configurations and its comparison with an electromagnetic 3D approach." in *IEEE/PES General Meeting*, Calgary, Canada, Jul. 2009.

[45] Y. Nakachi, R. Hatano, T. Matsubara, and Y. Uemura, "Calculation of transformer saturated leakage inductance based on field test data," in *Proc. IEEE Power Engineering Society General Meeting*, 2006, p. 7pp.

[46] F. de Leon and J. A. Martinez, "Dual three-winding transformer equivalent circuit matching leakage measurements," *IEEE Trans. Power Del.*, vol. 24, no. 1, pp. 160–168, Jan. 2009.

[47] A. Semlyen and F. De Leon, "Eddy current add-on for frequency dependent representation of winding losses in transformer models used in computing

electromagnetic transients," *IEE Proceedings Generation, Transmission and Distribution*, vol. 141, no. 3, pp. 209–214, May 1994.

[48] T. Noda, H. Nakamoto, and S. Yokoyama, "Accurate modeling of core-type distribution transformers for electromagnetic transient studies," *IEEE Trans. Power Del.*, vol. 17, no. 4, pp. 969–976, Oct. 2002.

[49] W. L. A. Neves, H. W. Dommel, and W. Xu, "Practical distribution transformer models for harmonic studies," *IEEE Trans. Power Del.*, vol. 10, no. 2, pp. 906–912, Apr. 1995.

[50] C. Andrieu, E. Dauphant, and D. Boss, "A frequency-dependent model for a MV/LV transformer," in *IPST'99 - International Conference on Power System Transients*, no. 098Ű18.2, Budapest, Hungary, Jun. 1999, pp. 468–473.

[51] B. Gustavsen, "Wide band modeling of power transformers," *IEEE Trans. Power Del.*, vol. 19, no. 1, pp. 414 – 422, Jan. 2004.

[52] M. Popov, L. van der Sluis, G. C. Paap, and H. De Herdt, "Computation of very fast transient overvoltages in transformer windings," *IEEE Trans. Power Del.*, vol. 18, no. 4, pp. 1268–1274, Oct. 2003.

[53] M. Popov, L. van der Sluis, R. P. P. Smeets, and J. L. Roldan, "Analysis of very fast transients in layer-type transformer windings," *IEEE Trans. Power Del.*, vol. 22, no. 1, pp. 238–247, Jan. 2007.

[54] M. Steurer and K. Frohlich, "The impact of inrush currents on the mechanical stress of high voltage power transformer coils," *IEEE Trans. Power Del.*, vol. 17, no. 1, pp. 155–160, Jan. 2002.

[55] J. F. Witte, F. P. DeCesaro, and S. R. Mendis, "Damaging long-term overvoltages on industrial capacitor banks due to transformer energization inrush currents," *IEEE Trans. Ind. Appl.*, vol. 30, no. 4, pp. 1107–1115, Jul. 1994.

[56] G. H. Cheng and Z. Xu, "Analysis and control of harmonic overvoltages during power system restoration," in *Proc. IEEE/PES Transmission and Distribution Conference and Exhibition: Asia and Pacific*, 2005, pp. 1–7.

[57] V. L. C. Soares, F. Reichert, R. L. Manenti, R. Zenker, J. L. Rosa, A. G. Teixeira, O. Borges, G. Gil, and A. Mena, "Disturbances related to the effects of the energization transients of large autotransformer banks," in *Proceedings of the 35th Session. International Conference on Large High Voltage Electric Systemss*, vol. vol.2, Paris, France, 1995, pp. 36 – 302.

[58] R. A. Turner and K. S. Smith, "Resonance excited by transformer inrush current in inter-connected offshore power systems," in *Proc. IEEE Industry Applications Society Annual Meeting IAS '08*, Oct. 5–9, 2008, pp. 1–7.

[59] A. Clerici, A. Ardito, M. Rioual, B. Shperling, G. Sybille, C. Van der Merwe, O. Volker, B. Wahlstrome, and E. Zaima, "Temporary overvoltages test case results," *Electra*, no. 188, pp. 70 – 87, Feb. 2000.

[60] S. G. Abdulsalam, W. Xu, and V. Dinavahi, "Modelling and simulation of three-phase transformers for inrush current studies," *IEE Proceedings-Generation, Transmission and Distribution*, vol. 152, no. 3, pp. 328–333, May 6, 2005.

[61] A. Tokic, I. Uglesic, and F. Jakl, "An algorithm for calculations of low frequency transformer transients," in *IPST'03 - International Conference on Power Systems Transients*, no. 9a-2, New Orleans, Louisiana, USA, Sep. 2003.

[62] A. Tokic, V. Madzarevic, and I. Uglesic, "Numerical calculations of three-phase transformer transients," *IEEE Trans. Power Del.*, vol. 20, no. 4, pp. 2493–2500, Oct. 2005.

[63] J. J. Rico, E. Acha, and M. Madrigal, "The study of inrush current phenomenon using operational matrices," *IEEE Trans. Power Del.*, vol. 16, no. 2, pp. 231–237, Apr. 2001.

[64] M. Laasonen and R. Hirvonen, "Inrush currents of three-winding transformers," in *International Conference on Power Systems Transients. IPST '95 Proceedings*, Lisbon, Portugal, 1995, pp. 142–7.

[65] L. Prikler, G. Banfai, G. Ban, and P. Becker, "Reducing the magnetizing inrush current by means of controlled energization and de-energization of large power transformers," *Electric Power Systems Research*, vol. 76, no. 8, pp. 642–649, May 2006.

[66] R. Yacamini and H. Bronzeado, "Transformer inrush calculations using a coupled electromagnetic model," *IEE Proceedings-Science, Measurement and Technology*, vol. 141, no. 6, pp. 491 – 8, Nov. 1994.

[67] R. Apolonio, J. C. de Oliveira, H. S. Bronzeado, and A. B. de Vasconcellos, "Transformer controlled switching: a strategy proposal and laboratory validation," in *11th International Conference on Harmonics and Quality of Power*, IEEE, Ed., Sep. 2004, pp. 625 – 630.

[68] H. S. Bronzeado, J. C. Oliveira, R. Apolonio, and A. B. Vasconcellos, "Transformer inrush mitigation - Part I: modeling and strategy for controlled switching," in *Cigré international technical colloquium*, C. SCA3, Ed., Rio de Janeiro, Brazil, Sep. 12–13 2007.

[69] H. S. Bronzeado, S. Oliveira Pinto, J. C. Oliveira, M. L. R. Chaves, and P. Jonsson, "Transformer inrush mitigation - Part II: Field test on a 100MVA three-phase transformer," in *Cigré international technical colloquium*, C. SCA3, Ed., Rio de Janeiro, Brazil, Sep. 12–13 2007.

[70] W. Schmidt, "Vergleich der groesstwerte des kurzschluss- und einschaltstromes von einphasentransformatoren," *Elektrotechnische Zeitschrift – Edition A*, vol. 79, no. 21, pp. 801–806, 1958, Comparison of maximum values of short circuit and inrush currents of single-phase transformers.

[71] N. Richard and N. Szylowicz, "Comparison between a permeance network model and a 2D finite element model for the inrush current computation in a three phase transformer," *IEEE Trans. Magn.*, vol. 30, no. 5, pp. 3232–3235, Sep. 1994.

[72] J. Faiz, B. M. Ebrahimi, and T. Noori, "Three- and two-dimensional finite-element computation of inrush current and short-circuit electromagnetic forces on windings of a three-phase core-type power transformer," *IEEE Trans. Magn.*, vol. 44, no. 5, pp. 590–597, May 2008.

[73] L. Pierrat and T. Tran-Quoc, "Influence of random variables on transformer inrush current," in *International Conference on Power Systems Transients. IPST '95 Proceedings*, Lisbon, Portugal, 1995, pp. 148–52.

[74] H. Bronzeado and R. Yacamini, "Phenomenon of sympathetic interaction between transformers caused by inrush transients," *IEE Proceedings -Science, Measurement and Technology*, vol. 142, no. 4, pp. 323–329, Jul. 1995.

[75] A. Wiszniewski, W. Rebizant, D. Bejmert, and L. Schiel, "Ultrasaturation phenomenon in power transformers: Myths and reality," *IEEE Trans. Power Del.*, vol. 23, no. 3, pp. 1327–1334, Jul. 2008.

[76] W. Schmidt, "Ueber den einschaltstrom bei drehstromtransformatoren," *Elektrotechnische Zeitschrift – Edition A*, vol. 82, no. 15, pp. 471–474, Jul. 1961, Switch-on current in 3-phase a-c transformers.

[77] G. Bertagnolli, *Short-Circuit Duty of Power Transformers, Second Revised Edition*. ABB, 1996.

[78] T. R. Specht, "Transformer magnetizing inrush current," *AIEE Trans*, vol. 70, pp. 323–328, 1951.

[79] J. F. Holcomb, "Distribution transformer magnetizing inrush current," *Transactions of the American Institute of Electrical Engineers, Part III (Power Apparatus and Systems)*, vol. 80, no. 57, pp. 697–702, Dec. 1961.

[80] R. Yacamini and A. Abu-Nasser, "The calculation of inrush current in three-phase transformers," *IEE Proceedings B (Electric Power Applications)*, vol. 133, no. 1, pp. 31–40, Jan. 1986.

[81] L. Sainz, F. Corcoles, J. Pedra, and L. Guasch, "Theoretical calculation of inrush currents in three- and five-legged core transformers," *IEEE Trans. Power Del.*, vol. 22, no. 2, pp. 986–995, Apr. 2007.

[82] Y. Wang, S. G. Abdulsalam, and W. Xu, "Analytical formula to estimate the maximum inrush current," *IEEE Trans. Power Del.*, vol. 23, no. 2, pp. 1266–1268, Apr. 2008.

[83] R. S. Girgis and E. G. teNyenhuis, "Characteristics of inrush current of present designs of power transformers," in *Proc. IEEE Power Engineering Society General Meeting*, Jun. 24–28, 2007, pp. 1–6.

[84] H. Ito, "Controlled switching technologies, state-of-the-art," in *Proc. Transmission and Distribution Conference and Exhibition 2002: Asia Pacific. IEEE/PES*, vol. 2, Oct. 6–10, 2002, pp. 1455–1460.

[85] P. C. Y. Ling and A. Basak, "Investigation of magnetizing inrush current in a single-phase transformer," *IEEE Trans. Magn.*, vol. 24, no. 6, pp. 3217–3222, Nov. 1988.

[86] H. S. Bronzeado and J. C. de Oliveira, "The influence of tap position on the magnitude of transformer inrush current," in *IPST'99 - International Conference on Power System Transients*, Budapest, Hungary, 1999, pp. 457–61.

[87] *Controlled switching of HVAC CBs - Planning, Specifications & Testing*, CIGRÉ SC A3 WG A3.07, Jan. 2004.

[88] J. H. Brunke and K. J. Frohlich, "Elimination of transformer inrush currents by controlled switching. I. Theoretical considerations," *IEEE Trans. Power Del.*, vol. 16, no. 2, pp. 276–280, April 2001.

[89] J. H. Brunke and K. J. Frohlich, "Elimination of transformer inrush currents by controlled switching. II. Application and performance considerations," *IEEE Trans. Power Del.*, vol. 16, no. 2, pp. 281–285, April 2001.

[90] U. Krusi, K. Frohlich, and J. H. Brunke, "Controlled transformer energization considering residual flux-implementation and experimental results," in *Proceedings of the IASTED International Conference Power and Energy Systems*, Anaheim, CA, USA, 2001, pp. 155–60.

[91] A. Mercier, E. Portales, Y. Filion, and A. Salibi, "Transformer controlled switching taking into account the core residual flux - a real case study," in *CIGRÉ, Session 2002*, no. 13-201, 2002.

[92] H. Kohyama, K. Kamei, and H. Ito, "Application of controlled switching system for transformer energization taking into account a residual flux in transformer core," in *CIGRE SC A3&B3 Joint Colloquium in Tokyo*, 2005.

[93] A. Ebner, M. Bosch, and R. Cortesi, "Controlled switching of transformers - effects of closing time scatter and residual flux uncertainty," in *Proc. 43rd International Universities Power Engineering Conference UPEC 2008*, Sep. 2008, pp. 1–5.

[94] S. G. Abdulsalam and W. Xu, "A sequential phase energization method for transformer inrush current reductiontransient performance and practical considerations," *IEEE Trans. Power Del.*, vol. 22, no. 1, pp. 208–216, Jan. 2007.

[95] E. Colombo and G. Santagostino, "Results of the enquiries on actual network conditions when switching magnetizing and small inductive currents and on transformer and shunt reactor saturation characteristics," *Electra*, vol. 94, pp. 35–53, May 1984.

[96] Y. Husianycia and M. Rioual, "Determination of the residual fluxes when deenergizing a power transformer/comparison with on-site tests," *2005 IEEE Power Engineering Society General Meeting (IEEE Cat. No. 05CH37686)*, vol. 3, pp. 2492–2497, 2005.

[97] L. M. Ganatra, P. G. Mysore, K. K. Mustaphi, A. Mulawarman, B. A. Mork, and G. Gopakumar, "Application of reclosing schemes in the presence of capacitor bank ringdown," *Proc Am Power Conf*, vol. 61-2, pp. 967–972, 1999.

[98] J. Pearson, P. T. Squire., and D. Atkinson, "Which anhysteretic magnetization curve?" *IEEE Trans. Magn.*, vol. 33, no. 5 pt 2, pp. 3970–3972, 1997.

[99] S. N. Talukdar, J. K. Dickson, R. C. Dugan, M. J. Sprinzen, and C. J. Lenda, "On modeling transformer and reactor saturation characteristics for digital and analog studies," *IEEE Trans. Power App. Syst.*, vol. 94, no. 2, pp. 612–621, Mar 1975.

[100] S. Prusty and M. Rao, "A direct piecewise linearized approach to convert rms saturation characteristic to instantaneous saturation curve," *IEEE Trans. Magn.*, vol. 16, no. 1, pp. 156–160, 1980.

[101] S. Prusty and M. Rao, "A novel approach for predetermination of magnetization characteristics of transformers including hysteresis," *IEEE Trans. Magn.*, vol. 20, no. 4, pp. 607–612, 1984.

[102] W. L. A. Neves and H. W. Dommel, "On modelling iron core nonlinearities," *IEEE Trans. Power Syst.*, vol. 8, no. 2, pp. 417–422, 1993.

[103] G. W. Swift, "Power transformer core behavior under transient conditions," *IEEE Trans. Power App. Syst.*, no. 5, pp. 2206–2210, Sep. 1971.

[104] C. C. Wong, "A dynamic hysteresis model," *IEEE Transactions on Magnetics*, vol. 24, no. 2, pp. 1966 – 8, Mar. 1988.

[105] A. Medina, A. M. Maldonado, L. Sanchez, and C. M. Sanchez, "Experimental determination of magnetic saturation and hysteresis characteristics in power transformers with the WVAV method," in *Proc. IEEE Power Engineering Society Summer Meeting*, vol. 4, Jul. 16–20, 2000, pp. 2434–2438.

[106] A. Medina, G. Saucedo, C. M. Sanchez, A. M. Maldonado, and L. Sanchez, "Saturation and hysteresis characteristics obtained by measurements in multil-

imb power transformers using DC excitation," in *Proc. IEEE Power Engineering Society Winter Meeting*, vol. 2, Jan. 27–31, 2002, pp. 1389–1393.

[107] E. F. Fuchs and Y. You, "Measurement of λ-i characteristics of asymmetric three-phase transformers and their applications," *IEEE Trans. Power Del.*, vol. 17, no. 4, pp. 983–990, Oct. 2002.

[108] M. Elleuch and M. Poloujadoff, "Analytical model of iron losses in power transformers," *IEEE Trans. Magn.*, vol. 39, no. 2, pp. 973–980, Mar. 2003.

[109] A. Gaudreau, P. Picher, L. Bolduc, and A. Coutu, "No-load losses in transformer under overexcitation/inrush-current conditions: tests and a new model," *IEEE Trans. Power Del.*, vol. 17, no. 4, pp. 1009–1017, Oct. 2002.

[110] E. J. Tarasiewicz, A. S. Morched, A. Narang, and E. P. Dick, "Frequency dependent eddy current models for nonlinear iron cores," *IEEE Trans. Power Syst.*, vol. 8, no. 2, pp. 588–597, May 1993.

[111] W. L. A. Neves and H. W. Dommel, "Transformer core modelling," in *International Conference on Power Systems Transients. IPST '95 Proceedings*, Lisbon, Portugal, 1995, pp. 125 – 30.

[112] G. Bertotti, *Hysteresis in magnetism for physicist, materials scientists, and engineers*. San Diego, CA, USA: Academic Press, 1998.

[113] F. Liorzou, B. Phelps, and D. L. Atherton, "Macroscopic models of magnetization," *IEEE Trans. Magn.*, vol. 36, no. 2, pp. 418–428, Mar. 2000.

[114] R. Girgis, M. Hastenrath, and J. Schoen, "Electrical steel and core performance," Presentation, Oct. 2009. [Online]. Available: http://www.transformerscommittee.org/info/f09-presentations.htm

[115] S. N. Talukdar and J. R. Bailey, "Hysteresis models for system studies," *IEEE Trans. Power App. Syst.*, vol. 95, no. 4, pp. 1429–1434, Jul. 1976.

[116] F. de Leon and A. Semlyen, "A simple representation of dynamic hysteresis losses in power transformers," *IEEE Trans. Power Del.*, vol. 10, no. 1, pp. 315–321, 1995.

[117] J. G. Frame, N. Mohan, and T. Liu, "Hysteresis modeling in an electromagnetic transient program," *IEEE Trans. Power App. Syst.*, vol. PAS-101, pp. 3403–3412, Sep. 1982.

[118] S. Dennetière, J. Mahseredjian, M. Martinez, M. Rioual, A. Xémard, and P. Bastard, "On the implementation of a hysteretic reactor model in EMTP," in *IPST'03 - International Conference on Power Systems Transients*, New Orleans, USA, Sep. 2003.

[119] D. A. Philips, L. R. Dupre, and J. A. Melkebeek, "Comparison of Jiles and Preisach hysteresis models in magnetodynamics," *IEEE Trans. Magn.*, vol. 31, no. 6 pt 2, pp. 3551–3553, Nov. 1995.

[120] D. C. Jiles and D. L. Atherton, "Ferromagnetic hysteresis." *IEEE Transactions on Magnetics*, vol. MAG-19, no. 5, pp. 2183 – 2185, 1983.

[121] D. C. Jiles and D. L. Atherton, "Theory of ferromagnetic hysteresis. (invited)." *Journal of Applied Physics*, vol. 55, no. 6 pt 2B, pp. 2115–2120, 1983.

[122] D. C. Jiles and D. L. Atherton, "Theory of ferromagnetic hysteresis," *Journal of Magnetism and Magnetic Materials*, vol. 61, no. 1-2, pp. 48 – 60, Sep. 1986.

[123] D. C. Jiles, "Modelling the effects of eddy current losses on frequency dependent hysteresis in electrically conducting media," *IEEE Trans. Magn.*, vol. 30, no. 6, pp. 4326–4328, Nov. 1994.

[124] W. Chandrasena, P. G. McLaren, U. D. Annakkage, and R. P. Jayasinghe, "An improved low-frequency transformer model for use in gic studies," *IEEE Trans. Power Del.*, vol. 19, no. 2, pp. 643–651, Apr. 2004.

[125] W. Chandrasena, P. G. McLaren, U. D. Annakkage, R. P. Jayasinghe, D. Muthumuni, and E. Dirks, "Simulation of hysteresis and eddy current effects in a power transformer," *Electric Power Systems Research*, vol. 76, no. 8, pp. 634–641, May 2006.

[126] D. C. Jiles and J. B. Thoelke, "Theory of ferromagnetic hysteresis: determination of model parameters from experimental hysteresis loops," *IEEE Trans. Magn.*, vol. 25, no. 5, pp. 3928–3930, Sep. 1989.

[127] D. C. Jiles, J. B. Thoelke, and M. K. Devine, "Numerical determination of hysteresis parameters for the modeling of magnetic properties using the theory of ferromagnetic hysteresis," *IEEE Trans. Magn.*, vol. 28, no. 1, pp. 27–35, Jan. 1992.

[128] X. Wang, D. W. P. Thomas, M. Sumner, J. Paul, and S. H. L. Cabral, "Characteristics of Jiles-Atherton model parameters and their application to transformer inrush current simulation," *IEEE Trans. Magn.*, vol. 44, no. 3, pp. 340–345, Mar. 2008.

[129] M. Toman, G. Stumberger, and D. Dolinar, "Parameter identification of the Jiles-Atherton hysteresis model using differential evolution," *IEEE Trans. Magn.*, vol. 44, no. 6, pp. 1098–1101, Jun. 2008.

[130] R. P. Jajasinghe and P. G. McLaren, "Transformer core models based on the Jiles-Atherton algorithm," in *Proc. IEEE WESCANEX 97: Communications, Power and Computing*, May 22–23, 1997, pp. 121–125.

[131] U. D. Annakkage, P. G. McLaren, E. Dirks, R. P. Jayasinghe, and A. D. Parker, "A current transformer model based on the Jiles-Atherton theory of ferromagnetic hysteresis," *IEEE Trans. Power Del.*, vol. 15, no. 1, pp. 57–61, Jan. 2000.

[132] M. Popov, L. Van Der Sluis, G. C. Paap, and P. H. Schavemaker, "On a hysteresis model for transient analysis," *IEEE Power Eng. Rev.*, vol. 20, no. 5, pp. 53–55, May 2000.

[133] I. D. Mayergoyz, "Mathematical models of hysteresis," *IEEE Transactions on Magnetics*, vol. MAG-22, no. 5, pp. 603 – 8, Sep. 1986.

[134] G. Bertotti, "Dynamic generalization of the scalar preisach model of hysteresis," in *Proc. International Magnetics Conference Digests of Intermag '92*, Apr. 13–16, 1992, p. 206.

[135] G. Bertotti and M. Pasquale, "Physical interpretation of induction and frequency dependence of power losses in soft magnetic materials," *IEEE Trans. Magn.*, vol. 28, no. 5, pp. 2787–2789, Sep. 1992.

[136] S. Y. R. Hui and J. Zhu, "Numerical modelling and simulation of hysteresis effects in magnetic cores using transmission-line modelling and the Preisach theory," *IEE Proceedings -Electric Power Applications*, vol. 142, no. 1, pp. 57–62, Jan. 1995.

[137] J. M. Prousalidis, N. D. Hatziargyriou, and B. C. Papadias, "Geometrical transformer model including hysteresis," in *International Conference on Power Systems Transients. IPST '95 Proceedings*, Lisbon, Portugal, 1995, pp. 113 – 18.

[138] L. Dube and I. Bonfanti, "MODELS: A new simulation tool in the EMTP," *European transactions on electrical power engineering*, vol. 2, no. 1, pp. 45 – 50, 1992.

[139] L. Dube, "Users guide to MODELS in ATP," DEI Simulation Software, Tech. Rep., Apr. 1996.

APPENDIX A

IMPLEMENTATION OF THE JILES-ATHERTON MODEL IN ATP

The Jiles-Atherton model has been implemented as a module in ATP using the MODELS language and a type-94 NORTON component [138, 139]. The routine receives as input the guessed voltage to ground of the type-94 component at each time-step. The model computes and returns the total current into the terminal, the Norton current source and conductance at each time-step. The code may be further enhanced to achieve a faster computation speed.

```
MODEL JA_NRd
 comment ------------------------------------------------------------------
 |                                          _______                       |
 | Internal circuit:  1-2 : JA ind         |       |                      |
 |                                       1 o       -- GND                 |
 |                                         |_______|                      |
 |                                                                        |
 |                                                                        |
 |                                                                        |
 | Built for use as a 1-phase type-94 NORTON component                    |
  ------------------------------------------------------------ endcomment

 comment ------------------------------------------------------------------------
 | First, declarations required for any type-94 iterated model                  |
 |   (the values of these data and input are loaded automatically by ATP)       |
 |   (the values of these outputs are used automatically by ATP)                |
 |   (DO NOT MODIFY THE SEQUENCING OF THE DATA, INPUT, AND VAR IN THIS GROUP)   |
 |   (the names may be modified, except 'n')                                    |
 |   (when built for n=1, the array notation is not required)                   |
  ------------------------------------------------------------------- endcomment
 DATA  n                    -- number of node pairs
       ng {dflt: n*(n+1)/2} -- number of matrix elements

 INPUT v          -- guessed voltage across terminals 1-2
       v0         -- steady-state voltage across terminals 1-2
       i0         -- steady-state current into terminal 1

 VAR   i          -- current(t) into terminal 1
       is         -- Norton source(t+timestep) at terminal 1
       g          -- conductance(t+timestep) at terminal 1
       flag       -- set to 1 whenever a conductance value is modified

 OUTPUT i, is, g, flag

 comment ------------------------------------------------------------------------
 | Next, declarations of user-defined data for this particular model            |
 | (values which must be defined when using this model as a type-94 component)  |
  ------------------------------------------------------------------- endcomment
 DATA    Y0 {DFLT: 0} -- Residual Flux initialization

         -- relative dimension of the tested material
         Arel {DFLT:1}
         Lrel {DFLT:1}

         -- anhysteretic curve
       Linf      -- saturated inductance
         ImSat     -- saturation level
         a1
         a2
         a3

         -- loss parameters
         alpha     -- mat. const. (inter-domain coupling)
         c         -- Material constant
         K         -- Material constant
         k1        -- classical eddy current coefficient
         k2        -- excess losses coefficient

         ResOut {DFLT: 0} -- aut. calculation of Res Flux for SS initialization
         Ref {DFLT: 0}

 comment ------------------------------------------------------------------------
 | Next, declarations private to the operation of this model                    |
  ------------------------------------------------------------------- endcomment
 CONST epsilon {VAL: 1E-10}      -- iteration accuracy
       maxloop {VAL: 1E3}

       Qmin {VAL: 0}
       Qmax {VAL: 1}

 VAR   st    -- used for converting Laplace s to time domain
       L     -- and any other variables needed in the procedure
       Q, Qnew, delta
       Y, Ie, Im, IeEff, ImAn
       dltY, dltIeMax
       dImdIe, Ldiff, dltL, g0
       loop, finish
       term1, term2, term3
       dY
       Ymin, Ymax, Yres, dYres, Yout
       MLL, NQZ

 INIT
  st := 2/timestep  -- trapezoidal rule conversion from Laplace
  Q := 0.5          -- Q reaches 1 when in heavy saturation
```

```
 Ymin := 1E8
 Ymax := 1E-8

 MLL := 0; NQZ := 0

 flag := 1
ENDINIT

HISTORY  INTEGRAL(v) {DFLT: Y0}
HISTORY  Y {DFLT: 0}
HISTORY  Ie {DFLT: i0}
HISTORY  Im {DFLT: Y/Linf - Ie}
HISTORY  ImAn {DFLT: Im}
HISTORY  IeEff {DFLT: Ie}

EXEC

 Y := INTEGRAL(v)
 Y := Y/Arel -- rescale to the sampled material condition of flux density

 IF ResOut=1 AND t>0.01 --delay to avoid initial transients
 THEN
   Ymin := min(Y,Ymin)
   Ymax := max(Y,Ymax)
   IF t>stoptime-timestep
   THEN
     dYres := -((Ymax-Ymin)/2+Ymin)
     Yres := Y0+dYres
     WRITE('JA'Ref ': New residual flux for SS: ' Yres ', adjustment: ' dYres)
   ENDIF
 ENDIF
 loop := 0
 finish := false

 -- ==> Calculation of y and dy (incremental flux) with trapezoidal rule of integration:
 dltY := Y-prevval(Y)

 -- ==> estimation of the electric and magnetic current components:
 dltIeMax := dltY/Linf

 -- optimization of Q
 WHILE loop<maxloop AND finish=false DO
   loop := loop+1

   Ie := prevval(Ie)+ dltIeMax*Q
   Im := prevval(Im)+ dltIeMax*(1-Q)

   -- ==> calculate dim/die
   delta := sign(dltY);
   IeEff := Ie+alpha*Im;

   -- anhysteretic curve
   ImAn := ImSat*(a1*abs(IeEff)+IeEff**2)/(a3+a2*abs(IeEff)+IeEff**2)*sign(IeEff)

   IF (ImAn-Im)*delta>0 THEN
     term2 := (ImAn-Im) / ( (delta*K/Linf) - (alpha*(ImAn-Im)/(1-c)) )
   ELSE
     term2 := 0
   ENDIF

   term1 := c*(ImAn-prevval(ImAn))/(IeEff-prevval(IeEff))
   term3 := 1 - alpha*term1
   dImdIe:= (term1 + term2) / term3

   -- ==> compare assumed Q and the one coming from the calculations.
   Qnew := 1/(dImdIe+1)
   IF abs(Q-Qnew)<=epsilon THEN
     IF Q>=Qmin AND Q<=Qmax AND Qnew>=Qmin AND Qnew<=Qmax THEN
       finish := true
     ENDIF
   ENDIF

   -- Set the new Q for the next iteration based on the number of loops
   -- to be improved for better efficiency...
   IF loop<20 THEN
     Q := Qnew
   ELSIF loop<50 THEN
     Q := Q+(Qnew-Q)*0.5
   ELSIF loop<150 THEN
     Q := Q+(Qnew-Q)*0.05
   ELSIF loop<400 THEN
     Q := Q+(Qnew-Q)*0.005
   ELSE
     Q := Q+(Qnew-Q)*0.0005
   ENDIF
```

```
    IF Q<0 THEN
      Q := abs(Q)
    ENDIF

  ENDWHILE

  -- final calculation at the end of the iterations
  Ldiff := Linf*(dImdIe+1)

  -- OUTPUT
  dY := v -- DERIV(Y)

  g := 1/(st*(Ldiff+prevval(Ldiff))/2) + k1 + k2/sqrt(abs(dY))
  g := g *Lrel/Arel -- conductance

  IF t=0
  THEN
    i := i0
    is := -i-g*v0
  ELSE
    i := (Ie + k1*dY + k2*sqrt(abs(dY))*sign(dY)) *Lrel -- with eddy components
    is := -i-g*v
  ENDIF
  g0 := g

  Yout := Y*Arel

 ENDEXEC
ENDMODEL
```

APPENDIX B

JOURNAL PUBLICATIONS AND CONFERENCE PROCEEDINGS

JOURNAL PAPER

Analytical algorithm for the calculation of magnetization and loss curves of delta connected transformers

N. Chiesa, H. K. Høidalen

2009

IEEE Transaction on Power Delivery

Accepted for publication

TPWRD-00589-2009

Analytical Algorithm for the Calculation of Magnetization and Loss Curves of Delta Connected Transformers

Nicola Chiesa, and Hans Kristian Høidalen, *Member, IEEE*.

Abstract

This paper proposes an analytical algorithm for the computation of the magnetization and loss curves for a transformer from standard no-load test report data. This is the input to standard transformer models for power system simulation. In the case of delta coupled windings the conversion from test report rms line quantities to peak phase values requires processing of the triplen harmonics in the current. This is handled analytically in the paper with utilization of the concept of incremental inertance and conductance. The analysis shows that only the third harmonic needs to be treated to reach sufficient accuracy within the measurement errors. The test case with a 290 MVA GSU transformer shows an increase in the calculated current of above 10% at rated voltage with proper triplen harmonic handling. This difference will increase considerably with excitation voltage.

Index Terms

Power transformer, magnetization, nonlinearities, harmonic distortion, Fourier series, power system transients.

NOTATION

- *triplen harmonic:* an odd harmonic of order multiple of three (3rd, 9th, 15th, 21st, 27th...);
- *inertance:* inverse of an inductance: $\Gamma = 1/L$;
- *capital letter:* rms value (e.g.: I);
- *small letter:* peak value (e.g.: i);
- *variable dependency:* instantaneous value (e.g.: $i(t)$);
- *over-tilde character:* contribution from each incremental inertance or conductance segment (e.g.: $\tilde{i}$);
- *index h:* triplen harmonic order (e.g.: I_h);
- *index n:* excitation level, $1 \leq n \leq N$, where N is the total number of points specified in the test-report;
- *indices j and m:* summation intervals, $1 \leq j \leq n$ and $1 \leq m \leq j$;
- *indices p and l:* phase and line quantities respectively.

I. INTRODUCTION

THE power transformer is an essential component in power systems. The standard models used to predict its transient behavior are poor due to lack of data, measurements, and knowledge. Transformer modeling is an active topic

in the research community with papers published on different issues. References [1]–[3] present a comprehensive and up to date review of transformer models for electromagnetic transients.

One of the critical aspects of transformer modeling is the description of nonlinear and frequency dependent parameters. Among others, nonlinear core magnetization and losses (hysteresis and eddy current) play an important role in transient studies such as inrush and ferroresonance. The typical data available when modeling a power transformer are from the factory test report [4]. In such circumstances it is common to model the magnetic core with a nonlinear $R-L$ parallel impedance for each phase and to neglect the frequency dependent and dynamic hysteresis effects of the magnetization current. Peak values of quantities in magnetization and loss curves are specified in transformer models, thus a conversion from rms test report data is required.

The conversion process has been extensively addressed and developed over the years [5]–[12]. A first reference by Talukdar *et al.* [5] addresses the conversion problem and proposes a numerical iterative technique. Beside the limitation of an iterative algorithm, this approach neglects the core losses and does not take into consideration multiple phase systems. An analytical technique is proposed by Prusty and Rao [6], but iron-core losses and handling of multiple phase windings is not considered. The same analytical approach is also reported in [7] by Dommel *et al.* and is currently the main tool used in EMTP/ATP to convert a rms V/I to a λ/i characteristic [9], [10]. Neves and Dommel present in [8] an extended analytical algorithm that takes into account the influence of the no-load losses. The same authors in a follow up paper [11] discuss the handling of a delta connection using a numerical approach that was implemented in ATP as documented in [12]. A natural further step and the main contribution of our paper is the development of an analytical algorithm able to handle a delta connection.

The next section gives an overview of the algorithm and outlines the main issues involved. The following sections detail and discuss each step of the algorithm. The method of the incremental inertance and conductance is presented in section III. The proper processing of the inductive current in case of a delta coupling is treated analytically and presented in section IV. The resistive current must be processed before the inductive current, however it is initially briefly examined and then further developed in section V as the emphasis is on the dominating inductive current. Section VI discusses a case study and verifies the proposed method with field measurements.

II. LINE, PHASE QUANTITIES AND TRIPLEN HARMONIC ELIMINATION

According to IEEE Standards [4], the variables to be measured in a no-load test of a three-phase transformer are the rms line voltages, the rms line currents, and the active losses, irrespectively of the transformer connection and the core construction. For delta-connected transformer, the phase currents are not available from measurements. The three currents are in general different for three-phase transformers due to the asymmetry of the core structure. Mainly, only the mean

value of these currents is given in the test report, therefore the three currents are assumed to be equal even if they are slightly different.

For the case of single-phase transformer the distinction between line and phase quantities has no significance:

$$I_p = I_l \ ; \ V_p = V_l \tag{1}$$

Based on the assumption of a sinusoidal voltage, the standard relations apply to wye-connected three-phase transformers:

$$I_p = I_l \ ; \ V_p = V_l/\sqrt{3} \tag{2}$$

Due to the distorted nature of the current, the same analogous relations based on the $\sqrt{3}$ are not suitable for delta-connected three-phase transformers:

$$I_p \neq I_l/\sqrt{3} \ ; \ V_p = V_l \tag{3}$$

This last case is of most interest and will be examined in detail. The approach proposed in [11] recommends to deal with triplen harmonic elimination. Under the assumption of equal currents in all the three phases, the triplen harmonics (the odd harmonics of order multiple of three) are confined inside the delta-connected winding and cannot be seen when measuring line currents. However, if the triplen harmonics are present in the delta-connected winding they also contribute to the magnetization and loss currents. A decrease in accuracy is experienced if the line current measured at the terminal is used to calculate the magnetization and loss curves without taking into account the presence of triplen harmonics.

The conversion from rms open circuit measurements to flux-linkage v.s. peak current is done in steps as outlined in Fig. 1. First, the total no-load line current is split into the loss and magnetization components. The loss curve can be directly obtained from the measured no-load losses. Triplen harmonic elimination is not required for the calculation of the loss curve because under the assumption of sinusoidal voltage only the fundamental harmonic of the current contributes to active losses. However, as the loss curve is nonlinear, the resulting phase loss current will contain harmonics and triplen harmonics need to be removed before the conversion to line loss current in case of a delta coupled winding.

The magnetization curve can then be obtained by equalizing the measured and calculated rms magnetization line currents for each point of the characteristic. The phase current waveform is calculated from a nonlinear magnetization characteristic initially unknown and then converted to line current. In the case of a delta coupled winding, the triplen harmonics should be eliminated from the calculated phase current before the conversion to line current. The algorithm presented in the following sections of the paper computes the magnetization characteristic recursively and analytically, without trial and error iterations, and with a particular consideration for the case of delta connected windings.

III. THE METHOD OF INCREMENTAL INERTANCE AND CONDUCTANCE

The method of incremental inertance and conductance contributes to a clear mathematical formulation and an easy processing of the harmonics. With this

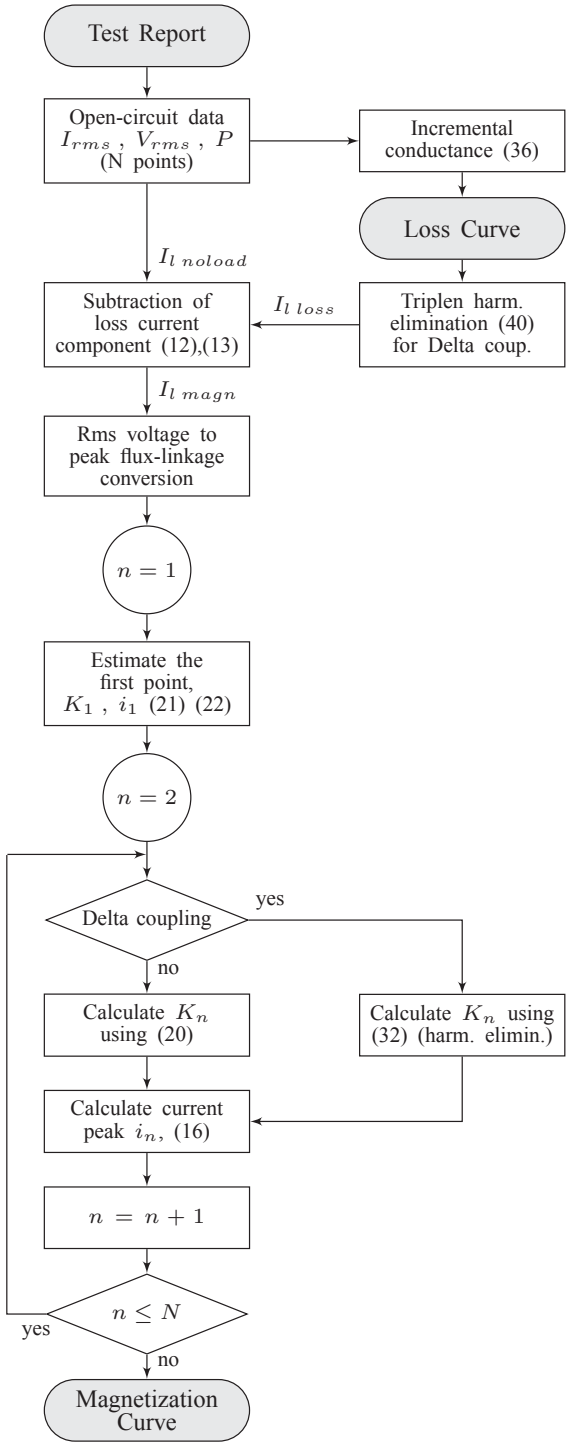

Fig. 1. Flow chart: test report to loss and magnetization curve conversion.

approach one of the limits of the rms integration interval remains constant and the formula of the rms value is simplified in a plain sum. The technique is presented here and its application will be clarified in the following sections.

The magnetization curve is described as a piecewise linear curve defined by pairs of flux-linkage/current values, shown by a continuous line in Fig. 2. The slope of each segment is defined as S_n:

$$S_n \triangleq \frac{i_n - i_{n-1}}{\lambda_n - \lambda_{n-1}} \tag{4}$$

An alternative way to describe the same curve is to define straight lines with the origin at the same abscissa ($\lambda_0 = 0$) but different ordinates (i_0, i_1, i_2) as represented by dashed lines in Fig. 2. The slope of the lines is defined by the *"incremental inertance"* K_n:

$$K_n \triangleq S_n - S_{n-1} \tag{5}$$

Equations (4) and (5) define the absolute and the incremental inertances, respectively, with a dimension of henry to the minus one: $\frac{i}{\lambda} = \frac{1}{L} = \Gamma$, $[H^{-1}]$.

Consider now the incremental inertance segments of Fig. 2 and a sinusoidal flux-linkage with peak value λ_n. It is possible to assemble a current waveform as qualitatively shown in Fig. 3. A partial current waveform $\tilde{i}_j(\theta)$ is created for every incremental inertance segment and can be expressed as a function of λ_n and the electric angle $\theta = \omega t$ as:

$$\tilde{i}_j(\theta) = K_j \cdot (\lambda_n(\theta) - \lambda_{j-1}) \cdot H(\lambda_n(\theta) - \lambda_{j-1}) \tag{6}$$

where $\lambda_n(\theta) = \lambda_n \cdot \sin(\theta)$ and $H(\cdot)$ is the Heaviside step function. The total current is the sum of the calculated partial waveforms:

$$i_n(\theta) = \sum_{j=1}^{n} \tilde{i}_j(\theta) \tag{7}$$

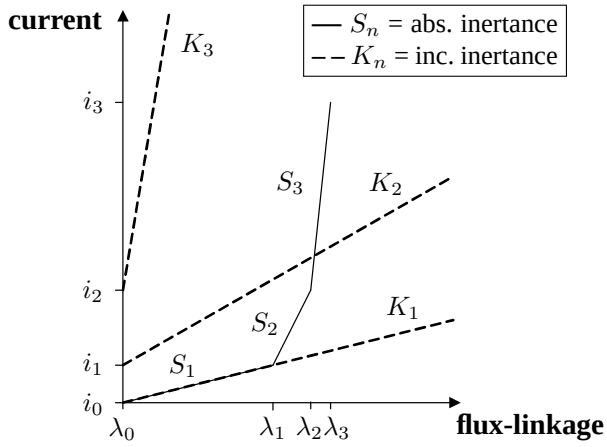

Fig. 2. Piecewise linearised magnetization curve, incremental inertance definition.

Assuming a sinusoidal flux-linkage with peak value λ_n, the angle α_j is defined as:

$$\alpha_j \triangleq \arcsin \frac{\lambda_j}{\lambda_n} \tag{8}$$

α_j is the electrical angle corresponding to a change in the slope of the piecewise linearized magnetization curve. Due to the assumption of a sinusoidal flux-linkage, a direct relation exists between flux-linkage and electrical angles for any defined value of flux-linkage. Therefore, (6) can now be reformulated as:

$$\tilde{i}_j(\theta) = K_j \cdot (\lambda_n(\theta) - \lambda_{j-1}) \cdot H(\theta - \alpha_{j-1}) \tag{9}$$

In this form the Heaviside function is a direct function of the electrical angle θ.

The *"incremental conductance"* G_n is defined in an analogous way to the incremental inertance. The same approach is used and only the final result is reported:

$$i_{loss\,n}(\theta) = \sum_{j=1}^{n} \tilde{i}_{loss\,j}(\theta) \tag{10}$$

$$\tilde{i}_{loss\,j}(\theta) = G_j \cdot (v_n(\theta) - v_{j-1}) \cdot H(\theta - \alpha_{j-1}) \tag{11}$$

Sections IV-B and V detail how to obtain the incremental inertance and conductance coefficients, respectively.

IV. MAGNETIZATION CHARACTERISTIC

The measured rms no-load current is the sum of the current contributions from magnetization and no-load losses. Due to the orthogonality of the two current components, the magnetization current (inductive component) can be separated from the total no-load current:

$$I_{l\,magn} = \sqrt{I^2_{l\,noload} - I^2_{l\,loss}} \tag{12}$$

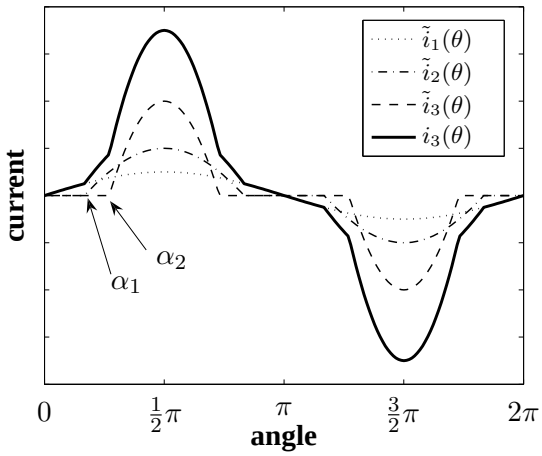

Fig. 3. Current waveform assembled by sum of incremental current waveforms contribution.

The calculation of $I_{l\,loss}$ is investigated in section V.

Phase quantities are now used to present a general formulation. The case of delta connection requires more explanation as it involves the handling of harmonics and (12) becomes:

$$I_{l\,magn} = \sqrt{3}\big(I_{p\,magn} - \sum_h I_{h\,magn}\big) = \\ = \sqrt{I^2_{l\,noload} - 3\big(I_{p\,loss} - \sum_h I_{h\,loss}\big)^2} \tag{13}$$

as triplen harmonics flow in the delta and are neither transferred to the line current nor measurable from the terminals. This will be further investigated in section IV-C.

The subscript *"magn"* is implied in the following part of this section.

A. Conversion from rms Voltage to Flux-linkage

This step is straightforward if the open-circuit test voltage is assumed sinusoidal:

$$\lambda = \frac{\sqrt{2}\cdot V_p}{\omega} = \frac{\sqrt{2}\cdot V_p}{2\cdot\pi\cdot f} \tag{14}$$

The exciting current of a transformer contains many harmonic components. Any source of power has some internal impedance that leads to the creation of harmonics in the voltage. If present, these harmonics cause a reduction of the accuracy of any method that takes advantage of the sinusoidal voltage assumption. It is difficult to take into account this phenomena based only on the standard test report data. A power source with low internal impedance should be used for the testing of a transformer. Moreover, it is important to verify the voltage distortion, in [13] the THD factor is suggested to be maintained lower than 15%.

B. Conversion from rms to peak current

The rescaling of current from rms to peak is more elaborate than the previous step. Commonly, the conversion is performed in ATP by the numerical routines SATURATION or LOSSY SATURATION [9], [10], [12]. The use of the *incremental inertance method* developed and presented in section III leads to a refined analytical formulation.

For an odd function the rms value of the magnetization current is defined as:

$$I_n = \sqrt{\frac{1}{T}\int_0^T i_n^2(t)\,dt} = \sqrt{\frac{2}{\pi}\int_0^{\frac{\pi}{2}} i_n^2(\theta)\,d\theta} \tag{15}$$

with i_n defined as in (7):

$$i_n(\theta) = \sum_{j=1}^{n} \tilde{i_j}(\theta) = \sum_{j=1}^{n} K_j\cdot(\lambda_n(\theta) - \lambda_{j-1})\cdot H(\theta - \alpha_{j-1}) \tag{16}$$

The periodicity and symmetry of the current waveform allow to calculate the integral over just one fourth of the period, say $[0, \pi/2]$. Substituting (16) in (15) for i_n^2, this gives:

$$\begin{aligned} I_n^2 &= \frac{2}{\pi}\int_0^{\frac{\pi}{2}} \sum_{j=1}^{n}\left(\tilde{i}_j^2(\theta) + 2\cdot\tilde{i}_j(\theta)\cdot\sum_{m=1}^{j-1}\tilde{i}_m(\theta)\right) d\theta = \\ &= \sum_{j=1}^{n} K_j^2\cdot A_j + 2\cdot\sum_{j=1}^{n}\sum_{m=1}^{j-1} K_j\cdot K_m\cdot B_{j,m} = \\ &= K_n^2\cdot\underbrace{A_n}_{A} + 2\cdot K_n\cdot\underbrace{\sum_{m=1}^{n-1} K_m\cdot B_{n,m}}_{B} + \\ &\quad + \underbrace{\sum_{j=1}^{n-1} K_j^2\cdot A_j + 2\sum_{j=1}^{n-1}\sum_{m=1}^{j-1} K_j\cdot K_m\cdot B_{j,m}}_{C'} = \\ &= K_n^2\cdot A + 2\cdot K_n\cdot B + C' \end{aligned} \tag{17}$$

with A_j and $B_{j,m}$ having analytical solutions:

$$\begin{aligned} B_{j,m} = \frac{2}{\pi}\cdot\Big[&\lambda_n^2\cdot\Big(\frac{\pi}{4} - \frac{\alpha_{j-1}}{2} + \frac{1}{4}\cdot\sin(2\cdot\alpha_{j-1})\Big) + \\ &+ \lambda_{j-1}\cdot\lambda_{m-1}\cdot\Big(\frac{\pi}{2} - \alpha_{j-1}\Big) + \\ &- \lambda_n\cdot(\lambda_{j-1} + \lambda_{m-1})\cdot\cos(\alpha_{j-1})\Big] \end{aligned} \tag{18}$$

$$A_j = B_{j,j} \tag{19}$$

The only unknown quantity is K_n: the incremental inertance of the point n. The values of all the K_j ($1 \le j \le n-1$) are known from the calculations of the previous points of the magnetization characteristic. It is then possible to isolate the term K_n and solve (17): A, B and $C = C' - I_n^2$ are the coefficients of a quadratic equation that can be solved for K_n:

$$K_n = \frac{-B \pm \sqrt{B^2 - A\cdot C}}{A} \tag{20}$$

It can be proved that only the solution with "+" is valid for this problem.

The point $i_0 - \lambda_0$ is set to zero; the segment connecting $i_0 - \lambda_0$ to $i_1 - \lambda_1$ can be assumed linear with:

$$i_1 = I_1\cdot\sqrt{2} \tag{21}$$

Thus follows:

$$K_1 = \frac{i_1}{\lambda_1} \tag{22}$$

Equation (20) is used to find the incremental inertance for each of the following point.

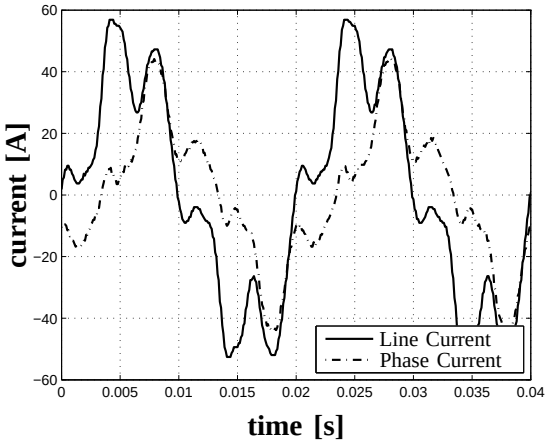

Fig. 4. Measured line and phase current at rated voltage, delta connected transformer (test object).

C. Three-Phase Delta-Coupling Case

In case of a single-phase or a three-phase wye-connected transformer, standard routines and the hereby presented routine lead to the same numeric result. A three-phase delta-connected transformer requires more attention.

Fig. 4 shows the line and phase currents at rated voltage for a delta-connected transformer; the curves refer to the transformer considered in the case study in section VI. The high content of harmonics is noticeable and for this reason the rms values of phase and line currents are not related by the factor $\sqrt{3}$.

Line and phase currents of a delta connected transformer can be decomposed in their harmonic contents:

$$I_p = \sqrt{I_{p1}^2 + I_{p3}^2 + I_{p5}^2 + I_{p7}^2 + I_{p9}^2 + \ldots + I_{p\infty}^2} \tag{23}$$

$$I_l = \sqrt{3} \cdot \sqrt{I_{p1}^2 + I_{p5}^2 + I_{p7}^2 + I_{p11}^2 + \ldots + I_{p\infty}^2} \tag{24}$$

Phase currents contain all the odd harmonics. Line current harmonics have value $\sqrt{3}$ the phase current harmonics, but the triplen harmonics are not present due to their elimination in the delta.

The value of the rms line current is known from the test report, so (23) and (24) can be rewritten as:

$$\frac{I_l^2}{3} = I_p^2 - I_{p3}^2 - I_{p9}^2 - I_{p15}^2 - \ldots - I_{ph}^2 = I_p^2 - \sum_h I_{ph}^2 \tag{25}$$

where the I_p^2 can be replaced by (17).

The triplen harmonics can be expressed analytically and for an odd function the Fourier series is:

$$\mathcal{F}(\theta) = \sum_{h=1}^{\infty} b_h \, \sin(h \cdot \theta) \tag{26}$$

$$b_h = \frac{1}{\pi} \int_{-\pi}^{\pi} \mathcal{F}(\theta) \cdot \sin(h \cdot \theta) \, d\theta = \frac{4}{\pi} \int_0^{\frac{\pi}{2}} \mathcal{F}(\theta) \, \sin(h \cdot \theta) \, d\theta \tag{27}$$

The last equation is valid due to the assumptions of sinusoidal voltage, and a symmetric and non-hysteretic magnetization loop. For $\mathcal{F}(\theta) = i_p(\theta)$, b_n will be the harmonic component of the current:

$$b_h = i_h = \sqrt{2}\, I_{p\,h} \tag{28}$$

The integral of (27) can be simplified if a piecewise linear magnetization characteristic is assumed and the incremental inertance method is used. Equation (16) is inserted in (27):

$$\begin{aligned} i_h &= \sum_{j=1}^{n} \frac{4}{\pi} \int_{\alpha_{j-1}}^{\frac{\pi}{2}} \tilde{i}_j(\theta)\, \sin(h\cdot\theta)\, d\theta = \sum_{j=1}^{n} \tilde{i}_{h,j} \\ &= K_n \cdot A_{h,n} + \sum_{j=1}^{n-1} K_j \cdot A_{h,j} = \\ &= K_n \cdot A_{h,n} + C_{h,n} \end{aligned} \tag{29}$$

where $\tilde{i}_{h,j}$ is the portion of the total current of the harmonic h due to the incremental inertance segment j. $A_{h,j}$ is obtained solving the integral in (29):

$$\begin{aligned} A_{h,j} = \frac{2}{\pi} \cdot \Big[\lambda_n \cdot \Big(\frac{\sin((h+1)\cdot\alpha_{j-1})}{h+1} - \frac{\sin((h-1)\cdot\alpha_{j-1})}{h-1} \Big) + \\ - 2 \cdot \lambda_{j-1} \cdot \frac{\cos(h\cdot\alpha_{j-1})}{h} \Big] \end{aligned} \tag{30}$$

The values of the $A_{h,j}$ and K_j terms are known. The only unknown term is K_n: the incremental inertance for the point n. $C_{h,n}$ is constant for each considered harmonic.

Equations (17), (25) and (29) can be redeveloped in:

$$\begin{aligned} K_n^2 \cdot \underbrace{\left(A - \sum_h \frac{A_{h,n}^2}{2} \right)}_{D} + 2 \cdot K_n \cdot \underbrace{\left(B - \sum_h \frac{A_{h,n} \cdot C_{h,n}}{2} \right)}_{E} + \\ + \underbrace{C' - \frac{I_l^2}{3} - \sum_h \frac{C_{h,n}^2}{2}}_{F} = 0 \end{aligned} \tag{31}$$

that gives a quadratic equation solvable for K_n:

$$K_n = \frac{-E + \sqrt{E^2 - D \cdot F}}{D} \tag{32}$$

V. CORE LOSSES CHARACTERISTIC

Losses are responsible for part of the no-load current. A reduced accuracy in the estimation of the magnetization curve is experienced if the nonlinearity of the no-load losses is not taken into account. For consistency, the formulation presented in [8] is reformulated here using the incremental conductance approach.

No-load losses are available in the test report as a function of the line voltage. It is assumed that the applied voltage is sinusoidal and that for three-phase systems the losses are equally distributed within the three phases. In case of a non-sinusoidal voltage, the total losses may be corrected combining the reading of rms and rectified-average voltmeters [13], [14]. Due to the different length of the magnetic circuit, the losses distribute in different proportions in the three phases [15]. However, the assumption of equally distributed losses within the three phases of a transformer is reasonable for the detail level of this approach. Resistive losses of the winding are not taken into account because they are negligible in no-load tests.

Using an energetic approach, the losses per phase ($P_n = P_0/3$) are:

$$P_n = \frac{2}{\pi}\int_0^{\frac{\pi}{2}} v_n(\theta)\cdot i_n(\theta)\, d\theta = \frac{2}{\pi}\int_0^{\frac{\pi}{2}} v_n(\theta)\cdot i_{loss\,n}(\theta)\, d\theta \tag{33}$$

where $i_{loss}(\theta)$ is the current component in phase with the voltage (resistive component). At excitation level n, using the *incremental loss conductance* approach:

$$i_{loss\,n}(\theta) = \sum_{j=1}^{n} \tilde{i}_{loss\,j}(\theta) = \sum_{j=1}^{n} G_j\cdot(v_n(\theta) - v_{j-1})\cdot H(\theta - \alpha_{j-1}) \tag{34}$$

This equation is analogous to (16) for the case of the incremental inertance. $\tilde{i}_{loss\,j}$ is the portion of the current attributed to the incremental loss conductance G_j. The losses per phase can be expressed as:

$$P_n = \sum_{j=1}^{n} \frac{2}{\pi}\int_{\alpha_{j-1}}^{\frac{\pi}{2}} v_n(\theta)\cdot\tilde{i}_{loss\,j}(\theta)\, d\theta = \sum_{j=1}^{n} \tilde{P}_j \tag{35}$$

$$\tilde{P}_j = \frac{G_j}{2\cdot\pi}\cdot\Big(v_n^2\cdot(\pi - 2\cdot\alpha_{j-1} + \sin(2\cdot\alpha_{j-1})) + - 4\cdot v_n\cdot v_{j-1}\cdot\cos(\alpha_{j-1})\Big) \tag{36}$$

The only unknown value in this equation is G_n: the incremental conductance for the point n. The procedure has to be repeated for each of the points specified in the test report to identify the nonlinear loss characteristic in a similar way as has been done for the incremental inertance. The result will be a peak-voltage/peak-current nonlinear loss characteristic, similar to the curve shown in Fig. 5(b).

The current flowing trough the nonlinear resistance contains harmonics and its rms value has to be analytically computed from the nonlinear loss characteristic in order to apply (12) for single-phase and three-phase wye-connected windings, or (13) for three-phase delta connected windings. The phase rms value can be found substituting λ with v and K_j with G_j in (17), (18) and (19). In this case all the G_j are known and the unknown quantity is the rms value of the loss current:

$$I_{loss\,n}^2 = \sum_{j=1}^{n} G_j^2\cdot A_{loss\,j} + 2\cdot\sum_{j=1}^{n}\sum_{m=1}^{j-1} G_j\cdot G_m\cdot B_{loss\,j,m} \tag{37}$$

$$B_{loss\,j,m} = \frac{2}{\pi}\cdot\Big[v_n^2\cdot\Big(\frac{\pi}{4} - \frac{\alpha_{j-1}}{2} + \frac{1}{4}\cdot\sin(2\cdot\alpha_{j-1})\Big) + \\ + v_{j-1}\cdot v_{m-1}\cdot\Big(\frac{\pi}{2} - \alpha_{j-1}\Big) + \\ - v_n\cdot(v_{j-1} + v_{m-1})\cdot\cos(\alpha_{j-1}) \tag{38}$$

$$A_{loss\,j} = B_{loss\,j,j} \tag{39}$$

The line current can then be found for single-phase and three-phase wye-connected windings. An additional step is required for three-phase delta-connected windings as the triplen harmonics needs to be eliminated as defined in (13). The value of each triplen harmonic can be found with a slightly modified version of (29):

$$i_{h\,loss} = \sum_{j=1}^{n} i_{h\,loss,j} = \sum_{j=1}^{n} G_j\cdot A_{loss\,h,j} \tag{40}$$

$$A_{loss\,h,j} = \frac{2}{\pi}\cdot\Big[v_n\cdot\Big(\frac{\sin((h+1)\cdot\alpha_{j-1})}{h+1} - \\ - \frac{\sin((h-1)\cdot\alpha_{j-1})}{h-1}\Big) - 2\cdot v_{j-1}\cdot\frac{\cos(h\cdot\alpha_{j-1})}{h}\Big] \tag{41}$$

The rms value of the loss current is not correctly estimated and leads to an inaccurate magnetization current if the triplen harmonic correction is not taken into account. This correction is however of minor significance for the calculation of the magnetization characteristic. It can be explained with the lower magnitude of the resistive current being approximately an order lower than the inductive current. An error quantified below 1% is introduced in the estimation of the magnetization characteristic when the triplen harmonic elimination is ignored in the calculation of the resistive rms line current.

VI. CASE STUDY

A 290 MVA GSU transformer has been used as a case study. Table I details the transformer test report data obtained from factory measurements. The open circuit test has been performed on the low-voltage delta-connected winding. The analytical algorithm proposed in the previous sections has been implemented in a Matlab function and is now used to calculate the magnetization curve.

Two different results are presented in Fig. 5(a). One curve has been obtained with no triplen harmonic elimination, the other with harmonics elimination. Fig. 5(b) shows the nonlinear loss characteristic. The numeric results are reported in Table II.

Fig. 6 shows the accuracy of the result as a function of the number of harmonics taken into account. The reference value “Peak current p.u. = 1” refers to the current peak calculated taking into account a large number of harmonics (up to the 6000-th). The summation converges rapidly and one term (elimination of only the third harmonic) seems to give sufficient accuracy (error $< 0.2\%$). The first point of Fig. 6(a) is the result obtained with no delta correction. This figure shows how disregarding the triplen harmonic elimination leads to errors higher than 10% in the estimation of the current peak of Fig. 4 (rated excitation).

TABLE I
GENERATOR STEP-UP TRANSFORMER TEST-REPORT.

Main data	[kV]	[MVA]	[A]	Coupling
HS	432	290	388	YN
LS	16	290	10465	d5
Open-circuit	E_0[kV,(%)]	[MVA]	I_0[%]	P_0[kW]
LS	12(75)	290	0.05	83.1
	14(87.5)	290	0.11	118.8
	15(93.75)	290	0.17	143.6
	16(100)	290	0.31	178.6
	17(106.25)	290	0.67	226.5
Short-circuit	[kV]	[MVA]	ek, er[%]	P_k[kW]
HS/LS	432/16	290	14.6, 0.24	704.4

TABLE II
NONLINEAR CHARACTERISTICS.

Loss Curve			
Peak Current [A]	Peak Voltage [kV]	Rms Line Current [A]	
		No Harm. Elim.	Harm. Elim.
3.264	16.970	3.998	3.998
4.240	19.798	4.847	4.840
5.038	21.213	5.455	5.444
6.350	22.627	6.454	6.434
8.054	24.041	7.855	7.817

Magnetization Curve		
Peak Current [A]	Peak Current [A]	Flux-linkage [Wb-t]
No Harm. Elim.	Harm. Elim.	
2.756	2.756	54.018
12.948	14.403	63.022
21.105	24.107	67.523
42.879	50.171	72.025
99.428	118.773	76.526

The ATPDraw circuit shown in Fig. 7 is used to test the model. The blocks named “RMS meter” and “W meter” are models used to measure rms current and active power as defined by the standards and normally performed during a factory test [4]. Magnetization and loss curves are inserted in an ATPDraw circuit as type-98 nonlinear inductor and type-99 nonlinear resistor [10]. The hysteretic behavior of the model is shown in Fig. 8 (only half of the loop is shown due to symmetry). The value of the nonlinear inductance is assigned first according to the first column (no harmonic elimination) and then to the second column (triplen harmonic elimination) of Table II. Based on this circuit the proposed algorithm is benchmarked using two different strategies: comparison with measurements and consistency of the results with the input data.

The simulated waveform of the line current is compared with the measured waveform. The result at rated excitation level is shown in Fig. 9. The agreement between measured and simulated waveforms is rather poor if the algorithm does

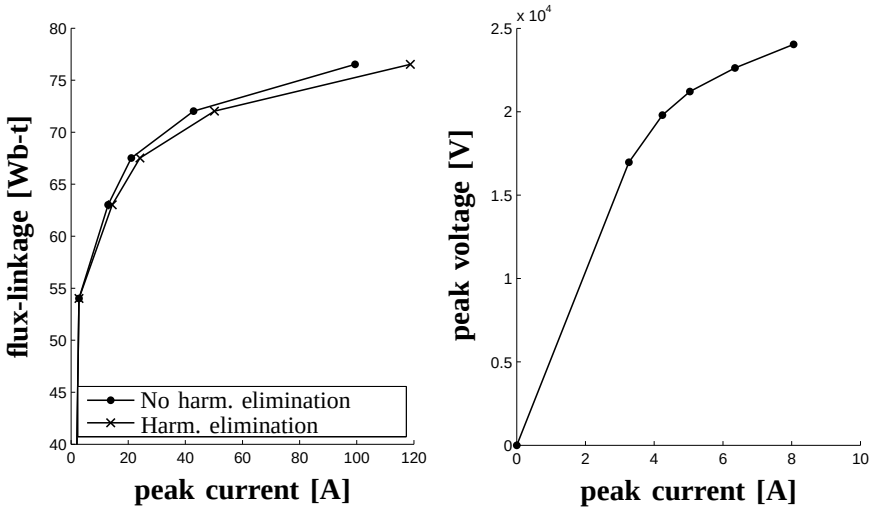

(a) Magnetization curve. (b) Loss curve.

Fig. 5. Nonlinear characteristics, phase quantities.

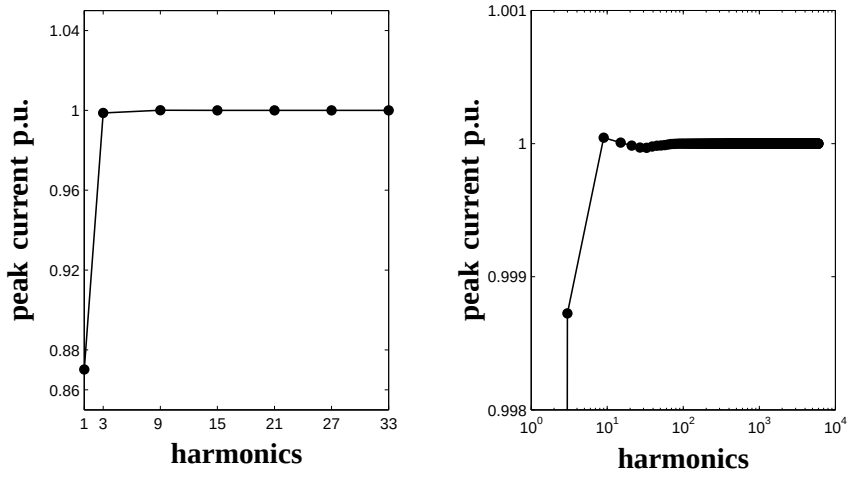

(a) Linear scale, harmonics 1-33. (b) Logaritmic scale, harm. 3-6000.

Fig. 6. Current peak functions of the number of eliminated harmonics at rated excitation. (Harmonic=1 refers to no harmonic elimination.)

not use the harmonic elimination. The proposed method gives a better accuracy in close proximity with the peaks where the current magnitude is linked with the magnetization curve, but does not modify the behavior in the shoulder area characterized by the loss curve. The harmonic content of line and phase currents for the simulated waveforms is shown in Fig. 10. The importance of triplen harmonic elimination increases with the excitation level. Beyond the knee point, the magnetization characteristic is flat and the current difference between the two characteristics for a certain magnetization level becomes even more marked.

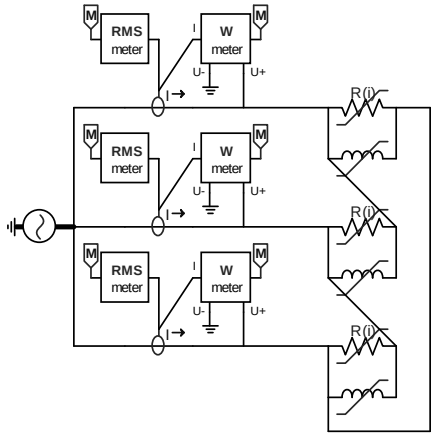

Fig. 7. ATPDraw test circuit.

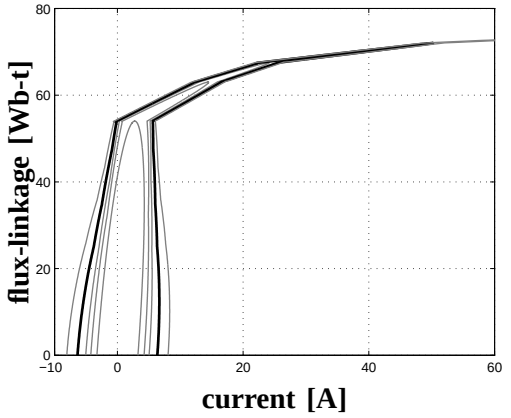

Fig. 8. Hysteretic behavior of the R-L model.

The no-load rms current and active loss are calculated in the simulation and compared with the test report values specified as input data of the routine. The results are reported in Table III. Input data and calculated line rms current differ up to 15% for the highest excitation level if triplen harmonic elimination is not taken into account. The difference is expected to increase further as the excitation level increases due to the nonlinear nature of the inductance. On the other hand, a very good agreement is obtained with the correct processing of the input data.

VII. DISCUSSION

Compared to the previously available algorithms (Talukdar [5], Prusty [6] and Neves [8], [11]), the use of a complete and general analytical algorithm for the calculation of loss and magnetization curves of transformers is the main contribution of this paper. The new algorithm enables the verification of the result

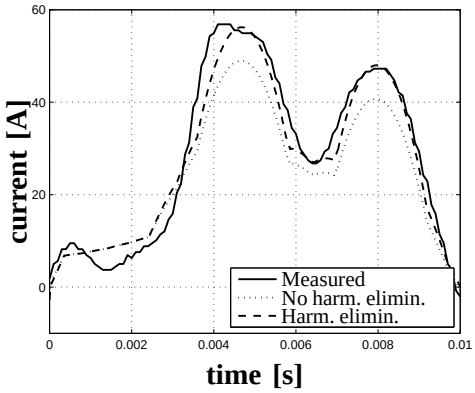

Fig. 9. Measured and simulated line current waveforms at rated voltage.

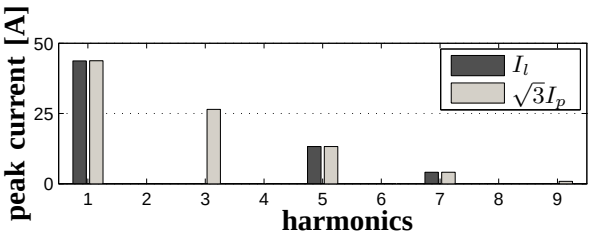

Fig. 10. Harmonics of phase and line currents (rated excitation and triplen harmonic elimination).

accuracy against the number of harmonics taken into account. In [11] it is suggested that harmonics up to the 99th order should be treated, while Fig. 6 shows that eliminating harmonics higher than the third does not significantly improve the accuracy. Finally, the model has been verified with measurement and validated against the input data.

The assumption of a sinusoidal voltage may be doubtful specially when a relatively low power generator is used to perform open circuit test of large transformer units. If the sinusoidal voltage assumption is not considered valid, the test report

TABLE III
RESULTS COMPARISON.

Excitacion	**Test Report**		**Simulation**		
Voltage [kV]	Current [A]	Loss [kW]	Current [a] [A]	Current [b] [A]	Loss [kW]
12	5.23	83.1	5.2323	5.2323	83.1
14	11.51	118.8	10.759	11.536	118.8
15	17.79	143.6	15.362	17.812	143.59
16	32.44	178.6	28.334	32.445	178.59
17	70.11	226.5	59.376	70.075	226.48

[a] no harmonic elimination
[b] triplen harmonic elimination

data alone are not adequate to establish the correct magnetization characteristic of a transformer. Transformer manufacturers and customers aware of this may decide to provide/require an additional and more comprehensive set of open circuit data than rms values.

The extrapolation of the magnetization curve beyond the last measured point and into extreme saturation remains uncertain. Possible approaches are linear extrapolation, air core inductance (connected to the last point of the magnetization curve), and curve fitting. The choice of a correct extrapolation method is important for inrush current and ferroresonance studies. A comparison between inrush calculation based on linear extrapolation and curve fitting (Frolich equation) is shown in [16].

While the parallel R-L representation treated in this paper lacks an accurate hysteresis and eddy current losses representation, the method presented here is a valid tool for parameter estimation of more accurate hysteretic models. An example of the use of the magnetization curve for the extraction of the Jiles-Atherton model parameters is given in [17].

The currents measured in a no-load test are the line currents. These currents are in general different for three-phase transformers due to the asymmetry of the core structure. The method presented in this paper does not take into account the core topology of a transformer and assume the three phases of a transformer to be identical. Topologically correct models exist and their use is suggested in case of unbalanced operation and where an accurate representation of the effect of the magnetic coupling between phases is important for the type of study investigated. When the central focus of the study is not on the transformer itself, a simpler and computationally more efficient representation of the transformers may be desired. In this case the presented approach can be used.

VIII. CONCLUSION

An algorithm for the computation of the magnetization curve from rms V/I to peak λ/i has been presented. The algorithm is analytical and implements the processing of no-load losses and delta connected winding. Other algorithms are analytical but neglect the handling of losses and delta connected winding, or are based on numerical and iterative approaches.

This paper focuses mainly on the handling of delta connected winding. Disregarding the transformer winding coupling type leads to significant inaccuracies that can be easily avoided with the proposed analytical algorithm. The test case with a 290 MVA GSU transformer shows an increase in the calculated peak current of above 10% at rated voltage with proper triplen harmonic handling. This difference will increase considerably with excitation voltage.

ACKNOWLEDGMENT

The research team at NTNU and SINTEF Energy Research acknowledge the Norwegian Research Council, Hafslund Nett, Statnett SF, Statkraft Energi AS, NVE, EDF, Nynäs Petroleum AB and ABB for their support in the project “Thermal and electromagnetic performance of transformers”.

REFERENCES

[1] F. de Leon and A. Semlyen, "Complete transformer model for electromagnetic transients," *IEEE Trans. Power Del.*, vol. 9, no. 1, pp. 231–239, 1994.

[2] J. A. Martinez and B. A. Mork, "Transformer modeling for low- and mid-frequency transients - a review," *IEEE Trans. Power Del.*, vol. 20, no. 2 II, pp. 1625–1632, 2005.

[3] J. A. Martinez, R. Walling, B. A. Mork, J. Martin-Arnedo, and D. Durbak, "Parameter determination for modeling system transients - part III: Transformers," *IEEE Trans. Power Del.*, vol. 20, no. 3, pp. 2051–2062, Jul. 2005.

[4] *IEEE standard test code for liquid-immersed distribution, power, and regulating transformers*, IEEE Std. C57.12.90-1999, 1999.

[5] S. N. Talukdar, J. K. Dickson, R. C. Dugan, M. J. Sprinzen, and C. J. Lenda, "On modeling transformer and reactor saturation characteristics for digital and analog studies," *IEEE Trans. Power App. Syst.*, vol. 94, no. 2, pp. 612–621, Mar 1975.

[6] S. Prusty and M. Rao, "A direct piecewise linearized approach to convert rms saturation characteristic to instantaneous saturation curve," *IEEE Trans. Magn.*, vol. 16, no. 1, pp. 156–160, 1980.

[7] H. W. Dommel, A. Yan, and S. Wei, "Harmonics from transformer saturation," *IEEE Trans. Power Del.*, vol. 1, no. 2, pp. 209–215, 1986.

[8] W. L. A. Neves and H. W. Dommel, "On modelling iron core nonlinearities," *IEEE Trans. Power Syst.*, vol. 8, no. 2, pp. 417–422, 1993.

[9] H. W. Dommel and et.al., *Electromagnetic Transients Program Reference Manual (EMTP Theory Book)*. Portland, OR: Prepared for BPA, Aug. 1986.

[10] *ATP Rule Book*, Leuven EMTP Center, Jul. 1987.

[11] W. L. A. Neves and H. W. Dommel, "Saturation curves of delta-connected transformers from measurements," *IEEE Trans. Power Del.*, vol. 10, no. 3, pp. 1432–1437, 1995.

[12] O. P. Hevia, "Inductor with losses in the ATP," in *EEUG News*, Aug. 2001, pp. 13–22.

[13] *Guide for Transformer Loss Measurement*, IEEE Std. C57.123, 2002.

[14] S. V. Kulkarni and S. A. Khaparde, *Transformer engineering: design and practice*, ser. Power engineering. New York, N.Y.: Marcel Dekker, Inc., 2004, vol. 25.

[15] P. Picher, L. Bolduc, R. Gagnon, and G. Sybille, "Study of the apparent load loss unbalance in three-phase transformers," in *Electrical and Computer Engineering, 2005. Canadian Conference on*. IEEE, May 2005, pp. 1481 – 1484.

[16] H. K. Høidalen, B. A. Mork, F. Gonzalez, D. Ishchenko, and N. Chiesa, "Implementation and verification of the hybrid transformer model in ATPDraw," *Electr. Power Syst. Res.*, vol. 79, no. 3, pp. 454 – 459, Mar. 2009, special Issue: Papers from the 7th International Conference on Power Systems Transients (IPST), 7th International Conference on Power Systems Transients.

[17] N. Chiesa and H. K. Høidalen, "Hysteretic iron-core inductor for transformer inrush current modeling in EMTP," in *PSCC 2008 - 16th Power Systems Computation Conference*, Glasgow, Scotland, Jul. 2008.

Nicola Chiesa was born in Italy in 1980. He received the MSc degree in Electrical Engineering from Politecnico di Milano in 2005. From 2005 to 2009 he joined the Department of Electric Power Engineering at the Norwegian University of Science and Technology as a PhD candidate. He is now with the Department of Energy Systems at SINTEF Energy Research.

Hans Kristian Høidalen (M'05) was born in Norway in 1967. He received his MSc and PhD from the Norwegian University of Science and Technology in 1990 and 1998, respectively. He is now a professor at the same institution with a special interest of electrical stress calculations and modeling.

CONFERENCE PROCEEDING

On the ringdown transient of transformers

N. Chiesa, A. Avendaño, H. K. Høidalen, B. A. Mork,
D. Ishchenko, and A. P. Kunze

2007

International Conference on Power Systems Transients (IPST'07)

Presented: Lyon, France, Jun. 4-7, 2007

Is not included due to copyright

CONFERENCE PROCEEDING

Hysteretic iron-core inductor for transformer inrush current modeling in EMTP

N. Chiesa,H. K. Høidalen

2008

16th Power Systems Computation Conference (PSCC 2008)

Presented: Glasgow, Scotland, Jul. 2008

HYSTERETIC IRON-CORE INDUCTOR FOR TRANSFORMER INRUSH CURRENT MODELLING IN EMTP

Nicola Chiesa
NTNU
Trondheim, Norway
nicola.chiesa@elkraft.ntnu.no

Hans K. Høidalen
NTNU
Trondheim, Norway
hans.hoidalen@elkraft.ntnu.no

Abstract - A crucial element of transformer models for transient simulation is the representation of the core. The modelling of non-linear hysteretic inductors required to properly represent a transformer core is a challenge in an electromagnetic transient program. The simulation of transients such as inrush and ferroresonance require a correct handling of nonlinear and frequency dependent losses, accurate hysteresis loop representation, possibility of flux initialization, and a proper automatic initialization by disconnection transients. This paper analyses standard available models and tests an advanced hysteretic model based on the Jiles-Atherton theory. This model is implemented in a topologically correct core representation and the parameters are obtained from test report data. Due to the interaction of several nonlinear elements, the solution of such model is still a challenge in an classical EMTP programs based on compensation method. Good agreement with ringdown and inrush measurements is achieved.

Keywords - Electromagnetic transients, inrush current, remanent magnetization, Jiles-Atherton, hysteresis, core losses, topologically correct core.

1 INTRODUCTION

THIS paper deals with the modelling of the magnetic core of transformers. A core model is required for simulations and studies that may involve dynamic excitation of the magnetic component of a transformer as low-frequency and slow-front transient analysis, [1]. These types of studies involve neither load flows, where only steady-state quantities are of interest, nor high-frequency and impulse transients, where the network capacitances are dominating the evolution of the transients. Areas of interest are inrush-current and ferroresonance studies, with practical application involving relay setting, inrush current mitigation, sympathetic inrush identification and investigation of resonances.

A transformer iron-core and any other ferromagnetic nonlinear inductance classically modeled in an electromagnetic transient program (EMTP) suffer from low accuracy. The main obstacle is the lack of input data: advanced models require detailed measurements for the estimation of parameters, while standard test report is usually the only source of data. An accurate representation of the losses (nonlinear and frequency dependent) is also a required feature of an accurate model.

Several hysteretic inductor models are presented in literature with the most noticeable summarized in [2]. The Jiles-Atherton (JA) and Preisach models are pre-

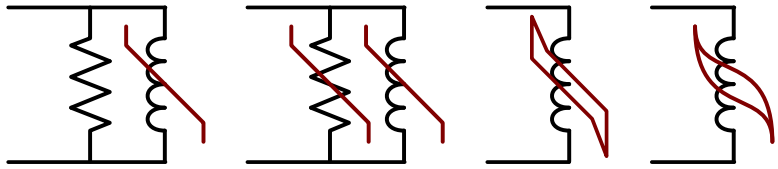

Figure 1: Representations of nonlinear inductor with losses.

ferred for their capability of representing minor loop operations and de-energization transients, thus their capability to estimate the remanent magnetization of an iron-core inductor. Among this two, the JA model has been preferred mainly because the model parameters can be obtained with fitting procedures as reported in [3], thus specific measurements are not required. The same reference also reveals a lower effort and a faster execution of the JA model. The same model has been reported successfully implemented in an electromagnetic transient program as described in [4, 5]. The Preisach model may give however better correspondence with the measurements especially in case of a large excitation range.

The implementation and the comparison of the various hysteretic iron-core inductor models is out of the scope of this paper. The main purpose is to present the significance of using such a model in electromagnetic transient simulations and to demonstrate the use of several instance of a hysteretic model in a topologically correct three-legged transformer model for representing disconnection and energization transients.

2 NONLINEAR CORE MODELLING

2.1 Single-phase representation

Iron-core inductor exhibits nonlinear characteristic of both magnetization current and iron losses as function of the applied voltage. The no-load current is the sum of the magnetization current and the current due to the core losses. Core losses are an important aspect to take into account; their nonlinear and frequency dependent nature makes the implementation in a transient simulation program not straight forward. Core losses can be divided in two parts: hysteresis losses and losses due to eddy current in laminations. Hysteresis losses per cycle are frequency independent, but they are affected by the excitation level. Eddy current losses vary nonlinearly with frequency. Fig. 1 shows different approaches used to model the behaviour of a nonlinear inductor. Each of this approach has its advantages and weaknesses.

The first distinction can be made between multi-elements (R-L representation) and true hysteretic models. In multi-elements models the losses are represented by either a linear or a nonlinear resistor, while the saturation curve is modeled with a nonlinear inductor. Hysteretic models include losses and saturation in the same model. R-L representation has the advantage of having a simple implementation and

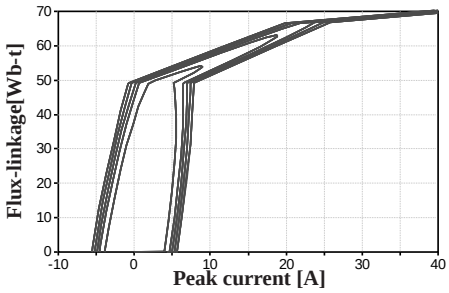

(a) Linear resistor.

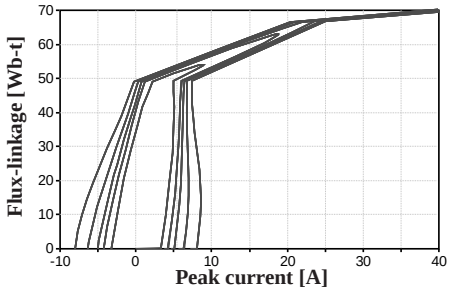

(b) Nonlinear resistor.

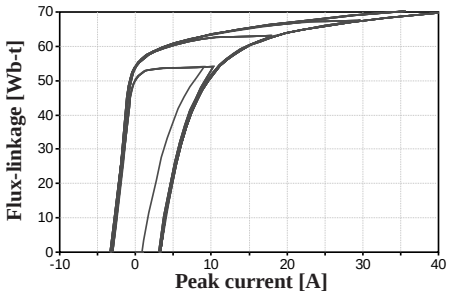

(c) Jiles-Atherton with eddy-current.

Figure 2: Hysteresis loops comparison; excitation 75–106%.

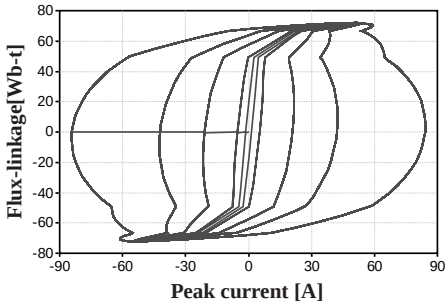

(a) Linear resistor.

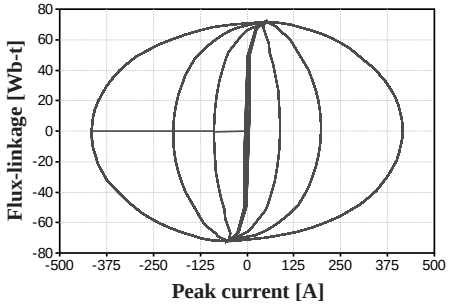

(b) Nonlinear resistor.

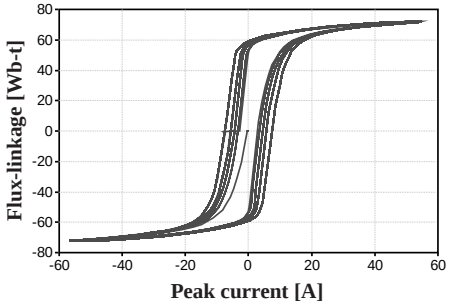

(c) Jiles-Atherton with eddy-current.

Figure 3: Frequency dependency; V/f constant.

relaying on standard available components. However, multi-elements models fails to reproduce remanent magnetization, [6].

The nonlinear inductor and resistor are usually characterized by piecewise-linear curves and are solved either by direct matrix change approach or compensation method, [7]. When a linear resistor is used, it is common to fix the resistance value to match losses at rated excitation. This gives overestimation of losses for lower level of excitation and underestimation for higher level of excitation. Better fitting of the losses can be achieved by a nonlinear resistor, however it has to be carefully implemented since hysteresis losses depend on maximum flux and not voltage, [8, 9]. A nonlinear resistor characteristic is defined as a $v - i$ curve: the differential resistance becomes lower (higher losses) as the voltage level increases. The losses reach their highest value at voltage peak, which correspond to the zero of the flux-linkage and to the base of the hysteresis loop.

Fig. 2 and 3 refer to a 290MVA 432/16kV 50Hz three-phase transformer, Table 1. The magnetization characteristic of the delta connected transformer has been obtained from positive-sequence data applying a triplen harmonic elimination method, [10]. In the first figure the supplied voltage has been varied between 75% and 106% of the rated voltage and constant rated frequency, while in the second figure the ratio V/f has been kept constant and the frequency varied as 1/4, 1, 4, 8, and 16 times the rated frequency.

The flux-current trajectory that may result from using a nonlinear piecewise resistor is unnatural and have a tendency to underestimate the losses in the vicinity of the knee area (this can be seen from the narrow width of the hysteresis loops in this area of the curve as shown in Fig. 2(b)). R-L representation may correctly represent losses at power frequency but does not provide a proper frequency dependency and may result in a bobbling effect of the hysteresis loop as reported in Fig. 3(b).

Concerning true hysteresis models, two approaches can be followed: path tracing, [11, 12], and mathematical representation, [2]. The path tracing approach is based on the scaling and expansion of a defined primary hysteresis loop. While this has been criticized mainly due to its simplistic representation of sub-loop operations, it allows residual flux and it requires a fairly limited input data. A physical description of a hysteretic model is unrealistic for a practical use due to the great level of uncertainty, and a mathematical representation based on measurement and parameter fitting should be preferred.

Fig. 2(c) and 3(c) represent the hysteresis loops obtained by the implementation of a Jiles-Atherton model that includes eddy-currents effects, [5, 13]. This model preserves the characteristic of the hysteresis loop for a wide range of excitation levels and frequencies. True hysteretic models have also a better relocation of the losses in the full area of the hysteresis loop than models that represent losses with a resistor in parallel to a nonlinear inductor. A limitation observed for the JA model is a poor fitting of the loss characteristic over a wide range of excitation, [14]. The Jiles-Atherton theory is quite mature and widely accepted, but has room for improvement in loss fitting.

Table 1: Generator Step-up Transformer Test-Report.

Main data	[kV]	[MVA]	[A]	Coupling
HS	432	290	388	YN
LS	16	290	10465	d5
Open-circuit	E_0[kV,(%)]	[MVA]	I_0[%]	P_0[kW]
LS	12(75)	290	0.05	83.1
	14(87.5)	290	0.11	118.8
	15(93.75)	290	0.17	143.6
	16(100)	290	0.31	178.6
	17(106.25)	290	0.67	226.5
Short-circuit	[kV]	[MVA]	ek, er[%]	P_k[kW]
HS/LS	432/16	290	14.6, 0.24	704.4

2.2 Extrapolation and final slope

A core model is usually based on the transformer open-circuit test measurement. Conventionally data at rated excitation is reported. Additional points are required in order to characterize the nonlinearity of the core and built a piecewise linear characteristic. Transformer manufacturers most commonly provide additional data for 90% and 110% excitation levels. Table 1 shows the test report data for a 290 MVA step-up transformer. In this case five results of the open-circuit test are provided, spanning from 75% to 106.25% of the rated voltage. The data provided by the open-circuit test report is sufficient when the purpose of the transient simulation does not involve heavy saturation of the transformer core. Note that the rms $V - I$ characteristic specified in a test report has to be converted to a peak $\lambda - i$ characteristic by use of the ATP CONVERT/SATURA routine [7] or a more advanced method that that can take into account the three-phase coupling [10].

Open-circuit test reports seldom include data above the 110% of excitation level; testing a power transformer in heavy saturation requires a large and stiff source, with rated power comparable to the power of the transformer. Indeed, no testing facility has the capability of performing such test on large units. Thus, the extension process is not straight forward.

Fig. 4 shows how a piecewise nonlinear characteristic is extended by linear extrapolation and curve fitting. The linear extrapolation method assumes a constant slope of the saturation curve after the last specified segment of the piecewise nonlinear curve. This approach becomes doubtful when the two last points of the piecewise nonlinear curve lie in the 100% to 110% excitation level range: the transformer has not reach the complete saturation during the open-circuit test and a linear extension of the curve will result in a severe underestimation of current for any excitation level above the last specified point. Curve fitting allows the definition of additional artificial points of the saturation characteristic, such that new segments can be added to the piecewise nonlinear curve. While linear extrapolation is most commonly used, the curve fitting approach should be preferred.

Without specific measurements it is difficult to verify how precisely the curve fitting method can represent the saturated region and mainly relay on the fitting function used. Here a modified version of the Frolich equation, [14], has been used as

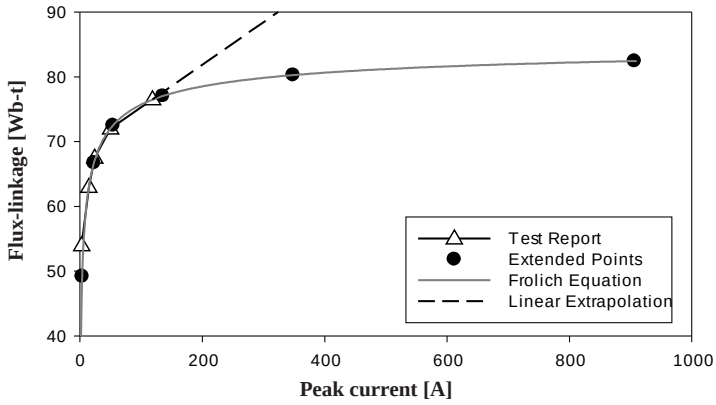

Figure 4: Representations of nonlinear inductor with losses.

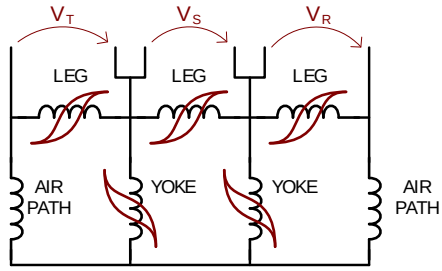

Figure 5: Topologically correct representation of three-legged transformer core.

indicative example:

$$\lambda = \frac{i}{a + b \cdot |i| + c \cdot \sqrt{|i|}} \tag{1}$$

with $a = 0.768 \cdot 10^{-3}$, $b = 11.6 \cdot 10^{-3}$, and $c = 16 \cdot 10^{-3}$.

Despite the fact that more advanced techniques exist [15], curve fitting is a simple method that requires no more than the standard test report data and allows the extension of the saturation characteristic. It is particularly useful to improve the nonlinear characteristic of a piecewise nonlinear inductor.

2.3 Three-phase representation

A three-phase transformer can either be represented as a single-phase equivalent model, or as a true three-phase model, [9, 16–19]. Most of the available models in transient simulation packages are of the first type. Such a model is a simplistic representation of a three-phase component and disregards the magnetic coupling between the phases. This approach may be accurate enough for steady state and balanced operations; however the approximations introduced are doubtful for transient analysis involving unbalanced operation. Practical cases that recommend true three-phase models are studies of single pole operations, single-phase faults, synchronized switching operations, energization and de-energization transient studies, and highly

nonlinear and stochastic behaviours as ferroresonance, just to mention some of them.

A true three-phase equivalent electric circuit model of a three-legged stacked core transformer is shown in Fig. 5. A full description of a transformer model that uses this approach can be found in [1, 20]. These references also greatly address the problem of parameters estimation based on three different sources of data: test report, design data, and typical values.

A transformer model developed as in Fig. 5 may correctly represent the intrinsic difference of the central and external phases, the induced voltage between phases in case of single- or bi-phase energization, and zero sequence behaviour. Such aspects are missing from a single phase equivalent representation.

All the transformer magnetic sections or limbs are build with the same material, thus has a common magnetic properties and $B-H$ hysteresis loop. The use of magnetic properties is not of great advantage because physical dimension are required to obtain the electric quantities and to express the hysteresis loop in term of more practical flux-linked and current-peak ($\lambda - i$) as shown in (2). Moreover, the magnetic properties of the ferromagnetic material do not take into account how a transformer core is manufactured in term of joint influence and inter-laminations air-gaps. Relative core dimensions (A_{REL} and l_{REL} respectively for relative cross section area and relative length) are of great advantage in the estimation of the core parameters such as anhysteretic curve or hysteresis loop, since the properties of a single section of core can be rescaled to any of the other sections of the magnetic core, (4). Core dimension ratios have the advantage of varying in a limited range regardless the size of the transformer and are easier to be estimated if not known.

$$\frac{B}{H} = \frac{\frac{\lambda}{AN}}{\frac{iN}{l}} = \frac{\lambda}{i} \cdot \frac{l}{A \cdot N^2} \tag{2}$$

$$\frac{\lambda_1}{i_1} \cdot \frac{l_1}{A_1} = \frac{\lambda_2}{i_2} \cdot \frac{l_2}{A_2} \tag{3}$$

$$\frac{\lambda_2}{i_2} = \frac{\lambda_1}{i_1} \cdot \frac{l_1}{A_1} \cdot \frac{A_2}{l_2} = \frac{\lambda_1}{i_1} \cdot \frac{A_{REL}}{l_{REL}} \tag{4}$$

3 JILES-ATHERTON MODEL

The Jiles-Atherton model presented in [5] has been implemented in the ATP version of EMTP using the MODEL language. The original JA model is expressed in term of magnetic quantities, (5). Here the set of equation has been revisited in term of electric quantities, (6). This allows to obtain unique parameters for a section of the core and rescaling the input and output quantities by the relative cross section area and length for different sections of the core.

$$B = \mu_0 \left(M + H\right) \tag{5}$$

$$\lambda = L_{inf} \left(i_M + i_E\right) \tag{6}$$

The basic Jiles-Atherton equations in term of $\lambda - i$ are:

$$i_{Eeff} = i_E + \alpha\, i_M \tag{7}$$

$$i_{Man} = i_{Msat}\, \frac{a_1\, i_{Eeff} + i_{Eeff}^2}{a_3 + a_2\, i_{Eeff} + i_{Eeff}^2} \tag{8}$$

$$\delta = sign\left(\frac{di_E}{dt}\right) \tag{9}$$

$$\frac{di_M}{di_E} = \left(c\, \frac{di_{Man}}{di_{Eeff}} + T\right) \frac{1}{1 - \alpha\, c\, \dfrac{di_{Man}}{di_{Eeff}}} \tag{10}$$

$$T = \begin{cases} 0 & \text{for } (i_{Man} - i_M)\delta > 0 \\ \dfrac{i_{Man} - i_M}{\frac{\delta\, K}{L_{inf}} - \frac{\alpha(i_{Man} - i_M)}{1-c}} & \text{for } (i_{Man} - i_M)\delta \leq 0 \end{cases} \tag{11}$$

These can be implemented in an EMTP program based on the trapezoidal rule of integration as follows:

$$\Delta\lambda = \left((V(t - dt) + V(t))\frac{dt}{2}\right) \cdot \frac{1}{A_{REL}} \tag{12}$$

$$\lambda(t) = \lambda(t - dt) + \Delta\lambda \tag{13}$$

$$\begin{cases} \Delta i_E = Q \cdot \Delta i_{max} \\ \Delta i_{max} = \frac{\Delta\lambda}{L_{inf}} \\ \Delta i_M = \Delta i_{max} - \Delta i_E \\ i_E(t) = i_E(t - dt) + \Delta i_E \\ i_M(t) = i_M(t - dt) + \Delta i_M \\ \frac{di_M}{di_E} = \ldots \text{ from (10)} \end{cases} \tag{14}$$

$$Q = \frac{1}{\frac{di_M}{di_E} + 1} \tag{15}$$

$$\begin{cases} L_{diff} = L_{inf}\, \left(\frac{di_M}{di_e} + 1\right) \\ i(t) = (i_E(t) + i_{clc}(t) + i_{exc}(t)) \cdot l_{REL} = \\ \qquad = \left(i_E(t) + k_1\, v(t) + k_2\, \sqrt{v(t)}\right) \cdot l_{REL} \end{cases} \tag{16}$$

where the set of equation (14) uses a guessed initial value of Q ($(0 < Q < 1)$) and

has to be iterated in order to satisfy (15)[1], and with:

λ: flux-linkage;
i_E: electric current;
i_{Eeff}: effective electric current;
i_M: magnetization current;
i_{Man}: anhysteretic magnetization current.

A total of eight (plus two optional) parameters have to be estimated:

L_{inf} : inductance in complete saturation;
i_{Msat} : saturation level of the anhysteretic curve;
a_1, a_2, a_3 : parameters of the anhysteretic curve;
α : interdomain coupling, controls the slope of the hysteresis loop;
c : ratio of the initial normal to the initial anhysteretic susceptibility, controls the transition smoothness of the knee area;
K : width of the base of the hysteresis loop, main contribution to the losses;
k_1, k_2 : rate dependent terms for classical and excessive eddy current (optional).

A comprehensive explanation of the function and the numerical determination of each parameter can be found in [21].

No special measurements are required to estimate the parameters. Data from a standard test report and a fitting procedure may be sufficient. The fitting is done in two steps. First the anhysteretic curve parameters are estimated by numerical fitting of the magnetization current subtracted by the losses, as explained in section 2.2 and [10]. Then the losses are fitted using the complete model and the remaining parameters are estimated. An additional optional step is required to fit the two rate dependent terms; extensive measurements at different values of excitation frequency are needed in this case.

For three-phase transformer with a topologically correct core model, the fitting procedure is non-trivial. The core is divided in several section as shown in Fig. 5. The parameters to be estimated remain the same and do not multiply by the number of sections. However the models of the different sections have to be solved together and converge to the RMS values reported in the test report.

When multiple instances of a hysteretic model are used in EMTP simulation software the implementation is not trivial as the different models have to interact and

[1]This equation is incorrect in the originally published paper.

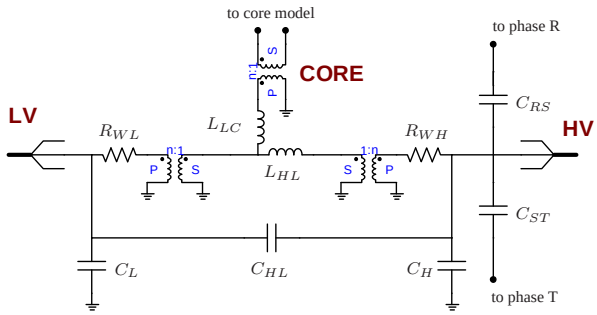

Figure 6: Transformer model, central phase, no core.

be solved together with the rest of the circuit. EMTP/ATP offers two different approaches based either on compensation or iteration method (type-94) for the implementation of user defined models. The compensation method has been preferred due to a faster computation time, and has been verified to give negligible error compared to the iteration method for a relatively small time step.

4 CASE STUDY

A 300kVA, 11430/235V YNyn three-legged transformer has been used as test object to verify the model. Fig. 6 shows the model used in the simulations. Only the central phase S without the core representation is shown in the figure. The other two phases are analogue and the core has been modeled with five JA hysteretic inductor as in Fig. 5. Ideal transformer has been used to allow the connection to the core and keep the freedom to have both wye and delta configuration by changing the coupling on the primary side of the ideal transformers. R_{WL} and R_{WH} are the winding resistances and are calculated from short-circuit test data. L_{HL} represent the main leakage channel and is calculated from the short-circuit test data. L_{LC} is the leakage channel between low-voltage winding and a fictitious winding on the core surface, [1]. It is assumed $L_{LC} = L_{HL}/2$. Capacitances to ground (C_L and C_H), between low and high voltage coils (C_{HL}) and between high voltage coils of different phases (C_{RS} and C_{ST}) are calculated from design data.

The result from the no-load test (RMS no-load current and active no-load losses) are compared in Fig. 7 with the result of simulations performed with corresponding conditions as during the measurements. While an accurate matching of the RMS current is achieved, the model shows a poor agreement with the core losses. This is due to the already mentioned difficulties in fitting the JA parameters over several excitation levels. The fitting below rated voltage has been preferred as the core is the principal dissipative element during de-energization transients, while winding resistance has a dominant role during inrush transients, [6].

The steady-state no-load current waveforms are compared in Fig. 8. The agreement between simulation and measurement is quite satisfactory. While there is a good estimation of the peaks of all the three phases, the current in the shoulder area

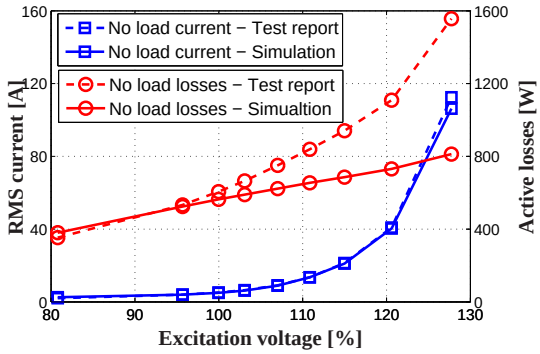

Figure 7: Comparison between measured and simulated test-report.

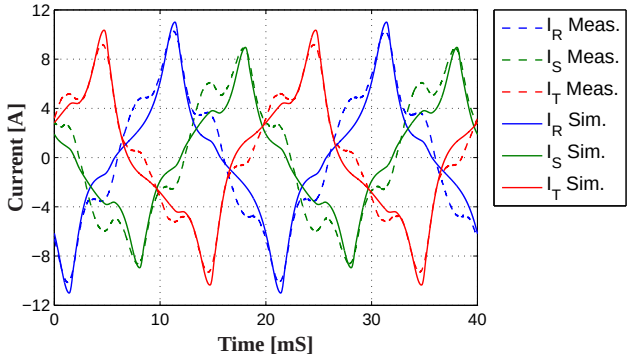

Figure 8: Noload current at rated excitation.

is underestimated. This can in part be imputed to the underestimation of the no-load losses. To be noticed is the correct representation of the different magnitude of the peaks for the different phases. Not only the current in the central phase is lower as expected, but the model can also represent the minor difference between phase R and T. This phenomenon is unexplained and may be further investigated in future research.

The model has been verified against inrush-current measurements with the transformer fed from the 11kV grid. Fig. 9 shows one of these measurements compared with the simulation results. A perfect matching between measurements and simulations is not expected as several parameters of the network feeding the transformer are unknown, and the voltage at the HV terminals was not recorded. In addition a 600kVA transformer was located in parallel to the tested one and the two transformers were controlled by a common circuit breaker. This configuration may have influenced the ringdown transient as the two transformers interact together during the de-energization. The inrush transient may have been influenced as well as much higher inrush current had to be fed by the network causing a higher voltage drop on the feeding line. The second transformer could not be modeled due to complete lack of data.

While the transformer model is quite advanced, the models of other network com-

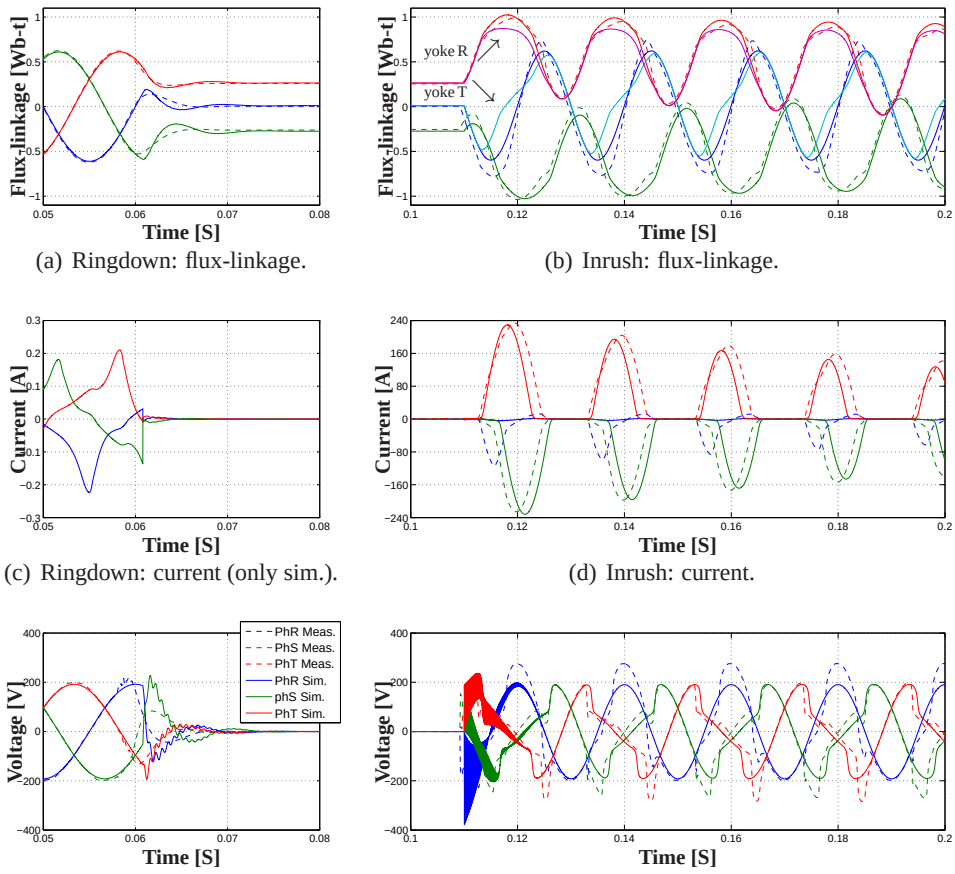

(a) Ringdown: flux-linkage.
(b) Inrush: flux-linkage.
(c) Ringdown: current (only sim.).
(d) Inrush: current.
(e) Ringdown: induced voltage.
(f) Inrush: induced voltage.

Figure 9: 300kVA three-legged transformer: ringdown and inrush.

ponent are very basic. Network components as circuit breaker (arc modelling and delay between poles), cable, lines, stray capacitances and other machines connected to the network can highly influence the insertion and disconnection transient of a nonlinear device. At this stage the main purpose is to test the accuracy of the core model, not the interaction with the rest of the network. The core model is highly depended from the linkage-flux. For this reason a suitable value of line impedance has been used in order to obtain a good match of the first peak of flux-linkage during inrush. Moreover, in order to obtain a good matching with the remanent fluxes the disconnection instant has been tuned within $\pm 2ms$ from the measured disconnection instant. It is important to remark that no tuning of the JA parameters has been done to obtain good matching with measurements. JA parameters were left as first derived from the open-circuit test data. Such a good agreement was obtain because an extended open-circuit test report with excitation covering the range between 80% and 130% was available.

The fluxes measured are obtained from the integration of the voltage on the low-voltage terminals. The simulated fluxes are the fluxes of the different section of

the core: legs and yokes. During steady-state condition and ringdown transients the fluxes in the yokes are equal to the fluxes of the correspondent legs. However as shown in Fig. 9(b), during inrush transients the fluxes in the yokes differ from the fluxes in the legs. This is due to the zero-sequence component of the flux that flows in air (air-path linear inductances in Fig. 5).

The shift in time of the inrush currents may be explained by a non perfect synchronization of the three poles of the circuit breaker. The model assumes a simultaneous closing of the poles, while a standard deviation is known to be in the range $\pm 1ms$. This aspect will be further investigated in future research when more advanced measurements will become available.

5 CONCLUSION

Different nonlinear inductor modelling techniques have been examined. When used in electromagnetic transient modelling, standard RL-representation introduce uncertainties concerned loss distribution and frequency dependent characteristic. Path tracing approach is a simple approximation of hysteretic behaviour. The investigation reveals the need of an advanced hysteretic model.

Curve fitting has been presented as an approach to reduce uncertainties at high saturation level when piecewise nonlinear inductor and linear extrapolation are used. The authors believe that curve fitting can increase the accuracy of transient simulations like inrush and ferroresonance, and any other study that demand an accurate model of the heavy saturated area of transformers and iron-core devices.

The Jiles-Atherton model has been successfully implemented in a topologically correct core model. The Jiles-Atherton model tested has a good potential, but more work has to be done to refine the loss model. The proposed core model has shown a good agreement with ringdown and inrush current measurements.

It has been verify that the Jiles-Atherton model parameters can be estimated from standard available data as test report with sufficient accuracy needed to model inrush current transient. However, fitting should be based on extended test report as the knowledge of very few point of the no-load test may strongly reduce the accuracy of the method.

Further work involves the improvement of the hysteretic model to obtain better fitting of the losses, a better verification of the capability of the model to reach the correct value of residual flux, a better measurement setup to record more relevant inrush-current measurement with lower influence of the feeding network. Moreover, a simple, automatic and more accurate fitting procedure will be addressed.

REFERENCES

[1] B. A. Mork, F. Gonzalez, D. Ishchenko, D. L. Stuehm, and J. Mitra, “Hybrid transformer model for transient simulation: Part I: development and parameters,” *IEEE Trans. Power Del.*, vol. 22, no. 1, pp. 248–255, Jan. 2007.

[2] F. Liorzou, B. Phelps, and D. L. Atherton, “Macroscopic models of magnetization,” *IEEE Trans. Magn.*, vol. 36, no. 2, pp. 418–428, Mar. 2000.

[3] D. A. Philips, L. R. Dupre, and J. A. Melkebeek, "Comparison of Jiles and Preisach hysteresis models in magnetodynamics," *IEEE Trans. Magn.*, vol. 31, no. 6 pt 2, pp. 3551–3553, Nov. 1995.

[4] M. Popov, L. Van Der Sluis, G. C. Paap, and P. H. Schavemaker, "On a hysteresis model for transient analysis," *IEEE Power Eng. Rev.*, vol. 20, no. 5, pp. 53–55, May 2000.

[5] W. Chandrasena, P. G. McLaren, U. D. Annakkage, R. P. Jayasinghe, D. Muthumuni, and E. Dirks, "Simulation of hysteresis and eddy current effects in a power transformer," *Electric Power Systems Research*, vol. 76, no. 8, pp. 634–641, May 2006.

[6] N. Chiesa, A. Avendaño, H. K. Høidalen, B. A. Mork, D. Ishchenko, and A. P. Kunze, "On the ringdown transient of transformers," in *IPST'07 - International Conference on Power System Transients*, no. IPST-229, Lyon, France, Jun. 2007.

[7] H. W. Dommel and et.al., *Electromagnetic Transients Program Reference Manual (EMTP Theory Book)*. Portland, OR: Prepared for BPA, Aug. 1986.

[8] A. Gaudreau, P. Picher, L. Bolduc, and A. Coutu, "No-load losses in transformer under overexcitation/inrush-current conditions: tests and a new model," *IEEE Trans. Power Del.*, vol. 17, no. 4, pp. 1009–1017, Oct. 2002.

[9] J. A. Martinez, R. Walling, B. A. Mork, J. Martin-Arnedo, and D. Durbak, "Parameter determination for modeling system transients - part III: Transformers," *IEEE Trans. Power Del.*, vol. 20, no. 3, pp. 2051–2062, Jul. 2005.

[10] W. L. A. Neves and H. W. Dommel, "Saturation curves of delta-connected transformers from measurements," *IEEE Trans. Power Del.*, vol. 10, no. 3, pp. 1432–1437, 1995.

[11] J. G. Frame, N. Mohan, and T. Liu, "Hysteresis modeling in an electro-magnetic transient program," *IEEE Trans. Power App. Syst.*, vol. PAS-101, pp. 3403–3412, Sep. 1982.

[12] S. Dennetière, J. Mahseredjian, M. Martinez, M. Rioual, A. Xémard, and P. Bastard, "On the implementation of a hysteretic reactor model in EMTP," in *IPST'03 - International Conference on Power Systems Transients*, New Orleans, USA, Sep. 2003.

[13] U. D. Annakkage, P. G. McLaren, E. Dirks, R. P. Jayasinghe, and A. D. Parker, "A current transformer model based on the Jiles-Atherton theory of ferromagnetic hysteresis," *IEEE Trans. Power Del.*, vol. 15, no. 1, pp. 57–61, Jan. 2000.

[14] N. Chiesa and H. K. Høidalen, "Modeling of nonlinear and hysteretic iron-core inductors in ATP," in *EEUG Meeting 2007, European EMTP-ATP Conference*, Leon, Spania, Sep. 2007.

[15] S. G. Abdulsalam, W. Xu, W. L. A. Neves, and X. Liu, "Estimation of transformer saturation characteristics from inrush current waveforms," *IEEE Trans. Power Del.*, vol. 21, no. 1, pp. 170–177, Jan. 2006.

[16] W. Enright, O. B. Nayak, G. D. Irwin, and J. Arrillaga, "An electromagnetic transients model of multi-limb transformers using normalized core concept," in *IPST'97 - International Conference on Power System Transients*, Seattle, Washington, Jun. 1997, pp. 93–98.

[17] W. Enright, O. Nayak, and N. Watson, "Three-phase five-limb unified magnetic equivalent circuit transformer models for PSCAD V3," in *IPST'99 - International Conference on Power System Transients*, Budapest, Hungary, Jul. 1999, pp. 462–467.

[18] J. A. Martinez and B. A. Mork, "Transformer modeling for low frequency transients - the state of the art," in *IPST'03 - International Conference on Power Systems Transients*, no. 9a-1, New Orleans, USA, Sep. 2003.

[19] ——, "Transformer modeling for low- and mid-frequency transients - a review," *IEEE Trans. Power Del.*, vol. 20, no. 2 II, pp. 1625–1632, 2005.

[20] B. A. Mork, F. Gonzalez, D. Ishchenko, D. L. Stuehm, and J. Mitra, "Hybrid transformer model for transient simulation: Part II: laboratory measurements and benchmarking," *IEEE Trans. Power Del.*, vol. 22, no. 1, pp. 256–262, Jan. 2007.

[21] D. C. Jiles, J. B. Thoelke, and M. K. Devine, "Numerical determination of hysteresis parameters for the modeling of magnetic properties using the theory of ferromagnetic hysteresis," *IEEE Trans. Magn.*, vol. 28, no. 1, pp. 27–35, Jan. 1992.

CONFERENCE PROCEEDING

Systematic switching study of transformer inrush current: simulation and measurements

N. Chiesa, H. K. Høidalen

2009

International Conference on Power Systems Transients (IPST'09)

Presented: Kyoto, Japan, Jun. 2009

Is not included due to copyright

JOURNAL PAPER

Transformer model for inrush current calculations: simulations, measurements and sensitivity analysis

N. Chiesa, B. A. Mork, H. K. Høidalen

2010

IEEE Transaction on Power Delivery

Accepted for publication

TPWRD-00942-2009

Transformer Model for Inrush Current Calculations: Simulations, Measurements and Sensitivity Analysis

Nicola Chiesa, Bruce A. Mork, *Senior Member, IEEE*
and Hans K. Høidalen, *Member, IEEE*.

Abstract

The modeling of inrush currents that occur upon energization of a transformer is a challenge for EMTP-type programs due to limitations in available transformer models and ability to determine and specify initial flux. The estimation of transformer model parameters is also an issue. This paper presents a transformer model for low- and mid- frequency transient studies with focus on the behavior in saturation and the estimation of residual fluxes. The comparison of the simulation results with analytical calculations and measurements proves the capability of the model to accurately represent energization and de-energization transients of a three-legged-core distribution transformer. A novel property is the ability of auto initialization after disconnection, made possible by the implementation of a hysteretic core model which properly simulates and remembers residual flux from the previous de-energization. Special attention is paid to parameter estimation. Detailed core and winding design data are not used as they are seldom available from the manufacturer. A sensitivity analysis is performed to verify the influence of each parameter on the inrush current envelope curve. It is observed that the parameter that most influences the current amplitude is the slope of the magnetization curve at extreme saturation.

Index Terms

Transformer modeling, inrush current, residual flux, nonlinearities, power system transients.

I. INTRODUCTION

TRANSFORMERS have the greatest exposure to electrical transients with the exception of transmission lines [1]. The standard models used in electromagnetic transient programs to predict their behavior are not always adequate due to lack of data, measurements, and knowledge. The aim of this paper is the modeling of power transformers where inrush current during energization is an issue related to relay settings, inrush mitigation by synchronized switching, voltage harmonic distortion, control of switching overvoltages, and internal mechanical stress reduction.

The shape, magnitude and duration of the inrush current depends on several factors as network topology, transformer construction, winding coupling, residual fluxes, and circuit breaker's current-chopping characteristic. The highest current-peak calculated on the basis of the combination of these factors and occurring in the

first period after the energization of a transformer is defined as worst-case inrush current. This current decays after several periods to reach the steady-state value of the magnetization current. Analytical equations exist to approximately calculate worst-case inrush current and decay of single-phase transformers [2], [3].

References [4]–[7] present a comprehensive and up-to-date review of transformer models for electromagnetic transients. Topologically correct models based on the transformer geometry should be preferred for transient studies as each individual limb of the magnetic circuit contributes to the magnetization characteristic. This approach can represent any type of core such that unbalance operations are accurately reproduced, but requires a more detailed set of parameters than the less accurate single-phase equivalent transformer models. Standardly available models that adopt this approach are the unified magnetic equivalent circuit (UMEC) model in PSCAD/EMTDC [8]–[10], and the hybrid transformer model (XFMR) implemented in ATPDraw [11]–[14].

The models UMEC and XFMR have limitations related to the accuracy at extreme saturation and the proper representation of the hysteretic behavior of the core. A large variation between the two models in the prediction of an inrush transient is reported in [14]. In addition, neither model can retain a residual flux value after de-energization and the manual specification of initial residual fluxes is complex. The simulations are therefore restricted to the case of zero residual flux initial condition. To overcome these weak points, the model proposed here is based on a topologically correct hysteretic core, with special consideration of behavior in extreme saturation. The capability of auto initialization after disconnection of the model overcomes the common problem of manually initializing the residual fluxes. Manual initialization of the residual fluxes is also possible.

Section II presents the development and the topology of the proposed transformer model. Section III shows the performance of the model compared to measurements. Section IV outlines standard analytical inrush formulas and relates these to simulations. A sensitivity study of the most important parameters is performed in Section V in order to establish the crucial factors that may influence the model performance, and to enhance their estimation procedure.

II. TRANSFORMER MODEL

This new transformer model is developed in a way somewhat equivalent to that of the hybrid model presented in [11], [12]. The topology of a three-legged two-winding transformer is shown in Fig. 1. The magnetic paths in the iron (nonlinear reluctances) and in air (linear reluctances) are detailed in the figure. The magnetic circuit of Fig. 2 is then deduced according to the physical topology of the transformer. The nonlinear reluctances (black rectangles) refer to the saturable transformer limbs ($\mathfrak{R}_{Leg}$, $\mathfrak{R}_{Yoke}$). The linear reluctances (white rectangles) account for the main leakage channel between the high- and low-voltage windings ($\mathfrak{R}_{HL}$), a secondary leakage channels between the inner winding and the core ($\mathfrak{R}_{LC}$), and the zero sequence leakage ($\mathfrak{R}_0$).

The equivalent electric circuit of Fig. 3 is obtained by duality transformation of the magnetic circuit. Ideal transformers account for the winding turns ratio and

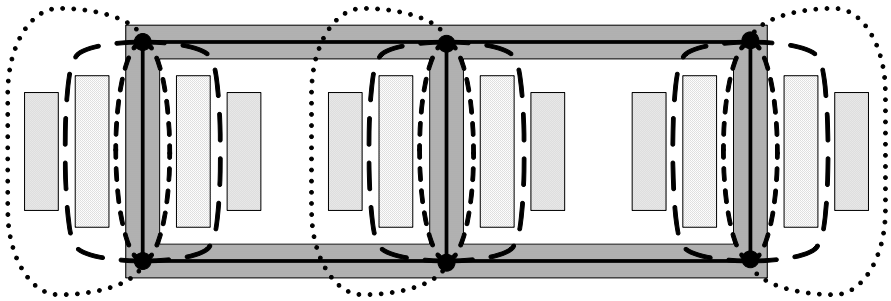

Fig. 1. Physical structure of three-legged transformer with magnetic paths.

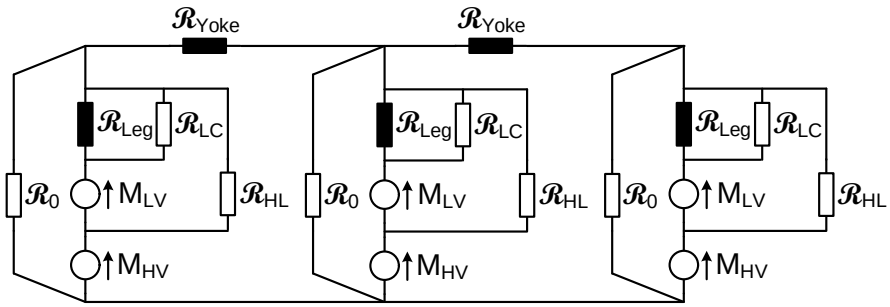

Fig. 2. Magnetic circuit of a three-legged transformer.

interface the dual electric circuit with the external electric network. The winding resistances are connected at the transformer terminals. The coupling and phase-shift (e.g. Δ, Y, auto) are achieved by external connections of the transformer terminals. The capacitance network is shown in Fig. 4 and is connected to each end of the winding terminals.

This model is implemented in ATP/EMTP and is intended to be a general purpose model for electromagnetic transient studies. It can be easily extended to five-legged core transformers by modeling the external legs with two additional non-linear reactances. The development of a topological multi-winding transformer model is more challenging and is partially addressed in [15]. Model parameters are obtained from standard test data that are usually acquired at the transformer factory before delivery. If available, a relatively small amount of low detail and easily accessible design data can be used to accurately tune some parameters and greatly enhance the performance of the transformer model when operating in heavy saturation. The design data used in this model are limited to the main dimensions of core (cross-sectional area and limb length) and windings (number of turns, height, internal and external diameter), and are given in Table I in the appendix. Although additional detailed information is relevant for models target to higher frequencies, detailed construction information about core and winding construction is not usually disclosed by manufacturers.

Existing models are not capable of retaining residual flux values after ringdown as they commonly use combinations of parallel R-L sections to represent the core.

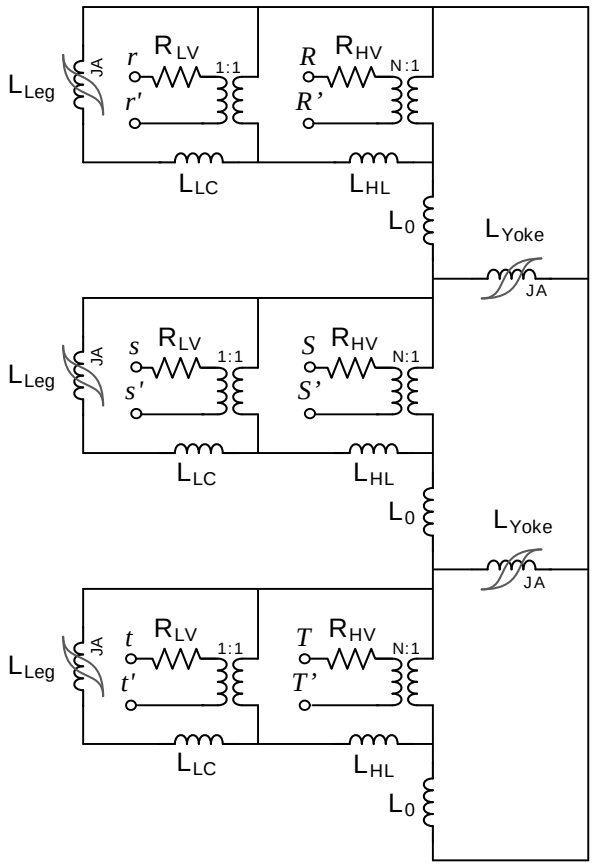

Fig. 3. Equivalent electric circuit of a three-legged transformer with ideal transformers and winding resistances.

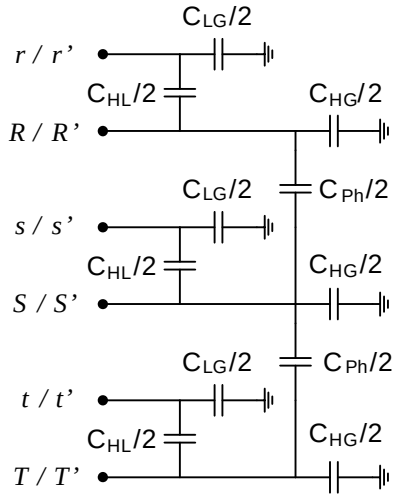

Fig. 4. Transformer model: capacitances.

A single-valued nonlinear L fails to reach any residual flux value as no energy can be stored in the core [16]. A more sophisticated core model is therefore required to predict a de-energization transient. This is a natural LC response that appears as the stored magnetic and electrostatic energy dissipate whenever a transformer is de-energized [16], [17]. At the end of a de-energization transient, both voltage and current decrease to zero. However, the flux in the core retains a value defined as residual flux. In the proposed model each section of the core is modeled separately to correctly represent the core topology of the transformer. Each of the three main legs and the two outer yokes is modeled with a Jiles-Atherton hysteretic model [18]–[20] capable of predicting the residual fluxes in the core.

In addition to hysteresis, the representation of saturation and air-core inductance is included in the Jiles-Atherton hysteretic model which is depicted in Fig. 3 as an inductor with superimposed hysteresis loop. Eddy current and excessive losses in the core can also be taken into account by this model [19]. The Jiles-Atherton theory was originally developed as a function of the magnetic quantities $M-H$ and has been converted here to be directly used with electromagnetic quantities $\lambda - i$ [20]. The implementation of the Jiles-Atherton model has not been detailed in this study and the focus is only on the estimation of the model parameter L_{inf} that defines the incremental inductance in complete saturation.

A detailed leakage model is required if energization inrush current transients need to be represented. When the magnetic core is highly saturated, the final slope of the core inductance is determined by the leakage and air-core paths. The ability to measure or estimate this parameter limits the detail level of the model. The magnetic paths in the core and in air shown in Fig. 1 give the most advantageous discretization level. Higher degree of discretization of the model would require input data beyond the short-circuit nameplate data and the main winding and core dimensions. A lower degree of discretization cannot guarantee a good accuracy of the model.

III. VALIDATION OF THE MODEL

A 300-kVA 11.43-0.235-kV Yyn three-legged core transformer is used as test object and is energized from the 11-kV side by a vacuum circuit breaker. The laboratory setup and test procedure is further detailed in [21]. The approach used in the hybrid model for the parameter estimation [11], [14] serves as a starting point and the numerical values of the parameters used for the verification of the model with measurements are reported in Table II in the appendix.

When the model is de-energized from steady-state by opening the circuit breaker, the ringdown transient is initiated and the proper level of residual flux for each limb is established by the Jiles-Atherton hysteretic core model. Fig. 5 shows the comparison of the measured and simulated waveforms of a de-energization transient of line current, induced voltage, and flux-linkage. The high frequency oscillation at the disconnection instant cannot be accurately reproduced in the simulation, however the main purpose here is to predict the steady-state value of residual fluxes. Fig. 6 shows simulated and measured residual fluxes as a function of the opening instant of the circuit breaker. Considering the large statistical variation

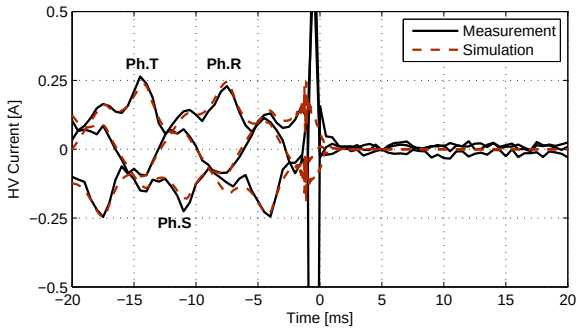

(a) Line current, high voltage side.

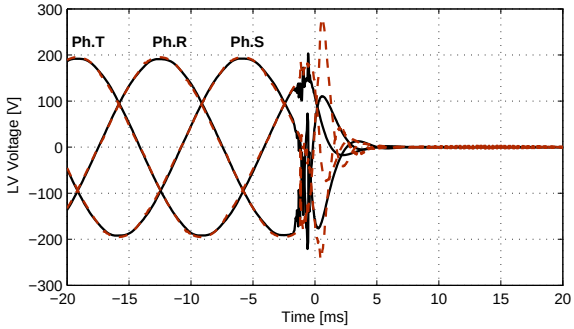

(b) Phase voltage, low voltage side.

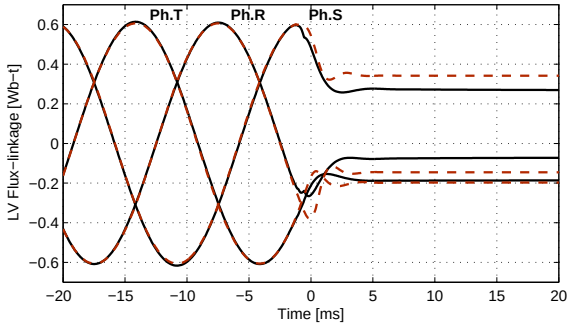

(c) Flux-linkage, low voltage side.

Fig. 5. De-energization of a 11.43/0.235 kV, 300 kVA, Yyn transformer.

of the measurements, the model well approximates the trend of the residual flux values and their correlation in the three phases.

Fig. 7 compares measurements with ATP/EMTP simulations for the first few periods of an inrush transient. The applied voltage on the HV terminals is shown in Fig. 7(a), the inrush current waveforms measured on the HV terminals are shown in Fig. 7(b), the induced voltage on the LV terminals is shown in Fig. 7(c), and the flux-linkage obtained by integration of the induced voltage is shown in Fig. 7(d). The residual fluxes of the model are auto-initialized by a de-energization transient

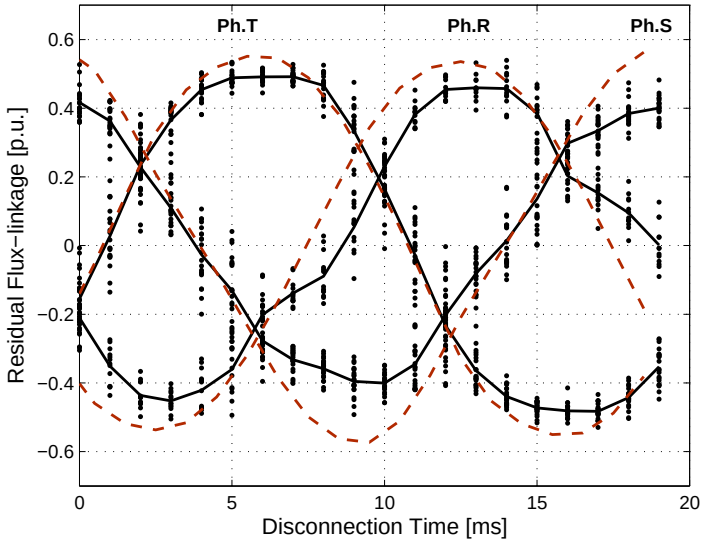

Fig. 6. Residual flux function of the disconnection time (dots: measurements, solid lines: average of 20 measurements, dashed lines: simulation).

simulation, and the measured residual fluxes are obtained from the recording of the transformer's de-energization preceding the investigated energization. For the case shown, the model is able to reach the inrush current first peak with a 7% difference, and the waveform shape of the highly distorted induced voltage is very close.

The verification of a model with a single inrush current measurement is insufficient as several parameters interact to determine the inrush peak and attenuation. Fig. 8 shows the envelope of the inrush current peaks of phase R for three different switching instants that lead to different inrush current amplitudes (switching angles given in Table III in the appendix). The comparison between measurements and simulations for the first five seconds and for three different inrush current magnitudes proves that the model with the calculated parameters is able to reproduce a wide range of inrush current transients with an error below 1 p.u. (overestimated in case 1 and underestimated in cases 2 and 3). Possible reasons for the difference in the maximum inrush current are:

1) Residual flux estimation, i.e. in Fig. 7(d) the initialization flux is slighty higher for phase R in the simulation giving the higher current of Case 1.
2) The shape of the saturation characteristic in the knee area defined by the Jiles-Atherton model. This determines when the transformer enters into saturation and is only significant for the cases with low inrush current.
3) Non exact switching time and simultaneous closing of the poles during the measurements.
4) Uncertainties in the parameter estimation.

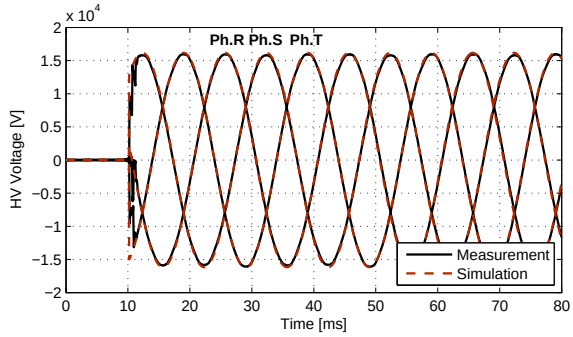

(a) Line voltage, high voltage side.

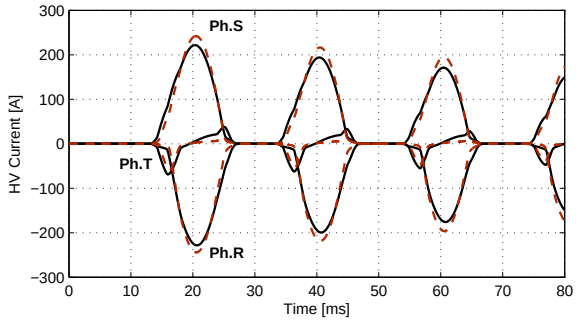

(b) Line current, high voltage side.

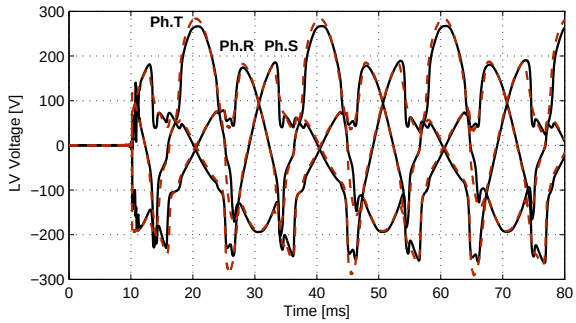

(c) Phase voltage, low voltage side.

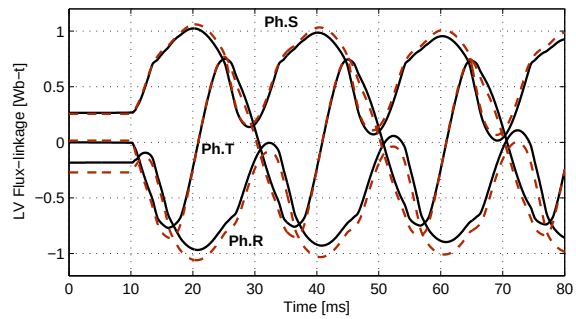

(d) Flux-linkage, low voltage side. Auto-initialized residual flux-linkage.

Fig. 7. Energization of a 11.43/0.235 kV, 300 kVA, Yyn transformer. Recorded worst case inrush current transient, waveforms.

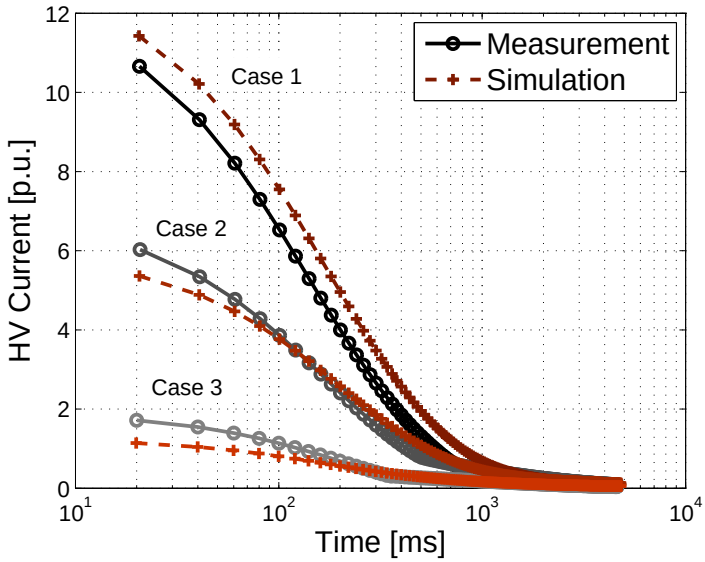

Fig. 8. Inrush envelope decay, phR. Comparison between measurement and simulation for three different inrush current magnitudes, Yyn.

IV. ANALYTICAL FORMULAS FOR INRUSH CURRENT ESTIMATION

Three standard analytical formulas for the calculation of inrush current, plus the calculation provided by the manufacturer are compared with the model results to further verify its performance.

The following analytical expressions are used:

$$i(t) = \frac{\sqrt{2}U}{\sqrt{R_W^2 + \omega^2 L_{air-core}^2}} \cdot \cdot \left(\sin(\omega t - \phi) - e^{-\frac{R_W}{L_{air-core}}(t-t_s)} \sin(\omega t_s - \phi) \right) \tag{1}$$

$$i(t) = \frac{\sqrt{2}U}{\omega L_{air-core}} \left(1 - \frac{B_S - B_N - \tilde{B_R}}{B_N}\right) \tag{2}$$

$$\tilde{B_R}(new) = \tilde{B_R}(old) - B_N \cdot \frac{R_W}{\omega L_{air-core}} \cdot 2(\sin\theta - \theta\cos\theta)$$

$$i(t) = \frac{\sqrt{2}U}{\sqrt{R_W^2 + \omega^2 \cdot L_{air-core}^2}} \left(\frac{2 \cdot B_N + B_R - B_S}{B_N} \right) \cdot e^{-\frac{t_n}{\tau}} \tag{3}$$

with (1), (2) and (3) proposed by Holcomb [22], Specht [23] and Bertagnolli [24] respectively. Equation (1) and (2) are quite similar in the way that the current decay is considered during saturation ($B > B_S$). On the contrary, (3) is based

on a sustained exponential decay of inrush that results in a larger rate of decay. Equation (1) can analytically calculate the full current and flux waveforms, while (2) and (3) only calculate the envelope of the inrush current peaks.

Parameters R_W and $L_{air-core}$ are the same in all three equations, with R_W being the DC resistance of the energized HV winding and $L_{air-core}$ the air-core inductance of the same winding calculated as:

$$L_{air-core} = \mu_0 \cdot N_{HV}^2 \cdot \frac{A_{HV}}{h_{eq\_HV}} \tag{4}$$

with A_{HV} the mean cross-sectional area of the high voltage winding and h_{eq_HV} its equivalent height including fringing effects. The equivalent height is obtained by dividing the winding height by the Rogowski factor K_R (< 1.0) [3]. This factor is usually determined empirically and is a function of the height, mean diameter, and radial width of a winding. For this specific transformer K_R is estimated as 0.747.

Analytical formulas approximate inrush peak and rate of decay. They are based on single-phase transformer theory, and empirical factors are used to rescale the calculations to account for the number of phases, core construction and coupling of the transformer [2], [3]. The simulation of a transformer connected in grounded-wye configuration is compared with the results from the analytical formulas in order to avoid the use of uncertain and questionable empirical factors.

Since the analytical formulas are used to calculate the worst case value, the residual flux has been assumed 0.6 p.u. in agreement with Fig. 6. The model has been manually initialized to a residual flux of 0.6, -0.3, -0.3 p.u. for the main limbs of phase R, S, and T respectively. For a three-legged core, the residual fluxes of the two yokes are assumed equal to those of the outer legs (phase R and T). Setting the breaker to close at voltage zero crossing of phase R produces the worst case condition for phase R and the result is comparable to the analytical formulas.

As shown in Fig. 9, the simulation gives a result very similar to (1) and (2). Equation (3) has too much damping compared to the other expressions and the simulation result. The calculation given by the manufacturer is based on (3) with in-house empirically calculated coefficients. This results in a curve with only slightly higher first-peak current, but even larger decay. The authors are confident that the model, (1), and (2) are accurate due to the good match of the model results to the measurements for the ungrounded-wye case shown in the previous section.

The proposed model is able to provide a result comparable to the analytical equations. While the applicability of these formulas is restricted to the worst case scenario, the model can be used to test different energization conditions and the interaction of a transformer with the external network.

V. PARAMETER ESTIMATION AND SENSITIVITY ANALYSIS

The estimation of the parameters of the model is discussed in this section with exception of the hysteretic core model. The Jiles-Atherton model is presented in [18], [19] and its implementation and parameter estimation are discussed in [20].

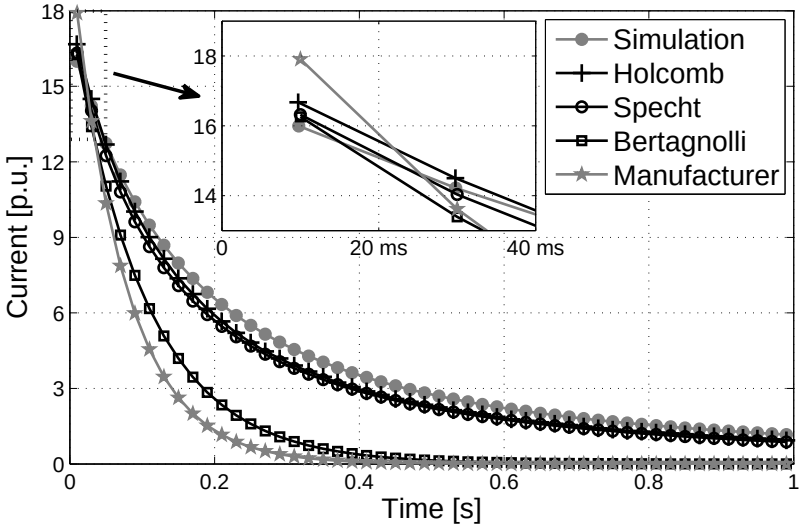

Fig. 9. Comparison of analytical formula for the calculation of inrush, with detail of the first two points (YNyn).

In parallel to the guidelines for the parameter estimation, a sensitivity analysis is performed to verify the influence of each parameter on the inrush current peak and decay. The most significant parameters are identified and the methods for estimating them are outlined. Fig. 6, 7 and 8 shows that the set of parameters in Table II well reproduce the de-energization and energization transients and therefore it is used as the reference point. The sensitivity analysis is performed for both YNyn and Yyn connections and the envelope curves of the first 200 ms of the inrush of phase R are reported. The transformer is initialized to a residual flux of 0.6, -0.3, -0.3 p.u. for the three phases respectively and the breaker closes at voltage zero crossing of phase R to simulate the worst case condition.

A. Leakage inductances L_{HL} and L_{LC}

The leakage inductance between high and low voltage winding (L_{HL}) is obtained directly from the short-circuit test measurement. The leakage inductance between low voltage winding and core (L_{LC}) cannot be directly measured but is assumed to be:

$$L_{LC} \approx K \cdot L_{HL} \tag{5}$$

Short-circuit reactances can be calculated from winding dimensions with standard equations reported in [3] chapter 3.1. Assuming a winding of zero thickness on the core surface, the reactance between low voltage winding and core can be estimated

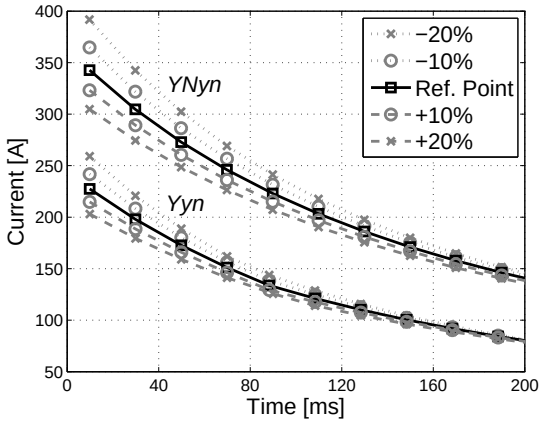

Fig. 10. Parameter Sensitivity: L_{HL}.

from the core and winding geometry:

$$L_{ij} = \frac{\mu_0 \pi N^2}{h_{eq}} \cdot \sum_{k=1}^{n} ATD_{ij} \tag{6}$$

$$\sum ATD_{HL} = 1/3 \cdot T_L \cdot D_L + T_{g\,HL} \cdot D_{g\,HL} + 1/3 \cdot T_H \cdot D_H \tag{7}$$

$$\sum ATD_{LC} = 1/3 \cdot T_L \cdot D_L + T_{g\,LC} \cdot D_{g\,LC} \tag{8}$$

with ATD being the area of the Ampere-Turn Diagram, D the mean diameter, T the radial width of a winding, and T_g the thickness of the air-gap between two windings [3]. An initial estimation of $K = 0.5$ is proposed in [14] assuming that:

1) the insulation clearance between core and low-voltage winding $T_{g\,LC}$ is approximately equal to half the distance between low- and high-voltage windings $T_{g\,HL}$,
2) the cross-sectional dimensions of low- and high-voltage windings are similar ($T_L \approx T_H$ and $h_{eq\,L} \approx h_{eq\,H}$),
3) the mean winding diameter can be approximated to $D_L \approx D_H = D$.

The value calculated with actual winding dimensions is used in the model and is:

$$K = \sum ATD_{LC} / \sum ATD_{HL} \approx 0.33 \tag{9}$$

Fig. 10 shows a mean variation of 12% in the inrush first peak for a variation of 20% of L_{HL}. According to (5), a variaton of L_{HL} implies a change in L_{LC} as well.

Fig. 11 shows the influence of the parameter K in the estimation of L_{LC}. A smaller value K results in a lower voltage drop on the low-voltage to core reactance, thus in a higher inrush current peak.

B. Air-core inductance L_{inf}

Air-core theory is based on the concept that once the magnetic core is fully saturated it behaves like air with permeability μ_0. The analytical formulas (1), (2)

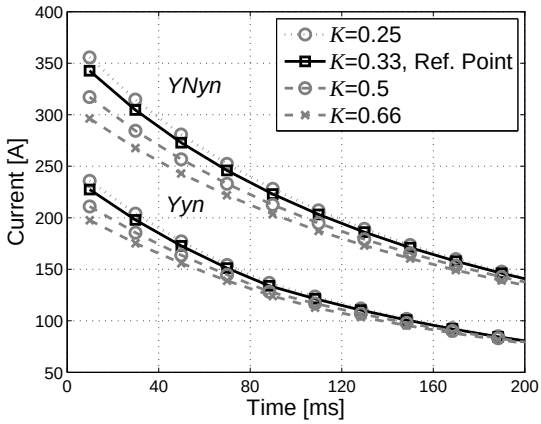

Fig. 11. Parameter Sensitivity: L_{LC}.

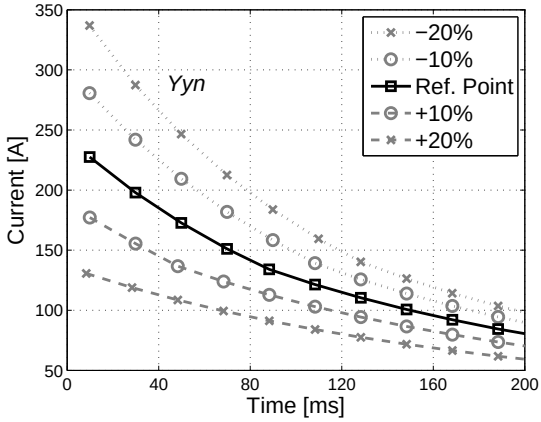

(a) Ungrounded-wye.

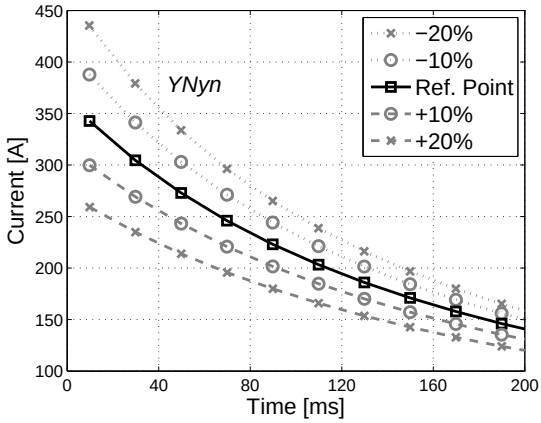

(b) Grounded-wye.

Fig. 12. Parameter Sensitivity: L_{inf}.

and (3) are based on this concept and denote *air-core inductance* as the inductance of a winding with no magnetic core. Neglecting the effect of the yokes as the first approximation, the quantity in the transformer model equivalent to the air-core inductance defined in (4) is the incremental inductance at high saturation given by:

$$L_{air-core} \approx L_{HL} + L_{LC} + L_{inf} \tag{10}$$

where L_{inf} is the slope of the magnetization curve at complete saturation defined by L_{inf} in the Jiles-Atherton model, which cannot be directly measured, but can be calculated from design data as:

$$L_{inf} = \mu_0 \cdot N^2 \cdot \frac{A_{limb}}{l_{limb}} \tag{11}$$

Reference [25] discusses the importance of the air-core inductance and proposes analytical formulas for its calculation, however these require a detailed knowledge of the core and winding structure.

Numerically, (4) and (10) agree within 5% for the calculated parameters:

$$L_{HL} + L_{LC} + L_{inf} = 107.3\,\text{mH} \tag{12}$$

$$L_{air-core} = 112.8\,\text{mH} \rightarrow \text{from (4)} \tag{13}$$

with numerical values of (12) from Table II and rescaled to the HV-side voltage reference for comparison with (4).

L_{inf} accounts for one third of the total air-core inductance (10), but peak inrush current is highly sensitive to variations in L_{inf} as seen from Fig. 12. A variation of 20% of L_{inf} gives a mean variation in the inrush first peak of 45% for ungrounded-wye and 26% for grounded-wye.

C. Zero-sequence inductance L_0

The flux in the three legs may not sum up to zero during unbalanced operations, generating a zero sequence flux. Referring to Fig. 1, this flux flows in the zero sequence paths of the transformer, for instance from one leg, through the oil and the tank wall and back to the core. Three zero sequence paths can therefore be identified, one around each leg of a three-legged transformer. Although the zero sequence path includes the tank (normally made of magnetic material), it can be safely assumed that zero sequence inductances are linear due to the dominant effect of the oil gap between the core and the tank. The value of the zero sequence inductances is best found from a zero sequence test where the three phases of a transformer are energized in parallel. The total current is measured and the total zero sequence inductance is equally split on each of the three phases:

$$L_0 = \frac{L_{zero}}{3} \tag{14}$$

$$L_{zero} = \frac{\lambda_{zero}}{i_{zero}} = \frac{V_{zero}}{\omega \cdot I_{zero}} \tag{15}$$

The variation of the zero-sequence inductance within $\pm 20\%$ has no effect on inrush current transients.

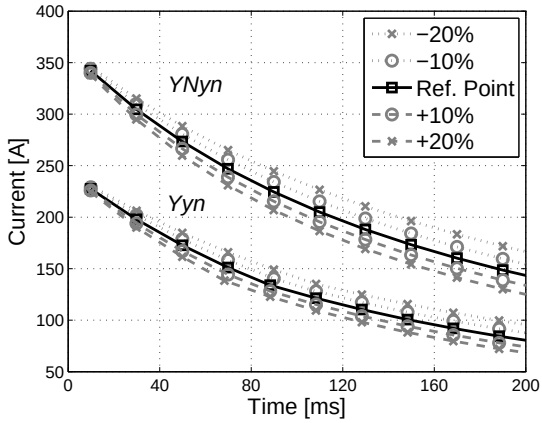

Fig. 13. Parameter Sensitivity: R_{HV}.

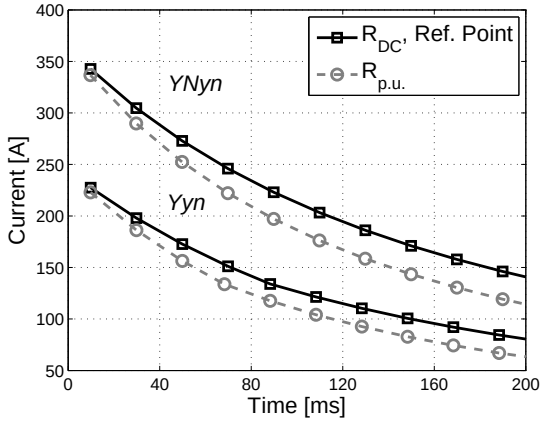

Fig. 14. Parameter Sensitivity: R_{HV} and R_{LV} splitting.

D. Winding resistances R_{HV} and R_{LV}

The winding resistances are concentrated at the terminals of each winding. It is common to estimate the winding resistance based only on a short-circuit measurement and then equally split the value on a per unit basis between high and low voltage resistances.

To achieve higher accuracy, here the values are allocated based on DC winding resistance measurements [26]:

$$r_{AC\,HV} = r_{AC\,sc} \cdot \frac{r_{DC\,HV}}{r_{DC\,HV} + r_{DC\,LV}} \tag{16}$$

$$r_{AC\,LV} = r_{AC\,sc} \cdot \frac{r_{DC\,LV}}{r_{DC\,HV} + r_{DC\,LV}} \tag{17}$$

where r is the resistance expressed in per unit. The splitting of the AC resistance based on DC resistance measurements usually results in $r_{AC\,HV} < r_{AC\,LV}$ on a per

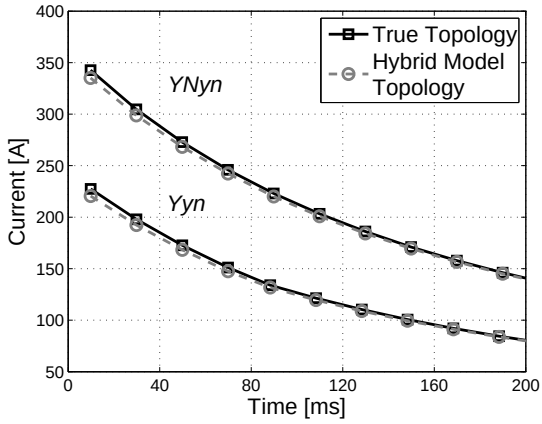

Fig. 15. Parameter Sensitivity: Core Connection.

unit basis. When the transformer is energized from the high voltage side (normal situation for power and distribution transformer) the voltage drop caused by the winding resistance is smaller than for an equal split, resulting in a lower inrush current damping.

Fig. 13 shows how a variation of winding resistance has a minor effect on the inrush-current first peak, while the current damping is substantially affected. The inrush-current half value is reached approximately one period earlier and two periods later if the high-voltage winding resistance is increased and decreased by 20% respectively. Fig. 14 compares the resulting inrush current damping when the winding resistances are split based on the per unit and DC resistance methods.

E. Core connection

In order to simplify the model representation, the hybrid model [11], [14] assumes that the leakage inductances are much smaller than the core inductances. This allows concentrating the core and leakage networks in two distinct and separate modules. This assumption is correct under normal conditions, but becomes doubtful at high saturation where the incremental core inductance approaches the air-core inductance.

The validity of this approximation has been tested on the proposed model by connecting the right section of the core model (yoke and zero-sequence representation) in parallel with the leg representation. As shown in Fig. 15, the topologically correct core results in a slightly higher value of inrush current. The approximation in the topology of the hybrid model introduces a relatively small inaccuracy and can be considered reasonable.

F. Residual flux

After examining the main model parameters, attention is turned to the initial conditions which have a considerable influence in the determination of the inrush

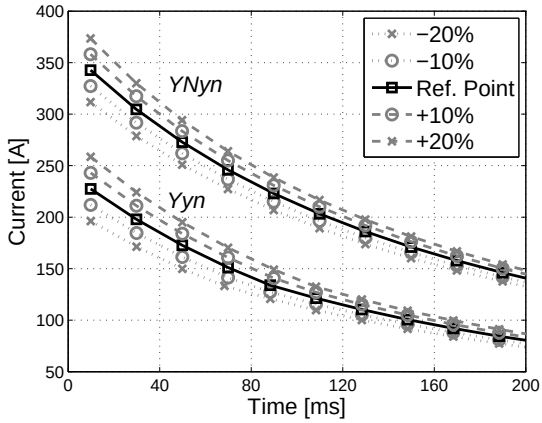

Fig. 16. Parameter Sensitivity: Residual Flux.

current. The residual flux in the transformer's limbs prior the energization defines the initial magnetization state and affects the energization transient.

Fig. 16 shows how the inrush current magnitude is related to the residual flux amplitude. For a variation of 20% of the residual fluxes, a mean variation of 9% for ungrounded-wye and 14% for grounded-wye is experienced in the inrush first peak.

G. Winding and shunt capacitances

An accurate estimation of the transformer capacitances is important both to extend the validity of the model to higher frequency, and to correctly predict the residual fluxes. The influence of shunt capacitance on the residual flux has been discussed in [16].

Capacitances are estimated from direct capacitance measurements at the transformer terminals. These measurements are highly susceptible to error and inaccuracy, thus it is suggested that redundant data be acquired to verify the calculated parameters. The recommended minimum set of measurements is:

- HV+LV to G:
$$C_{meas} = C_{LG} /\!/ C_{HG} \tag{18}$$
- LV to G+HV:
$$C_{meas} = C_{LG} /\!/ C_{HL} \tag{19}$$
- HV to G+LV:
$$C_{meas} = C_{HG} /\!/ C_{HL} \tag{20}$$
- HV_{phR} to G+LV+HV_{phS}+HV_{phT}:
$$C_{meas} = C_{HGphR} /\!/ C_{HL} /\!/ C_{Ph} \tag{21}$$
- HV_{phS} to G+LV+HV_{phR}+HV_{phT}:
$$C_{meas} = C_{HGphS} /\!/ C_{HL} /\!/ C_{Ph} /\!/ C_{Ph} \tag{22}$$

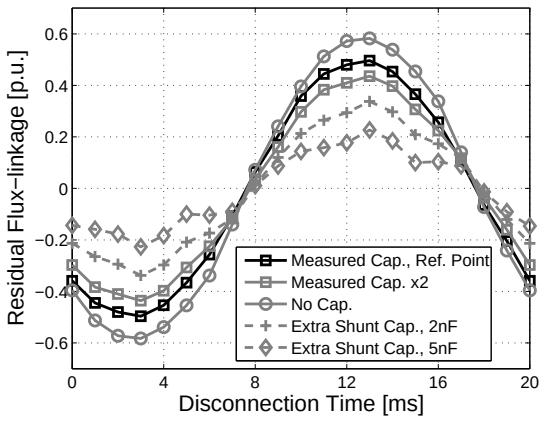

Fig. 17. Parameter Sensitivity: Capacitances.

- HV_{phT} to G+LV+HV_{phR}+HV_{phS}:

$$C_{meas} = C_{HGphT} \,//\, C_{HL} \,//\, C_{Ph} \tag{23}$$

with // representing a parallel connection, and as an example *"HV+LV to G"* refers to the measurement of the capacitance between all the terminals of the high and low voltage windings connected together (HV+LV) and the transformer tank (G).

Measurements (18) to (23) together with $C_{HG} = C_{HG\,phR} + C_{HG\,phS} + C_{HG\,phT}$ are sufficient to estimate the capacitance values, while other coupling combinations can be measured in addition and used to verify the calculations. The capacitance C_{HL}, C_{HG} and C_{LG} estimated from solving these equations are total capacitances. Per-phase capacitances with a value of 1/3 of the total capacitances have to be used in the model.

The measurements (21) to (23) are used to estimate the asymmetry of the capacitance to ground of the high voltage winding and can be performed only if the three high voltage windings are accessible independently. This is however seldom possible on a power transformer. C_{HG} can be assumed to be equally distributed among the three phases in case of lack of such measurements. Series winding capacitances have been neglected in the model as they cannot be measured from the bushing terminals and their estimation must be based exclusively on highly detailed winding design information [3], [27].

Fig. 17 shows the residual flux estimated by the model as a function of the disconnection instant for different values of transformer winding capacitances and supplementary system shunt capacitances connected to the HV terminals. Shunt capacitances installed in the system between the circuit breakers and the transformer terminals (cables and shunt capacitances on both LV and HV sides) should be included in the model as they may affect the residual flux estimation.

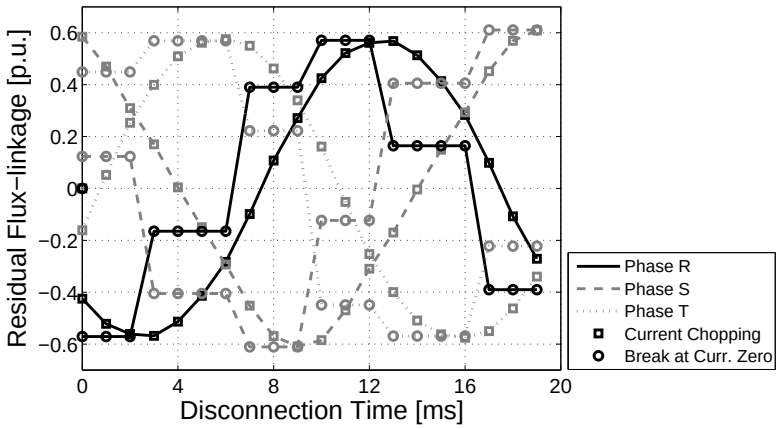

Fig. 18. Parameter Sensitivity: Circuit Breaker and Current Chopping.

H. Current chopping characteristic of the breaker

The residual flux estimation is expected to be affected by the circuit breaker's chopping characteristic. The vacuum circuit breaker used during the measurements can be considered a good approximation of an ideal breaker due to its high current chopping capability. Fig. 18 shows the simulation result of the residual flux as a function of the opening time when the circuit breaker is modeled to interrupt the currents at any magnitude or only at its zero crossing. These two modeled cases represent the two extreme situations and prove the importance of a correct circuit breaker model. The investigation of a circuit breaker model is beyond the scope of this paper.

VI. DISCUSSION

The analysis of the parameters emphasize the importance of the leakage inductances L_{HL}, L_{LC}, and L_{inf} in a transformer model. The main leakage inductance L_{HL} is a parameter directly measurable with a short-circuit test and is always represented in a transformer model. It accounts for the interaction between windings and describes the short-circuit behavior of a transformer. The other two inductances have significance only when the effect of the core must be analyzed. Most important is the contribution from the incremental inductance L_{inf} as it has a major current limiting effect when the core is saturated. This inductance can be considered in series with a saturable nonlinear inductance that represents the core, and it accounts for the slope of the magnetization curve in complete saturation. Transformer models rarely take this parameter into account, however it is important not only to add a series inductor L_{inf} to the core representation, but also to ensure the saturation of the core. The saturated core inductance L_{inf} is not measurable from the transformer terminals, but a good estimation can be obtained from design data according to (11). The leakage between the innermost winding and the core L_{LC} is also not measurable but determinable from design data according to (9). The required design

data for the estimation of L_{inf} and L_{LC} are those reported in Table I. A transformer manufacturer not willing to reveal design data of a transformer may provide these two parameters according to the referenced equations as part of test report data.

Different models have been proposed to represent the hysteresis phenomenon, but only a few of them can represent demagnetization correctly [18]. The Jiles-Atherton model is selected over the Preisach model for its simpler implementation and reduced computational effort. The novel use of this model for three-phase power transformer modeling is presented here to prove its applicability and effectiveness. The capability of this model to predict residual fluxes with different disconnection conditions should to be further verified. For instance, the disconnection of a transformer connected to a long cable is of particular interest as it produces a long-lasting ringdown transient. In addition, records on a large population of transformers are needed to obtain a more accurate assessment and a better knowledge of the residual flux range variation in power transformers.

Other recent studies [7], [28], [29] prove the effectiveness of this approach in the modeling of transformers. The use of a modified Jiles-Atherton model with non-constant parameters is suggested to overcome some accuracy issues experienced for simulations with a wide variation of field strength. Further development is recommended to improve the loss representation and simplify the parameter estimation procedure without the need of specific measurements [20].

VII. CONCLUSION

A model has been developed based on transformer topology with special concern for extreme saturation and inrush currents. This results in a true topologically-correct three-phase representation. A novel characteristic of the model is the possibility to retain residual fluxes in the limbs and therefore to be auto initialized. The model is suitable for any electromagnetic transient where saturation is a concern.

The capability of the model to determine residual flux and correctly initialize inrush transients has been validated with measurements. The parameters obtained from test report and limited design data have been utilized to accurately reproduce the inrush current first-peak and decay of energization transients with different current magnitudes.

The model has been compared to analytical formulas and gives similar results. Formulas are limited to the estimation of the worst-case scenario and refer to a single-phase-equivalent representation. They are therefore not beneficial to transient studies. The use of the proposed model is of great advantage for energization studies where the interaction of the transformer with other network component needs to be investigated.

Parameter estimation together with a sensitivity study is effectively used to identify the most critical parameters. The conclusion is that the parameter that most influences the inrush current amplitude is the slope of the magnetization curve at extreme saturation, L_{inf}.

APPENDIX

TABLE I
CORE AND WINDINGS DESIGN DATA.

CORE	**Legs**	**Yokes**
Net cross-sectional area	0.0175 m^2	0.0198 m^2
Max lamination width	0.150 m	0.170 m
Window height	0.500 m	
Legs dist. center-to-center	0.290 m	

WINDINGS	**Low Voltage**	**High Voltage**
Number of turns	21	1074
Height	0.452 m	0.452 m
Inner diameter	0.162 m	0.222 m
Thickness	0.017 m	0.0225 m

TABLE II
MODEL PARAMETERS.

Parameter	**Value**	**Reference**
L_{HL}	$23.2 \cdot 10^{-3}$ mH	LV side
L_{LC}	$0.33 \cdot L_{HL}$	LV side
L_{inf}	$14.5 \cdot 10^{-3}$ mH	LV side
L_0	1.52 mH	LV side
R_{LV}	1.2 mΩ	LV side
R_{HV}	1.78 Ω	HV side

TABLE III
SWITCHING ANGLES OF FIG. 8

	Opening Angle	**Closing Angle**
Case 1	-12.6 °	140.4 °
Case 2	84.6 °	145.8 °
Case 3	34.2 °	75.6 °

Note: angles are relative to phR zero crossing.

ACKNOWLEDGMENT

The research team at NTNU, MTU and SINTEF Energy Research acknowledge the Norwegian Research Council, Hafslund Nett, Statnett SF, Statkraft Energi AS, NVE, EDF, Nynäs Petroleum AB and ABB for their support in the project “Thermal and electromagnetic performance of transformers”.

REFERENCES

[1] A. Greenwood, *Electrical Transients in Power Systems*, 2nd ed. Troy, N.Y.: John Wiley and Sons, Inc., 1991.

[2] L. F. Blume, *Transformer engineering : a treatise on the theory, operation, and application of transformers*, 2nd ed. New York, N.Y.: John Wiley and Sons, Inc., 1951.

[3] S. V. Kulkarni and S. A. Khaparde, *Transformer engineering: design and practice*, ser. Power engineering. New York, N.Y.: Marcel Dekker, Inc., 2004, vol. 25.

[4] F. de Leon and A. Semlyen, "Complete transformer model for electromagnetic transients," *IEEE Trans. Power Del.*, vol. 9, no. 1, pp. 231–239, 1994.

[5] J. A. Martinez and B. A. Mork, "Transformer modeling for low frequency transients - the state of the art," in *IPST'03 - International Conference on Power Systems Transients*, no. 9a-1, New Orleans, USA, Sep. 2003.

[6] J. A. Martinez and B. A. Mork, "Transformer modeling for low- and mid-frequency transients - a review," *IEEE Trans. Power Del.*, vol. 20, no. 2 II, pp. 1625–1632, 2005.

[7] A. D. Theocharis, J. Milias-Argitis, and T. Zacharias, "Three-phase transformer model including magnetic hysteresis and eddy currents effects," *IEEE Trans. Power Del.*, vol. 24, no. 3, pp. 1284–1294, Jul. 2009.

[8] W. Enright, O. B. Nayak, G. D. Irwin, and J. Arrillaga, "An electromagnetic transients model of multi-limb transformers using normalized core concept," in *IPST'97 - International Conference on Power System Transients*, Seattle, Washington, Jun. 1997, pp. 93–98.

[9] W. Enright, O. Nayak, and N. Watson, "Three-phase five-limb unified magnetic equivalent circuit transformer models for PSCAD V3," in *IPST'99 - International Conference on Power System Transients*, Budapest, Hungary, Jul. 1999, pp. 462–467.

[10] Y. Zhang, T. Maguire, and P. Forsyth, "UMEC transformer model for the real time digital simulator," in *IPST'05 - International Conference on Power System Transients*, no. IPST05-77, Montreal, Canada, Jun. 2005.

[11] B. A. Mork, F. Gonzalez, D. Ishchenko, D. L. Stuehm, and J. Mitra, "Hybrid transformer model for transient simulation: Part I: development and parameters," *IEEE Trans. Power Del.*, vol. 22, no. 1, pp. 248–255, Jan. 2007.

[12] B. A. Mork, F. Gonzalez, D. Ishchenko, D. L. Stuehm, and J. Mitra, "Hybrid transformer model for transient simulation: Part II: laboratory measurements and benchmarking," *IEEE Trans. Power Del.*, vol. 22, no. 1, pp. 256–262, Jan. 2007.

[13] B. A. Mork, D. Ishchenko, F. Gonzalez, and S. D. Cho, "Parameter estimation methods for five-limb magnetic core model," *IEEE Trans. Power Del.*, vol. 23, no. 4, pp. 2025–2032, Oct. 2008.

[14] H. K. Høidalen, B. A. Mork, F. Gonzalez, D. Ishchenko, and N. Chiesa, "Implementation and verification of the hybrid transformer model in ATPDraw," *Electr. Power Syst. Res.*, vol. 79, no. 3, pp. 454 – 459, Mar. 2009, special Issue: Papers from the 7th International Conference on Power Systems Transients (IPST), 7th International Conference on Power Systems Transients.

[15] T. Henriksen, "Transformer leakage flux modeling," in *IPST'01 - International Conference on Power System Transients*, no. 059, Rio de Janeiro, Brazil, Jun. 2001.

[16] N. Chiesa, A. Avendaño, H. K. Høidalen, B. A. Mork, D. Ishchenko, and A. P. Kunze, "On the ringdown transient of transformers," in *IPST'07 - International Conference on Power System Transients*, no. IPST-229, Lyon, France, Jun. 2007.

[17] L. M. Ganatra, P. G. Mysore, K. K. Mustaphi, A. Mulawarman, B. A. Mork, and G. Gopakumar, "Application of reclosing schemes in the presence of capacitor bank ringdown," *Proc Am Power Conf*, vol. 61-2, pp. 967–972, 1999.

[18] F. Liorzou, B. Phelps, and D. L. Atherton, "Macroscopic models of magnetization," *IEEE Trans. Magn.*, vol. 36, no. 2, pp. 418–428, Mar. 2000.

[19] W. Chandrasena, P. G. McLaren, U. D. Annakkage, R. P. Jayasinghe, D. Muthumuni, and E. Dirks, "Simulation of hysteresis and eddy current effects in a power transformer," *Electric Power Systems Research*, vol. 76, no. 8, pp. 634–641, May 2006.

[20] N. Chiesa and H. K. Høidalen, "Hysteretic iron-core inductor for transformer inrush current modeling in EMTP," in *PSCC 2008 - 16th Power Systems Computation Conference*, Glasgow, Scotland, Jul. 2008.

[21] N. Chiesa and H. K. Høidalen, "Systematic switching study of transformer inrush current: simulation and measurements," in *IPST'09 - International Conference on Power System Transients*, no. IPST-139, Kyoto, Japan, Jun. 2009.
[22] J. F. Holcomb, "Distribution transformer magnetizing inrush current," *Transactions of the American Institute of Electrical Engineers, Part III (Power Apparatus and Systems)*, vol. 80, no. 57, pp. 697–702, Dec. 1961.
[23] T. R. Specht, "Transformer magnetizing inrush current," *AIEE Trans*, vol. 70, pp. 323–328, 1951.
[24] G. Bertagnolli, *Short-Circuit Duty of Power Transformers, Second Revised Edition*. ABB, 1996.
[25] M. Rioual, T. Guillot, and C. C., "Determination of the air-core reactance of transformers by analytical formulae for different topological configurations and its comparison with an electromagnetic 3D approach." in *IEEE/PES General Meeting*, Calgary, Canada, Jul. 2009.
[26] B. A. Mork, F. Gonzalez, and D. Ishchenko, "Parameter estimation and advancements in transformer models for EMTP simulations. Task MTU-7: Model Performance and Sensitivity Analysis," Bonneville Power Admin., Portland, OR, Tech. Rep., Jun. 2004.
[27] E. Bjerkan, "High frequency modeling of power transformers," Ph.D. dissertation, NTNU, 2005.
[28] X. Wang, D. W. P. Thomas, M. Sumner, J. Paul, and S. H. L. Cabral, "Characteristics of Jiles-Atherton model parameters and their application to transformer inrush current simulation," *IEEE Trans. Magn.*, vol. 44, no. 3, pp. 340–345, Mar. 2008.
[29] M. Toman, G. Stumberger, and D. Dolinar, "Parameter identification of the Jiles-Atherton hysteresis model using differential evolution," *IEEE Trans. Magn.*, vol. 44, no. 6, pp. 1098–1101, Jun. 2008.

Nicola Chiesa was born in Italy in 1980. He received the MSc degree in Electrical Engineering from Politecnico di Milano in 2005. From 2005 to 2009 he joined the Department of Electric Power Engineering at the Norwegian University of Science and Technology as a PhD candidate. He is now with the Department of Energy Systems at SINTEF Energy Research.

Bruce A. Mork (M'82, SM'08) was born in Bismarck, ND, on June 4, 1957. He received the BSME, MSEE, and Ph.D. from North Dakota State University in 1979, 1981 and 1992 respectively. He joined the faculty of Michigan Technological University in 1992, where he is now Associate Professor of Electrical Engineering, and Director of the Power & Energy Research Center.

Hans K. Høidalen (M'05) was born in Norway in 1967. He received his MSc and PhD degrees from the Norwegian University of Science and Technology in 1990 and 1998, respectively. He is now a professor at the same institution with a special interest of electrical stress calculations and modeling.

JOURNAL PAPER

Novel approach for reducing transformer inrush currents. Laboratory measurements, analytical interpretation and simulation studies

N. Chiesa, H. K. Høidalen

2010

IEEE Transaction on Power Delivery

Accepted for publication

TPWRD-00953-2009

Novel Approach for Reducing Transformer Inrush Currents. Laboratory Measurements, Analytical Interpretation and Simulation Studies

Nicola Chiesa, and Hans Kristian Høidalen, *Member, IEEE*.

Abstract

Transformer inrush currents can lead to a reduction of transformer life time and inadvertent tripping of relays. This paper investigates a novel approach for minimizing the inrush current with a potential application in circuit breaker control strategies without independent-pole operation and residual flux estimation. For the analyzed transformer, the worst case inrush current is halved compared to the rapid-closing switching strategy. Measurements of inrush current transients are performed on an unloaded 11 kV distribution transformer varying disconnection and connection instants systematically. This reveals a characteristic pattern in the extremal value of the inrush current as a function of switching times. The pattern is reproduced with simulations and extended to alternative winding configurations. A condition for minimum inrush currents, consistent for all phases and winding configurations, is identified and explained physically. The impact of the current chopping capability of the circuit breaker is important and is discussed in this paper.

Index Terms

Inrush current, residual flux, controlled switching, transformer modeling.

I. INTRODUCTION

TRANSFORMERS energized in no-load condition experience a transient with overvoltages and high currents known as the inrush current transient. The first peak of the inrush current can reach a value that is several times higher than the transformer's rated current. This is not an issue for small transformers, but becomes important for large and medium power transformers. Aggregation of several relatively small units energized at the same time is another situation where energization transients are an issue. The inrush current is asymmetric and unbalanced among the phases, and may place a heavy stress on the network and the transformer itself. The mechanical forces within the transformer windings can have similar increases in amplitudes as those in short circuits but with longer duration time [1]. The correct understanding and prediction of energization transients are required to extend the lifespan of the transformer's paper insulation by minimizing internal stresses and limiting switching overvoltages. In addition, the power quality

of a network can be improved by reducing the voltage distortion created by the energization of large transformers. Finally, the misoperation of protection schemes can be avoided by using refined relay strategies.

The inrush current behavior in transformers has been generally understood and analytical equations exist to approximately calculate the inrush current's first peak and the rate of decay of single-phase transformers [2]–[6]. However, it remains a challenge to accurately predict the inrush current transient of a three-phase transformer installed in a network and interacting with several other electrical components. The magnitude of the inrush current varies as a function of the instant of energization and the residual flux in the core. The residual flux in the core is determined by the ringdown transient [7], [8] and is a function of the opening time of the circuit breaker. Therefore the initial conditions of a transformer can be changed by varying the opening and closing switching times.

Several technologies exist to mitigate energization transients in transformers. The most common are closing resistors and point-on-wave (POW) controlled closing. The state of the art is to use synchronized switching, however this requires independent-pole circuit breakers and knowledge of residual fluxes to achieve optimal energization [9]–[13].

The aim of this paper is to investigate a simplified approach to minimize the inrush current. This is achieved via a systematic switching study of the energization of a distribution transformer. Section II presents the laboratory setup and the automated measurement procedure. In Section III a new method for the visualization of the inrush current's first peak is proposed. A graphical pattern is identified and a simplified physical explanation is discussed. The measurements are compared with EMTP simulations and the analysis is extended to the most common winding couplings. Section IV investigates a novel mitigation scheme based on a consistent condition of minimum inrush current as a function of the switching in and out times. Practical implementation issues and benefits of this method are discussed in Section V.

II. MEASUREMENT SETUP AND PROCEDURE

A distribution transformer is used for laboratory investigations. The test object is oil filled with a three-legged core. The transformer is rated 300 kVA 11.430/0.235 kV Yyn, and connected to a low-impedance 11-kV medium voltage grid. It is energized by two sets of controlled circuit breakers and the 235-V side is unloaded as shown in Fig. 1. The components in the dashed box of Fig. 1 are a fixed laboratory installation and cannot be modified. A vacuum breaker is placed before the test object terminals in order to decouple the ringdown of the two transformers and record only the test object response. The vacuum breaker can be effectively used to chop the magnetization current (<1 A) at any instant and does not limit the interruption to the zero crossing of the current. The available vacuum breaker is not suitable for the energization of the transformer due to contact bouncing, therefore the main breaker is used to energize the test object. It has been verified that the simultaneous energization of the two transformers does not influence the

energization transient as a result of the low impedance of the 11-kV network. More detailed information on the laboratory equipment is given in [14].

The breakers have a stable operation time and can be controlled with accuracy and repeatability of approximately ± 1 ms. Two trigger signals that are synchronous to the zero crossing of the line voltage V_{RS} on the high voltage side are used to control the time when de-energization and energization occur. The de-energization and energization transients are linked together as the ringdown transient determines the value of the residual fluxes in the transformer that is a fundamental initial condition for the following energization. The residual flux is calculated by integration of the induced voltage during the ringdown transient and once it reaches a stable value it is assumed constant until the next energization. In order to limit the uncertainties on the residual flux estimation, the de-energization and energization transients are performed in rapid sequence with a delay of approximately 2 s. The measurement procedure consists of two separate recordings as the frequency of power systems is not fixed at 50 Hz but shows slow fluctuations. A double triggering and double acquisition procedure is therefore necessary to accurately synchronize the operation of the circuit breakers with the point-on-wave (POW) timings. As shown in Fig. 2, the opening time (Δt_{open}) is relative to the trigger signal t_{trg1} and is varied systematically between 0 ms and 20 ms. In the same way, the closing time (Δt_{close}) is relative to the trigger signal t_{trg2} and is varied systematically between 0 ms and 20 ms. The systematic variation of the opening and closing times of the breakers with a time resolution of 1 ms allows a total of 400 (20x20) measurements to be performed in order to map the whole range of inrush current and residual flux combinations in a period.

The automated sequence of operations for the acquisition of a de-energization and energization sequence is shown in Fig. 3 and can be outlined in six repeating stages:

- *Steady State:* The transformer is energized and in steady state (no-load).
- *Ringdown:* The vacuum breaker opens at $t_{trg1}+\Delta t_{open}$ and the de-energization transient initiates. The main breaker opens slightly later without any effect on the test object. The transient is recorded for the duration of 1 s.
- *Storing Data:* Recorded data are stored and a delay of 1 s is introduced between the ringdown and inrush stages.
- *Inrush:* The vacuum breaker closes without delay. The main circuit breaker closes at $t_{trg2} + \Delta t_{close}$ and the energization transient initiates. The transient is recorded for a duration of 20 s.
- *Storing Data & Delay:* Recorded data are stored followed by a 10 s delay where the transformer reaches steady state.
- *Ready for Next Run:* The system is ready and in steady state. A new measurement sequence can start.

III. INRUSH CURRENT PATTERNS

A. Measured pattern

The maximum absolute values of the inrush current in the three phases are extracted from each of the 400 measurements. The current peaks occur at different

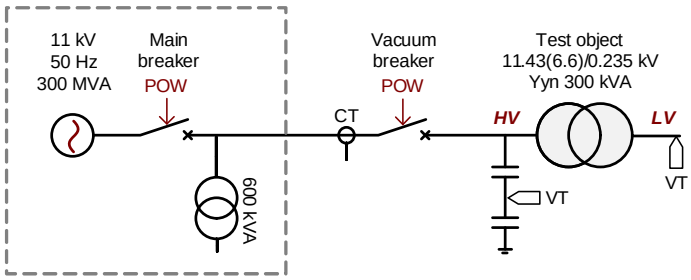

Fig. 1. Laboratory layout.

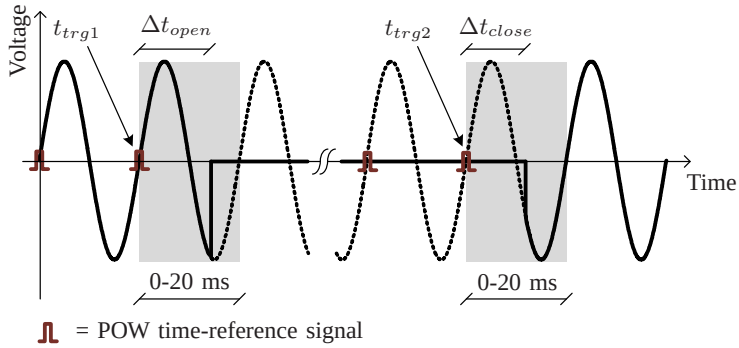

Fig. 2. Trigger signals and systematic variation of the switching times.

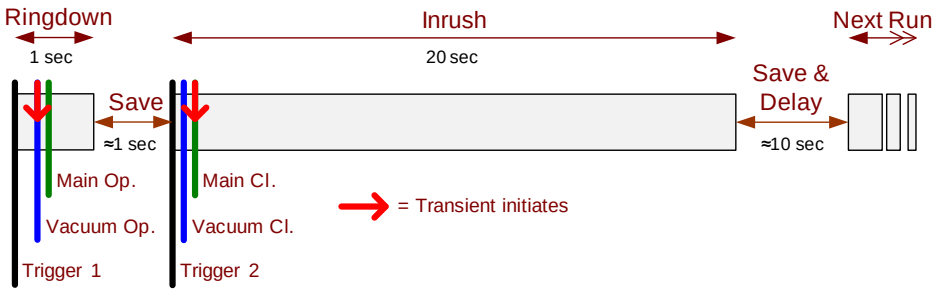

Fig. 3. Double triggering procedure.

times and have a positive or negative sign. The absolute values of these currents are then plotted in a contour plot as a function of Δt_{close} and Δt_{open} as shown in Fig. 4 for each of the three phases. The times when the peak currents occur are disregarded. The resolution in the contour plot is set to 20 A and the absolute value of the current is used to avoid a cluttered plot. Dark areas represent a lower magnitude of inrush currents, while lighter shades indicate higher inrush currents.

The purpose of Fig. 4 is to outline the magnitude of the inrush current in the three phases for different switching times. The $time = 0$ in the figure is synchronous to the triggering events, that is the zero crossing of the line voltage V_{RS} on the high voltage side. The opening time and the residual flux are constant when the figure

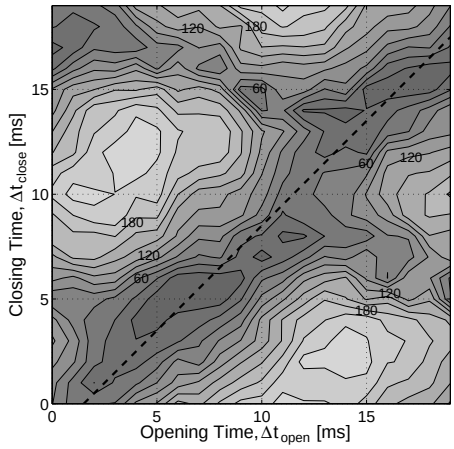

(a) Phase R

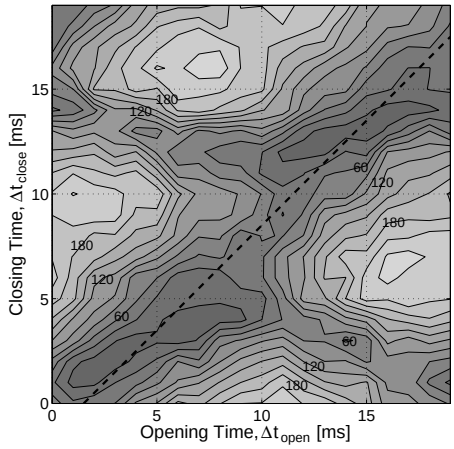

(b) Phase S

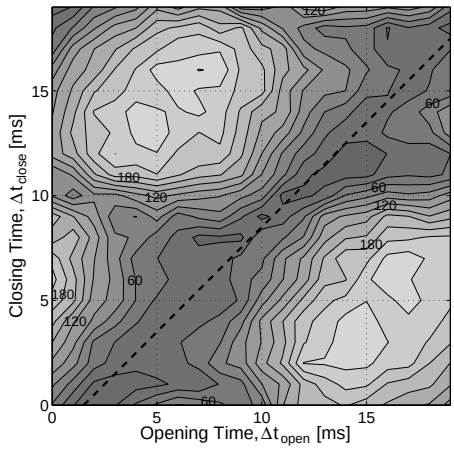

(c) Phase T

Fig. 4. Measurements of the first peak inrush current pattern, Yyn coupling. The opening and closing times are relative to the trigger signals.

is observed along a vertical line. The variation of the inrush current as a function of only the closing time can therefore be examined. Moving on a horizontal line denotes a fixed energization instant, and the inrush current variation for different disconnection times of the circuit breaker (i.e. different values of residual flux) can be investigated.

The worst-case inrush current peak measured is slightly below 240 A, almost 16 times the rated current of the transformer. The highest contour lines shown in Fig. 4 are for 220 A meaning that the measurements inside these defined areas have inrush current peaks higher than 220 A.

In a 20-by-20 ms grid the inrush current has two main summits that have alternating positive and negative values creating a graphical pattern. This pattern repeats itself due to the periodicity of the waveforms. The transition from positive to negative values is gradual and creates regions where the inrush current has a minimum value. The dashed lines in Fig. 4 identify an area that is consistent in all the three phases where the current peak is less severe and mainly remains lower than 3 times the transformer rated current in all the three phases concurrently.

B. Simplified physical explanation

The saturation of the magnetic core of a transformer is the main cause of an inrush current transient. The energization of a transformer yield to the most severe case of inrush current and the flux in the core can reach a maximum theoretical value of two to three times the rated flux peak [2].

The magnitude of the flux in the core at the energization instant is the residual flux. The integral of the applied voltage at the instant of energization can be called the "prospective" flux in the sense that it will be reached only at steady state [9], as shown in Fig. 5. The prospective flux can be described as a function of time:

$$\lambda_{j\,pros}(t) = \lambda_{peak} \cdot \sin(wt + \theta_j) \tag{1}$$

where $1 \leq j \leq 3$ is the phase index and $\theta_j = [0, -\frac{2\pi}{3}, \frac{2\pi}{3}]$ is the phase shift for a three-phase system. A flux offset is created if the residual flux is not equal to the prospective flux at the instant of energization and is defined as:

$$\lambda_{j\,offs}(\Delta t_{open}, \Delta t_{close}) = \lambda_{j\,res}(\Delta t_{open}) - \lambda_{j\,pros}(\Delta t_{close}) \tag{2}$$

Neglecting the damping of the offset flux as the first approximation, the flux in the core after the energization is:

$$\lambda_{j\,core}(t) = \lambda_{j\,pros}(t) + \lambda_{j\,offs}(\Delta t_{open}, \Delta t_{close}) \tag{3}$$

For this specific transformer and vacuum breaker setup, the ringdown measurements reveal that there is a periodical dependency of the residual flux from the disconnection time [14], [15]. A similar residual flux pattern is also reported in [13]. The periodical variation of the residual flux can be represented by a Fourier series that when simplified to the first term can be described by the function:

$$\lambda_{j\,res}(\Delta t_{open}) = \xi \cdot \lambda_{peak} \cdot \sin(\omega \Delta t_{open} + \theta_j + \beta) \tag{4}$$

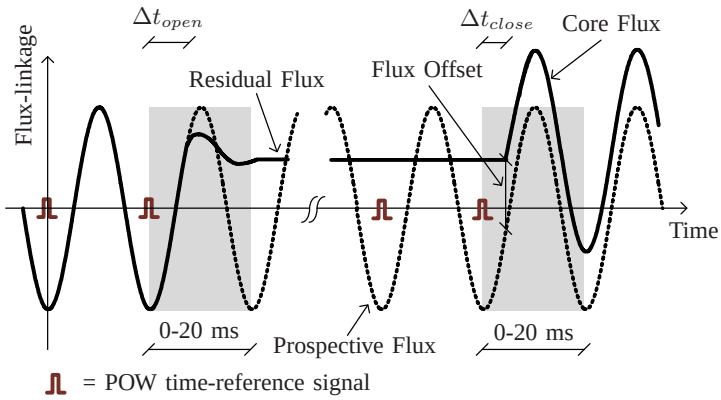

Fig. 5. Definition of fluxes.

with β describing the phase shift of the residual flux wave and ξ the ratio between rated and residual flux.

The residual flux is assumed to remain constant after de-energization [11]. Therefore the time lapse between the disconnection and the following energization of the transformer is not relevant. The opening and closing instants have a relative POW time delay defined as:

$$\Delta t_{POW} = \Delta t_{open} - \Delta t_{close} \tag{5}$$

Equation (2) can be described analytically:

$$\begin{aligned}
&\lambda_{j\,offs}(\Delta t_{open}, \Delta t_{close}) = \\
&= \lambda_{j\,res}(\Delta t_{close} + \Delta t_{POW}) - \lambda_{j\,pros}(\Delta t_{close}) = \\
&= \lambda_{peak} \cdot [\xi \cdot \sin(\omega \Delta t_{close} + \omega \Delta t_{POW} + \theta_j + \beta) + \\
&\qquad - \sin(\omega \Delta t_{close} + \theta_j)] = \\
&= \lambda_{peak} \cdot [\sin(\omega \Delta t_{close} + \theta_j) \cdot (\xi \cdot \cos(\omega \Delta t_{POW} + \beta) - 1) + \\
&\qquad + \cos(\omega \Delta t_{close} + \theta_j) \cdot (\xi \cdot \sin(\omega \Delta t_{POW} + \beta))] = \\
&= \lambda_{peak} \cdot C(\xi, \Delta t_{POW}, \beta) \sin(\omega \Delta t_{close} + \theta_j + \gamma)
\end{aligned} \tag{6}$$

with

$$C(\xi, \Delta t_{POW}, \beta) = \sqrt{\xi^2 + 1 - 2\xi \cos(\omega \Delta t_{POW} + \beta)} \tag{7}$$

$$\gamma = \tan^{-1} \frac{\sin(\omega \Delta t_{POW} + \beta)}{\cos(\omega \Delta t_{POW} + \beta) - \xi^{-1}} \tag{8}$$

Equation (6) proves that λ_{offs} is periodic and its magnitude is a function of Δt_{POW}. The magnitude of the inrush current is related to the flux offset as this is responsible for the development of the energization transient. The flux offset is reduced by minimizing C or the sine in (6). The minimum value of $C(\xi, \Delta t_{POW}, \beta)$ is $1 - \xi$ for

$$\Delta t_{POW} \mid_{min(|\lambda_{offs}|)} = -\frac{\beta}{\omega} \tag{9}$$

while $\sin(\omega\Delta t_{close} + \theta + \gamma) = 0$ for

$$\Delta t_{j\,close}\,|_{min(|\lambda_{offs}|)} = -\frac{\theta_j + \gamma + n\pi}{\omega} \tag{10}$$

The minimum amplitude of λ_{offs} occurs with a constant Δt_{POW} independently of the phase shifts θ_j as shown in (9). This corresponds to the dashed lines in Fig. 4 and identifies a consistent region for minimum inrush currents in all three phases. Equation (10) identifies also a region where λ_{offs} is zero. However, this is a nonlinear relationship that is dependent on the phase shift θ_j. In Fig. 4 this region can be identified as valleys curved around the summits with a different location for each phase.

The map of the inrush current as a function of Δt_{open} and Δt_{close} can be obtained theoretically. However, the function describing the relation current-flux is nonlinear as the behavior is ruled by the saturation of the magnetic core. In addition, the electric and magnetic couplings of the three phases complicate any further explanation without the use of a simulation model.

C. Confirmation and extension to other winding configurations by simulations

In order to confirm the observed behavior, the pattern measured in Fig. 4 is reproduced with ATP/EMTP simulations. The transformer model required to represent the systematic measurements is sophisticated as it needs to replicate both disconnection and energization transients. Standard models available in ATP/EMTP and PSCAD cannot represent the residual flux in a transformer after the disconnection transient, and the representation of the transformer energization transient is uncertain, showing considerable differences in transient situations [16].

The model proposed in [14], [15], [17] has the required characteristic and is used in this study. The transformer model is based on a topologically correct core model derived by duality transformation of the transformer's magnetic circuit. Each transformer limb is modeled by a nonlinear hysteretic inductor based on Jiles-Atherton theory. A hysteretic model is required for an accurate representation of disconnection transients and the determination of residual fluxes. The shunt capacitances in the winding are taken into account in the model as they influence the residual flux estimation [8], [15] and are modeled as connected to the terminals of the windings. In addition to the main leakage inductance between low and high voltage windings, the air-core inductance is also taken into account as it has a considerable inrush current limiting effect. The model parameters are calculated from standard test report data and a relatively small amount of low-detail design data. Special attention is paid to the parameter estimation to enhance the performance of the transformer model in saturation. It has been verified that the set of parameters used in the model predict the worst case inrush current within a 10% error and accuracy is maintained over a large range of inrush current magnitude. The parameter estimation technique and the verification of the model are discussed in [14], [15]. The capability of the model to determine the residual fluxes is an important feature for this study and is proved in Fig. 6 in [15].

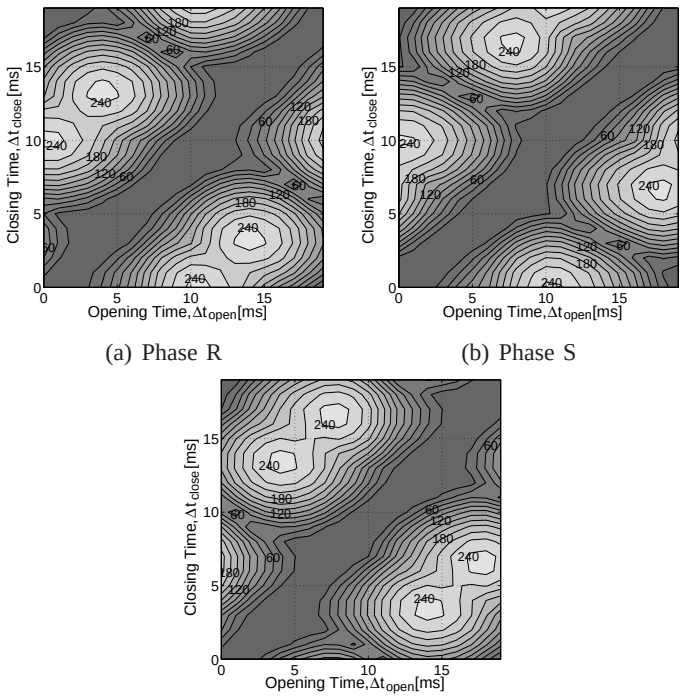

(a) Phase R (b) Phase S

(c) Phase T

Fig. 6. Simulated inrush pattern, Yyn.

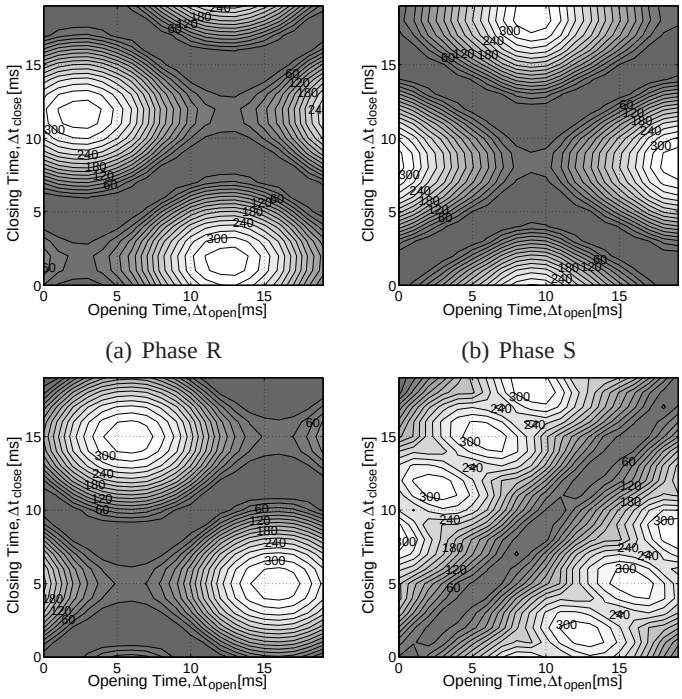

(a) Phase R (b) Phase S

(c) Phase T (d) Neutral

Fig. 7. Simulated inrush pattern, YNyn (similar to Dyn, phase currents).

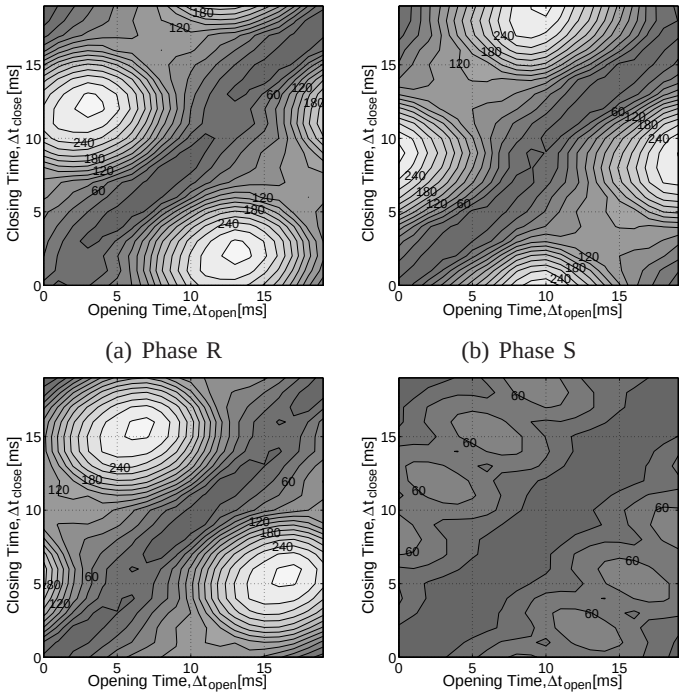

(a) Phase R (b) Phase S

(c) Phase T (d) Neutral

Fig. 8. Simulated inrush pattern, YNd (similar to Yd).

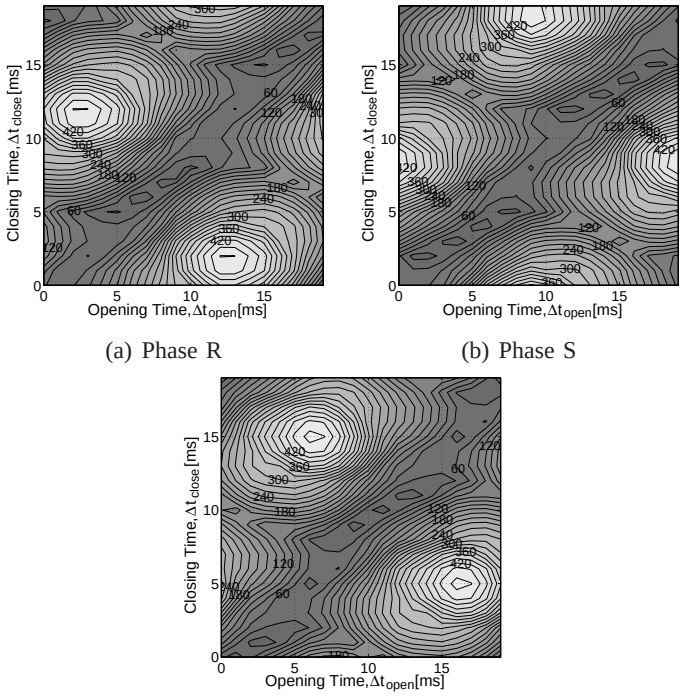

(a) Phase R (b) Phase S

(c) Phase T

Fig. 9. Simulated inrush pattern, Dyn, line currents.

A total of four hundred simulations were performed. For each simulation the model is initialized to steady state, the breaker opens and remains open to reach a stationary residual flux, and then closes as illustrated in Fig. 5. The opening and closing instants vary for each simulation in a range of 0-20 ms with a resolution of 1 ms. After the opening of the breaker, each section of the core in the model corresponding to a different transformer limb is self initialized to its residual flux value. The absolute value of the first current peak in each phase is recorded and displayed in Fig. 6 for the three phases. Some differences are noticeable between the measured pattern in Fig. 4 and the simulated pattern in Fig. 6, however the shape of the patterns is very close. The main source of inaccuracy derives from the control of the circuit breaker as accurate timing is achieved in the simulation, while the real circuit breaker has minor stochastic behavior that results in more rough lines in the measured pattern.

The simulations of the inrush peak pattern for different winding configurations are shown in Figs. 7-9. While measurements are not available for winding couplings other than Yyn, the validity of these simulation results is supported by the extensive verification of the model in [14], [15] and by the validation of Fig. 6.

Table I summarizes the result of Figs. 6-9 by comparing the influence of the winding connection with the worst case inrush current peak. The standard factor k reported in the literature [2], [3], [18], [19], is normally used to scale analytically calculated inrush current for single-phase transformer to three-phase:

$$I_{max\_3ph} = k \cdot I_{max\_1ph} \tag{11}$$

where the single-phase transformer has a rated voltage equal to the rated phase voltage of the three-phase transformer. The k factor is derived by semi-empirical considerations based on the core topology, and the current circulation and distribution in the windings. The main assumption is that the saturation involves only one phase. In Table I the simulated maximum current peak for grounded-wye coupling is used as a reference and set to 100%. The inrush current in pu is calculated as:

$$I_{inrush\_pu} = \frac{I_{inrush\_max}}{I_n} = I_{inrush\_max} \frac{\sqrt{3} \cdot V_l}{S} \tag{12}$$

and the percent value refers to:

$$I_{inrush}\% = \frac{I_{inrush\_max}}{I_{inrush\_max\_YNyn}} \cdot \frac{V_l}{V_{l\_YNyn}} \cdot 100 \tag{13}$$

The ratio between inrush maximum peaks for YNyn and Yyn is in agreement with the value reported in the literature. Discrepancies between 15% and 20% appear in the presence of a delta-connected winding, either on the primary or secondary sides of the transformer. The presence of a delta winding reduces the line current amplitude as part of the triple harmonics can circulate inside the delta without being transferred to the transformer terminals. Current zero sequence paths in a transformer affect the amplitude of inrush current as they allow, limit or block the development of triple harmonics in the line current.

A further comparison of the inrush current patterns in Figs. 6-9 reveals:

TABLE I
WINDING COUPLING INFLUENCE ON INRUSH PEAK.

Coupling	Current Peak	Neutral Peak	*k* Factor
YNyn	336A, 22pu, *(100%)*	318 A (95%)	1
YNd	287A, 19pu, (85%)	74 A (22%)	1
Yyn	248A, 16pu, (74%)	//	0.7-0.85
Yd	272A, 18pu, (81%)	//	2/3
Dyn	468A, 18pu, (80%)	//	1
Dyn (Ph. curr.)	319A, 21pu, (95%)	//	//

- The minimum inrush current pattern observed in the measurements is present in all the winding couplings.
- The pattern is nearly equal in all the three phases and is shifted by $\frac{T}{3} = 6.6\text{ms}$ in both the opening and closing time axes.
- In the Yyn case, the peak has a double-summit shape as the inrush current return path is through another phase (due to the insulated neutral). Thus the inrush current is induced in two phases simultaneously.
- Comparing YNyn and YNd, the neutral current becomes considerably attenuated if a secondary delta winding is present.
- The line current for the Dyn case in p.u. is lower than the phase current (Table I).
- The pattern for the winding coupling Yd is not reported here but is similar to the pattern for the YNd coupling (with the lack of the neutral current). In the same way, the pattern of the phase current in Dyn is not shown here but is similar to the pattern for the YNyn coupling (with the lack of the neutral current).

These considerations are valid only for three-legged core-type transformers. The five-legged, shell and transformer banks require further investigation as the magnetic circuit of the model changes according to the core topology.

IV. MINIMUM OF FIRST PEAK INRUSH CURRENT

The region where the peak inrush current is less severe is identified in Fig. 4 and a simplified physical explanation is given in Section III-B. To simplify the analysis of the maximum inrush current, the simulation results are now further extracted as shown in Figs. 10-13. The maximum inrush current in the three phases, both positive and negative, of each of the 400 simulations in Figs. 6-9 are now plotted as a function of $\Delta t_{POW} = \Delta t_{open} - \Delta t_{close}$. The points having the same closing time are connected by lines. In addition, due to the periodicity of the waveforms, the range from -20 ms to 0 ms maps the range from 0 ms to 20 ms and only positive values of Δt_{POW} are shown in these figures. For the 300-kVA transformer test object, it is estimated from Figs. 10-13 that the less severe inrush currents occur in the range $0\text{ ms} \leq \Delta t_{POW} \leq 2\text{ ms}$. This is independent of the winding configuration and confirms the simplified estimation of Δt_{POW} in (9) with a negative value of β. This range depends on the ringdown transient of a transformer. It is mainly

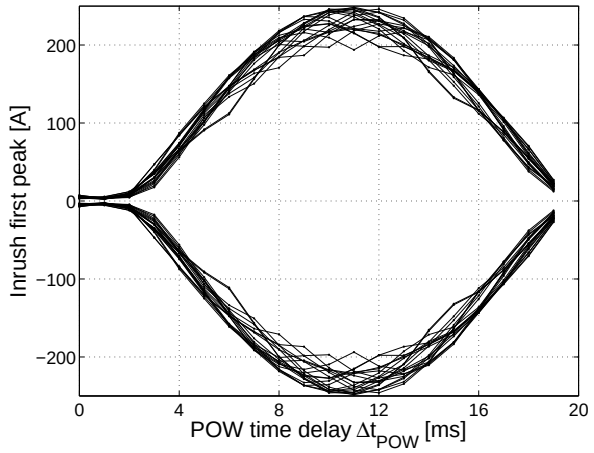

Fig. 10. Inrush current first peak, Yyn.

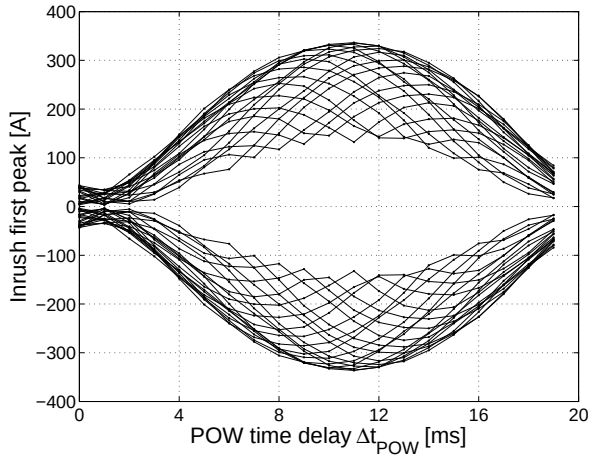

Fig. 11. Inrush current first peak, YNyn.

influenced by the transformer itself, the circuit breaker and the stray capacitances of the system.

The amplitude of the inrush current transient may be minimized by using a POW triggering control and without the need to measure and compute residual fluxes. This can be performed in two simple steps by the circuit breaker control mechanism:

1) The breaker opens and the point-on-wave time Δt_{open} is recorded.
2) The breaker closes at a point-on-wave instant $\Delta t_{close} = \Delta t_{open} - \Delta t_{POW}$

Steps one and two do not need to be in rapid succession, but any number of periods between the two operations can occur. The residual flux is assumed to stay constant in this interval.

The rapid-closing switching strategy [9], [10] and the novel simultaneous-closing switching strategy based on (9) are compared in Fig. 14 and Fig. 15 for a YNyn

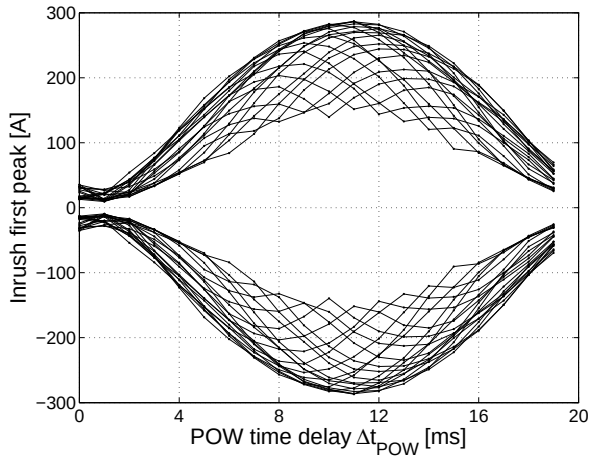

Fig. 12. Inrush current first peak, YNd.

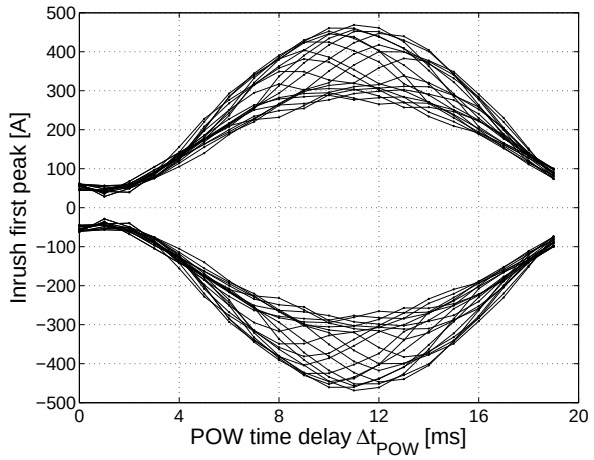

Fig. 13. Inrush current first peak, Dyn.

connection. In Fig. 14 the rapid-closing strategy is applied assuming that no information is available on residual fluxes. The first phase closes at voltage peak (phase R) and the other two phases are delayed 5 ms. Assuming that there is no control of the circuit breaker opening, the inrush current mitigation is not always optimal and the worst case energization with controlled switching gives an inrush current of $6\,I_n$ for the rapid-closing strategy. Fig. 15 shows the proposed simultaneous-closing strategy resulting in only $2.5\,I_n$ for the worst case energization.

V. DISCUSSION

The measurements and the analysis performed on the 300-kVA distribution transformer indicate that a simultaneous-closing strategy can be applied to mitigate inrush current transients. This technology does not require an independent-pole circuit breaker and may be employed in a lower voltage system as it is economically

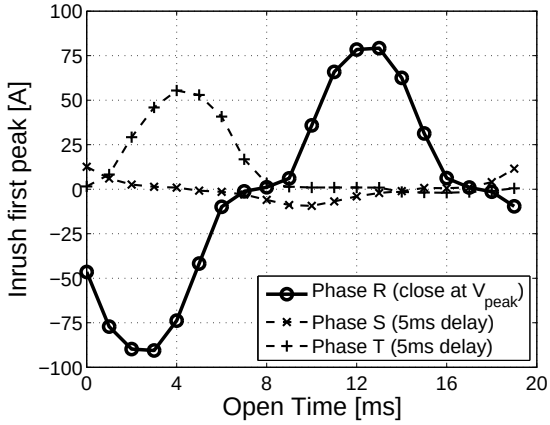

Fig. 14. Inrush current first peak with rapid-closing strategy, YNyn.

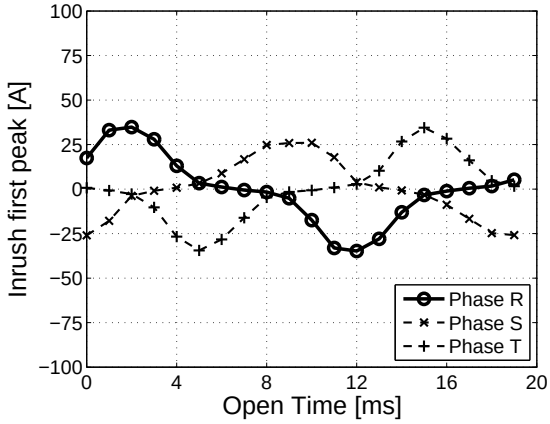

Fig. 15. Inrush current first peak with simultaneous-closing strategy, YNyn.

and technologically feasible. Previous studies report that residual fluxes in all three phases have to be known, and there are constraints on the residual flux magnitude which limit the applicability of the method [9], [10]. The current study shows how a simultaneous-closing strategy can be effectively used to limit the inrush current to $2.5\,I_n$, utilizing only the measured disconnection instant and without constraints or the need to calculate residual fluxes.

The transformer capacitances have influence on the maximum residual flux as shown in Fig. 17 in [15]. Larger capacitances result in lower maximum residual fluxes and according to (6) and (9) in a larger value of λ_{offs}. A less effective mitigation of inrush currents will be achieved with the proposed method for transformers with larger capacitances.

The vacuum circuit breaker used in the test setup has the capability to interrupt the no-load current at any instant (not zero crossing). The effect of circuit breakers with different current chopping capability has to be investigated as well. The

validity of (4) is essential for the applicability of the methods. Equation (4) implies that there is a relation between the prospective flux and the residual flux. This is verified in Fig. 6 in [15] with the use of a vacuum breaker and in Fig. 2 in [13] with the use of a solid state switch (IGBT). In Fig. 8 in [8] low-voltage molded-case circuit breakers are used and the validity of (4) is more doubtful. This may be explained by the lower current chopping capability of the circuit breakers and the lack of a perfect simultaneous interruption of the magnetizing current in all three phases. Fig. 18 in [15] shows the simulation result of the residual flux as a function of the opening time when the circuit breaker is modeled to interrupt the currents at any magnitude or only at its zero crossing. These two cases represent the two extreme situations and prove that when the breaker opens at the current zero crossing of each phase, a negative phase shift in the residual flux waveform is produced. Equation (4) is still verified for the fundamental harmonic of the residual flux curve and the novel current mitigation strategy can be applied, however reduced inrush current mitigation is achieved.

VI. CONCLUSION

The main result from this paper is the definition of a novel minimum inrush current condition. This condition is first observed in systematic measurements when the first peak inrush current pattern is analyzed. The condition is verified analytically and with simulations that confirm its applicability for all phases and winding configurations. The validity of the minimum inrush current pattern scheme is only verified for an unloaded 300-kVA distribution transformer. Further investigations are necessary to determine the general applicability of this approach.

The inrush current mitigation method derived from this study may find application in lower voltage grids where three-pole vacuum breakers are used and there is a low margin for extra investments. The applicability to higher voltage grids requires further investigation.

The inrush current pattern is proposed as an innovative way to effectively represent the first inrush current peak obtained with systematic measurements. This pattern is a suitable tool to verify a transformer model with measurements as the overall transformer response is better represented compared to a single time-domain curve. When inrush current damping is also an interesting factor in the study, inrush patterns representing the first and following inrush peaks can be shown.

Simulations have been used to calculate the maximum inrush peak for different winding couplings, and the ratios are compared with the semi-empirical k factor. A finding is that the contribution of delta-coupled windings to the reduction of inrush current is higher than what is normally considered. A difference up to 20% is observed when comparing the standard k factor with simulations. It is clear from these results that the validity of the k factor is somewhat doubtful and further work supported by measurements and simulations is required to update the analytical calculation method of the inrush current for a three-phase transformer based on the k factor.

ACKNOWLEDGMENT

The research team at NTNU and SINTEF Energy Research acknowledge the Norwegian Research Council, Hafslund Nett, Statnett SF, Statkraft Energi AS, NVE, EDF, Nynäs Petroleum AB and ABB for their support in the project "Thermal and electromagnetic performance of transformers".

REFERENCES

[1] M. Steurer and K. Frohlich, "The impact of inrush currents on the mechanical stress of high voltage power transformer coils," *IEEE Trans. Power Del.*, vol. 17, no. 1, pp. 155–160, Jan. 2002.

[2] L. F. Blume, *Transformer engineering : a treatise on the theory, operation, and application of transformers*, 2nd ed. New York, N.Y.: John Wiley and Sons, Inc., 1951.

[3] S. V. Kulkarni and S. A. Khaparde, *Transformer engineering: design and practice*, ser. Power engineering. New York, N.Y.: Marcel Dekker, Inc., 2004, vol. 25.

[4] J. F. Holcomb, "Distribution transformer magnetizing inrush current," *Transactions of the American Institute of Electrical Engineers, Part III (Power Apparatus and Systems)*, vol. 80, no. 57, pp. 697–702, Dec. 1961.

[5] T. R. Specht, "Transformer magnetizing inrush current," *AIEE Trans*, vol. 70, pp. 323–328, 1951.

[6] G. Bertagnolli, *Short-Circuit Duty of Power Transformers, Second Revised Edition*. ABB, 1996.

[7] L. M. Ganatra, P. G. Mysore, K. K. Mustaphi, A. Mulawarman, B. A. Mork, and G. Gopakumar, "Application of reclosing schemes in the presence of capacitor bank ringdown," *Proc Am Power Conf*, vol. 61-2, pp. 967–972, 1999.

[8] N. Chiesa, A. Avendaño, H. K. Høidalen, B. A. Mork, D. Ishchenko, and A. P. Kunze, "On the ringdown transient of transformers," in *IPST'07 - International Conference on Power System Transients*, no. IPST-229, Lyon, France, Jun. 2007.

[9] J. H. Brunke and K. J. Frohlich, "Elimination of transformer inrush currents by controlled switching. I. Theoretical considerations," *IEEE Trans. Power Del.*, vol. 16, no. 2, pp. 276–280, April 2001.

[10] J. H. Brunke and K. J. Frohlich, "Elimination of transformer inrush currents by controlled switching. II. Application and performance considerations," *IEEE Trans. Power Del.*, vol. 16, no. 2, pp. 281–285, April 2001.

[11] *Controlled switching of HVAC CBs - Planning, Specifications & Testing*, CIGRÉ SC A3 WG A3.07, Jan. 2004.

[12] L. Prikler, G. Banfai, G. Ban, and P. Becker, "Reducing the magnetizing inrush current by means of controlled energization and de-energization of large power transformers," *Electric Power Systems Research*, vol. 76, no. 8, pp. 642–649, May 2006.

[13] A. Ebner, M. Bosch, and R. Cortesi, "Controlled switching of transformers - effects of closing time scatter and residual flux uncertainty," in *Proc. 43rd International Universities Power Engineering Conference UPEC 2008*, Sep. 2008, pp. 1–5.

[14] N. Chiesa and H. K. Høidalen, "Systematic switching study of transformer inrush current: simulation and measurements," in *IPST'09 - International Conference on Power System Transients*, no. IPST-139, Kyoto, Japan, Jun. 2009.

[15] N. Chiesa, B. A. Mork, and H. K. Høidalen, "Transformer model for inrush current calculations: Simulations, measurements and sensitivity analysis," *IEEE Trans. Power Del.*, 2010, accepted for publication, TPWRD-00942-2009.

[16] H. K. Høidalen, B. A. Mork, F. Gonzalez, D. Ishchenko, and N. Chiesa, "Implementation and verification of the hybrid transformer model in ATPDraw," *Electr. Power Syst. Res.*, vol. 79, no. 3, pp. 454 – 459, Mar. 2009, special Issue: Papers from the 7th International Conference on Power Systems Transients (IPST), 7th International Conference on Power Systems Transients.

[17] N. Chiesa and H. K. Høidalen, "Hysteretic iron-core inductor for transformer inrush current modeling in EMTP," in *PSCC 2008 - 16th Power Systems Computation Conference*, Glasgow, Scotland, Jul. 2008.

[18] W. Schmidt, "Ueber den einschaltstrom bei drehstromtransformatoren," *Elektrotechnische Zeitschrift – Edition A*, vol. 82, no. 15, pp. 471–474, Jul. 1961, Switch-on current in 3-phase a-c transformers.
[19] R. Yacamini and A. Abu-Nasser, "The calculation of inrush current in three-phase transformers," *IEE Proceedings B (Electric Power Applications)*, vol. 133, no. 1, pp. 31–40, Jan. 1986.

Nicola Chiesa was born in Italy in 1980. He received the MSc degree in Electrical Engineering from Politecnico di Milano in 2005. From 2005 to 2009 he joined the Department of Electric Power Engineering at the Norwegian University of Science and Technology as a PhD candidate. He is now with the Department of Energy Systems at SINTEF Energy Research.

Hans Kristian Høidalen (M'05) was born in Norway in 1967. He received his MSc and PhD degrees from the Norwegian University of Science and Technology in 1990 and 1998, respectively. He is now a professor at the same institution with a special interest of electrical stress calculations and modeling.

never been so close...
(c.b.)

ISBN 978-82-471-2086-6 (printed ver.)
ISBN 978-82-471-2087-3 (electronic ver.)
ISSN 1503-8181

NTNU
Norwegian University of
Science and Technology